SAPIENZA
UNIVERSITÀ DI ROMA

The Enduring Menace of Antibiotic Resistance: Multidimensional Adaptation in High-Impact Clinical Pathogens and Prospects of Novel Interventions

Department of Public Health and Infectious Diseases

PhD Programme in Advances in Infectious Diseases, Microbiology, Legal Medicine and Public Health Sciences

PhD Candidate

Astri Dwyanti Tagueha

Supervisors

Prof. Cecilia Ambrosi

Daniela Scribano, PhD

The Enduring Menace of Antibiotic Resistance: Multidimensional Adaptation in High-Impact Clinical Pathogens and Prospects of Novel Interventions

Department of Public Health and Infectious Diseases

PhD Programme in Advances in Infectious Diseases, Microbiology, Legal Medicine and Public Health Sciences

XXXVIII Cycle

PhD Candidate

Astri Dwyanti Tagueha

Supervisors

Prof. Cecilia Ambrosi

Daniela Scribano, PhD

Coordinator

Prof. Stefano D'Amelio

Academic year: 2025/2026

Summary

This PhD thesis explores how high-impact clinical pathogens adapt under sustained antibiotic pressure and examines complementary strategies to counteract their persistence. Focusing on *Acinetobacter baumannii*, Uropathogenic *Escherichia coli* and *Streptococcus agalactiae*, the work shows how resistance genes, virulence factors, and niche-specific phenotypes interact to sustain survival in hospital and community settings, including the emergence of multidrug-resistant and hypervirulent lineages. Within this framework, the thesis evaluates probiotic-based and nanotechnology-based approaches as antibiotic-sparing options to limit colonization and infection by these priority pathogens.

The thesis begins with an extensive review of antibiotic classes, major resistance mechanisms, and the epidemiology and persistence strategies of the three selected pathogens, alongside emerging non-antibiotic interventions such as probiotics and nanoparticles. Subsequent project chapters dissect the genomic and phenotypic adaptation of *A. baumannii* and UPEC under clinical selective pressures, reveal the initial goblet-cell responses to *A. baumannii* in air-liquid interface cell models mimicking the airway epithelium, define the virulence–resistance landscape of colonizing and hypervirulent *S. agalactiae* isolates, and investigate the antagonistic potential of *Lactobacillus spp*. and serine-based gemini nanoparticles as tools to reshape pathogen–host–microbiota interactions.

Collectively, the findings reveal a coherent scenario in which resistance and virulence frequently co-evolve, challenging conventional antibiotic-centred management and underscoring the need for integrated ecological and physicochemical therapies. By combining detailed pathogen characterisation with proof-of-concept studies on probiotics and gemini-based nanoparticles, this thesis contributes to a broader understanding of how alternative interventions might be employed to reduce maternal colonization, lower the spread of multidrug-resistant lineages, and ultimately mitigate the burden of invasive bacterial disease.

Abbreviations

2D-ALI: 2-Dimension-Air Liquid Interface

8-8Ser: Anionic serine-based surfactant

ARGs: Antibiotic Resistance Genes

ATCC: American Type Culture Collection

BA: Bronchoalveolar Aspirate

BAL: Bronchoalveolar Lavage

BHI: Brain Heart Infusion

CFU: Colony Forming Unit

CLSI: Clinical and Laboratory Standard Institute

CMC: Critical Micelle Concentration

CRAB: Carbapenem Resistance *Acinetobacter baumannii*

DEGs: Differentially Expressed Genes

DMEM: Dulbecco's Modified Eagle Medium

DMPC: zwitterionic phospholipid 1,2-dimyristoyl-sn-glycero-3-phosphocholine

DMPG: anionic phospholipid 1,2-fimyristoyl-sn-glycero-3-phospho-rac- (1-glycerol) sodium salt

DNA: Deoxyribonucleic Acid

ESBL: extended spectrum beta-lactamase

EUCAST: European committee on antimicrobial susceptibility testing

ExPEC: Extraintestinal Pathogenic *Escherichia coli*

GBS: Group B Streptococcus

HLGR: High Level Gentamicin Resistance

HvgA: Hypervirulent GBS Adhesin

IAP: Intrapartum Antibiotic Prophylaxis

KEGG: Kyoto Encyclopedia of Genes and Genomes

LA: Luria-agar

LB: Luria-Bertani broth

LPS: Lipopolysaccharide

MDR: Multi Drug Resistance

MIC: Minimum Inhibitory Concentration

MLST: Multilocus Sequence Typing

MOI: Multiplicity of Infections

MTT: 3-(4,5-dimethylthiazol-2-yl)-2,5-diphenyl-2H-tetrazolium bromide

NCIMB: National Collection of Industrial, food, and Marine Bacteria

NPs: Nanoparticles

OD: Optical Density

OR: Odd Ratio

PCR: Polymerase Chain Reactions

PDR: Pan Drug Resistance

Pen/Strep: Penicillin Streptomycin

ROS: Reactive Oxygen Species

RNA: Ribonucleic Acid

ST: Sequence Type

STRING: Search Tool for the Retrieval of Interacting Genes/Proteins

TSA: Tryptic Soy Agar

TSB: Tryptic Soy Broth

UPEC: Uropathogenic *Escherichia coli*

UTI: Urinary Tract Infection

VGs: Virulence Genes

XDR: Extended Drug Resistance

Table of contents

Chapter 1. Introduction

1.1 Antibiotic Resistance as a Global Health Crisis

Antibiotic resistance (AR) has become the concerning challenges to global health in the 21st century, although the problem is not a recent phenomenon. AR has existed since the earliest use of antibiotics, including penicillin and streptomycin, discovered during the interwar period (1920s-1940s). Even before these antibiotics were widely introduced, bacteria had already begun developing resistance mechanisms as part of their natural evolutionary response [1]. Furthermore, along with the golden age of antibiotic discovery and subsequent decades of medical improvement, bacteria have shown an alarming capacity to counteract the effects through diverse resistance strategies. Consequently, infections that were previously treatable, such as urinary tract infections, pneumonia, and neonatal infections, are becoming increasingly difficult to manage with standard antibiotic therapies [2–4].

The emergence and spread of drug-resistant pathogens are significantly linked to high mortality, as well as clinical and economic consequences. Current mortality data showed that drug-resistant bacteria are directly responsible for 1.27 million deaths and contributed to 4.95 million deaths globally in 2019 [5]. By 2050, annual deaths attributable to antimicrobial resistance, mostly driven by resistant bacteria, are projected to reach 1.91 million (a 67.5% increase), while associated deaths could hit 8.22 million yearly [6]. AR complicates the treatment of healthcare-associated infections, including respiratory infections, urinary tract and bloodstream infections, surgical site complications, neonatal infections, and infections affecting cancer or transplant patients. AR prolongs hospital stay, increase treatment failures, and costly alternatives. Accordingly, antimicrobial current trends add $66 billion/year to global healthcare costs, and projected to rise to $1 trillion per year by 2050. If resistance accelerates continuously, global gross domestic product (GDP) could shrink to 1.1%-3.8% by 2050 due to lost productivity, reduced labor forces, and tourism declines, which then could push 28.3 million people living in extreme poverty [7,8].

The rapid evolution of bacterial resistance mechanisms is primarily driven by the overuse and misuse of antibiotics in clinical and agricultural settings. Factors contributing to the overuse of antibiotics in clinical settings include overprescription, poor regulation, a lack of rapid diagnostic tools, the underutilization of microbiological diagnostics, clinical misdiagnosis, and healthcare system challenges such as patient pressure. Private healthcare providers, especially in low-and middle-income countries, also play a significant role by overprescribing antibiotics to maximize their profits, as there is often a direct financial incentive to dispense medications [9,10]. Moreover, personal behavioral factors including self-medication, misconception, and the tendency to share and store leftover antibiotics exacerbate the issue [11]. In contrast, antibiotics are used prophylactically in industrial farming to increase livestock growth rates and prevent illness. A recent study showed that global antibiotic use in livestock could reach

approximately 143,481 tons by 2040, indicating a 25% upward trend from a baseline of approximately 110,777 tons in 2019, with Asia remaining the largest consumer [12]. The variation in regional policies regarding antibiotic use is another challenge. While European countries strictly enforced measures to reduce antibiotic consumption in the non-medical sector, almost 54% of 12,254 tons of antimicrobials sold in domestic agriculture under the US authority were classified as medically important [13]. This ongoing pressure fosters the emergence of resistance among bacteria in clinical, community, and environmental settings.

1.2 Classification of Antibiotic Resistance in Bacteria

Bacterial resistance to antibiotics has become a major concern for healthcare practitioners, scientists, and health organizations. In 2008, Dr. Louis B. Rice, introduced the acronym ESKAPE to highlight six clinically significant pathogens (*Enterococcus faecium, Staphylococcus aureus, Klebsiella pneumoniae, Acinetobacter baumannii, Pseudomonas aeruginosa,* and *Enterobacter* spp), regarding their ability to "escape" the effect of antibiotic treatment [14,15]. At around the same time, the urgency of addressing antibiotic resistance was reinforced by a joint initiative of the European Center for Disease Prevention and Control (ECDC) and the US Center for Disease Control and Prevention (CDC). As a result, in 2011, standardized definitions for multidrug-resistant (MDR), extensively drug-resistant (XDR), and pandrug-resistant (PDR) strains were officially adopted. These classifications are critical for guiding treatment decisions that are directly associated with the therapeutic complexity and clinical outcomes. MDR organisms (resistant to at least one of three or more antibiotic agents) may still respond to selected antibiotics. Conversely, XDR organisms (non-susceptibility to almost all but one or two categories) reveal greater treatment challenges, while PDR organisms (resistance to all tested antibiotics) frequently result in treatment failure [16]. These definitions are now widely applied to nosocomial pathogens owing to their epidemiological significance and emerging resistance patterns.

Based on these definitions, the World Health Organization (WHO) introduced the Bacterial Priority Pathogens List (BPPL) in 2017 to stratify antibiotic-resistant bacteria into critical, high-, and medium-priority groups. This stratification is based on several factors, including resistance profiles, global disease burden, transmission potential, and availability of effective treatment. The expansion of priority pathogen list from 12 pathogens in 2017 to 24 across 15 bacterial families by 2024 highlights the broad adaptation and transmission of antibiotic-resistant bacteria [17]. The BPPL has double functions, as a strategic tool for directing research and development of novel antibacterial agents and practical resource for policymakers, researchers, funders, and pharmaceutical industry [18]. To support appropriate antibiotic use, WHO also introduced the AWaRe classification system, which divides antibiotics into three groups: access (first-line essential treatments), watch (broad-spectrum agents requiring careful monitoring), and

reserve (last-resort antibiotics), thereby promoting rational prescription and global stewardship efforts [19].

Although MDR, XDR, and PDR classifications remain foundational for epidemiological surveillance, they present limitations when applied to clinical decision-making. The key shortcoming is the uniform weighting of all antibiotics based solely on in vitro susceptibility, without accounting for critical clinical parameters, such as drug efficacy, pharmacokinetics, and toxicity. This limitation restricts their usefulness at the bedside and may not accurately predict patient outcomes. To address this gap, the concept of difficult-to-treat resistance (DTR) was proposed in 2018, specifically for Gram-negative bacteria resistant to all first-line, high-efficacy, and low-toxicity antibiotics, including carbapenems, β-lactam-β-lactamase inhibitor combinations, and fluoroquinolones. Unlike MDR/XDR/PDR, which focus on the number of drug classes affected, DTR emphasizes the practical difficulty of treatment, offering more direct guidance to clinicians about therapeutic urgency and limited options. Together, both approaches share alignment in highlighting high-risk pathogens and reflect complementary strategies in tackling antimicrobial resistance at both the clinical and public health levels [20,21].

1.3 Antibiotic resistance mechanisms

Drug-resistant bacteria use a variety of molecular and cellular mechanisms to survive under antibiotic pressure, including enzymatic inactivation of the drug, alteration-modification-protection of target sites, reduced drug accumulation, functional bypass, and adaptive metabolic rewiring (Figure 1.1). Indeed, individual antibiotic classes are often countered by several mechanisms simultaneously (Table 1.1), and the underlying resistance genes may arise from chromosomal mutations or spread rapidly through horizontal gene transfer [22]. Notably, a previous palaeomicrobiology study showed that adapt-or-die strategies already existed in ancient environmental bacteria, underlining that resistance will continue to diversify as part of bacterial evolution in response to novel antibiotics [23].

Enzymatic inactivation or modification is a major and highly efficient bacterial resistance mechanism. These enzymes act as molecular effectors that either cleave or chemically modify antibiotic molecules, thereby neutralizing drug activity before reaching its target. This strategy covering a diverse set of adaptive protein and pathways, include hydrolysis, group transfer, and redox reactions. β-lactamases are well-known examples that inactivate penicillin, cephalosporins and carbapenems by hydrolysing the beta-lactam ring, an essential structure for antibiotic activity. The presence of extended-spectrum beta-lactamases (ESBLs)-producing strains marks a significant evolution step, as these enzymes can degrade modern penicillin and cephalosporin [24]. Similarly, aminoglycoside-modifying enzymes confer resistance to aminoglycosides by catalysing the transfer of chemical groups (e.g., acetyl, phosphate), directly onto the antibiotic molecule. This enzymatic modification alters the molecular structure of the drug and prevents effective binding to the bacterial ribosome [25]. Furthermore, the evolution of

antibiotic resistance enzymes appears inevitably since many of them arise within enzyme superfamilies that also contain housekeeping proteins involved in primary metabolism and cell wall synthesis [26]. For example, structural and phylogenetic analyses show that classes A, C, and D serine β-lactamases originated from actinomycete D-alanyl-D-alanine peptidases (penicillin-binding proteins), essential housekeeping enzymes that catalyse peptidoglycan cross-linking in cell wall synthesis, and that these β-lactamases are ancient, having emerged more than two billion years ago from a common PBP-like ancestor [27–29].This evolutionary relationship illustrates how enzymes with primary roles in cell wall metabolism can be repurposed into dedicated antibiotic resistance functions.

Table 1.1. Mode of action and resistance mechanisms of commonly used antibiotics [30].

Antibiotic class	Mechanism of action	Common resistance
β-lactams	Inhibit cell wall synthesis via PBPs	β-lactamases, altered PBPs, porin loss, efflux
Glycopeptides	Bind D-Ala-D-Ala to block peptidoglycan synthesis	D-Ala-D-Lac modification (VanA)
Macrolides	Inhibit 50S ribosome – block protein elongation	Efflux (msrA), ribosome methylation (erm)
Tetracyclines	Inhibit 30S ribosome – block tRNA binding	Efflux (tetA), ribosome protection (tetM)
Aminoglycosides	Bind 30S ribosome – cause mRNA misreading	Modifying enzymes (aac, ant), 16S methylation
Fluoroquinolones	Inhibit DNA gyrase & topoisomerase IV	gyrA/parC mutations, efflux (qnr), plasmids
Sulfonamides	Inhibit folic acid synthesis via DHPS	dhps mutations, PABA overproduction, efflux
Oxazolidinones	Inhibit 50S – block ribosome assembly	23S rRNA mutation, cfr methylation
Polymyxins	Disrupt cell membrane	LPS modification (mcr-1), efflux
Lincosamides	Inhibit 50S – block protein elongation	erm-mediated methylation, efflux
Rifamycins	Inhibit RNA polymerase – block transcription	rpoB mutations, efflux

Second resistance mechanism are alteration, modification, and protection of the target sites of the antibiotic which operates similarly to the lock and key principle. If the antibiotic is the key designed to fit a specific lock inside the bacterium, resistance occurs when the bacterium changes the lock, so that the antibiotic will no longer bind effectively. Besides enzymatic deactivation, β-lactam resistance also occurs through alteration in the structure and/or number of penicillin-binding-proteins (PBPs). Another example is

fluroquinolones resistance, which occurs through mutations in the genes encoding DNA gyrase (*gyrA/gyrB*) and topoisomerase IV (*parC/parE*). These mutations alter the conformation of the enzymes' active sites, reducing drug binding while preserving enzyme function for bacterial metabolism [31]. Beyond alteration, two other key strategies are modification and protection. Modification involves the additional of chemical group to the drug target, such as the methylation of rRNA by methyltransferases, which confers resistance to macrolides, lincosamides, and streptogramin [32]. In contrast, protection employs specific protein that bind to the target site, acting as physical shield from antibiotic. For instance, TetM/TetO proteins bind to the ribosome and dislodge tetracycline from its binding site [33,34].

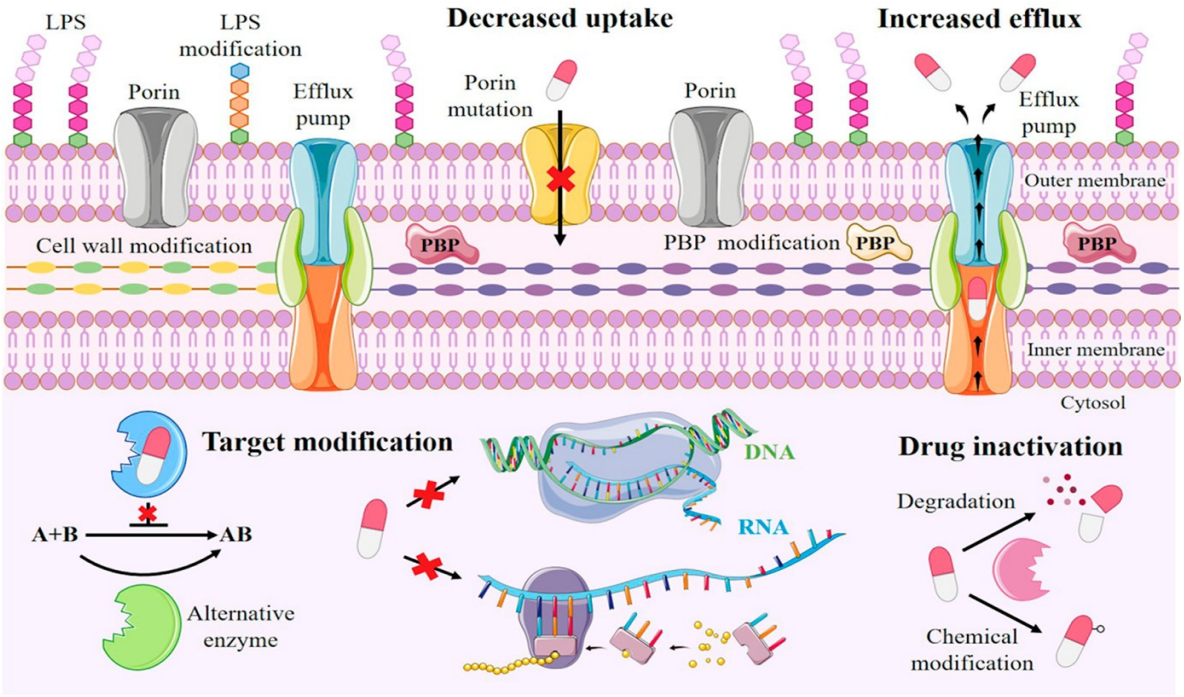

Figure 1.1. Schematic representation of different mechanism of antibiotic resistance in bacteria [35].

Reduced permeability is an antibiotic resistance mechanism works differently between Gram-negative and Gram-positive bacteria due to their distinct cell envelope structures. In Gram negative, outer membrane proteins (OMPs) form porins, a β-barrel formations that create water-filled channels in the outer membrane [36]. Porin as OmpC and OmpF of *Enterobacteriaceae*, with narrow and wide pore respectively, act as primary antibiotic entry point; their modification or loss reduces influx and limiting the entry of hydrophilic antibiotic like β-lactams and fluoroquinolones. Differently, the major outer membrane protein OmpA plays a distinct, structural role in resistance. Indeed, OmpA maintains the membrane integrity and stability by interacting with peptidoglycan layer. Its mutation causing direct permeability changes and affects the positioning and expression of other Omp including OmpF [36,37]. Furthermore, a stable membrane architecture is required

for the proper assembly and operation of efflux pumps, and OmpA acts a critical scaffold, ensuring the functionality of these fundamental bacterial antibiotic-resistance defensive machinery [37,38]. Five major superfamilies have been discovered (Figure 1.2). The RND (Resistance-Nodulation-Division) family is specific to Gram negative bacteria; its tripartite structure (e.g., AcrAB-TolC) expels a drug from the cytoplasm through the periplasm and out of the cell via membrane channels. This structure is then complemented by other superfamilies located in the inner membrane such as the MFS (Major Facilitator Superfamily), SMR (Small Multidrug Resistance), MATE (Multidrug and Toxic Compound Extrusion) pumps, and the ABC (ATP-Binding Cassette) family [36,39]. On the contrary, Gram-positive bacteria lack an outer membrane and thus have no equivalent to porins or the periplasm-spanning RND pumps. Their efflux systems are based exclusively on the MFS, SMR, MATE, and ABC families, which operate across the single cytoplasmic membrane. Therefore, their resistance mainly relies on cell wall modifications and membrane bound and single component efflux pump [40,41]. The absence of the complex, broad-spectrum RND efflux machinery and the initial porin barrier is what makes the Gram-negative defence against antibiotics far more sophisticated and effective [36,42].

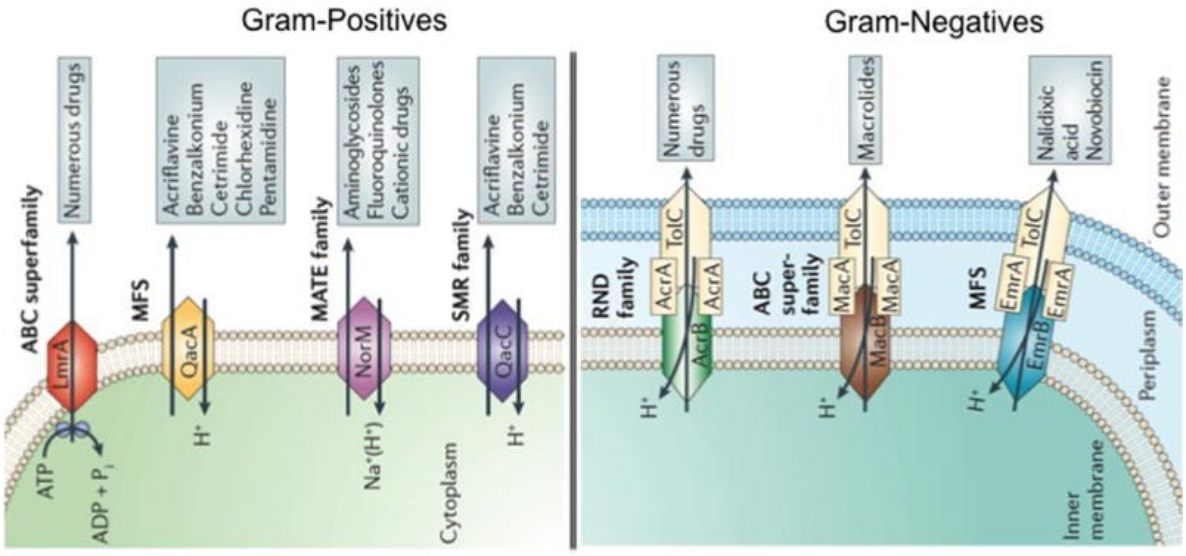

Figure 1.2. The five major families of efflux pumps. Each family have their source of energy, example of drugs, and compounds that serve as substrate [22].

Functional bypass and metabolic rewiring are two additional bacterial survival strategies when antibiotics block key metabolic pathways. In functional bypass, bacteria acquire or upregulate alternative enzymes or pathways that perform the same essential function as the antibiotic-inhibited target, so the blocked reaction is effectively circumvented [22]. This mechanism relies on stable genetic changes, such as point mutations, gene duplication, or horizontally acquired resistance genes, and therefore confers heritable resistance. The basic example is the resistance to sulfonamides and trimethoprim, an

antibiotic which target sequential steps in folate synthesis. Resistant bacteria often acquire plasmids carrying resistant gene to these antibiotics. Particular genes, such as *sul1* and *sul2,* encode alternative dihydropteroate synthases (DHPS), and *dfr* which encode variant dihydrofolate reductase (DHFR) enzyme, which help to neutralizing both antibiotics respectively [43,44]. In contrast, metabolic rewiring refers to dynamic, reversible reorganization of central metabolism including glycolysis, tricarboxylic acid (TCA) cycle, fermentation, amino acid and lipid metabolism, and redox balance that supports survival under antibiotic stress without necessarily modify drug targets [45]. For example, Gram-negative pathogen exposed to polymyxins remodel lipid A and outer membrane components, reducing the net negative charge and hindering electrostatic interactions with these cationic peptides [46]. However, a more drastic mechanism, observed notably in *Acinetobacter baumannii*, involves the complete loss of lipopolysaccharide (LPS) due to mutations in the lipid A biosynthesis pathway (e.g., *lpx* genes). This results in the total absence of the primary binding target, rendering the bacteria highly resistant to the drug [47,48]. Another example is tetracycline-resistant *E. coli* remodels its metabolism by downregulating the TCA cycle and disrupting redox homeostasis to support the proton motive force for tetracycline efflux, with at least 308 genes, including transcriptional regulators [49]. Whereas functional bypass directly replaces the inhibited molecular function, metabolic rewiring globally adjusts the metabolic network to promote tolerance and persistence, providing temporal period in which functional bypass and other stable resistance determinants can emerge and be selected [45].

Biofilm formation and desiccation tolerance combine physical protection (biofilm matrix, surface adherence, and microenvironments) with low-activity metabolic shifts as stress-adapted states, which are often coordinated by quorum sensing (QS) [50,51]. At high densities, QS-cell-to-cell communication via diffusible autoinducers synchronizes biofilm maturation, matrix production, and metabolic downregulation, while simultaneously enhances desiccation tolerance by inducing osmoprotectant synthesis and persister formation (Figure 1.3) [50,52]. Within biofilms, the formation of QS-driven steep oxygen and nutrients gradients lead interior cells to downregulate aerobic respiration and the TCA cycle, thereby inducing a switch to fermentation or alternative pathways such as denitrification or the glyoxylate shunt, forcing slow-growing or quasi-dormant states. This metabolic repression reduces membrane potential, lowers reactive oxygen species (ROS) production, and diminishes uptake and bactericidal activity of antibiotics dependent on active metabolism, such as aminoglycosides and many cell wall–active drugs [52,53]. Furthermore, under desiccation stress, QS coordinates water loss, and broad adaptive response to osmotic stress, and oxidative damage; these include accumulation of compatible solutes (such as L-glutamate, trehalose, and mannitol), the remodelling of membrane fatty acids, and a global slowing or arrest of growth and respiration. The result is anhydrobiotic-like state, which greatly

reduces turnover of antibiotic targets and energy-dependent drug uptake, thereby significantly limiting antibiotic killing [54–56].

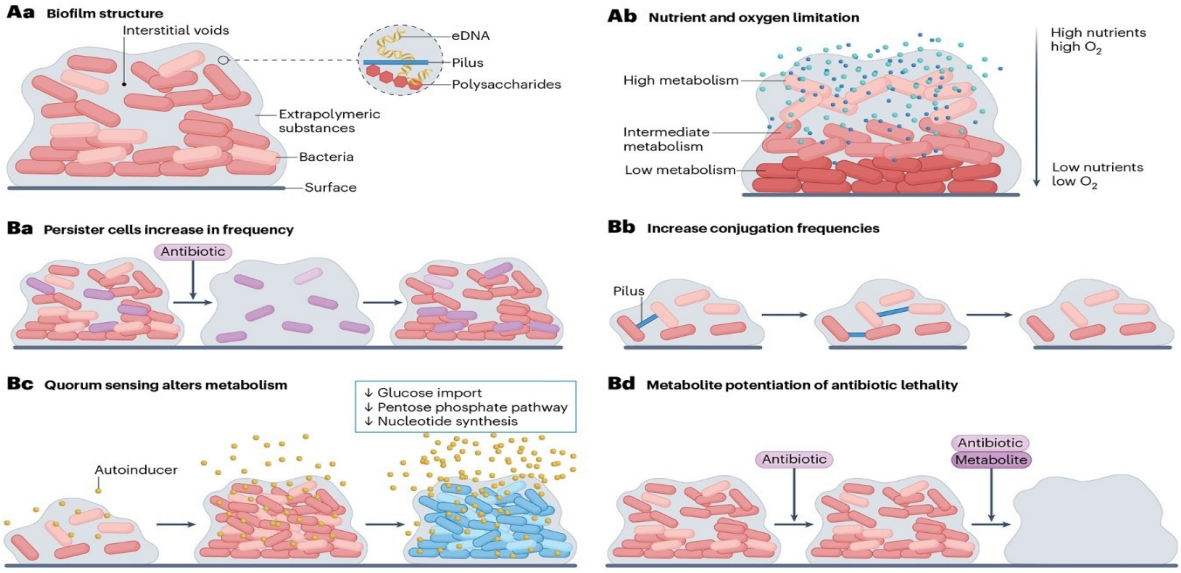

Figure 1.3. Unique properties of biofilm confer antibiotic tolerance via altered metabolism**.** Biofilm bacterial communities creating stratified layers with high and low metabolism in surface and deep layer respectively (Aa-Ab). Antibiotic exposure enriches dormant persister cells and promotes conjugation, accelerating the spread of resistance genes within the biofilm (Ba-Bb). Quorum sensing is intensified, rewiring metabolism (for example, reducing glucose uptake and pentose phosphate pathway and nucleotide synthesis), which further increases tolerance (Bc). Conversely, certain metabolites can restore or enhance antibiotic killing of biofilm bacteria (Bd) [52].

1.4 Case Studies of High-Impact Clinical Pathogens

High-impact clinical pathogens are bacterial species that combine a high burden of disease with resistance to multiple antibiotic classes, leading to severe, often difficult-to-treat infections and substantial clinical and economic costs. Representative examples include MDR *A. baumannii*, MDR *E. coli*, and MDR *S. agalactiae,* which are predominantly associated with human infections. According to the WHO, carbapenem-resistant *A. baumannii* and third-generation *E. coli* are classified in the Critical Priority tier of the top BPPL, while *S. agalactiae* is currently highlighted as a major cause of neonatal mortality, emphasizing the maternal vaccine are urgently needed (www.who.int). Altogether, these organisms represent major clinical syndromes, including: nosocomial pneumonia and sepsis, community and hospital urinary tract infections, and invasive neonatal and maternal disease, and illustrate distinct transmission routes, virulence strategies, and resistance mechanisms. The following sections outline how genomic plasticity, virulence factors, and persistence phenotypes converge to sustain antibiotic resistance in these pathogens.

1.4.1 *Acinetobacter baumannii*

1.4.1.1 Etiology and epidemiology

A. baumannii is a Gram-negative, strictly aerobic, non-fastidious, pleomorphic coccobacillus bacterium (Figure 1.4). Biochemically, it is catalase-positive, oxidase-negative, coagulase-negative, able to grow at high temperatures up to 42^0C, and not-lactose-fermenter, producing colourless colonies on MacConkey agar [57]. This opportunistic pathogen is predominantly isolated from the respiratory tract, accounting for approximately 50.2% to 100% of all *A. baumannii* infection [58]. Beyond respiratory infections, *A. baumannii* infections are also associated with soft tissue and musculoskeletal sites (22.7%), urinary tract (17.1%), and bloodstream (10.4%) [59]. Regarding its persistence in abiotic environment, these bugs can be recovered from up to 91% of inanimate surfaces in ICU settings, including bedcovers, ventilators, doorknobs, patient clothes, bedrails, pillows, and surgical tools [60]. Furthermore, its presence in air conditioning systems and air samples suggest that airborne transmission may play role in its dissemination, particularly in enclosed clinical settings [61,62]. *A. baumannii* has also been detected in human body lice, which can remain colonize throughout their lifespan and excrete viable bacteria in their feces, therefore suggesting that these arthropods may contribute to skin colonization and could serve as potential vectors under poor hygiene condition [63,64].

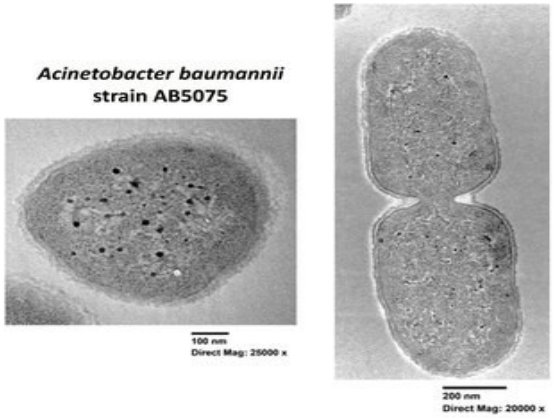

Figure 1.4. Transmission electron microscopy (TEM) micrographs of *A. baumannii* AB5075 (https://acinetobacterbaumannii.no/).

Among nosocomial pneumonia due to *A. baumannii* infection, mortality rates reach up to 70% for those caused by XDR strains [3]. Bacteremia often results from hematogenous spread of pneumonia or from the presence of an infected central venous catheter, contributing to mortality rate up to 39.5% within 30-90 days after infection. In addition, septic shock resulting from bacteremia associated with a mortality rate of 61.2% within 14 days [65]. Although UTIs caused by *A. baumannii* are associated with lower mortality rates, their incidence can be as high as 62.5% [59]. Infections of the central nervous system, wounds, and bones are less common but significantly complicate treatment

efforts [66]. The pathogen has also been reported to cause eye infections, endocarditis, nosocomial sinusitis, and peritonitis [67]. These infections mainly affect vulnerable ICU population, including critically ill children, neonates and premature infants, the elderly, patients with comorbidities, immunocompromised patients, nursing home residents, and patients with hematological malignancies [57,68,69]. Moreover, although community-acquired *A. baumannii* infections are less common, their occurrence suggests that the pathogen likely spreading beyond hospital setting. This implies that transmission is not only link to prior hospitalization but also involves environmental and animal reservoirs [67]. Particularly, carbapenem-resistant *A. baumannii* (CRAB) strains recovered from urban wastewater, livestock production systems, wildlife, and the food chain often belong to high-risk clones; these strains share resistance genes and sequences type with clinical isolates, further indicating interconnected environmental, animal, and human transmission routes [70–72].

Initially underestimated, *A. baumannii* began drawing global attention in the late 1970s when it started exhibiting MDR phenotypes. Nowadays, it is officially recognized as a critical priority pathogen on WHO's BPPL since 2017 [17]. CRAB is estimated for approximately one million infections annually worldwide, with an average mortality rate of around 35% (https://gardp.org/). In 2021 alone, CRAB strains were responsible for 100,000 deaths associated with nosocomial infections [6]. While colistin and cofiderocol are recommended for CRAB treatment, emerging reports of hetero-resistant phenotype among clinical strains further complicate the treatment [73,74].

1.4.1.2 Phylogeny and clonal lineages

A. baumannii clones circulating in healthcare settings is classified into high-risk international clones (IC) that dominate hospital-associated infections worldwide. These lineages are usually defined by multi-locus sequence typing (MLST), for which two schemes (Pasteur and Oxford) have been developed based on seven housekeeping genes. Within this framework, IC correspond to clonal complexes in the Pasteur scheme, which assigns IC1-IC9 (and more recently three novel IC) to specific clonal complexes and is therefore widely preferred for broad epidemiological surveillance, whereas the Oxford scheme offers higher resolution for local outbreak investigation but is more strongly affected by recombination in loci such as the capsule region [75,76]. As of mid-May 2026, the *A. baumannii* MLST database contains 1,080,715 unique sequences (www.pubmlst.org/abaumannii).

Among these lineages, IC1, IC2, and IC3 were first globally recognized high-risk clones and have played a central role in the spread of carbapenem-resistant *A. baumannii* across Europe, Asia, and the Americas. IC1 has undergone extensive recombination over several decades, particularly in genes encoding surface polysaccharides and outer membrane proteins, while sequentially acquiring diverse resistance determinants through plasmids and transposons [77]. IC2 has emerged as the most prevalent carbapenem-resistant clone worldwide, combining genomic flexibility with conserved resistance islands carrying

carbapenems resistant genes (most notably *bla*$_{OXA-23}$ on Tn2006/Tn2007) and overexpression of multidrug efflux systems, which underpin its remarkable success and environmental resilience [78,79]. Conversely, IC3, once an important clone, is now less frequently reported and is often associated with non-human sources, although carbapenem-resistant IC3 strains continue to be detected in some regions [80,81].

Other IC show more restricted but still clinically relevant distributions. IC4 and IC5 predominate in South America and are sometimes referred to as Pan-American clones, yet both ICs are also detected in Europe. Both lineages share core carbapenem resistance traits but differ in accessory resistance gene content and integron associations [82,83]. IC6–IC9 comprise additional emerging or regionally enriched lineages reported from Europe, Asia, and South America, with several examples of rapid acquisition of carbapenem and, in some instances, colistin resistance, as well as occasional overlap between human and animal reservoirs [84,85]. Recently, three novel IC have emerged (IC10-IC12): IC10 shows limited transmission in Middle East [86], IC11 has caused outbreaks in Danish hospitals [87], whereas IC12 was found across the continent but predominantly in the Middle East [88]. Collectively, these ICs illustrate how clonal diversification, horizontal gene transfer, and recombination continually remodel the global population structure of *A. baumannii* strains.

1.4.1.3 Genomic plasticity and mobile elements

A. baumannii is notable for its remarkable genomic plasticity, reflected in an open pan-genome and a relatively small core genome of around 2,500 genes, which comprises only about one-fifth of its total gene content. Its genome size typically ranges from approximately 3.4 to 4.2 Mb, with some clinical isolates carrying even larger genomes, and features a G+C content around 39%, which appears permissive for the acquisition of exogenous DNA [89,90]. Large comparative analyses of hundreds of genomes have identified 185 unique antibiotic resistance genes and 139 virulence genes distributed between core and accessory gene pools. Moreover, the identification of over 25,000 insertion sequence elements, 3,000 prophage regions, and 3,709 of integron-mediated resistance determinants, underscores the rapid evolutionary turnover of its accessory genome [90].

A central feature of this plasticity is the presence of genomic resistance islands that integrate at specific sites, often flanked by short direct repeats and exhibiting distinct G+C content compared to the surrounding chromosome. In IC-1, AbaR-type islands can span tens to over one hundred kilobases and carry multiple antibiotic as well as heavy-metal resistance genes [91]. By contrast, in IC-2, AbGRI1–3 typically encode combined resistance to aminoglycosides, beta-lactams, tetracyclines, sulfonamides, and chloramphenicol. These islands differ in size, structure, and gene cargo, but collectively provide modular platforms for the stepwise accumulation of resistance traits across lineages [92,93].

The architecture and mobility of these islands are driven by embedded mobile genetic elements such as transposons, insertion sequences, and integrons, which mediate the capture, rearrangement, and expression of resistance genes. *bla*$_{OXA-23}$ are frequently carried on Tn2006-like transposons inserted into larger resistance island backbones, while insertion sequences such as ISAba1 can provide strong promoters that enhance expression and promote local genomic rearrangements [93]. Class 1 integrons within the resistance islands further expand the resistome by recruiting gene cassettes encoding additional determinants such as *aadA1* and *aacA4* [78].

Plasmids add an important additional layer to the mobilome of *A. baumannii* by acting as vehicles that disseminate resistance determinants. Clinically important plasmid families frequently carry carbapenemase genes embedded in composite transposons [94,95]. Depending on their size and backbone, *A. baumannii* plasmids may encode resistance to one or several antibiotic classes: small plasmids such as pRAY (~6 kb) typically carry single aminoglycoside resistance genes (for example, *aadB* conferring gentamicin and tobramycin resistance), whereas larger plasmids including pD46-4 or pAB3 often harbor a broader repertoire, including genes such as *oxa23*, *strAB*, *sul2, and tetA(B)* [96,97]. Conjugative plasmids equipped with transfer functions can not only spread tetracycline and other resistance determinants but also modulate bacterial physiology, including type VI secretion, metabolic pathways, and virulence-associated phenotypes [98].

1.4.1.4 Mechanisms of persistence and infection

A. baumannii employs multiple strategies to persist in diverse environments, including resistance to desiccation, disinfectants, osmotic changes, and oxidative stress. Its long-term environmental survival is strongly supported by capsular polysaccharide biosynthesis and biofilm formation, which allow cells to remain viable on dry surfaces for months, with the K locus–encoded capsule and outer membrane lipo-oligosaccharide (LOS) contributing to water retention and membrane stability. Biofilm development (Figure 1.5), initiated by surface adherence and reinforced by cell–cell aggregation within an exopolysaccharide matrix, provides additional protection against drying and chemical exposure [99,100]. In addition, resistance under stress is further enhanced by RecA-mediated repair of DNA damage, overexpression of catalases (for example, *katG* and *katE* often driven by ISAba1-linked promoters) to detoxify ROS, uptake of compatible solutes such as glycine betaine and glutamate for osmoprotection, and activity of multiple efflux systems (RND pumps like AdeABC and AbeD, MFS transporters such as EmrAB and AmvA, and others including AbuO and AceI) that extrude disinfectants and toxic compounds [100].

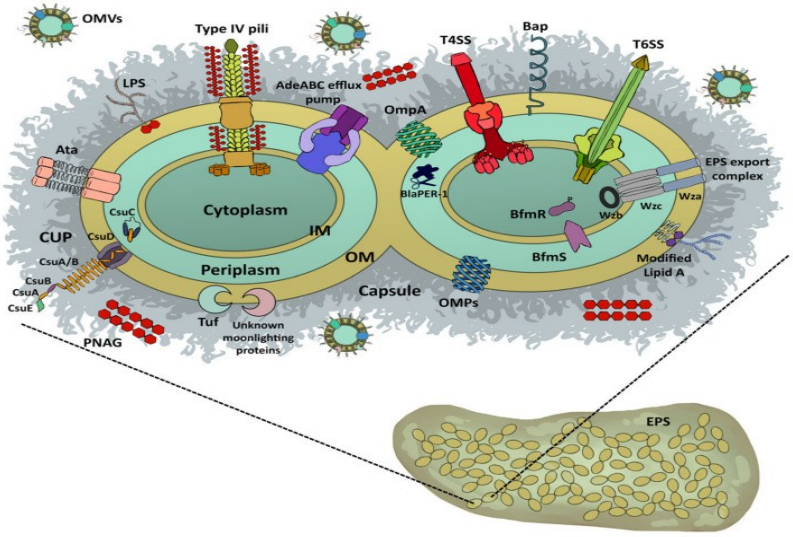

Figure 1.5. *A. baumannii* forming a biofilm with the bacterial cells embedded in the extracellular polymeric substance. The surface protein involved including AdeABC, RND efflux pump; Ata, autotransporter; Bap, biofilm-associated protein; BfmRS, two-component system; BlaPER-1, extended-spectrum β-lactamase; CUP, chaperone-usher pili; EPS, extracellular polymeric substance; IM, inner membrane; LPS, lipopolysaccharide; OM, outer membrane; OMPs, outer membrane proteins; OMVs, outer membrane vesicles; PNAG, poly-β-(1-6)-N-acetylglucosamine; T4SS, type IV secretion system; T6SS, type VI secretion system; Tuf, moonlighting protein; Wza-Wzb-Wzc system [99].

Adhesion to abiotic surfaces and host cells is a critical first step in infection. Csu pili are central to the colonization of plastic and other medical device materials, anchoring early biofilm formation on catheters and endotracheal tubes. Omps are similarly crucial, with OmpA acts as a major adhesin that promotes attachment to epithelial cells, contributes to biofilm formation, and shapes host–pathogen interactions, by mediating bacterial adhesion and invasion and modulating host cellular responses [101,102]. Beyond OmpA, other OmpA-like proteins such as PsaB, and ArfA, YiaD further support cell envelope integrity and contribute to antibiotic resistance [100,103]. Type IV pili, known for mediating twitching motility, also facilitate binding to pharyngeal and lung carcinoma cell lines, thereby supporting colonization of the respiratory tract. In addition, *A. baumannii* exploits host extracellular matrix components and receptors through autotransporter adhesins: the trimeric autotransporter Ata (T5cSS) binds multiple collagens and laminin, while FhaB (T5bSS) interacts with integrins and fibronectin via RGD-containing motifs. These interactions with collagen, elastin, fibrillin, laminin, and fibronectin, together with engagement of CEACAM-1/-5/-6 and ChoP-dependent binding to platelet-activating factor receptors on lung epithelial cells, enable tight contact with mucosal surfaces and create a platform for subsequent invasion [100,104].

Once attached, *A. baumannii* can invade respiratory epithelial cells and persist intracellularly. The bacterium is internalized through a zipper-like process and resides within membrane-bound vacuoles in bronchial and alveolar cells. Major porins such as

OmpA and Omp33 contribute to this phenotype by inducing apoptosis and subverting host autophagy. In particular, OmpA blocks autophagosome–lysosome fusion, allowing bacteria to survive in immature autophagosomes and enhancing inflammatory cytokine release. In parallel, *A. baumannii* exploits several host receptors to promote adhesion and internalization: ChoP-decorated OmpA/OprD engages the platelet-activating factor receptor (PAFR), triggering a G-protein–coupled endocytic cascade, and CEACAM-1/-5/-6 further mediate bacterial uptake and LC3-associated phagocytosis in pneumocytes. Pattern-recognition receptors such as TLR2 and TLR4 on type II pneumocytes sense bacterial lipoproteins and LOS and activate major mitogen-activated protein kinases (MAPKs) p38 and Erk1/2, as well as the nuclear factor NF-κB, leading to IL8 mediated neutrophil recruitment. Infection also activates factor EB and remodels the autophagosome–lysosome pathway, including reduced lysosomal acidification, thereby facilitating intracellular trafficking, inflammatory responses, and long-term persistence in lung cells (Figure 1.6). Together with receptor-driven apoptosis of bronchial epithelial cells, these processes suggest that both intracellular survival and programmed cell death are exploited by *A. baumannii* to disseminate to deeper tissues and promote invasive disease [100].

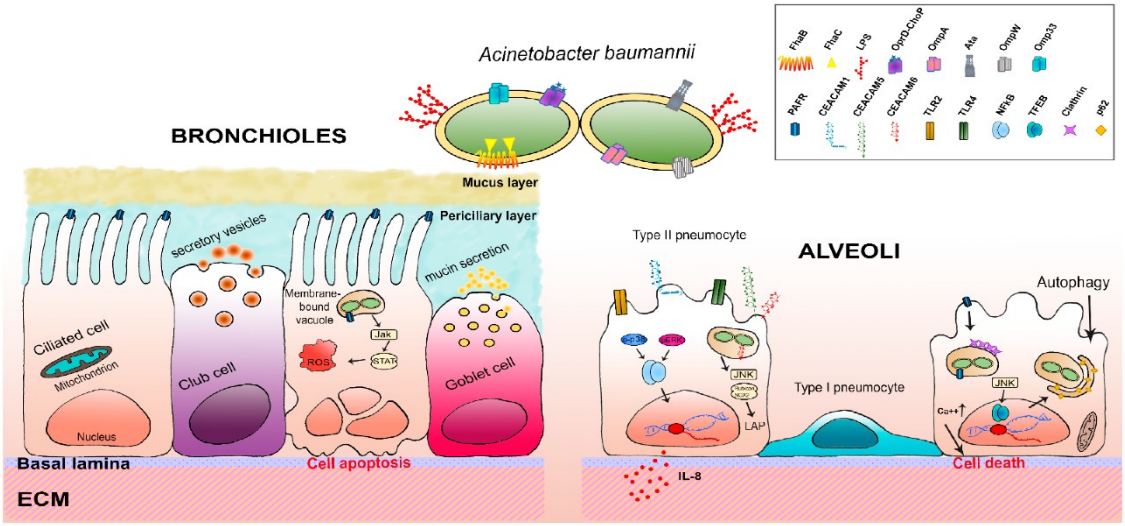

Figure 1.6. Schematic representation of the interrelations between *A. baumannii* and the respiratory epithelium [100].

1.4.2 Uropathogenic *E. coli*

1.4.2.1 Etiology and epidemiology

Uropathogenic *E. coli*, a member of extraintestinal pathogenic *E. coli*, is a Gram-negative, facultative anaerobic, and motile rod (Figure 1.7). In the CHROMAgar, the bacteria form smooth and convex colonies with light moist or dry appearance and dark pink to reddish color. Biochemically, UPEC is catalase-positive and oxidase-negative, ferments lactose, producing acid and gas. These strains causes of urinary tract infections (UTI), accounting for up to 90% on community-acquired uncomplicated cases and 65% of complicated UTIs

[105,106]. UPEC also frequently causes bacteremia in children, with possible maternal transmission leading to neonatal blood and cerebrospinal infection [107,108]. Its success in both community and hospital settings has driven the global spread of multidrug-resistant lineages, including ESBL strains which are resistant to third-generation cephalosporins, representing second line antibiotics [109].

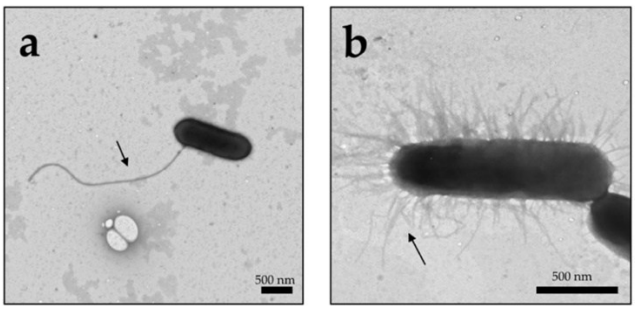

Figure 1.7. UPEC strain CFT073 with surface appendages appearance.
The arrow show (a) flagellum and (b) type 1 fimbriae [110].

UPEC typically originate from the intestinal reservoir, where it may behave as harmless commensals, and under favorable conditions colonize the periurethral area and introitus. The capability to tightly adhere to bladder cells represents the hallmark of UPEC pathogenesis. It mainly causes cystitis; however, it can also migrate into the upper urinary tract, promote pyelonephritis, and even enter the bloodstream, resulting in urosepsis [105,106]. Women are at high risk due to the short urethra and proximity of the urethral opening to the anus. In addition, women with UTI history were likely to experience recurrent UTI within months from the initial infections caused by the same strains, which highlighted the persistence of bacteria [2,111].

To colonize and persist in the urinary tract, UPEC must adapt to hostile conditions, including fluctuating pH, high osmolality, low oxygen, and the denaturing effects of urea [112,113]. UPEC respond by modulating central metabolism, osmoprotection pathways, and stress responses, and by producing proteases and toxins that damage uroepithelial cells, release nutrients, and promote dissemination. UPEC also readily form biofilms on the bladder mucosa and indwelling devices such as catheters, which further protect them from host immunity and antimicrobial agents and contribute to chronic and recurrent infection [105,113,114].

1.4.2.2 Phylogenetic and serotyping classification

E. coli populations are structured into several phylogroups (A, B1, B2, C, D, E, F and the cryptic clade I), defined by specific combinations of housekeeping genes [115]. Commensal strains are typically grouped within phylogroups A and B1, whereas extraintestinal pathogenic *E. coli*, including most UPEC, populate phylogroups B2 and D. UPEC from these phylogroups tend to harbor a higher burden of virulence factors and

are frequently associated with multidrug-resistant phenotypes, including resistance to extended-spectrum cephalosporins and fluoroquinolones [109,116].

Serotyping based on O (lipopolysaccharide) and H (flagellar) antigens further refines epidemiological classification. Certain serotypes, such as O1, O2, O4, O6, O7, O8, O15, O16, O18, O21, O22, O25, O75, and O83, are frequently associated with UPEC isolates [117]. Among these, the O25:H4 serotype is strongly associated with phylogroup B2, belong to the pandemic ST131 clone, which combines high virulence potential with resistance to third-generation cephalosporins and fluoroquinolone [109,118]. Other serotypes, including O15:H31 and O16:H5, are also associated with MDR and particular virulence factors [109,119].

Integration of phylogenetic grouping, serotyping, and MLST has enabled the identification of globally disseminated UPEC such as ST69, ST73, ST95, and most particularly ST131 [119]. ST131-O25b:H4 clone has attracted special attention because of its diverse virulence potential, for long-term intestinal colonization, its association with ESBL production and fluoroquinolone resistance, and its prominent role in both community- and hospital-acquired UTIs [120,121]. Together, these molecular typing approaches reveal that UPEC pathogenesis and resistance are concentrated in defined clonal lineages that have adapted efficiently to the urinary tract niche.

1.4.2.3 Genomics feature and mobile genetic elements

Genomic analysis of UPEC revealed a distinct, diverse, and adaptable genome that distinguishes UPEC from other *E. coli* pathotypes. Based on whole-genome data, UPEC strains diverged from commensal *E. coli* over 32 million generations, suggesting that uropathogenicity is ancient and maintained its survival trait [122]. UPEC has a large pan-genome; approximately 5,500 genes, 50-54% are conserved genes shared with commensal *E. coli* and the remainder constituting an accessory genome enriched in genomic islands, prophages, transposons, integrons, and plasmids [123]. Many of these accessory regions are organized as pathogenicity islands (PAIs), which often integrate at tRNA loci, display atypical G+C content, and have mosaic structures containing numerous mobile element fragments. PAIs are strongly enriched in UPEC compared with commensal strains and encode a wide array of virulence determinants, including adhesins, toxins, iron-acquisition systems, and immune-evasion factors [114,122].

The highly prevalence of PAIs among UPEC strains is a hallmark distinguishing this pathogen; specifically, >95% of PAIs were found in UPEC strains compare to commensal strains [124]. Among the PAIs already identified, some contain genes encoding adhesins and toxins (PAI I_{J96}), are associated with iron acquisition and immune evasion (PAI II_{CFT073}), are linked to increased bacterial survival in the urinary tract (PAI IV_{536}), or carry genes that enhance colonization and persistence (PAI V_{536}), while (PAI_{usp}) harbors the gene encoding the uropathogenic-specific protein Usp. Among clinical isolates, strains encoding PAI II_{CT073} were associated with pyelonephritis, prostatitis, and sepsis

[125,126]. The deletion of PAIs in reference strains caused virulence reduction in animal models, which showed their significant impact in UPEC pathogenesis [127].

Plasmids and other mobile genetic elements further shape the UPEC genome. Large conjugative plasmids (50 to over 200 kb), especially those of the IncF and IncI/B families, frequently carry ESBL genes, additional antibiotic resistance determinants, and virulence-associated genes such as bacteriocins, siderophore systems, or complement resistance [128]. Interestingly, some of UPEC plasmids exhibit high transferability within biofilms, a process influenced by biofilm biomass or on oxygen availability [129,130]. Deep genomic analyses of strains carrying two plasmids have revealed recombination events mediated by IS elements such as IS3 and IS21, TN21-family transposons, and resistance islands that occur not only between plasmids but also between plasmids and the chromosome, driving genomic rearrangements and mobilizing resistance and virulence genes among UPEC strains [131]. Finally, class 1 integrons, Tn-3 like transposons, and insertion sequences promote capture and expression of various virulence and resistance genes, thereby accelerating the genetic diversification of UPEC [131,132].

1.4.2.4 Mechanisms of infection and urinary tract colonization

In the bladder, UPEC utilizes type 1 fimbriae (T1F), primarily through the FimH adhesin to initiate infections. FimH binds to mannosylated uroplakins and α3β1 integrins on umbrella cells, activating Rho-family GTPases, driving actin rearrangement, and promoting bacterial internalization by a zipper-like process. Once inside, UPEC evade host defences and antibiotics by forming intracellular bacterial communities (IBCs). Host sensing of lipopolysaccharide via TLR4 activates an AC3-dependent cyclic AMP signalling cascade that induces exocytosis of superficial cells, allowing the pathogen to re-enter the urothelial surface, seed new IBCs, or establish quiescent intracellular reservoirs (QIRs), small non-replicating population within deeper transitional cells. The pore-forming toxin α-haemolysin (HlyA) lyses host cells, promotes epithelial exfoliation, and favors the release of iron. Pathogen then uses multiple sidesphore system to scavenge this extracellular iron, supporting survival and deeper colonization of uroepithelial layers. Cytotoxic necrotizing factor 1 (CNF1) binds to basal cell adhesion molecule (BCAM) receptor and constitutively activates Rho GTPases, causing actin remodelling, membrane ruffling, and activation of anti-apoptotic pathways that prolong survival of infected epithelial cells (Figure 1.8) [105].

Kidney's colonization is mediated by the P fimbriae, via the PapG adhesin, to globoside-containing receptors highly expressed in the upper urinary tract. PapG modulates the local secretory-antibody immune response by interacting with TLR4 signalling to downregulate the expression of polymeric immunoglobulin receptor, impairing IgA transport, and weakening mucosal defences. These additional virulence factors enable UPEC to penetrate the tubular epithelial barrier of the kidney, enter the bloodstream, and cause urosepsis. In catheter-associated urinary tract infections (CAUTIs), UPEC follows a similar overall pathogenic sequence but initially exploits

catheter-induced inflammation. Inflammation-driven leakage leads to fibrinogen accumulation on the catheter surface. The pathogen then uses specific fibrinogen-binding adhesins to attach densely to this protein layer, form and proliferate as a biofilm on the catheter, and resist neutrophil clearance. Once established, UPEC can ascend to the kidneys via the mechanisms described above, leading to serious complications (Figure 1.8) [105].

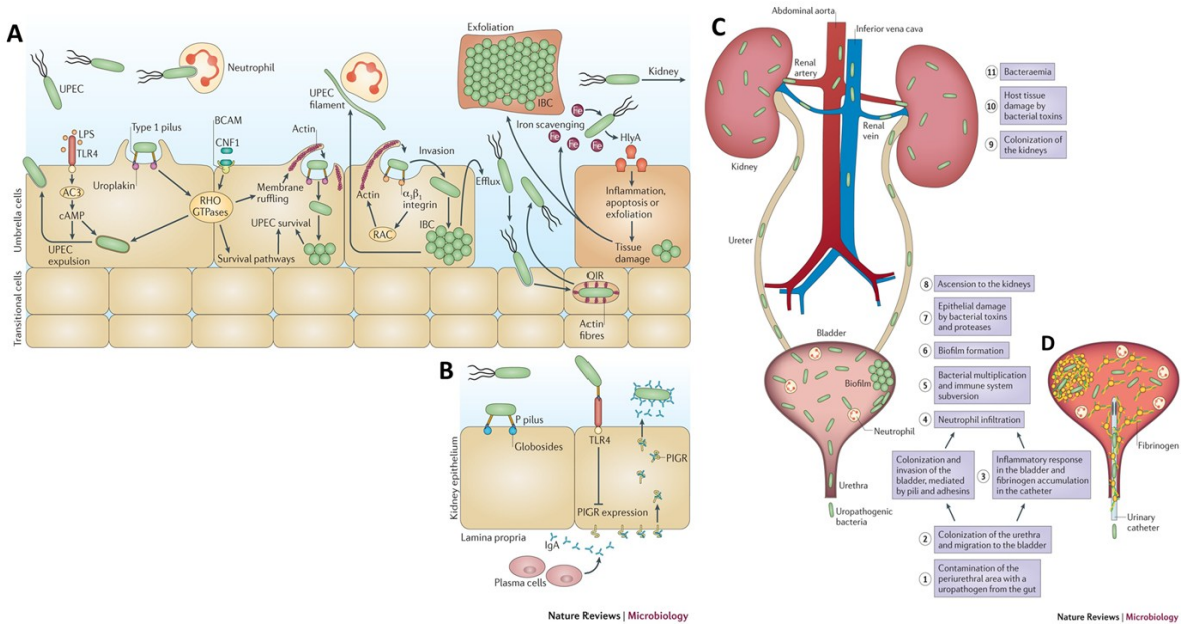

Figure 1.8. Pathogenesis and ascending infection of UPEC. Schematic representation of UPEC infection showing bladder colonization and intracellular lifestyles (A), pili-mediated adherence in the kidney and modulation of local immune responses (B), overview of ascending infection from bladder to kidney (C), and catheter-associated UPEC (D) [105].

Beyond T1F and P fimbriae, UPEC adherence to host cells is also mediate by other adhesin factors, such as S. fimbriae, F1C fimbriae, Afa/Dr fimbriae, afimbrial adhesins, and curli fibers (Figure 1.9). S fimbriae have specificity for alpha-sialyl-2,3-alpha-galactose residues present on the glycoproteins of urothelial tissues in the bladder and kidneys [133]. The Afa/Dr adhesins activate signal transduction pathways that induce structural and functional injuries at brush border and junctional domains, trigger proinflammatory responses, and engage β_1 integrin to facilitate entry in the host by a zipper-like, raft- and microtubule-dependent mechanism [134]. Non-fimbrial adhesins such as type one secretion A (TosA) can bind to human kidney and epithelial cells in the upper urinary tract [135]. Curli fibers, functional amyloid fimbriae widely distributed among UPEC strains, promote adhesion to bladder epithelial cells and biofilm formation and enhance urinary tract colonization and persistence, acting as an important fitness and virulence factor [136,137]. Together, these adhesin factors, iron-uptake strategies, toxins, and intracellular lifestyles, providing a multilayered framework that supports long-term survival, treatment failure, and relapse [106], [126].

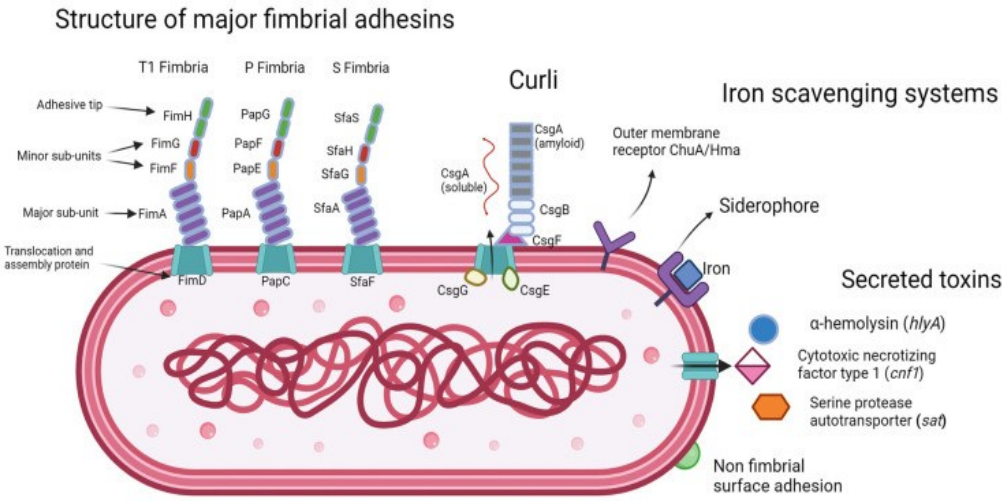

Figure 1.9. Schematic Representation of UPEC major fimbrial adhesion and iron-acquisition systems [114].

1.4.3 *Streptococcus agalactiae*

1.4.3.1 Etiology and epidemiology

Streptococcus agalactiae, known as group B Streptococcus (GBS), is Gram-positive bacterium. GBS is a β-hemolytic coccus that grows in chains (Figure 1.10), catalase-negative, facultative anaerobic, non-sporing, and ferments carbohydrates to lactic acid [138]. The pathogen colonizes primarily mucosal surfaces of the gastrointestinal and genitourinary tracts [139]. Like UPEC, GBS can behave as a commensal in healthy adults yet transition to an opportunistic pathogen when host or ecological conditions favor invasion, highlighting a shared theme of colonization-to-disease progression.

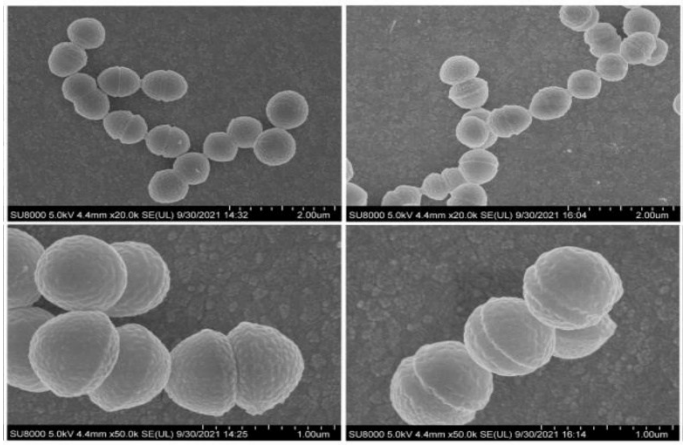

Figure 1.10. Microstructural visualization of *S. agalactiae* [140]

S. agalactiae has been first recognized in 1887 as an important veterinary pathogen, classically associated with bovine mastitis and major milk-production losses in dairy herds [141]. It was classified into Lancefield group B in 1933, and first described as a cause of human disease in 1938; however, the clinical significance of invasive neonatal and maternal infections was not fully recognized until the 1960s, coinciding with the advent of improved microbiological methods and clinical surveillance [142,143]. The pathogen was later detected in fish hatcheries in 1966 and has since been implicated in outbreaks affecting diverse aquaculture species in both farmed and natural environments, as well as in foodborne infection with severe blood poisoning [144–146]. These historical observations establish GBS as a versatile species capable of crossing host-species barriers and causing disease in both animals and humans.

S. agalactiae causes a wide spectrum of invasive infections, including bacteremia, skin/soft tissue infection, osteomyelitis/septic arthritis, endocarditis, pneumonia, and UTI, across all age group [147]. In recent years, invasive disease has increasingly been reported among older adults, particularly elderly women [148,149]. The highest incidence and most severe outcomes, however, occur in neonates and in pregnant and postpartum women. Maternal rectovaginal colonization is common; around 20% pregnant women worldwide have been colonized by GBS, creating a substantial reservoir for vertical transmission [150,151]. Even relatively low maternal carriage densities have been associated with vertical transmission to newborns, transmission rates among colonized mothers estimated at approximately 41-72% [152]. Vertical transmission is therefore the primary cause of early-onset disease, typically presenting as sepsis and pneumonia in the first week of life, leaving survivors at risk of long-term neurodevelopmental impairment [153]. Late-onset GBS disease, often presents as meningitis, can result from mucosal colonization at birth followed by postnatal overgrowth or from exposure to colonized caregivers, breast milk, and other sources [154]. Mothers may also develop postpartum infections such as endometritis, and rarely, severe sepsis [155]. Due to this combined burden on mothers and infants, perinatal GBS disease has become a major target for prevention; this has led to global implementation of intrapartum antibiotic prophylaxis (IAP) [156,157]. However, the widespread application of IAP has reshaped the epidemiology and resistance profile of *S. agalactiae*-human isolated. While the microorganism remains uniformly susceptible to penicillin, increasing resistance to macrolides, lincosamides, and tetracyclines has been documented, and multidrug-resistant (MDR) lineages have emerged in several regions [4,158]. High-level gentamicin resistance, mediated by acquired aminoglycoside-modifying enzymes, has also been reported, compromising synergistic therapy options and raising concern for the management of severe invasive infections [159,160]. These trends, together with persistent global burdens of neonatal sepsis, meningitis, and maternal disease, underscore the evolving threat posed by resistant GBS and the urgent need to develop maternal GBS vaccination as a complementary strategy to reduce stillbirths and neonatal morbidity and mortality [156,157].

1.4.3.2 Population structure and serotypes

The population structure of *S. agalactiae* is organized into clonal complexes (CCs) defined by MLST, which correlate strongly with capsular serotypes and host or disease niches. Ten main capsular polysaccharide (CPS) serotypes (Ia, Ib, II–IX) are recognized, with Ia, Ib, II, III and V accounting for most human colonizing and invasive isolates worldwide. In many regions, serotypes Ia and III predominate among vaginal and rectal colonizing strains, and serotype III, followed by Ia, is are most frequently associated with neonatal invasive disease [161–163].

Specific correlations between CCs and serotypes show marked associations with clinical syndromes. For instance, CC17, typically comprising serotype III/ST17 strains, is classically described as a "hypervirulent" lineage strongly linked to late-onset neonatal meningitis and invasive disease in infants, although it also causes infections in adults [164,165]. CC23 (often serotype Ia), CC19 (serotypes II/III), CC1 (serotype V/II), and CC10/CC12 (various serotypes) are major lineages involved in maternal colonization and neonates disease, as well as infections in non-pregnant adults [166]. Capsular switching events, such as the emergence of CC17 strains expressing serotype IV, illustrate ongoing recombination at the *cps* locus and have implications for serotype-based vaccine coverage [167].

Comparative genomic studies also found that some human lineages may share ancestry with animal-associated strains and have acquired a broad ecological range. For example, close relatedness between the human ST17 and bovine ST61 serotypes indicates past cross-species transmission [168]. In contrast, serotype III ST238, which was identified as an invasive lineage in non-pregnant adults, has also been found in farmed freshwater fish, pointing to bidirectional host switching between humans and fish [169–171]. In recent years, ST238 has emerged as a foodborne zoonotic clone, causing outbreaks of invasive disease in Hongkong and Singapore linked to consumption or handling of raw freshwater fish dishes [146,172]. Altogether, these lineages highlight the broad niche range and zoonotic potential of GBS.

The widely used of macrolides and lincosamides for GBS treatment raising concerns about reduced treatment options for β-lactam-allergic women. These trends are not uniform across the species but are strongly shaped by clonal background. Genomic analyses indicate that the high prevalence of tetracycline resistance in major human-infecting CCs (such as CC1, CC10, CC17, CC19, CC23, and CC26) reflects historical tetracycline use, which imposed a strong selective bottleneck and favoured global expansion of a Tc-resistant strains [141,173]. In several regions, macrolide- and clindamycin-resistant isolates are increasingly concentrated within CC1 and CC19 lineages, commonly harbouring *erm* and *mef*/*msr* genes on conjugative elements such as Tn916-like transposons [174]. The hypervirulent CC17 lineage traditionally considered fully susceptible to β-lactams, now frequently exhibits resistance to at least two antibiotic

classes in some region, underscoring the risk that continued selection from IAP may drive the emergence and spread of MDR GBS clones [175,176].

1.4.3.3 Genomic feature and virulence repertoire

The GBS genome, typically 1.53 – 2.38 Mbps in size, contains approximately 2,000 protein-encoding genes and a relatively high number of tRNA-coding sequences (≈80), ABC transporter genes (≈60), and two-component system genes [177]. The genome consists of conserved backbone of core housekeeping genes and a diverse accessory genome containing mobile genetic elements, genomic islands, and phages that encode many virulence and resistance determinants (Figure 1.11). Notably, about 20% of predicted open reading frames remain functionally uncharacterized, leaving substantial scope for the discovery of new molecular mechanisms and regulatory systems [177,178].

Capsular polysaccharide, pili, serine-rich (Srr) proteins, and multiple surfface adhesins, including fibrinogen binding proteins (FbsABC), plasminogen binding-surface protein (PbsP), the hypervirulent adhesin HvgA, streptococcal fibrinogen-binding protein A (SfbA), αC protein (ACP), and laminin-binding protein (Lmb), are central to initial attachment, mucosal colonization, and tissue invasion. Capsular polysaccharide is the basis for serotype classification and promotes vaginal colonization [179]. GBS pili involves in adhesion and biofilm formation, thereby supporting persistent colonization. PilA, the pilus tip adhesin of PI-1, binds collagen and triggers integrin-mediated signaling, enhancing adhesion to and invasion of brain microvascular endothelial cells and contributing to central nervous system tropism [180]. The high molecular-weight Srr1 and Srr2 proteins form mucin-like structures that promote aggregation and attachment to vaginal and cervical epithelial cells by binding fibrinogen, keratin, plasminogen, and plasmin; noteworthy, Srr2 is closely associated with hypervirulent ST-17 lineages [181,182]. FbsABC further support vaginal colonization and dissemination by mediating fibrinogen-dependent adhesion, facilitating bacterial transit in the bloodstream and fixation at sites of tissue injury; increased FbsA and FbsB expression correlates with stronger tissue association and invasion in animal models [183]. PbsP facilitates plasminogen-dependent invasion of brain microvasculature endothelial cells, and its expression is regulated by the SaeR/S and CovR/S systems, deletion of the *pbsP* reduces brain bacterial burden and mortality in experimental meningitis [184]. HvgA, a hallmark of ST-17 strains, is crucial for epithelial colonization and crossing of the intestinal, blood-brain, blood-cerebrospinal fluid barrier during neonates meningitis, in part via robust interactions with clathrin that facilitate transcytosis across the choroid plexus [161,185]. SfbA contributes to infection of vaginal and cervical epithelium as well as adhesion to brain microvascular endothelial cells, whereas ACP binds glycosaminoglycans to mediate attachment to cervical epithelial cells and translocation across epithelial layers [161,185]. Lmb binds laminin in the extracellular matrix, supporting close contact with host tissue [177,179].

Immune evasion is driven largely by the sialylated capsule, complement-modifying enzymes, cytolytic toxins, and global regulatory system. Terminal N-acetylneuraminic acid residues on the capsule mediate molecular mimicry of host sialylated glycans, impairing complement deposition and promoting interaction with inhibitory Siglecs on leukocytes; these interactions dampen neutrophil oxidative burst and reduce bacterial killing [177,186]. C5a peptidase (ScpB) is a surface-anchored enzyme that cleaves complement component C5a, thereby diminishing opsonophagocytic clearance [187]. Beyond their role in barrier damage, β-hemolysin/cytolysin (βH/C), CAMP factor, granadaene, and HylB contribute directly to immune evasion: βH/C neutralizes reactive oxygen species and protects GBS from phagocyte-derived oxidative stress, CAMP factor forms pores in host cell membranes and damages immune cells and erythrocytes, granadaene is strongly cytotoxic to neutrophils and is overproduced in CovR-deficient hyper-hemolytic, hyper-pigmented strains, and HylB reduces neutrophil reactive oxygen species production, limiting bacterial killing [188,189]. GBS pili can further promote inflammation-driven barrier disruption and cytokine release, increasing local permeability of the blood–brain barrier and favoring persistence. The cell surface-associated protein CspA promotes fibrin-like aggregate formation, protects against neutrophil phagocytosis, and interferes with leukocyte chemotaxis, thereby shielding bacteria from immune attack. Finally, two-component regulatory systems, including CovR/S, CiaR/H, LiaR/H, SaeR/S, and HssR/S, orchestrate context-dependent expression of these virulence traits in different host niches; HssR/S regulates transcription of the heme export machinery, whereas HrtA/B mitigates intracellular heme toxicity, and tight control of heme homeostasis is essential for survival during systemic infection, where both heme exposure and immune pressure are high [177,184].

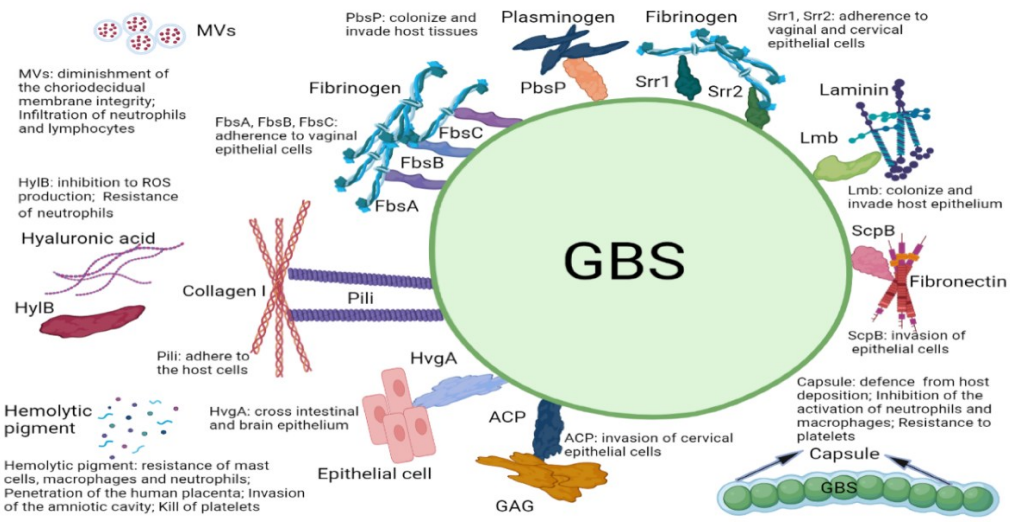

Figure 1.11. Summary of *S. agalactiae* virulence factors [179].

1.4.3.4 Mechanism of infection: vaginal colonization and fetoplacental invasion

S. agalactiae initiates infection by adhering to various epithelial surfaces, including the vaginal epithelium, placental membranes, respiratory tract epithelium, and blood-brain barrier endothelium. This adherence is maximal in the acidic pH of the vaginal tract, supporting stable colonization and vertical transmission to the newborn. A low-affinity GBS interaction with epithelial cells is mediated by its amphiphilic cell wall-associated lipoteichoic acid, whereas higher affinity interactions with host cells are mediated by a series of size-variable, pronase-sensitive, and hydrophobic GBS surface proteins that engage extracellular matrix components such as fibronectin, fibrinogen, and laminin, which in turn interact with host cell-anchored integrins [139,190].

After adhesion, GBS can invade chorionic epithelial cells and placental membranes, weakening their tensile strength through infection-induced inflammatory pathways, including increased prostaglandin E_2 production and oxidative stress, thereby predisposing to preterm membrane rupture and intra-amniotic infection [191,192]. Similar mechanisms works also at the blood–brain barrier, where GBS adheres to brain microvascular endothelial cells, is internalized, and crosses these cells by transcytosis, allowing bacteria to enter the brain and cause meningitis [139]. Transcytosis in this context denotes uptake of GBS into vesicles on the blood-facing side of endothelial cells, vesicular transport across the cytoplasm, and release on the brain side, a process that is accompanied by modulation of P-glycoprotein activity and may favor bacterial persistence within the central nervous system [193]. In addition, GBS can invade the CNS via a nose-to-brain route, initially infecting the olfactory mucosa and subsequently reaching the olfactory bulb and trigeminal nerve, where it persists in glial cells before spreading further into the brain in experimental infection models [194]. Once tissue barriers are crossed, GBS should evades innate and adaptive immune responses to persist and disseminate, a process that relies heavily on its sialylated capsule and other surface factors that limit opsonophagocytic clearance [139,177].

Upon breaching tissue barriers and replicates, GBS replication provokes a strong inflammatory response that can progress to sepsis and organ dysfunction. GBS cell wall components and secreted toxins trigger massive cytokine release (including TNF and IL-1) and the upregulation of inducible nitric oxide synthase (iNOS), driving vasodilation, hypotension, and tissue injury. In the lungs, this manifests as acute inflammatory damage to epithelial and endothelial layers, whereas in the central nervous system, barrier disruption and cytokine production lead to neutrophilic inflammation, vasculopathy, and neuronal apoptosis, hallmarks of GBS meningitis [139]. The overall mechanism is summarized in Figure 1.12.

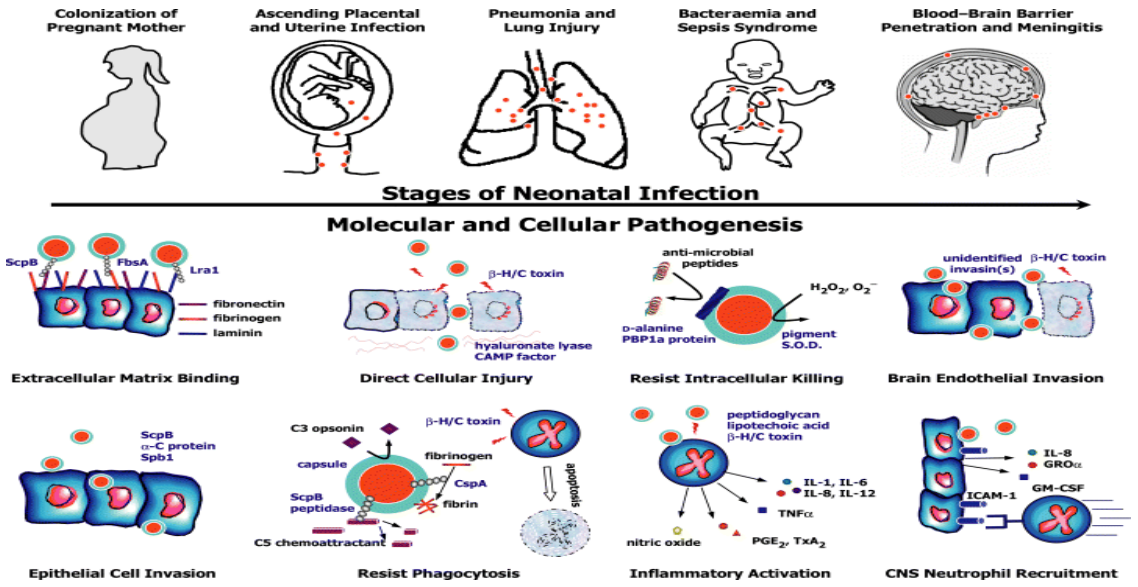

Figure 1.12. Stages in the molecular and cellular pathogenesis of neonatal group B *Streptococcal* (GBS) infection. β-H/C, beta-haemolysin/cytolysin; S.O.D., superoxide dismutase; IL, interleukin; TNFα, tumour necrosis factor-alpha; PGE_2, prostaglandin E_2; TxA2, thromboxane A_2; GROα, growth-related oncogene-alpha; ICAM-1, intercellular adhesion molecule 1; GM-CSF, granulocyte-macrophage colony-stimulating factor [139].

1.5 Novel Therapeutic Strategies Against MDR Bacteria

The global expansion of MDR and XDR pathogens has questioned the effectiveness of conventional antibiotic-based strategies. Indeed, the development of new antibiotics is a long and costly process, while high-impact clinical pathogens can acquire and disseminate resistance within relatively short time, thus challenging the introduction of novel drugs [195]. Similarly, combinate therapies can broaden antimicrobial spectra or enhance bactericidal activity, but can increased toxicity, disruption of microbiota, and selection of highly resistant strains, highlighting the need to explore complementary approaches [196,197].

To address these problems, a range of innovative strategies has been proposed to overcome or bypass classical resistance mechanisms, including antibiotic carriers and adjuvants that enhance existing drug efficacy, bacteriophages and their derived enzymes which offer targeted bacterial lysis, antimicrobial peptides with broad-spectrum activity, anti-virulence agents that disarm pathogens without directly killing them, nanotechnology-based delivery systems such as nanoparticles for targeted intervention, and microbiota or probiotic-based interventions aimed at restoring host defense [198–200] (Figure 1.13). Among these, nanoparticles and probiotics represent distinct, complementary adjunct approaches against MDR pathogens. Both differ mechanistically and conceptually from other non-antibiotic strategies, which tend to be more target-specific or pathway-focused. Nanoparticles mainly act through direct physicochemical

damage and smart drug delivery, while probiotics primarily reshape the microbial and immune environment to reduce MDR colonization and virulence [198,201].

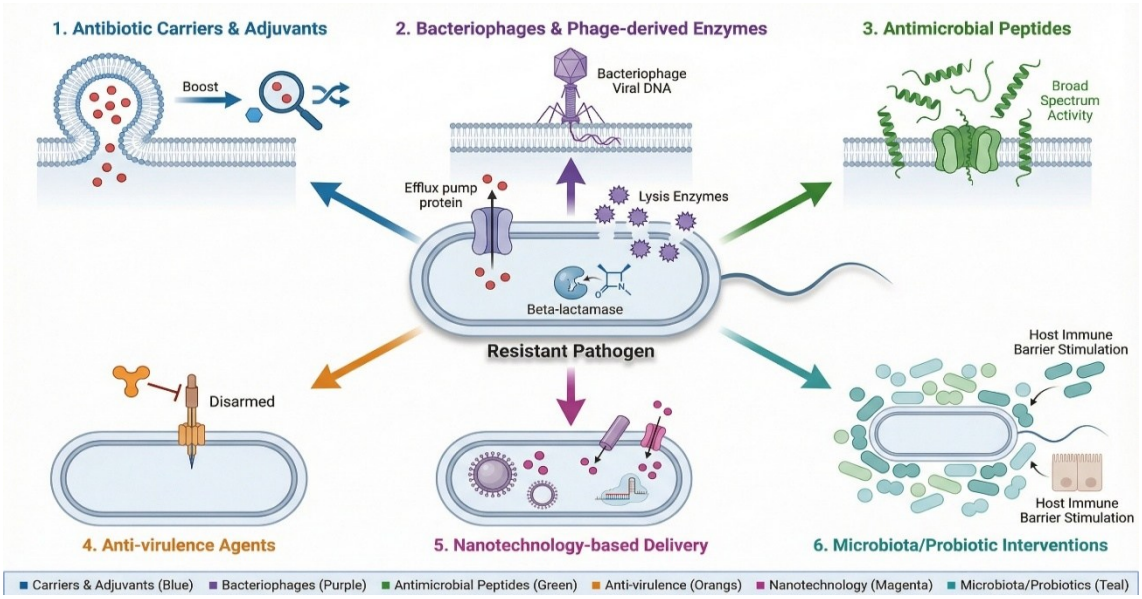

Figure 1.13. Innovative non-antibiotic strategies to combat antibiotic-resistant pathogens. The figure was created with FigureLabs.

1.5.1 Nanoparticles-based antibiotic delivery systems

Nanoparticles (NPs) designed against MDR bacteria can be classified into several categories: inorganic (e.g. metallic NPs, silica NPs, and mesoporous silica NPs), organic (e.g. polymeric, liposomes, and dendrimers), carbon-based (e.g. carbon nanotubes, Graphene NPs, and Fullerens), and hybrid structures. These materials typically sized below 100 nm, exhibit advantageous properties such as a high surface-area-to-volume ratio and tunable surface charge and coatings which can be engineered for specific functions. Antibacterial NPs can be categorized based on direct and indirect effect. The direct effect often involves NPs interacting with and disrupting cell wall integrity, leading to the leakage of cellular contents. Subsequent entry to bacterial cell trigger ROS formation, which cause oxidative damage to proteins, lipids, and DNA, as well as inhibition of enzymes, imbalance in electrolyte levels, and change in gene expression. As an indirect functions, NPs act as carriers enhancing local antibiotic concentration, thus overcoming efflux and permeability barriers. Within biofilms, NPs can penetrate the extracellular polymeric substance (EPS), disrupt matrix structure, and killing biofilm-resident cells, which are highly tolerant to conventional antibiotics [198,199,202]. The overall mechanisms of nanoparticles action are summarized in Figure 1.14.

Within this framework, inorganic nanomaterials are often further divided into metallic and non-metallic systems, which show distinct antibacterial strategies rooted in their physicochemical structures [198,199,202]. Metallic NPs (such as Ag, Au, Cu, and ZnO) possess intrinsic bactericidal properties driven by multiple aggressive mechanisms,

including the release of metal ions, physical damage to the cell wall, and the generation of ROS which induces oxidative stress [203,204]. For instance, silver NPs (AgNPs) and copper NPs exhibit broad-spectrum efficacy by compromising cell integrity and triggering immunostimulatory effects [204]. Specifically, AgNPs have proven their efficacy against *A. baumannii* clinical strains by downregulating the expression of *oprD* and *carO*, two genes contributing to carbapenem resistance [205]. Similarly, Zinc Oxide (ZnO) NPs are highly effective against antibiotic-resistant bacteria, utilizing ROS generation and physical disruption of the membrane to prevent bacterial proliferation [206].

In contrast, non-metallic and organic NPs (such as polymeric NPs, liposomes, and biocompatible carbon-based carriers) often function by encapsulating and delivering antimicrobial agents, or by mimicking biological structures to interfere with bacterial metabolism and enhance drug bioavailability. Rather than relying solely on oxidative toxicity, these carriers overcome issues like hydrophobicity and instability associated with traditional antibiotics or natural compounds like curcumin [207]. For example, liposome NPs can disrupt the biofilm formation of Methicillin-resistant *Staphylococcus aureus* (MRSA) and *Pseudomonas aeruginosa* [208]. Furthermore, biopolymers like chitosan exhibit dual actions: serve as biocompatible coatings that release therapeutic agents and inherently disrupt biofilm formation through surface charge interactions, thereby reducing bacterial adherence, such as UPEC binding to bladder cells [209,210]. In addition, biopolymer aerogels and nanocellulose emphasize biocompatibility and controlled release, serving as advanced delivery systems that facilitate antimicrobials penetration into complex bacterial communities [211,212].

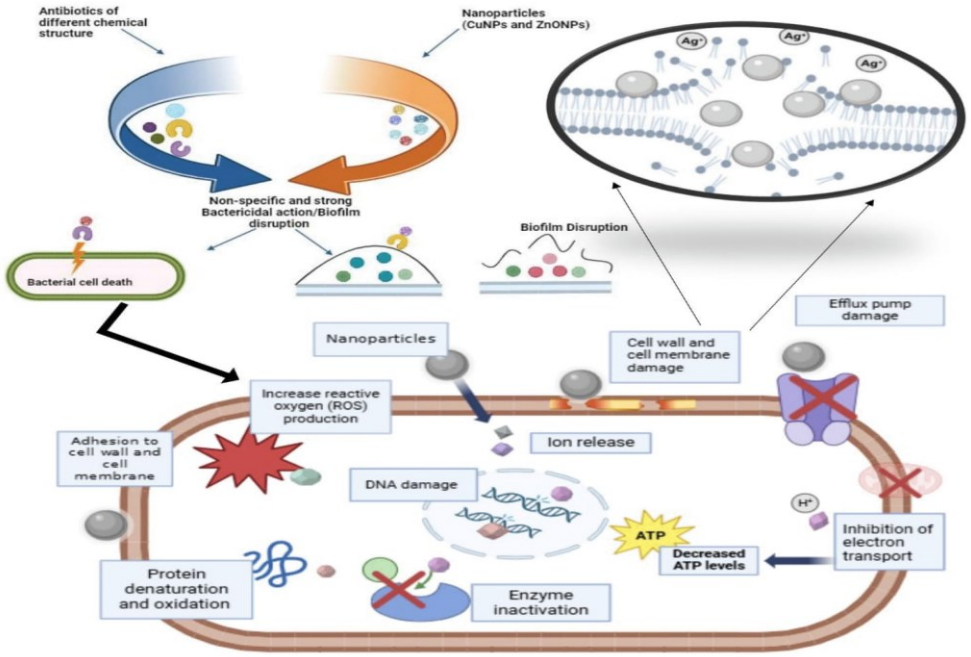

Figure 1.14. Schematic representation of the dual action of NPs, disrupting bacterial integrity both externally and internally [202].

1.5.2 Probiotic

Probiotics, commonly *Lactobacillus*, *Bifidobacterium*, some *Enterococcus*, and *Saccharomyces* strains, act primarily by restoring or reinforcing colonization resistance. In the intestine, they contribute to colonization resistance against pathogens by competing for nutrients and adhesion sites, producing acids, bacteriocins and other antimicrobials, reinforcing mucus and tight junctions, and modulating innate and adaptive immunity [201,213]. It was shown that these ecosystem-level effects limit pathogen overgrowth and reduce antibiotic-associated diarrhea, thereby lowering the risk or the severity of infections such as *Clostridioides difficile* and MDR *Enterobacterales* [214,215].

In respiratory infections, probiotics are being explored as adjuncts to antibiotics to limit pathogen colonization, reduce inflammation, and improve barrier function in the airways and distal organs [216,217]. Co-culture transcriptomics show that commensals and probiotics such as *Lactobacillus reuteri* can downregulate the expression of siderophore and adhesion-related genes in *Klebsiella pneumoniae* and *A. baumannii* during contact with host cells, indicating direct modulation of MDR pathogen virulence [216]. Moreover, the gut microbiota has been shown to support alveolar macrophage function, highlighting the importance of the gut-lung axis. However, the broad-spectrum antibiotics can disrupt this connection, promoting the overgrowth of pathogens such as *K. pneumoniae*, *S. pneumoniae*, and *P. aeruginosa*. Restoring a healthy microbiota, especially with probiotics, may therefore restore lung immunity [218,219]. Consistently, cell-free supernatants of *Lactobacillus plantarum* and *Lactobacillus rhamnosus* displayed rapid killing of both planktonic and biofilm-associated *P. aeruginosa* isolates from cystic fibrosis patients and suppressed expression of several quorum-sensing-regulated virulence factors [220].

In the urovaginal tract, probiotics treatment helps to restore a *Lactobacillus*-dominated flora characterized by their strong adhesion to urogenital epithelia, the production of lactic acid regulating the vaginal pH, production of hydrogen peroxide, and biosurfactant [221,222]. *L. reuteri* provides protection against diverse UPEC strains by blocking pathogen adhesion to and invasion of bladder cells and by enhancing host response through increased macrophage activity and balanced cytokine production [223]. Probiotic co-aggregation, initially forms a physical barrier followed by pathogen displacement and exclusion, thereby protecting host cells from vaginal pathogens such as *Candida glabrata*, *Neisseria gonorrheae*, and *Trichomonas vaginalis* [224]. Oral administration can also seed the rectum and perianal region with beneficial *Lactobacilli*, from where they can ascend to the vagina, supporting the restoration of the vaginal microbiota [225,226]. This concept has been applied to reduce *S. agalactiae* colonization, the frequency of premature rupture of membranes of amnio-chorionic membranes, and the need for IAP in pregnant women [227].

Advantages of probiotic adjuncts include relative safety of well-characterized strains, suitability for oral or vaginal administration, low production cost, and mechanisms that support microbiome resilience rather than causing further disruption. However, their clinical application remains constrained by heterogeneous clinical evidence, strain- and indication-specific effects, and limited colonization persistence in heavily antibiotic-exposed hosts. These challenges highlight the need for standardized outcome measures and optimized strategies to improve colonization capacity and sustain therapeutic effects across diverse patient populations [201,228]. Figure 1.15 schematically illustrates the interactions between probiotics, host tissues, and pathogens that confer protection.

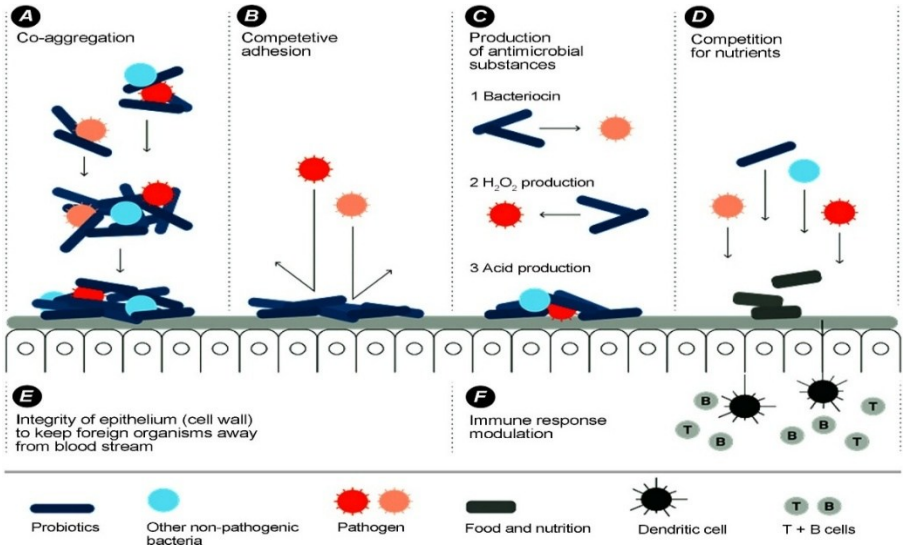

Figure 1.15. Effects of probiotic bacteria on the host epithelium and their interaction with potential pathogens. Probiotics compete with pathogens for binding sites (A, B) and nutrients (D), and secrete antimicrobial compounds such as bacteriocins, hydrogen peroxide, and organic acids (C). In parallel, they help maintain epithelial barrier integrity (E) and modulate dendritic cells as well as T and B lymphocytes [213].

References

1. Davies, J. & Davies, D. Origins and Evolution of Antibiotic Resistance. *Microbiol. Mol. Biol. Rev.* **74**, 417–433 (2010).
2. Tamadonfar, K. O., Omattage, N. S., Spaulding, C. N. & Hultgren, S. J. Reaching the End of the Line: Urinary Tract Infections. *Microbiol. Spectr.* **7**, 7.3.17 (2019).
3. Najafabadi, M. K. & Soltani, R. Carbapenem-resistant Acinetobacter baumannii and Ventilator-associated Pneumonia; Epidemiology, Risk Factors, and Current Therapeutic Approaches. *J. Res. Pharm. Pract.* **13**, 33–40 (2024).
4. Bostanghadiri, N. *et al.* Global Antimicrobial Resistance Trends in Group B *Streptococcus* Isolates From Pregnant Women: Systematic Review and Meta-Analysis. *MicrobiologyOpen* **14**, e70087 (2025).
5. Murray, C. J. L. *et al.* Global burden of bacterial antimicrobial resistance in 2019: a systematic analysis. *The Lancet* **399**, 629–655 (2022).
6. Naghavi, M. *et al.* Global burden of bacterial antimicrobial resistance 1990–2021: a systematic analysis with forecasts to 2050. *The Lancet* **404**, 1199–1226 (2024).
7. Jonas, O. B., Alec, I., Berthe, F. C. J., Le Gall, F. G. & Marquez, P. V. *Drug-Resistant Infections: A Threat to Our Economic Future (Vol. 2 of 2) : Final Report*. 141 http://documents.worldbank.org/curated/en/323311493396993758 (2017).
8. McDonnell, A. *et al. Forecasting the Fallout from AMR: Economic Impacts of Antimicrobial Resistance in Humans. A Report from the EcoAMR Series*. https://doc.woah.org/dyn/portal/index.xhtml?page=alo&aloId=44174 (2024) doi:10.20506/ecoAMR.3539.
9. Chokshi, A., Sifri, Z., Cennimo, D. & Horng, H. Global Contributors to Antibiotic Resistance. *J. Glob. Infect. Dis.* **11**, 36–42 (2019).
10. Sulis, G. *et al.* Antibiotic overuse in the primary health care setting: a secondary data analysis of standardised patient studies from India, China and Kenya. *BMJ Glob. Health* **5**, e003393 (2020).
11. Poluektova, O., Robertson, D. A., Rafferty, A., Cunney, R. & Lunn, P. D. A scoping review and behavioural analysis of factors underlying overuse of antimicrobials. *JAC-Antimicrob. Resist.* **5**, dlad043 (2023).
12. Acosta, A. *et al.* The future of antibiotic use in livestock. *Nat. Commun.* **16**, 2469 (2025).
13. U.S. Food and Drug Administration. 2021 Summary Report On Antimicrobials Sold or Distributed for Use in Food-Producing Animals. (2022).
14. Rice, L. B. Federal Funding for the Study of Antimicrobial Resistance in Nosocomial Pathogens: No ESKAPE. *J. Infect. Dis.* **197**, 1079–1081 (2008).
15. Rice, L. B. Progress and Challenges in Implementing the Research on ESKAPE Pathogens. *Infect. Control Hosp. Epidemiol.* **31**, S7–S10 (2010).
16. Magiorakos, A.-P. *et al.* Multidrug-resistant, extensively drug-resistant and pandrug-resistant bacteria: an international expert proposal for interim standard definitions for acquired resistance. *Clin. Microbiol. Infect.* **18**, 268–281 (2012).
17. WHO. *WHO Bacterial Priority Pathogens List 2024: Bacterial Pathogens of Public Health Importance, to Guide Research, Development, and Strategies to Prevent and Control Antimicrobial Resistance*. (World Health Organization, Geneva, 2024).
18. Sati, H. *et al.* The WHO Bacterial Priority Pathogens List 2024: a prioritisation study to guide research, development, and public health strategies against antimicrobial resistance. *Lancet Infect. Dis.* **25**, 1033–1043 (2025).

19. Mudenda, S., Daka, V. & Matafwali, S. K. World Health Organization AWaRe framework for antibiotic stewardship: Where are we now and where do we need to go? An expert viewpoint. *Antimicrob. Steward. Healthc. Epidemiol.* **3**, e84 (2023).

20. Dettori, S., Portunato, F., Vena, A., Giacobbe, D. R. & Bassetti, M. Severe infections caused by difficult-to-treat Gram-negative bacteria. *Curr. Opin. Crit. Care* **29**, 438–445 (2023).

21. Walker, M. K. *et al.* Using a difficult-to-treat resistance index to gauge imbalance between countries' antibiotic resistance prevalence and access to antibiotics: a scoping review and concept proposal. *Clin. Microbiol. Infect.* **31**, 1126–1138 (2025).

22. Munita, J. M. & Arias, C. A. Mechanisms of Antibiotic Resistance. *Microbiol. Spectr.* **4**, 4.2.15 (2016).

23. Waglechner, N., Culp, E. J. & Wright, G. D. Ancient Antibiotics, Ancient Resistance. *EcoSal Plus* **9**, eESP-0027-2020 (2021).

24. Wright, G. Bacterial resistance to antibiotics: Enzymatic degradation and modification. *Adv. Drug Deliv. Rev.* **57**, 1451–1470 (2005).

25. Ramirez, M. S. & Tolmasky, M. E. Aminoglycoside modifying enzymes. *Drug Resist. Updat.* **13**, 151–171 (2010).

26. Morar, M. & Wright, G. D. The Genomic Enzymology of Antibiotic Resistance. *Annu. Rev. Genet.* **44**, 25–51 (2010).

27. Lee, H. *et al.* Structural comparison of substrate-binding pockets of serine β-lactamases in classes A, C, and D. *J. Enzyme Inhib. Med. Chem.* **40**, 2435365 (2025).

28. Hall, B. G. & Barlow, M. Evolution of the serine β-lactamases: past, present and future. *Drug Resist. Updat.* **7**, 111–123 (2004).

29. Lamotte-Brasseur, J. *et al.* The Structures and Catalytic Mechanisms of Active-Site Serine β-Lactamases. *Biotechnol. Genet. Eng. Rev.* **12**, 189–230 (1994).

30. Nazir, A. *et al.* The Global Challenge of Antimicrobial Resistance: Mechanisms, Case Studies, and Mitigation Approaches. *Health Sci. Rep.* **8**, e71077 (2025).

31. Reygaert, W. C. An overview of the antimicrobial resistance mechanisms of bacteria. *AIMS Microbiol.* **4**, 482–501 (2018).

32. Darby, E. M. *et al.* Molecular mechanisms of antibiotic resistance revisited. *Nat. Rev. Microbiol.* **21**, 280–295 (2023).

33. Li, W. *et al.* Mechanism of tetracycline resistance by ribosomal protection protein Tet(O). *Nat. Commun.* **4**, 1477 (2013).

34. Arenz, S., Nguyen, F., Beckmann, R. & Wilson, D. N. Cryo-EM structure of the tetracycline resistance protein TetM in complex with a translating ribosome at 3.9-Å resolution. *Proc. Natl. Acad. Sci.* **112**, 5401–5406 (2015).

35. Matamoros-Recio, A. *et al.* Understanding the Antibacterial Resistance: Computational Explorations in Bacterial Membranes. *ACS Omega* **6**, 6041–6054 (2021).

36. Zhou, G. *et al.* Outer Membrane Porins Contribute to Antimicrobial Resistance in Gram-Negative Bacteria. *Microorganisms* **11**, 1690 (2023).

37. Benn, G. *et al.* OmpA controls order in the outer membrane and shares the mechanical load. *Proc. Natl. Acad. Sci.* **121**, e2416426121 (2024).

38. Samsudin, F., Ortiz-Suarez, M. L., Piggot, T. J., Bond, P. J. & Khalid, S. OmpA: A Flexible Clamp for Bacterial Cell Wall Attachment. *Structure* **24**, 2227–2235 (2016).

39. Auda, I. G., Ali Salman, I. M. & Odah, J. Gh. Efflux pumps of Gram-negative bacteria in brief. *Gene Rep.* **20**, 100666 (2020).

40. Schindler, B. D. & Kaatz, G. W. Multidrug efflux pumps of Gram-positive bacteria. *Drug Resist. Updat.* **27**, 1–13 (2016).

41. Evans, J. J. & Bolz, D. D. Regulation of virulence and antibiotic resistance in Gram-positive microbes in response to cell wall-active antibiotics. *Curr. Opin. Infect. Dis.* **32**, 217–222 (2019).

42. Gaurav, A., Bakht, P., Saini, M., Pandey, S. & Pathania, R. Role of bacterial efflux pumps in antibiotic resistance, virulence, and strategies to discover novel efflux pump inhibitors. *Microbiology* **169**, (2023).

43. Ambrose, S. J. & Hall, R. M. *dfrA* trimethoprim resistance genes found in Gram-negative bacteria: compilation and unambiguous numbering. *J. Antimicrob. Chemother.* **76**, 2748–2756 (2021).

44. Venkatesan, M. *et al.* Molecular mechanism of plasmid-borne resistance to sulfonamide antibiotics. *Nat. Commun.* **14**, 4031 (2023).

45. Acierno, C. *et al.* Metabolic Rewiring of Bacterial Pathogens in Response to Antibiotic Pressure—A Molecular Perspective. *Int. J. Mol. Sci.* **26**, 5574 (2025).

46. Hurst, M. N. *et al.* A Bacterial Signaling Network Controls Antibiotic Resistance by Regulating Anaplerosis of 2-oxoglutarate. Preprint at https://doi.org/10.1101/2020.10.22.351270 (2020).

47. Thi Khanh Nhu, N. *et al.* The induction and identification of novel Colistin resistance mutations in Acinetobacter baumannii and their implications. *Sci. Rep.* **6**, 28291 (2016).

48. Moffatt, J. H. *et al.* Colistin Resistance in *Acinetobacter baumannii* Is Mediated by Complete Loss of Lipopolysaccharide Production. *Antimicrob. Agents Chemother.* **54**, 4971–4977 (2010).

49. Arrieta-Ortiz, M. L. *et al.* Disrupting the ArcA Regulatory Network Amplifies the Fitness Cost of Tetracycline Resistance in Escherichia coli. *mSystems* **8**, e00904-22 (2023).

50. Mukherjee, S. & Bassler, B. L. Bacterial quorum sensing in complex and dynamically changing environments. *Nat. Rev. Microbiol.* **17**, 371–382 (2019).

51. De La Viuda, V., Buceta, J. & Grobas, I. Physical communication pathways in bacteria: an extra layer to quorum sensing. *Biophys. Rev.* **17**, 667–685 (2025).

52. Ahmad, M., Aduru, S. V., Smith, R. P., Zhao, Z. & Lopatkin, A. J. The role of bacterial metabolism in antimicrobial resistance. *Nat. Rev. Microbiol.* **23**, 439–454 (2025).

53. Stewart, P. S. *et al.* Conceptual Model of Biofilm Antibiotic Tolerance That Integrates Phenomena of Diffusion, Metabolism, Gene Expression, and Physiology. *J. Bacteriol.* **201**, (2019).

54. Li, S. *et al.* Metabolomics-based response of Salmonella to desiccation stress and skimmed milk powder storage. *Front. Microbiol.* **14**, 1092435 (2023).

55. Dayton, H. *et al.* Cellular arrangement impacts metabolic activity and antibiotic tolerance in Pseudomonas aeruginosa biofilms. *PLOS Biol.* **22**, e3002205 (2024).

56. Lucidi, M. *et al.* The response to desiccation in *Acinetobacter baumannii*. *Virulence* **16**, 2490209 (2025).

57. Peleg, A. Y., Seifert, H. & Paterson, D. L. *Acinetobacter baumannii* : Emergence of a Successful Pathogen. *Clin. Microbiol. Rev.* **21**, 538–582 (2008).

58. Mohd Sazlly Lim, S., Zainal Abidin, A., Liew, S. M., Roberts, J. A. & Sime, F. B. The global prevalence of multidrug-resistance among Acinetobacter baumannii causing hospital-acquired and ventilator-associated pneumonia and its associated mortality: A systematic review and meta-analysis. *J. Infect.* **79**, 593–600 (2019).

59. Foglia, F. *et al.* Prevalence of Acinetobacter baumannii Multidrug Resistance in University Hospital Environment. *Antibiotics* **14**, 490 (2025).

60. Zenati, K., Touati, A., Bakour, S., Sahli, F. & Rolain, J. M. Characterization of NDM-1- and OXA-23-producing Acinetobacter baumannii isolates from inanimate surfaces in a hospital environment in Algeria. *J. Hosp. Infect.* **92**, 19–26 (2016).

61. Pustijanac, E. *et al.* Dissemination of Clinical Acinetobacter baumannii Isolate to Hospital Environment during the COVID-19 Pandemic. *Pathogens* **12**, 410 (2023).

62. Lu, H. *et al.* On-Site Dual Detection of Airborne Acinetobacter baumannii and Its Carbapenem-Resistant Gene blaOXA-23 Using a One-Pot Visual LAMP-CRISPR/Cas12a-Based Platform. *Microorganisms* **13**, 976 (2025).

63. Houhamdi, L. & Raoult, D. Experimental Infection of Human Body Lice with Acinetobacter baumannii. *Am. J. Trop. Med. Hyg.* **74**, 526–531 (2006).

64. Kempf, M. *et al.* Detection of Acinetobacter baumannii in human head and body lice from Ethiopia and identification of new genotypes. *Int. J. Infect. Dis.* **16**, e680–e683 (2012).

65. Russo, A. *et al.* Bloodstream infections caused by carbapenem-resistant Acinetobacter baumannii: Clinical features, therapy and outcome from a multicenter study. *J. Infect.* **79**, 130–138 (2019).

66. Yang, X. *et al.* Treatment of Central Nervous System Infection Caused by Multidrug-Resistant Acinetobacter baumannii with Intravenous and Intraventricular Colistin Sulfate: A Case Report and Literature Review. *Infect. Drug Resist.* **Volume 16**, 6029–6038 (2023).

67. Yehya, A. *et al.* The intricacies of Acinetobacter baumannii: a multifaceted comprehensive review of a multidrug-resistant pathogen and its clinical significance and implications. *Front. Microbiol.* **16**, 1565965 (2025).

68. Tekin, R. *et al.* Risk Factors for Extensively Drug-Resistant Acinetobacter baumannii in Neonatal Patients. *J. Pediatr. Infect. Dis.* **16**, 031–035 (2021).

69. Zhang, Y. *et al.* Insights into the epidemiology, risk factors, and clinical outcomes of carbapenem-resistant Acinetobacter baumannii infections in critically ill children. *Front. Public Health* **11**, 1282413 (2023).

70. Higgins, P. G., Hrenovic, J., Seifert, H. & Dekic, S. Characterization of Acinetobacter baumannii from water and sludge line of secondary wastewater treatment plant. *Water Res.* **140**, 261–267 (2018).

71. Savin, M. *et al.* Tracing clinically-relevant antimicrobial resistances in Acinetobacter baumannii-calcoaceticus complex across diverse environments: A study spanning clinical, livestock, and wastewater treatment settings. *Environ. Int.* **186**, 108603 (2024).

72. Chung, Y. S. *et al.* Prevalence and antimicrobial resistance of Acinetobacter baumannii in the livestock industry in South Korea under a One Health perspective. *One Health* **20**, 101071 (2025).

73. Kon, H. *et al.* Prevalence and Clinical Consequences of Colistin Heteroresistance and Evolution into Full Resistance in Carbapenem-Resistant Acinetobacter baumannii. *Microbiol. Spectr.* **11**, e05093-22 (2023).

74. Shields, R. K. *et al.* Frequency of cefiderocol heteroresistance among patients treated with cefiderocol for carbapenem-resistant *Acinetobacter baumannii* infections. *JAC-Antimicrob. Resist.* **6**, dlae146 (2024).

75. Tomaschek, F., Higgins, P. G., Stefanik, D., Wisplinghoff, H. & Seifert, H. Head-to-Head Comparison of Two Multi-Locus Sequence Typing (MLST) Schemes for Characterization of Acinetobacter baumannii Outbreak and Sporadic Isolates. *PLOS ONE* **11**, e0153014 (2016).

76. Gaiarsa, S. *et al.* Comparative Analysis of the Two Acinetobacter baumannii Multilocus Sequence Typing (MLST) Schemes. *Front. Microbiol.* **10**, 930 (2019).

77. Holt, K. *et al.* Five decades of genome evolution in the globally distributed, extensively antibiotic-resistant Acinetobacter baumannii global clone 1. *Microb. Genomics* **2**, (2016).

78. Šeputienė, V., Povilonis, J. & Sužiedėlienė, E. Novel Variants of AbaR Resistance Islands with a Common Backbone in Acinetobacter baumannii Isolates of European Clone II. *Antimicrob. Agents Chemother.* **56**, 1969–1973 (2012).

79. Ying, S., Zhang, Z. & Xiang, R. Metagenomic and whole-genome characterization of carbapenem-resistant Acinetobacter baumannii carrying blaOXA-23 gene within the Tn2006 transposon among ICU patients. *J. Glob. Antimicrob. Resist.* **44**, 180–185 (2025).

80. Levy-Blitchtein, S. *et al.* Emergence and spread of carbapenem-resistant *Acinetobacter baumannii* international clones II and III in Lima, Peru. *Emerg. Microbes Infect.* **7**, 1–9 (2018).

81. Klotz, P. *et al.* Seasonal Occurrence and Carbapenem Susceptibility of Bovine Acinetobacter baumannii in Germany. *Front. Microbiol.* **10**, 272 (2019).

82. Caldart, R. V., Fonseca, E. L., Freitas, F., Rocha, L. & Vicente, A. C. Acinetobacter baumannii infections in Amazon Region driven by extensively drug resistant international clones, 2016-2018. *Mem. Inst. Oswaldo Cruz* **114**, e190232 (2019).

83. Wohlfarth, E. *et al.* The evolution of carbapenem resistance determinants and major epidemiological lineages among carbapenem-resistant Acinetobacter baumannii isolates in Germany, 2010-2019. *Int. J. Antimicrob. Agents* **60**, 106689 (2022).

84. Sheck, E. A. *et al.* Epidemiology and Genetic Diversity of Colistin Nonsusceptible Nosocomial *Acinetobacter baumannii* Strains from Russia for 2013-2014. *Can. J. Infect. Dis. Med. Microbiol.* **2017**, 1–5 (2017).

85. Wilharm, G. *et al.* Relatedness of wildlife and livestock avian isolates of the nosocomial pathogen *Acinetobacter baumannii* to lineages spread in hospitals worldwide. *Environ. Microbiol.* **19**, 4349–4364 (2017).

86. Karah, N. *et al.* Emergence of *Acinetobacter baumannii* International Clone 10 predominantly found in the Middle East. Preprint at https://doi.org/10.1101/2023.10.09.561570 (2023).

87. Hansen, F. *et al.* Characterisation of carbapenemase-producing Acinetobacter baumannii isolates from danish patients 2014–2021: detection of a new international clone – IC11. *Int. J. Antimicrob. Agents* **62**, 106866 (2023).

88. Karah, N. *et al.* Global emergence of Acinetobacter baumannii International Clone 12 predominantly found in the Middle East. *Microb. Genomics* **11**, (2025).

89. Wongsuk, T., Boonsilp, S., Homkaew, A., Thananon, K. & Oonanant, W. Whole genome sequence of pan drug-resistant clinical isolate of Acinetobacter baumannii ST1890. *PLOS ONE* **17**, e0264374 (2022).

90. Pearl, S. & Anbarasu, A. Genomic landscape of nosocomial Acinetobacter baumannii: A comprehensive analysis of the resistome, virulome, and mobilome. *Sci. Rep.* **15**, 18203 (2025).

91. Fournier, P.-E. *et al.* Comparative Genomics of Multidrug Resistance in Acinetobacter baumannii. *PLoS Genet.* **2**, e7 (2006).

92. Hamed, S. M., Hussein, A. F. A., Al-Agamy, M. H., Radwan, H. H. & Zafer, M. M. Genetic Configuration of Genomic Resistance Islands in Acinetobacter baumannii Clinical Isolates From Egypt. *Front. Microbiol.* **13**, 878912 (2022).

93. Naderi, G. *et al.* Dissemination of the *Acinetobacter baumannii* isolates belonging to global clone 2 containing AbGRI resistance islands in a referral hospital. *Microbiol. Spectr.* **11**, e05373-22 (2023).

94. Lam, M. M. C. & Hamidian, M. Examining the role of Acinetobacter baumannii plasmid types in disseminating antimicrobial resistance. *Npj Antimicrob. Resist.* **2**, 1 (2024).

95. Tobin, L. A. *et al.* Genomic analysis of diverse environmental *Acinetobacter* isolates identifies plasmids, antibiotic resistance genes, and capsular polysaccharides shared with clinical strains. *Appl. Environ. Microbiol.* **90**, e01654-23 (2024).

96. Hamidian, M., Nigro, S. J. & Hall, R. M. Variants of the gentamicin and tobramycin resistance plasmid pRAY are widely distributed in Acinetobacter. *J. Antimicrob. Chemother.* **67**, 2833–2836 (2012).

97. Nigro, S. J. & Hall, R. M. A large plasmid, pD46-4, carrying a complex resistance region in an extensively antibiotic-resistant ST25 Acinetobacter baumannii. *J. Antimicrob. Chemother.* **72**, 3496–3498 (2017).

98. He, W. *et al.* Structural and mechanistic insights into the transcriptional regulation of chromosomal T6SS by large conjugative plasmid-encoded TetRs in *Acinetobacter baumannii*. *Nucleic Acids Res.* **53**, gkaf755 (2025).

99. Pompilio, A. *et al.* Gram-Negative Bacteria Holding Together in a Biofilm: The Acinetobacter baumannii Way. *Microorganisms* **9**, 1353 (2021).

100. Sarshar, M., Behzadi, P., Scribano, D., Palamara, A. T. & Ambrosi, C. Acinetobacter baumannii: An Ancient Commensal with Weapons of a Pathogen. *Pathogens* **10**, 387 (2021).

101. Zhao, D. *et al.* Effect of OmpA of Acinetobacter baumannii on apoptosis in pulmonary epithelial cells and its molecular mechanism. *Microb. Pathog.* **210**, 108193 (2026).

102. Liao, C. *et al.* Human neutrophil α-defensin HNP1 interacts with bacterial OmpA to promote Acinetobacter baumannii biofilm formation. *Nat. Commun.* **16**, 5629 (2025).

103. Scribano, D. *et al.* Acinetobacter baumannii OmpA-like porins: functional characterization of bacterial physiology, antibiotic-resistance, and virulence. *Commun. Biol.* **7**, 948 (2024).

104. Ambrosi, C. *et al.* Acinetobacter baumannii Targets Human Carcinoembryonic Antigen-Related Cell Adhesion Molecules (CEACAMs) for Invasion of Pneumocytes. *mSystems* **5**, e00604-20 (2020).

105. Flores-Mireles, A. L., Walker, J. N., Caparon, M. & Hultgren, S. J. Urinary tract infections: epidemiology, mechanisms of infection and treatment options. *Nat. Rev. Microbiol.* **13**, 269–284 (2015).

106. Zagaglia, C., Ammendolia, M. G., Maurizi, L., Nicoletti, M. & Longhi, C. Urinary Tract Infections Caused by Uropathogenic Escherichia coli Strains—New Strategies for an Old Pathogen. *Microorganisms* **10**, 1425 (2022).

107. Yun, K. W., Lee, M.-K., Kim, W. & Lim, I. S. Uropathogenic *Escherichia coli* ST131 in urinary tract infections in children. *Korean J. Pediatr.* **60**, 221 (2017).

108. Oldendorff, F. *et al.* Case Report: Fatal Outcome for a Preterm Newborn With Meningitis Caused by Extended-Spectrum β-Lactamase-Producing Escherichia coli Sequence Type 1193. *Front. Pediatr.* **10**, 866762 (2022).

109. Matsukawa, M. *et al.* Epidemiology and genotypic characterisation of dissemination patterns of uropathogenic *Escherichia coli* in a community. *Epidemiol. Infect.* **147**, e148 (2019).

110. Vega-Hernández, R. *et al.* Flagella, Type I Fimbriae and Curli of Uropathogenic Escherichia coli Promote the Release of Proinflammatory Cytokines in a Coculture System. *Microorganisms* **9**, 2233 (2021).

111. Engelsöy, U., Svensson, M. A. & Demirel, I. Estradiol Alters the Virulence Traits of Uropathogenic Escherichia coli. *Front. Microbiol.* **12**, 682626 (2021).

112. Withman, B., Gunasekera, T. S., Beesetty, P., Agans, R. & Paliy, O. Transcriptional Responses of Uropathogenic Escherichia coli to Increased Environmental Osmolality Caused by Salt or Urea. *Infect. Immun.* **81**, 80–89 (2013).

113. Alteri, C. J. & Mobley, H. L. T. Metabolism and Fitness of Urinary Tract Pathogens. *Microbiol. Spectr.* **3**, 3.3.17 (2015).

114. Whelan, S., Lucey, B. & Finn, K. Uropathogenic Escherichia coli (UPEC)-Associated Urinary Tract Infections: The Molecular Basis for Challenges to Effective Treatment. *Microorganisms* **11**, 2169 (2023).

115. Clermont, O., Bonacorsi, S. & Bingen, E. Rapid and Simple Determination of the *Escherichia coli* Phylogenetic Group. *Appl. Environ. Microbiol.* **66**, 4555–4558 (2000).

116. García-Meniño, I., García, V., Lumbreras-Iglesias, P., Fernández, J. & Mora, A. Fluoroquinolone resistance in complicated urinary tract infections: association with the increased occurrence and diversity of Escherichia coli of clonal complex 131, together with ST1193. *Front. Cell. Infect. Microbiol.* **14**, 1351618 (2024).

117. Li, D. *et al.* A multiplex PCR method to detect 14 Escherichia coli serogroups associated with urinary tract infections. *J. Microbiol. Methods* **82**, 71–77 (2010).

118. Totsika, M. *et al.* Insights into a Multidrug Resistant Escherichia coli Pathogen of the Globally Disseminated ST131 Lineage: Genome Analysis and Virulence Mechanisms. *PLoS ONE* **6**, e26578 (2011).

119. Mostaghimi, T. *et al.* Phylogenetic analysis, biofilm formation, antimicrobial resistance and relationship between these characteristics in Uropathogenic Escherichia coli. *Mol. Biol. Rep.* **51**, 327 (2024).

120. Vimont, S. *et al.* The CTX-M-15-Producing Escherichia coli Clone O25b: H4-ST131 Has High Intestine Colonization and Urinary Tract Infection Abilities. *PLoS ONE* **7**, e46547 (2012).

121. Duprilot, M. *et al.* Success of Escherichia coli O25b:H4 Sequence Type 131 Clade C Associated with a Decrease in Virulence. *Infect. Immun.* **88**, e00576-20 (2020).

122. Lo, Y., Zhang, L., Foxman, B. & Zöllner, S. Whole-genome sequencing of uropathogenic Escherichia coli reveals long evolutionary history of diversity and virulence. *Infect. Genet. Evol.* **34**, 244–250 (2015).

123. Lukjancenko, O., Wassenaar, T. M. & Ussery, D. W. Comparison of 61 Sequenced Escherichia coli Genomes. *Microb. Ecol.* **60**, 708–720 (2010).

124. Samei, A., Haghi, F. & Zeighami, H. Distribution of pathogenicity island markers in commensal and uropathogenic Escherichia coli isolates. *Folia Microbiol. (Praha)* **61**, 261–268 (2016).

125. Lai, Y. M., Zaw, M. T., Shamsudin, S. B. & Lin, Z. Evaluation of PAIusp subtyping to characterize uropathogenic E. coli isolates. *J. Infect. Dev. Ctries.* **10**, 1053–1058 (2016).

126. Firoozeh, F., Soleimani-Moorchekhorti, L. & Zibaei, M. Evaluation of pathogenicity islands in uropathogenic Escherichia coli isolated from patients with urinary catheters. *J. Infect. Dev. Ctries.* **11**, 557–562 (2017).

127. Mukherjee, K., Aschenbach, W., Hilger, A., Saur, J. & Dobrindt, U. Differential perception of virulence factors of uropathogenic Escherichia coli at the level of chromatin dynamics of infected host cells. *Front. Immunol.* **16**, 1642683 (2025).

128. Rozwandowicz, M. *et al.* Plasmids carrying antimicrobial resistance genes in Enterobacteriaceae. *J. Antimicrob. Chemother.* **73**, 1121–1137 (2018).

129. Król, J. E. *et al.* Increased Transfer of a Multidrug Resistance Plasmid in Escherichia coli Biofilms at the Air-Liquid Interface. *Appl. Environ. Microbiol.* **77**, 5079–5088 (2011).

130. Kuznetsova, M. V., Maslennikova, I. L., Pospelova, J. S., Žgur Bertok, D. & Starčič Erjavec, M. Differences in recipient ability of uropathogenic Escherichia coli strains in relation with their pathogenic potential. *Infect. Genet. Evol.* **97**, 105160 (2022).

131. Carvalho, R. *et al.* Genomic Characterization of Multidrug-Resistant Escherichia coli BH100 Sub-strains. *Front. Microbiol.* **11**, 549254 (2021).

132. Skurnik, D. *et al.* Integron-Associated Antibiotic Resistance and Phylogenetic Grouping of *Escherichia coli* Isolates from Healthy Subjects Free of Recent Antibiotic Exposure. *Antimicrob. Agents Chemother.* **49**, 3062–3065 (2005).

133. Behzadi, P. Uropathogenic Escherichia coli and Fimbrial Adhesins Virulome. in *Urinary Tract Infection - The Result of the Strength of the Pathogen, or the Weakness of the Host* (eds Jarzembowski, T., Daca, A. & Dębska-Ślizień, M. A.) (InTech, 2018). doi:10.5772/intechopen.71374.

134. Servin, A. L. Pathogenesis of Afa/Dr Diffusely Adhering *Escherichia coli*. *Clin. Microbiol. Rev.* **18**, 264–292 (2005).

135. Vigil, P. D. *et al.* The Repeat-In-Toxin Family Member TosA Mediates Adherence of Uropathogenic Escherichia coli and Survival during Bacteremia. *Infect. Immun.* **80**, 493–505 (2012).

136. Luna-Pineda, V. M. *et al.* Curli of Uropathogenic Escherichia coli Enhance Urinary Tract Colonization as a Fitness Factor. *Front. Microbiol.* **10**, 2063 (2019).

137. Hollenbeck, E. C. *et al.* Phosphoethanolamine cellulose enhances curli-mediated adhesion of uropathogenic *Escherichia coli* to bladder epithelial cells. *Proc. Natl. Acad. Sci.* **115**, 10106–10111 (2018).

138. Jobin, T. *et al.* Identification of an unusual Streptococcus agalactiae growing on MacConkey Agar and its confirmation by biochemical tests, qPCR and nanopore sequencing. *J. Vet. Anim. Sci.* **55**, 675–679 (2024).

139. Doran, K. S. & Nizet, V. Molecular pathogenesis of neonatal group B streptococcal infection: no longer in its infancy. *Mol. Microbiol.* **54**, 23–31 (2004).

140. Wu, Y. *et al.* In Vitro Pharmacodynamics and Bactericidal Mechanism of Fungal Defensin-Derived Peptides NZX and P2 against Streptococcus agalactiae. *Microorganisms* **10**, 881 (2022).

141. Chen, S. L. Genomic Insights Into the Distribution and Evolution of Group B Streptococcus. *Front. Microbiol.* **10**, 1447 (2019).

142. Lancefield, R. C. A SEROLOGICAL DIFFERENTIATION OF HUMAN AND OTHER GROUPS OF HEMOLYTIC STREPTOCOCCI. *J. Exp. Med.* **57**, 571–595 (1933).

143. Eickhoff, T. C., Klein, J. O., Daly, A. K., Ingall, D. & Finland, M. Neonatal Sepsis and Other Infections Due to Group B Beta-Hemolytic Streptococci. *N. Engl. J. Med.* **271**, 1221–1228 (1964).

144. Evans, J. J., Klesius, P. H., Pasnik, D. J. & Bohnsack, J. F. Human *Streptococcus agalactiae* Isolate in Nile Tilapia (*Oreochromis niloticus*). *Emerg. Infect. Dis.* **15**, 774–776 (2009).

145. Bowater, R. O. *et al.* Natural outbreak of *Streptococcus agalactiae* (GBS) infection in wild giant Queensland grouper, Epinephelus lanceolatus (Bloch), and other wild fish in northern Queensland, Australia. *J. Fish Dis.* **35**, 173–186 (2012).

146. FAO. *Risk Profile - Group B Streptococcus (GBS) – Streptococcus Agalactiae Sequence Type (ST) 283 in Freshwater Fish*. (FAO, 2021). doi:10.4060/cb5067en.

147. Raabe, V. N. & Shane, A. L. Group B *Streptococcus* (*Streptococcus agalactiae*). *Microbiol. Spectr.* **7**, 7.2.17 (2019).

148. Baldan, R. *et al.* Group B streptococcal colonization in elderly women. *BMC Infect. Dis.* **21**, 408 (2021).

149. Navarro-Torné, A., Curcio, D., Moïsi, J. C. & Jodar, L. Burden of invasive group B Streptococcus disease in non-pregnant adults: A systematic review and meta-analysis. *PLOS ONE* **16**, e0258030 (2021).

150. Gizachew, M., Tiruneh, M., Moges, F. & Tessema, B. Streptococcus agalactiae maternal colonization, antibiotic resistance and serotype profiles in Africa: a meta-analysis. *Ann. Clin. Microbiol. Antimicrob.* **18**, 14 (2019).

151. Manuel, G. *et al.* Group B streptococcal infections in pregnancy and early life. *Clin. Microbiol. Rev.* **38**, e00154-22 (2025).

152. Upadhyay, K. & Talati, A. Group B Streptococcal Infections in Neonates. *Newborn* **1**, 109–119 (2022).

153. Verani, J. R. & Schrag, S. J. Group B Streptococcal Disease in Infants: Progress in Prevention and Continued Challenges. *Clin. Perinatol.* **37**, 375–392 (2010).

154. Berardi, A. *et al.* Group B Streptococcal Colonization in 160 Mother-Baby Pairs: A Prospective Cohort Study. *J. Pediatr.* **163**, 1099-1104.e1 (2013).

155. Sosa, M., Eckert, L. O. & Kachikis, A. Understanding GBS infection in pregnancy: exploring adverse maternal and pregnancy outcomes and the prospect of a GBS vaccine. *Ther. Adv. Infect. Dis.* **12**, 20499361251343710 (2025).

156. Panneflek, T. J. R. *et al.* Intrapartum antibiotic prophylaxis to prevent Group B streptococcal infections in newborn infants: a systematic review and meta-analysis comparing various strategies. *eClinicalMedicine* **74**, 102748 (2024).

157. Thorn, N., Karampatsas, K., Le Doare, K. & Heath, P. T. Progress towards a Group B streptococcal vaccine – where are we now? *Vaccine* **62**, 127575 (2025).

158. Hsu, C.-Y. *et al.* Global patterns of antibiotic resistance in group B Streptococcus: a systematic review and meta-analysis. *Front. Microbiol.* **16**, 1541524 (2025).

159. Creti, R., Imperi, M., Berardi, A., Angeletti, S. & Gherardi, G. Laboratory breakpoints for assessing high level gentamicin resistance in Streptococcus agalactiae: it is the time for a consensus. *Clin. Microbiol. Infect.* **28**, 1050–1052 (2022).

160. Creti, R. *et al.* Emergence of High-Level Gentamicin Resistance in Streptococcus agalactiae Hypervirulent Serotype IV ST1010 (CC452) Strains by Acquisition of a Novel Integrative and Conjugative Element. *Antibiotics* **13**, 491 (2024).

161. Shabayek, S. & Spellerberg, B. Group B Streptococcal Colonization, Molecular Characteristics, and Epidemiology. *Front. Microbiol.* **9**, 437 (2018).

162. Creti, R. *et al.* Invasive Group B Streptococcal Disease in Neonates and Infants, Italy, Years 2015–2019. *Microorganisms* **9**, 2579 (2021).

163. EL-Lakany, R. R., Abdelmaged, E. S., Shams, M., Hassan, R. & Rizk, D. E. Incidence of virulence determinants among *Streptococcus agalactiae* isolated from pregnant women and association with their serotypes. *Egypt. J. Basic Appl. Sci.* **10**, 650–670 (2023).

164. Gong, X. *et al.* Genomic characterization and resistance features of Streptococcus agalactiae isolated from non-pregnant adults in Shandong, China. *J. Glob. Antimicrob. Resist.* **38**, 146–153 (2024).

165. Imperi, M., Gherardi, G., Alfarone, G. & Creti, R. Group B Streptococcus Infections in Non-Pregnant Adults, Italy, 2015–2019. *Pathogens* **13**, 807 (2024).

166. Khan, U. B. *et al.* Genetic markers associated with host status and clonal expansion of Group B Streptococcus in the Netherlands. *Front. Microbiol.* **15**, 1410651 (2024).

167. Teatero, S. *et al.* Characterization of Invasive Group B Streptococcus Strains from the Greater Toronto Area, Canada. *J. Clin. Microbiol.* **52**, 1441–1447 (2014).

168. Brochet, M. *et al.* Shaping a bacterial genome by large chromosomal replacements, the evolutionary history of *Streptococcus agalactiae*. *Proc. Natl. Acad. Sci.* **105**, 15961–15966 (2008).

169. Ip, M. *et al.* Identification of a *Streptococcus agalactiae* Serotype III Subtype 4 Clone in Association with Adult Invasive Disease in Hong Kong. *J. Clin. Microbiol.* **44**, 4252–4254 (2006).

170. Barkham, T., Sheppard, A., Jones, N. & Chen, S. L. Streptococcus agalactiae that caused meningitis in healthy adults in 1998 are ST283, the same type that caused a food-borne outbreak of invasive sepsis in 2015: an observational molecular epidemiology study. *Clin. Microbiol. Infect.* **24**, 923–925 (2018).

171. Schar, D. *et al.* Dispersal history and bidirectional human-fish host switching of invasive, hypervirulent Streptococcus agalactiae sequence type 283. *PLOS Glob. Public Health* **3**, e0002454 (2023).

172. Wang, Z. Exploring the role of PilY1 family proteins in natural transformation. (Simon Fraser Universiy, 2022).

173. Jones, S., Newton, P., Payne, M. & Furfaro, L. Epidemiology, Antimicrobial Resistance, and Virulence Determinants of Group B Streptococcus in an Australian Setting. *Front. Microbiol.* **13**, 839079 (2022).

174. Lopes, E. *et al.* Increasing macrolide resistance among Streptococcus agalactiae causing invasive disease in non-pregnant adults was driven by a single capsular-transformed lineage, Portugal, 2009 to 2015. *Eurosurveillance* **23**, (2018).

175. Alzayer, M. *et al.* Genomic insights into the diversity, virulence, and antimicrobial resistance of group B Streptococcus clinical isolates from Saudi Arabia. *Front. Cell. Infect. Microbiol.* **14**, 1377993 (2024).

176. Maladan, Y. *et al.* Genomic analysis of virulence, antimicrobial resistance, and capsular polysaccharide locus of group B Streptococcus isolated from Indonesia. *The Microbe* **7**, 100367 (2025).

177. Megli, C. J., Carlin, S. M., Giacobe, E. J., Hillebrand, G. H. & Hooven, T. A. Virulence and pathogenicity of group B *Streptococcus* : Virulence factors and their roles in perinatal infection. *Virulence* **16**, 2451173 (2025).

178. Hooven, T. A. *et al.* Complete Genome Sequence of Streptococcus agalactiae CNCTC 10/84, a Hypervirulent Sequence Type 26 Strain. *Genome Announc.* **2**, e01338-14 (2014).

179. Liu, Y. & Liu, J. Group B Streptococcus: Virulence Factors and Pathogenic Mechanism. *Microorganisms* **10**, 2483 (2022).

180. Banerjee, A. *et al.* Bacterial Pili exploit integrin machinery to promote immune activation and efficient blood-brain barrier penetration. *Nat. Commun.* **2**, 462 (2011).

181. Samen, U., Eikmanns, B. J., Reinscheid, D. J. & Borges, F. The Surface Protein Srr-1 of *Streptococcus agalactiae* Binds Human Keratin 4 and Promotes Adherence to Epithelial HEp-2 Cells. *Infect. Immun.* **75**, 5405–5414 (2007).

182. Six, A. *et al.* S rr2, a multifaceted adhesin expressed by ST -17 hypervirulent G roup B *S treptococcus* involved in binding to both fibrinogen and plasminogen. *Mol. Microbiol.* **97**, 1209–1222 (2015).

183. Gutekunst, H., Eikmanns, B. J. & Reinscheid, D. J. The Novel Fibrinogen-Binding Protein FbsB Promotes *Streptococcus agalactiae* Invasion into Epithelial Cells. *Infect. Immun.* **72**, 3495–3504 (2004).

184. Coppolino, F. *et al.* The SaeRS two-component system regulates virulence gene expression in group B *Streptococcus* during invasive infection. *mBio* **15**, e01975-24 (2024).

185. Aznar, E. *et al.* The hypervirulent Group B Streptococcus HvgA adhesin promotes central nervous system invasion through transcellular crossing of the choroid plexus. *Fluids Barriers CNS* **21**, 66 (2024).

186. Carlin, A. F. *et al.* Molecular mimicry of host sialylated glycans allows a bacterial pathogen to engage neutrophil Siglec-9 and dampen the innate immune response. *Blood* **113**, 3333–3336 (2009).

187. Bohnsack, J. F. *et al.* Genetic Polymorphisms of Group B Streptococcus *scpB* Alter Functional Activity of a Cell-Associated Peptidase That Inactivates C5a. *Infect. Immun.* **68**, 5018–5025 (2000).

188. Armistead, B. *et al.* The cyl Genes Reveal the Biosynthetic and Evolutionary Origins of the Group B Streptococcus Hemolytic Lipid, Granadaene. *Front. Microbiol.* **10**, 3123 (2020).

189. Armistead, B. *et al.* Lipid analogs reveal features critical for hemolysis and diminish granadaene mediated Group B Streptococcus infection. *Nat. Commun.* **11**, 1502 (2020).

190. Zabel, L. T., Neuer, A. & Manncke, B. Fibronectin Binding and Cell Surface Hydrophobicity Contribute to Adherence Properties of Group B Streptococci. *Zentralblatt Für Bakteriol.* **285**, 35–43 (1996).

191. Vanderhoeven, J. P. *et al.* Group B Streptococcal Infection of the Choriodecidua Induces Dysfunction of the Cytokeratin Network in Amniotic Epithelium: A Pathway to Membrane Weakening. *PLoS Pathog.* **10**, e1003920 (2014).

192. Park, H.-R. *et al.* Group B streptococcus activates transcriptomic pathways related to premature birth in human extraplacental membranes in vitro†,‡. *Biol. Reprod.* **98**, 396–407 (2018).

193. Kim, B. J. *et al.* Streptococcus agalactiae disrupts P-glycoprotein function in brain endothelial cells. *Fluids Barriers CNS* **16**, 26 (2019).

194. Chacko, A. *et al.* Streptococcus agalactiae Infects Glial Cells and Invades the Central Nervous System via the Olfactory and Trigeminal Nerves. *Front. Cell. Infect. Microbiol.* **12**, 793416 (2022).

195. Evans, E. J., Witt, P. D., Zhanel, G. G. & Klein, D. J. Rethinking the unmet need for novel antibiotics. *J. Antibiot. (Tokyo)* s41429-025-00880–1 (2026) doi:10.1038/s41429-025-00880-1.

196. De Nies, L., Kobras, C. M. & Stracy, M. Antibiotic-induced collateral damage to the microbiota and associated infections. *Nat. Rev. Microbiol.* **21**, 789–804 (2023).

197. Peto, L. *et al.* The impact of different antimicrobial exposures on the gut microbiome in the ARMORD observational study. Preprint at https://doi.org/10.7554/eLife.97751.2 (2025).

198. Yusuf, A., Almotairy, A. R. Z., Henidi, H., Alshehri, O. Y. & Aldughaim, M. S. Nanoparticles as Drug Delivery Systems: A Review of the Implication of Nanoparticles' Physicochemical Properties on Responses in Biological Systems. *Polymers* **15**, 1596 (2023).

199. Elshobary, M. E. *et al.* Combating Antibiotic Resistance: Mechanisms, Multidrug-Resistant Pathogens, and Novel Therapeutic Approaches: An Updated Review. *Pharmaceuticals* **18**, 402 (2025).

200. El-Sayed, S. E., Messiha, A. A. & Zafer, M. Effective alternative strategies to combat challenges associated with MDR bacterial infections: Drug repurposing, role of artificial intelligence, and novel therapeutic options. *J. Infect. Public Health* **19**, 103058 (2026).

201. Mazziotta, C., Tognon, M., Martini, F., Torreggiani, E. & Rotondo, J. C. Probiotics Mechanism of Action on Immune Cells and Beneficial Effects on Human Health. *Cells* **12**, 184 (2023).

202. Hayat, S. *et al.* Nanoparticle-mediated approaches to combat antibiotic resistance: a comprehensive review on current progress, mechanisms, and future perspectives. *RSC Adv.* **15**, 42460–42478 (2025).

203. Generalova, A. N. & Dushina, A. O. Metal/metal oxide nanoparticles with antibacterial activity and their potential to disrupt bacterial biofilms: Recent advances with emphasis on the underlying mechanisms. *Adv. Colloid Interface Sci.* **345**, 103626 (2025).

204. Hao, Z. *et al.* Synergistic antibacterial mechanism of silver-copper bimetallic nanoparticles. *Front. Bioeng. Biotechnol.* **11**, 1337543 (2024).

205. Shamsoddini, S. M., Davoudi, M., Shahbazi, S. & Karizi, S. Z. Green synthesis of silver nanoparticles using Acroptilon repens aqueous extract and their antibacterial efficacy against multidrug-resistant Acinetobacter baumannii. *Mol. Biol. Rep.* **52**, 47 (2025).

206. Pangprasit, N. *et al.* Evaluation of Antibacterial Properties of Zinc Oxide Nanoparticles Against Bacteria Isolated from Animal Wounds. *Pharmaceutics* **17**, 209 (2025).

207. Trigo-Gutierrez, J. K., Vega-Chacón, Y., Soares, A. B. & Mima, E. G. D. O. Antimicrobial Activity of Curcumin in Nanoformulations: A Comprehensive Review. *Int. J. Mol. Sci.* **22**, 7130 (2021).

208. Kannan, S., Solomon, A., Krishnamoorthy, G. & Marudhamuthu, M. Liposome encapsulated surfactant abetted copper nanoparticles alleviates biofilm mediated virulence in pathogenic Pseudomonas aeruginosa and MRSA. *Sci. Rep.* **11**, 1102 (2021).

209. Mendez-Pfeiffer, P. *et al.* Chitosan-Coated Silver Nanoparticles Inhibit Adherence and Biofilm Formation of Uropathogenic *Escherichia coli*. *ACS Infect. Dis.* **10**, 1126–1136 (2024).

210. Kumari, S. *et al.* Surface functionalization of chitosan as a coating material for orthopaedic applications: A comprehensive review. *Carbohydr. Polym.* **255**, 117487 (2021).

211. Wasim, M. *et al.* Development of bacterial cellulose nanocomposites: An overview of the synthesis of bacterial cellulose nanocomposites with metallic and metallic-oxide nanoparticles by different methods and techniques for biomedical applications. *J. Ind. Text.* **51**, 1886S-1915S (2022).

212. Yahya, E. B. *et al.* A Review on Revolutionary Natural Biopolymer-Based Aerogels for Antibacterial Delivery. *Antibiotics* **9**, 648 (2020).

213. Dordević, D., Jančíková, S., Vítězová, M. & Kushkevych, I. Hydrogen sulfide toxicity in the gut environment: Meta-analysis of sulfate-reducing and lactic acid bacteria in inflammatory processes. *J. Adv. Res.* **27**, 55–69 (2021).

214. Spinler, J. K., Ross, C. L. & Savidge, T. C. Probiotics as adjunctive therapy for preventing Clostridium difficile infection – What are we waiting for? *Anaerobe* **41**, 51–57 (2016).

215. Wieërs, G. *et al.* Do Probiotics During In-Hospital Antibiotic Treatment Prevent Colonization of Gut Microbiota With Multi-Drug-Resistant Bacteria? A Randomized Placebo-Controlled Trial Comparing Saccharomyces to a Mixture of Lactobacillus, Bifidobacterium, and Saccharomyces. *Front. Public Health* **8**, 578089 (2021).

216. Chan, A. P. *et al.* Multidrug resistant pathogens respond differently to the presence of co-pathogen, commensal, probiotic and host cells. *Sci. Rep.* **8**, 8656 (2018).

217. Stavropoulou, E. & Bezirtzoglou, E. Probiotics in Medicine: A Long Debate. *Front. Immunol.* **11**, 2192 (2020).

218. Schuijt, T. J. *et al.* The gut microbiota plays a protective role in the host defence against pneumococcal pneumonia. *Gut* **65**, 575–583 (2016).

219. Enaud, R. *et al.* The Gut-Lung Axis in Health and Respiratory Diseases: A Place for Inter-Organ and Inter-Kingdom Crosstalks. *Front. Cell. Infect. Microbiol.* **10**, 9 (2020).

220. Pompilio, A. *et al.* Cell-free supernatants from Lactobacillus strains exert antibacterial, antibiofilm, and antivirulence activity against Pseudomonas aeruginosa from cystic fibrosis patients. *Microbes Infect.* **26**, 105301 (2024).

221. Avitabile, E. *et al.* Protective Mechanisms of Vaginal Lactobacilli against Sexually Transmitted Viral Infections. *Int. J. Mol. Sci.* **25**, 9168 (2024).

222. Xu, H. *et al.* Vaginal colonization of Lactobacilli: Mechanism and function. *Microb. Pathog.* **198**, 107141 (2025).

223. Tantibhadrasapa, A. *et al.* Probiotic Limosilactobacillus reuteri KUB-AC5 decreases urothelial cell invasion and enhances macrophage killing of uropathogenic Escherichia coli in vitro study. *Front. Cell. Infect. Microbiol.* **14**, 1401462 (2024).

224. Malfa, P. *et al.* Evaluation of Antimicrobial, Antiadhesive and Co-Aggregation Activity of a Multi-Strain Probiotic Composition against Different Urogenital Pathogens. *Int. J. Mol. Sci.* **24**, 1323 (2023).

225. Reid, G., Beuerman, D., Heinemann, C. & Bruce, A. W. Probiotic *Lactobacillus* dose required to restore and maintain a normal vaginal flora. *FEMS Immunol. Med. Microbiol.* **32**, 37–41 (2001).

226. Reid, G. *et al.* Oral use of *Lactobacillus rhamnosus* GR-1 and *L. fermentum* RC-14 significantly alters vaginal flora: randomized, placebo-controlled trial in 64 healthy women. *FEMS Immunol. Med. Microbiol.* **35**, 131–134 (2003).

227. Arduini, M. *et al.* A Controlled, Retrospective, Single-Center Study to Evaluate the Role of a Probiotic Mixture Administered during Pregnancy in Reducing Streptococcus Agalactiae Swab Positivity and the Frequency of Premature Rupture of Amniochorionic Membranes. *Microorganisms* **12**, 1979 (2024).

228. Merenstein, D. J. *et al.* Is There Evidence to Support Probiotic Use for Healthy People? *Adv. Nutr.* **15**, 100265 (2024).

Chapter 2. Scope of The Thesis

The global increase in antibiotic resistance indicates that the post-antibiotic era is approaching. Without effective intervention, antibiotics could lose their ability to treat even common infections. This situation is alarming, as no new classes of antibiotics have been discovered since the 1970s, and only a few innovative drugs are currently in clinical trials. This highlights how bacteria continue to outsmart medicine by evolving into superbugs. In this context, high-impact clinical pathogens characterized by MDR or XDR phenotypes have emerged. Among them, *A. baumannii*, UPEC, and *S. agalactiae* are prominent pathogens responsible for severe hospital-acquired infections, urinary tract diseases, and pregnancy-associated complications. Their resistance, virulence, and ecological adaptability reflect multidimensional survival strategies that promote persistence, treatment failure, and recurrent infections.

The overall aim of this thesis is to elucidate how these high-impact clinical pathogens adapt and persist under contemporary clinical and ecological pressures and evaluate probiotic and nanoparticle strategies as adjunct or alternative approaches to counteract bacterial virulence and resistance.

This thesis follows a paper-based format, with each chapter representing a published article or manuscript, structured according to the following research objectives:

Objective 1 – Genomic and phenotypic adaptation of XDR *A. baumannii*

To elucidate the microevolution and phenotypic adaptation of carbapenem-resistant *A. baumannii* isolates collected from two distinct periods over the past decade by characterizing their genomic, virulence, and antimicrobial resistance profiles.

Objective 2 – Goblet-cell response to *A. baumannii* infection in differentiated primary human primary bronchial epithelial cells

To determine how human respiratory epithelia respond to *A. baumannii* colonization using advanced *in vitro* air liquid interface (ALI) models that mimic host physiological conditions.

Objective 3 – Interplay between resistance, virulence, and phylogeny of MDR UPEC

To investigate how specific virulence gene determinants and phylogroups of UPEC from two distinct clinical settings shape resistance phenotypes and influence potential clinical outcomes.

Objective 4 – Emergence of MDR *S. agalactiae* and interaction with probiotic *Lactobacillus* spp.

To characterize the resistance and virulence profiles of GBS clinical isolates collected from pregnant women and to evaluate the protective effects of selected *Lactobacillus* strains as an adjunct therapy against GBS colonization in an *in vitro* cervical epithelial cell adhesion model.

Objective 5 – Effectiveness of serine-based gemini NPs against various MDR pathogens

To assess the antimicrobial activity of serine-based gemini NP formulations against *Staphylococcus aureus* ATCC 6538, *E. coli* MG 1655, *A. baumannii* ATCC 17978, and *Pseudomonas aeruginosa* PAO1, and to determine their cytotoxicity in human lung epithelial cells.

Within this framework, the scope of this thesis focuses on specific bacterial pathogens and clinical scenarios: hospital-acquired, urinary tract, and pregnancy-related infections. This focus allows a comprehensive analysis of pathogen adaptation, virulence, and ecological interactions, followed by an evaluation of the potential of probiotics and NPs as complementary tools for the surveillance, prevention, and treatment of MDR bacterial infections.

Chapter 3. A decade of genomic and phenotypic adaptation of carbapenem-resistant *Acinetobacter baumannii*

Astri D. Tagueha[1†], Cartesio D'Agostini [2,3†], Daniela Scribano[1], Carlotta Fiorilla[3], Dolores Limongi[4,5], Silvia Fillo[6], Luca Corrent[6], Martina Lipari[6], Florigio Lista[6], Lucia Nencioni[7], Anna Teresa Palamara[7,8] and Cecilia Ambrosi[4,5*]

[1]Department of Public Health and Infectious Diseases, Sapienza University of Rome, Rome, Italy, [2]Department of Experimental Medicine, University of Rome Tor Vergata, Rome, Italy, [3]Laboratory of Clinical Microbiology, Policlinico Tor Vergata, Rome, Italy, [4]Department of Promotion of Human Sciences and Quality of Life, San Raffaele Open University, Rome, Italy, [5]Laboratory of Microbiology, Istituto di Ricovero e Cura a Carattere Scientifico (IRCCS) San Raffaele Roma, Rome, Italy, [6]Scientific Department, Army Medical Center, Defense Institute for Biomedical Sciences, Rome, Italy, [7]Department of Public Health and Infectious Diseases, Laboratory Affiliated to Institute Pasteur Italia Cenci Bolognetti Foundation, Sapienza University of Rome, Rome, Italy, [8]Department of Infectious Diseases, Istituto Superiore di Sanità, Rome, Italy.

Published on 30 April 2025

Journal

Frontiers in Cellular and Infection Microbiology

IF (May 2026): 4.8

doi

https://doi.org/10.3389/fcimb.2025.1527488

Abstract

Acinetobacter baumannii exhibits high genomic plasticity, enabling it to acquire virulence factors and antibiotic resistance (AR). Understanding its evolutionary adaptations is crucial for developing effective therapeutic strategies. Thirty clinical isolates collected from two distinct time periods, defined as older (2010–2013), and recent (2022–2023), were compared phenotypically (antibiotic resistance, growth, biofilm formation, desiccation tolerance, invasiveness) and genotypically (whole-genome sequencing). All isolates displayed an extensively drug-resistant phenotype. Overall, respiratory isolates harbored a higher content of antibiotic-resistant genes (ARGs), with older isolates showing 12.5% increases in the average number of ARGs compared to recent urine isolates ($P = 0.02$). More than 50% of the strains with faster growth, stronger biofilm formation, and increased lung cell invasiveness were recent respiratory isolates, while over 70% of older isolates showed greater desiccation tolerance and bladder cell invasiveness. Eleven virulence factor genes were shared between old and recent respiratory isolates, and eight were common between recent urinary and respiratory strains with no overlap among urinary isolates. Statistically significant positive correlations were observed between fast-growing and strong biofilm-forming respiratory isolates as well as their lung cell invasiveness. Conversely, negative correlations were found between collection time, isolation site, and host cell invasiveness. Analysis of macrocolony types revealed no link to phenotypic behavior. Significant genetic variability was found between past and recent isolates. Older isolates had more genes involved in adhesion and nutrient uptake, while recent respiratory strains demonstrated increased biofilm formation and invasiveness, reflecting adaptation to clinical pressures. These findings highlight the dynamic evolution of *A. baumannii*, providing insights for future therapeutic strategies and infection control.

3.1 Introduction

Acinetobacter baumannii is a major opportunistic pathogen responsible for severe nosocomial infections worldwide, primarily affecting the lungs and bloodstream; however, the number of isolates collected from urinary sites has recently increased significantly compared to the past [1,2] raising the possibility that either it was previously underestimated or that *A. baumannii* isolates adapted to urinary tract. Currently, respiratory and urinary isolates exhibit robust environmental and host persistence and several antibiotic resistance (AR) mechanisms [3,4]. Moreover, transmission is not limited to vulnerable and critically ill patients in intensive care units (ICUs), but also to patients in general wards with long-term care treatment [5,6]. According to European Antimicrobial Resistance Surveillance Network (EARS-Net) in 2023, 59% of the 8,429 *Acinetobacter* spp. invasive isolates collected from 25 European countries exhibited resistance to multiple classes of antibiotics (www.ecdc.europa.eu/en). As global mortality associated with multidrug-resistant (MDR) *A. baumannii* accounted for 132.000 cases in 2019 (www.iris.who.int) and is projected to increase further, new medical therapeutic countermeasures for this pathogen have been prioritized [7,8].

In the last decades, *A. baumannii* clinical isolates have been exposed to enormous stress conditions, particularly due to the extensive use of antibiotics. As a consequence, *A. baumannii* isolates undergo local clonal expansion and adapt progressively to environmental and host changes [9–12]. *A. baumannii* great genomic plasticity allowed the acquisition of a remarkable number of AR genes (ARGs) via horizontal gene transfer through plasmid splicing, integrons, transposons, and mutations [13,14]. Other mechanisms, such as changes in the outer membrane proteins, target modification, and efflux pumps, further promote *A. baumannii* extraordinary resistance to antibiotics [12,15,16]. Acquirable traits allow *A. baumannii* isolates to adapt and persist in healthcare settings by forming biofilms, tolerating desiccation, improving motility and invasiveness. Isolates that are more adapted to local stresses expand clonally; currently, eleven international clones (IC) have been identified [17,18]. From epidemiological studies, it is evident that IC2 is the predominant and more spread clone, especially in Europe, whereas the others show a particular geographic dominance [17–19]. Several evidence demonstrated the fast evolution of this opportunistic pathogen in the healthcare environments and in the host during infection driven by stress exposure to achieve maximal adaptation [20–22]. Therefore, the present study aimed to genotypically and phenotypically characterize a collection of endemic carbapenem-resistant *A. baumannii* clinical isolates, collected in two distinct periods nearly a decade apart to identify key features, including antibiotic resistance and virulence traits, to understand their successful microevolution in the nosocomial environment.

3.2 Methods

3.2.1 Bacterial isolates, growth curves, and antibiogram profiles

Thirty *A. baumannii* carbapenem-resistant isolates were collected from twoperiods (2010–2013) and (2022– 2023) from three hospitals in Rome, Italy, including Policlinico Umberto I (n=9), Policlinico Di Liegro (n=6), and Policlinico Tor Vergata (n=15). Inclusion criteria: Carbapenem-resistant *A. baumannii* strains isolated from respiratory or urinary specimens, reflecting prevalent infection sources and the high risk of progression to pan-drug resistance. Exclusion criteria: Strains not exhibiting carbapenem resistance; strains isolated from other clinical sources. A single *A. baumannii* strain per patient was included in this study and was isolated mainly from respiratory specimens, including sputum (n=6), bronchoalveolar lavage (BAL) (n=4), bronchoalveolar aspirate (BA) (n=12), whereas 8 from urinary infections (Table 3.1).

Species were identified by MALDI-TOF mass spectrometry. Strains were grown on Luria-Bertani (LB) broth and agar plates (LA). Growth kinetics in 96 well microplates were determined by measuring cell density (OD600) for 16 h at 37°C in LB with vigorous shaking (200 rpm) in triplicate wells for each strain, using the plate reader BioTek SynergyHT equipped with the software GEN5™. Three independent experiments were performed. The reference strains ATCC 17978 and ATCC 19606 were used as controls for all the assays, while strain AB5075 for surface associated motility only [23].

Antibiogram profiles were obtained using the VITEK®2 system (bioMérieux, Italia S.p.A, Grassina, Italy) with the AST-N397 panel, which included amikacin, gentamicin, tobramycin, imipenem, meropenem, piperacillin/tazobactam, ciprofloxacin, trimethoprim/ sulfamethoxazole, and colistin. Minimum inhibitory concentration (MIC) values were interpreted according to the European Committee on Antimicrobial Susceptibility Testing (EUCAST v13.0, 2023). Detailed MIC values and breakpoints are provided in Table 3.2.

Table 3.1. Strains used in the study.

Site of isolation	Strain ID	Year	Strain ID	Year
Sputum	SN11	2022	SO3	2012
	SN12	2022	SO5	2012
	SN24	2023	SO28	2010
BL	BLN17	2023	BLO34	2012
	BLN19	2023	BLO70	2010
BA	BN14	2022	BO27	2012
	BN15	2022	BO29	2010
	BN20	2023	BO47	2011
	BN21	2023	BO88	2010
	BN22	2023	BO90	2010
	BN25	2023	BO93	2010
Urine	UN16	2022	UO2	2012
	UN18	2023	UO4	2013
	UN23	2023	UO7	2013
	UN26	2023	UO8	2013

BL: bronchoalveolar lavage, B: bronchial aspirate, U: urine, O: old collection, N: new collection.

3.2.2 Whole genome sequencing, molecular typing, antibiotic and virulence factors profiles

DNA was extracted using a Bacterial Genomic Isolation Kit (BioVision, USA). Libraries were prepared using the Nextera XT DNA kit and were sequenced on Illumina NextSeq500 and NextSeq2000 platforms using High Output Kit v2.5 (300 cycles) and P2 reagents (300 cycles), respectively; following the manufacturer's instructions (Illumina, CA, USA). Raw reads (around 14M of reads per sample) were evaluated using FastQC v0.12.1 (2023–03–01) as post-sequencing Quality Control. Raw reads were filtered by Trimmomatic v0.39 [24] with following parameters: ILLUMINACLIP: TruSeq3-PE.fa:2:30:10, LEADING:3, TRAILING:3, SLIDINGWINDOW:4:20, and MINLEN:36. A Phred quality score threshold of Q20 was applied for read filtering. The whole-genome shotgun sequences of the isolates generated in this study were deposited in GenBank under the BioProject accession number PRJNA1173090. The *de novo* assembly was performed by SPAdes Assembler v3.14.1 (2020–08–25) [25] on high-quality paired-ends reads for each isolate. Each genomic assembly contained contigs longer than 200 bp according to NCBI instructions

(https://www.ncbi.nlm.nih.gov/genbank/wgsfaq/). ARGs were searched with AMRFinder Pathogen Detection (VERSION: 3.12.8, 2024-01-31.1). Multilocus Sequence Typing (MLST) with MLST Pasteur scheme (VERSION: 2024-03-09) (https://github.com/tseemann/mlst; accessed on March 2024). This scheme was selected for its high discriminatory power in *A. baumannii*, ability to provide stable sequence type (ST) assignments, and reliability in tracking clonal lineages across different hospitals and collection years. Additionally, it ensures comparability with previous epidemiological studies. DNA sequences of bacterial Virulence Factors (VFs) were retrieved from the Virulence Factors Database (VFDB). Virulence markers were searched with a minimal coverage of > 90% and an e-value cut off of 0.0000001. Analyses of the contigs sequences for each sample were performed using blastn v2.11.0+ (2020–10–11). Sequence analyses were performed using a commercial service (Bio-Fab Research srl, Roma, Italy).

3.2.3 Biofilm formation assay

Biofilm formation was assessed using the microtiter plate assay and categorized as biofilm-forming producers as previously described [9]. Three independent experiments were performed.

3.2.4 Desiccation tolerance assay

Overnight cultures were adjusted to $OD_{600} \approx 1.0$, harvested by centrifugation, and washed twice with 2 ml of sterile water. Cell suspensions (10 µL) were deposited into a 96-well polystyrene microplate in triplicate and air-dried for 2–3 h in a biosafety cabinet until they were visibly dry. Uncovered plates were then placed in an airtight transparent plastic bag with silica beads and incubated for up to six days at 25°C with a relative humidity of 25 ± 2%. After incubation, the bacteria were rehydrated with water, gently scraped, plates rocked for 30 min to collect all cells from the bottom of the microplates, serially diluted in PBS and plated onto LB agar containing ampicillin (100 µg/ml). The percentage survival was calculated as:

$$\% \text{ survival} = \frac{\text{final CFU/ml}}{\text{initial CFU/ml}} \text{ x } 100$$

3.2.5 Surfaced-associated motility, protease, and hemolytic activities

Surface-associated motility was evaluated by spotting 5 µL of an overnight culture on freshly prepared soft agar plates incubated at 37°C for 24 h., as previously described [12]. The motile clinical strains AB5075 and ATCC 17978, as well as the not motile ATCC 19606 were included as controls. Protease activity was assessed by spotting 5 µL on LB agar containing 1% skim milk. *Pseudomonas aeruginosa* PAO1 was included as the positive control. One microliter of the overnight culture was spotted onto Columbia agar plates (Becton Dickinson™, Milan, Italy) and incubated for 24 h to assess hemolytic activity and macrocolony types.

3.2.6 *In vitro* infection

The human A549 lung epithelial cell line type II (ATCC CCL185, lab collection) and bladder cell line 5637 HTB-9 (ATCC-LGC, Milan, Italy) were cultured in DMEM supplemented with 10% fetal bovine serum (FBS), 1% glutamine, 1% penicillin-streptomycin, and 50 µg/ml gentamycin. Cell monolayers on 35 mm culture dishes at a density of 2.5 x 10^5/ml were infected with clinical isolates at a multiplicity of infection (MOI) of 10 and incubated at 37°C with 5% CO_2 for 2.5 h before adding colistin (10 µg/ml, BioChemica) to kill extracellular bacteria. After 48 h, cell monolayers were washed five times with PBS and lysed with 1 ml 0.1% Triton X-100. The recovered bacteria were serially diluted and plated onto LA plates to determine the number of colony-forming units (CFU)/ml.

3.2.7 Statistical analyses

GraphPad Prism Software (10.3.1) was used for statistical analyses. Normality was assessed using the Shapiro-Wilk test or Kolmogorov-Smirnov test. Phenotypic characteristics were analyzed using one-way ANOVA, and followed by Dunnett's *post hoc* test for multiple comparisons. Pearson correlation was used to assess the relationships among phenotypic traits, with data transformed using the log (Y) function prior to analysis. To evaluate whether the number of antibiotic resistance genes (ARGs) influence MIC values, the same analysis was performed. Statistical significance for all tests was set at $P< 0.05$. Moreover, Supplementary Figures S1, S2 were generated with Microsoft Excel and GraphPad Prism, respectively.

3.2.8 Data availability

The data presented in the study are deposited in the NCBI GenBank repository, accession numbers PRJNA1173090.

Table 3.2. MIC values of clinical isolates.

	Aminoglycosides			Carbapenems		B-lactams	Quinolones	Sulfonamides	Polymyxins
Strain ID	GM	TM	AK	IMP	MRP	P/T	CIP	T/S	CST*
SO3	≥16	≥16	≤2*	≥16	≥16	≥128	≥4	≥320	≤0.5
SO5	≥16	≥16	32	≥16	≥16	≥128	≥4	≥320	2
SO28	≥16	≥16	≥64	≥16	≥16	≥128	≥4	≥320	≤0.5
SN11	≥16	≥16	≥64	≥16	≥16	≥128	≥4	≥320	≤0.5
SN12	8	≤1*	4*	≥16	≥16	≥128	≥4	≥320	≤0.5
SN24	≥16	≥16	≥64	≥16	≥16	≥128	≥4	≥320	≤0.5
BO27	≥16	≥16	≥64	≥16	≥16	≥128	≥4	≥320	≤0.5
BO29	≥16	≥16	≥64	≥16	≥16	≥128	≥4	≥320	≤0.5
BO47	≥16	≥16	≥64	≥16	≥16	≥128	≥4	≥320	≤0.5
BO88	≥16	≥16	≥64	≥16	≥16	≥128	≥4	160	≤0.5
BO90	≥16	≥16	≥64	≥16	≥16	≥128	≥4	≥320	≤0.5
BO93	8	≥16	8*	≥16	≥16	≥128	≥4	≥320	≤0.5
BN14	≥16	≥16	≤2*	≥16	≥16	≥128	≥4	≥320	≤0.5
BN15	>8	≥16	≤4*	≥16	≥16	≥128	≥4	≥320	≤0.5
BN20	≥16	≥16	≥64	≥16	≥16	≥128	≥4	≥320	≤0.5
BN21	≥16	≥16	8*	≥16	≥16	≥128	≥4	≥320	1
BN22	≥16	≥16	≥64	≥16	≥16	≥128	≥4	≥320	≤0.5
BN25	≥16	≥16	≥64	≥16	≥16	≥128	≥4	≥320	≤0.5
BLO34	≥16	≥16	≥64	≥16	≥16	≥128	≥4	≥320	≤0.5
BLO70	≥16	≥16	32	≥16	≥16	≥128	≥4	≥320	≤0.5
BLN17	≥16	≥16	≥64	≥16	≥16	≥128	≥4	160	≤0.5
BLN19	>8	≥16	>16	≥16	16	≥128	>1	≥320	≤0.5
UO2	≥16	≥16	≥64	≥16	≥16	≥128	≥4	≥320	≤0.5
UO4	≥16	≥16	≥64	≥16	≥16	≥128	≥4	≤20*	1
UO7	≥16	≥16	≥32	≥16	≥16	≥128	≥4	≥320	2
UO8	≥16	≥16	≥64	≥16	≥16	≥128	≥4	≥320	≤0.5
UN16	≥16	≥16	≥32	≥16	≥16	≥128	≥4	≥320	≤0.5
UN18	≥16	≥16	≥64	≥16	≥16	≥128	≥4	≥320	≤0.5
UN23	≥16	≥16	≥64	≥16	≥16	≥128	≥4	≥320	≤0.5
UN26	≥16	≥16	4*	≥16	≥16	≥128	≥4	≥320	≤0.5

AK: Amikacin (R>8), GM: Gentamicin (R>4), TM: Tobramicin (R>4), IMP: Imipenem R(>2); MRP: Meropenem (R>8), P/T: Piperacilin-tazobactam, CIP: Ciprofloxacin (R>1), T/S: Trimethoprim/Sulfamethoxazole (R>80), CST: Colistin (R>2). Asterix (*) indicated the susceptibility to the tested antibiotic. The classification was based on EUCAST clinical breakpoints (v13.0).

3.3 Results

3.3.1 Antibiogram profiles and genomic content of ARGs

The minimal inhibition concentration (MIC) was assessed for all isolates, and values were interpreted according to EUCAST 2023 criteria (Table 3.2). Based on MIC values, all isolates were classified as extensively drug-resistant (XDR). Apart from carbapenem-resistance, few isolates (7/30) were susceptible to amikacin, whereas only one to tobramycin (Table 2). All isolates were susceptible to colistin. Overall, strains collected from urine were more resistant compared with respiratory isolates. EUCAST was chosen over clinical and laboratory standard institute (CLSI) as it is the standard in Europe, and provides continuously updated breakpoints based on pharmacokinetic and clinical data, ensuring a more precise and stringent classification of resistance, particularly for carbapenems. To associate the clinical breakpoints to genotypic data, the genome of each isolate was extracted and sequenced. According to the Pasteur scheme, all *A. baumannii* isolates belonged to ST2; but one, isolate BO29, belonging to ST632 [26].

Genes directly and indirectly related to AR mechanisms were identified (Figure 3.1). Statistical analysis revealed a significant difference in the number of ARGs among isolates. On average, 46% (33/71) of conserved genes were harbored by older isolates, with older respiratory isolates exhibiting a 12.5% increase ARGs number compared to recent urine isolates (P = 0.02). Regarding the genes conferring resistance to aminoglycosides, 13 genes were found in the genomes' isolates (Figure 3.1), thereby accounting for the high levels of resistance found in the MIC data (Table 2). Notably, the number of aminoglycoside resistance genes showed a strong positive correlation with the MIC of gentamicin (r = 0.43, P = 0.02) and amikacin (r = 0.70, P = 0.00002). Among these, the *ant (3)-IIa* variant was present in all isolates, followed by *aph(3')-Ib* and *aph (6)-Id* (19/30), *armA* (18/19), *aph(3')-Ia* (15/30), *ant(2')-Ia* (10/30), *aadA2* (9/30), *aph(3')-VIa* (7/30), *aadA1* (6/30), *aac (6)-Ib'* (5/30); *aac (3)-Ia*, *aac(6')-Ian*, and *aac (6)-Ib3* were found in single isolates. Interestingly, the overall content of aminoglycoside resistant genes was found less in recently isolated strains in comparison to old ones, particularly for urinary strains (Figure 3.1).

Among class D OXA-type carbapenemases, the $bla_{OXA\text{-}23}$ gene was present in the vast majority of isolates (93%, 28/30) (Figure 3.1). Interestingly, the $bla_{OXA\text{-}51}$-like carbapenemase gene, including $bla_{OXA\text{-}66}$ and $bla_{OXA\text{-}82}$ variants, was carried by all isolates. Conversely, the $bla_{OXA\text{-}58}$ and $bla_{OXA\text{-}20}$ genes were carried by one strain each (3%, 1/30), and the class A gene, $bla_{TEM\text{-}1}$was found in 30% of isolates (9/30) (Figure 3.1). Several intrinsic *Acinetobacter*-derived cephalosporinases (ADCs) genes belonging to class C were found in the genomes of isolates (Figure 3.1). The most prevalent variants were $bla_{ADC\text{-}73}$(50%, 15/30), $bla_{ADC\text{-}33}$(27%, 8/30), and $bla_{ADC\text{-}30}$(13%, 4/30) (Figure 3.1). Other variants such as $bla_{ADC\text{-}152}$, and $bla_{ADC\text{-}175}$were identified only in old isolates BO70, and BO93, respectively (Figure 3.1). It was also identified the mutation A515V in the penicillin-binding protein 3, FtsI, an essential division component in fourteen isolates,

which is associated with an increase in meropenem MIC values [27]. From our data, the overall content of beta-lactamase and carbapenemase genes seems increased in recently collected strains from respiratory specimens, while it is stable among urinary isolates (Supplementary Figure S1A).

Moreover, the *parC_S84L* and *gyrA_S81L* genes conferring resistance to quinolones were found in 97 and 100% of the isolates, respectively (Figure 3.1). The *sul1* and *sul2* genes involved in sulfonamide resistance were less present, being both found in 53% of the genomes (16/30). The overall content of quinolone and sulfonamide resistance genes appears to have increased and decreased in recent respiratory strains, respectively. Conversely, while the content of quinolone resistance genes remains the same in both old and new urinary strains, there is an increase in sulfonamide resistance genes in recent urinary strains (Figure 3.1). Furthermore, five genes associated with tetracycline resistance mechanisms were identified, *tet(B), tet(M), tet (32), tetA (46)*, and *tetB (46)*, showing higher prevalence in recent respiratory isolates and lower prevalence in recent urinary strains (Figure 3.1). The *tet(B)* gene, an efflux pump (belonging to the major facilitator superfamily [MFS] superfamily) known to mediate resistance to tetracycline, doxycycline, and minocycline, was the most prevalent among our strain collection, accounting for 67% (20/30). The other tetracycline resistance genes, including *tet (32)*, *tet(M)*, conferring resistance to tetracycline by ribosomal protection, and *tetAB (46)*, encoding a predicted heterodimeric ABC transporter was only described in *Streptococcus australis* [28] were found only in strain BN25. To assess the contribution of these tetracycline resistance genes, we determined the MIC of tetracycline. BN25, BLN17, and UO7 exhibited MICs greater than 256 µg/ml, while other strains had MICs >16 µg/ml, highlighting the key role of Tet efflux pumps, including *tetB* [29].

Moreover, all isolates were colistin-susceptible, according to EUCAST breakpoints (https://www.eucast.org/). Notably, isolate UO7 carried the P233S mutation in the histidine kinase encoded by the *pmrB* gene, described as a key mutation for conferring resistance to polymyxins under certain conditions, accounting for the higher MIC value [30,31]. Although macrolide resistance was not tested, the *A. baumannii* common *mph(E)-msr(E)* operon was found in 57% of isolates (17/30). Differently, the *erm(B)*, and *msrA* genes were individually found in only two isolates, BN25 and BO70, respectively (Figure 3.1). Overall, macrolide resistance gene content was found increased in recent respiratory isolates, and decreased in recent urinary strains (Supplementary Figure S1). Furthermore, the *catB8* gene, encoding a chloramphenicol acetyltransferases protein type B [32], was identified in 17% (5/30) of isolates. Differently, the *floR* gene, conferring resistance to florfenicol and chloramphenicol, was found only in one isolate (Figure 3.1).

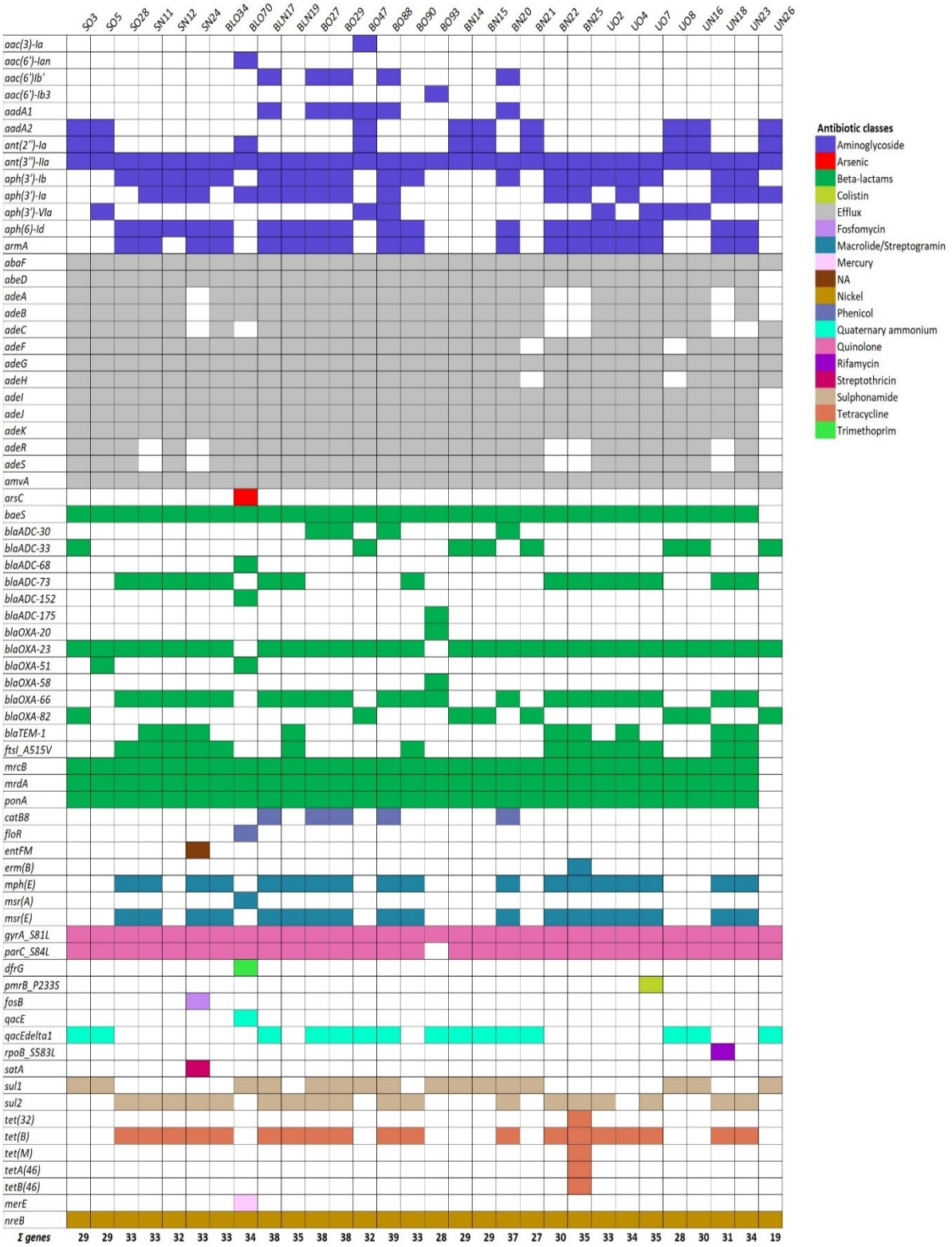

Figure 3.1. Genes directly and indirectly related to AR mechanisms detected in the isolate collection. Heat map of ARGs identified using whole genome sequence analysis. Color-code represents genes involved in the resistance of the different classes of antibiotics, heavy metals, and disinfectants, as indicated. NA, not applicable.

Several genes encoding multidrug efflux pumps were identified; the most prevalent ones were *amvA* and *abaF*, encoding MFS pumps, which were found in all isolates [33,34] (Figure 3.1). Differently, the *adeC* gene, encoding the outer membrane protein of the three-component efflux machinery of the resistance nodulation division (RND)-type superfamily [35], was found in 80% of isolates (24/30). Interestingly, the mutation P116L in the regulatory gene *adeR* associated with AdeAB overexpression was identified in only one isolate (1/30), UO7 (Figure 3.1) [36]. The RND efflux pump *adeFGH* were highly present in all isolates, ranging from 100% for adeG to 97% (29/30) for *adeF* and *adeH* (Figure 3.1). In addition, the efflux systems involving *qac* genes (*qacE* and *qacE* delta1) that confers resistance to biocides were present in 3 (1/30) and 50% (15/30) of isolates, respectively [37]. The nickel/cobalt tolerance gene *nreB* was found in all isolates [38]. Overall, we found a slight decrease in the content of efflux pump genes in both groups of recent strains (Figure 3.1; Supplementary Figure S1). Other genes involved in resistance to heavy metal efflux (*arsC*, and *merE*), fosfomycin (*abaF* and *fosB*), trimethoprim (*dfrG)*, rifamycin (*rpoB_S583L)*, and streptothricin *(satA)*, were the least prevalent among isolates (Figure 3.1). The highest content of ARGs was found in strain BO88 (39 genes), followed by strains BN17, BO29, and BO27 [38]. According to the antibiogram profile, the most common genotype in strains displaying the highest MIC values was: *ant(3")-IIa, abaF, abeD, adeABFGHJK, amvA, baeS,* $bla_{OXA\text{-}23}$, $bla_{OXA\text{-}51}$ (variants included*), mrcB, mrdA, ponA, gyrA_S81L, nreB, parC_S84L.*

3.3.2 Growth rates and genomic content of key metabolic genes

The growth properties of the isolates were evaluated. The two reference strains ATCC 17978 and ATCC 19606 were included as controls. As shown in Figure 3.2, eleven isolates collected from 2022, and mainly isolated from the respiratory tract (7/11), showed a significant faster growth in comparison to both reference strains ($P< 0.0001$). Key genes related to *A. baumannii* metal ion metabolism uptake systems were analyzed (Figure 3.3), including the *bar/bas/bau/entE* (synthesis, secretion, and uptake acinetobactin/enterobactin, *pbpG* (penicillin-binding protein 7 (PBP7), *fecIR/hemO/tonB* (hemin or hemoglobin), *pirA/slam/ybaN* (transporters), *znuABC* (zinc acquisition system), *zrlA* (zinc peptidase), *plc1/plc2/plcD* (phospholipases), and *lysR* (transcriptional regulator) [39–41]; *basD, plcD*, and *znuABC* were conserved in all isolates, while prevalent *basAB, bauA, entE, fecI, hemO*, and *plc2* (29/30, 97%) (Figure 3.3). According to growth rates, the most common genotype in fastest-growing isolates was: *basABD, bauA, entE, plc2, plcD, znuABC* (Figures 3.2, 3.3).

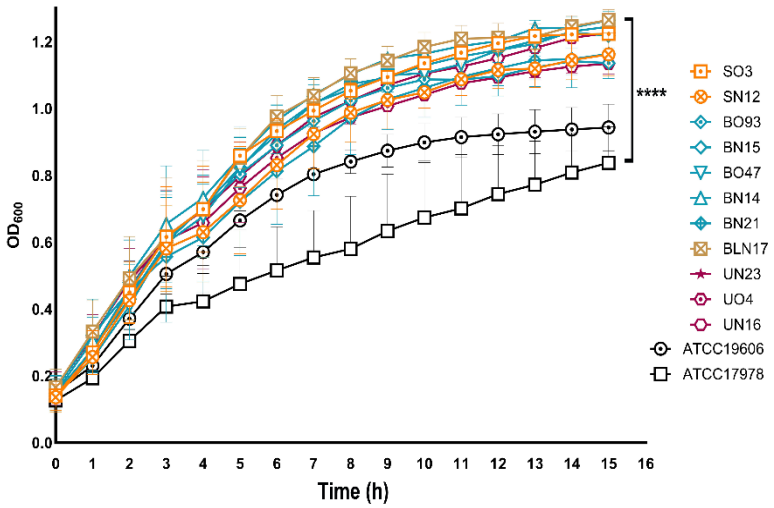

Figure 3.2. Growth rates of the clinical isolates. Overnight cultures were diluted to 1:100 in LB in a 96-wells microplate. The OD_{600} was determined every 30 min using a plate reader (BioTek SynergyHT). Only the growth curves of the 11 fastest-growing isolates, compared to both reference strains, are presented. Means and standard deviations were obtained from three independent experiments. **** $P < 0.0001$.

3.3.3 Biofilm-forming activity, desiccation tolerance and genomic content of related genes

The ability of *A. baumannii* clinical isolates to form biofilms represent crucial features in clinical settings. Therefore, the biofilm-forming ability on polystyrene microtiter plates of each isolate was measured by Crystal Violet staining (Figure 3.4). Isolates arbitrarily grouped according to A_{570}/A_{600} values as weak (<0. 47), moderate (0.47-0.70), and strong biofilm producers (>0.70) accounted for 16.7% (5/30), moderate for 23.3% (7/30), and strong for 60.0% (18/30), respectively (Figure 3.4A). Nine isolates (SN24, BO47, BO88, BN15, BN14, BN21, BN22, UO2, and UO8) showed significant differences in biofilm formation compared with both reference strains, with the majority belonging to the recently collected BA specimens (71.4%, 5/7). Isolates BO88 and UO2 were significant only in comparison with ATCC 19606 reference strain (Figure 3.4A). Interestingly, we found a significant positive correlation between biofilm producer strains and amikacin resistance ($r = 0.43$, $P = 0.016$). Several genes that contribute to biofilm formation were searched, including *bap/bap*-like proteins (biofilm associate proteins), *csuA-E* (chaperone-usher type I pili), *pil* and *fim* genes (type 4 pili), *pgaA-D* genes (poly-β-1,6-N-acetylglucosamine), *bfmRS* (the two-component system), *ompA* (the major Gram-negative porin), *hlyD* (Type 1 Secretion System) and *abaIRM* (quorum sensing). All isolates carried the *bpl2*, *bfmRS*, *ompA*, *csuD*, *pgaAB*, *pilBCGIJMQRSTUWY1*, and *fimTV* genes (Figure 3.3). Interestingly, the *bap* gene was identified in all but one (the BN20 isolate), while *bap1* and *bpl1* were identified only in BO47 and BO70, respectively (Figure 3.3).

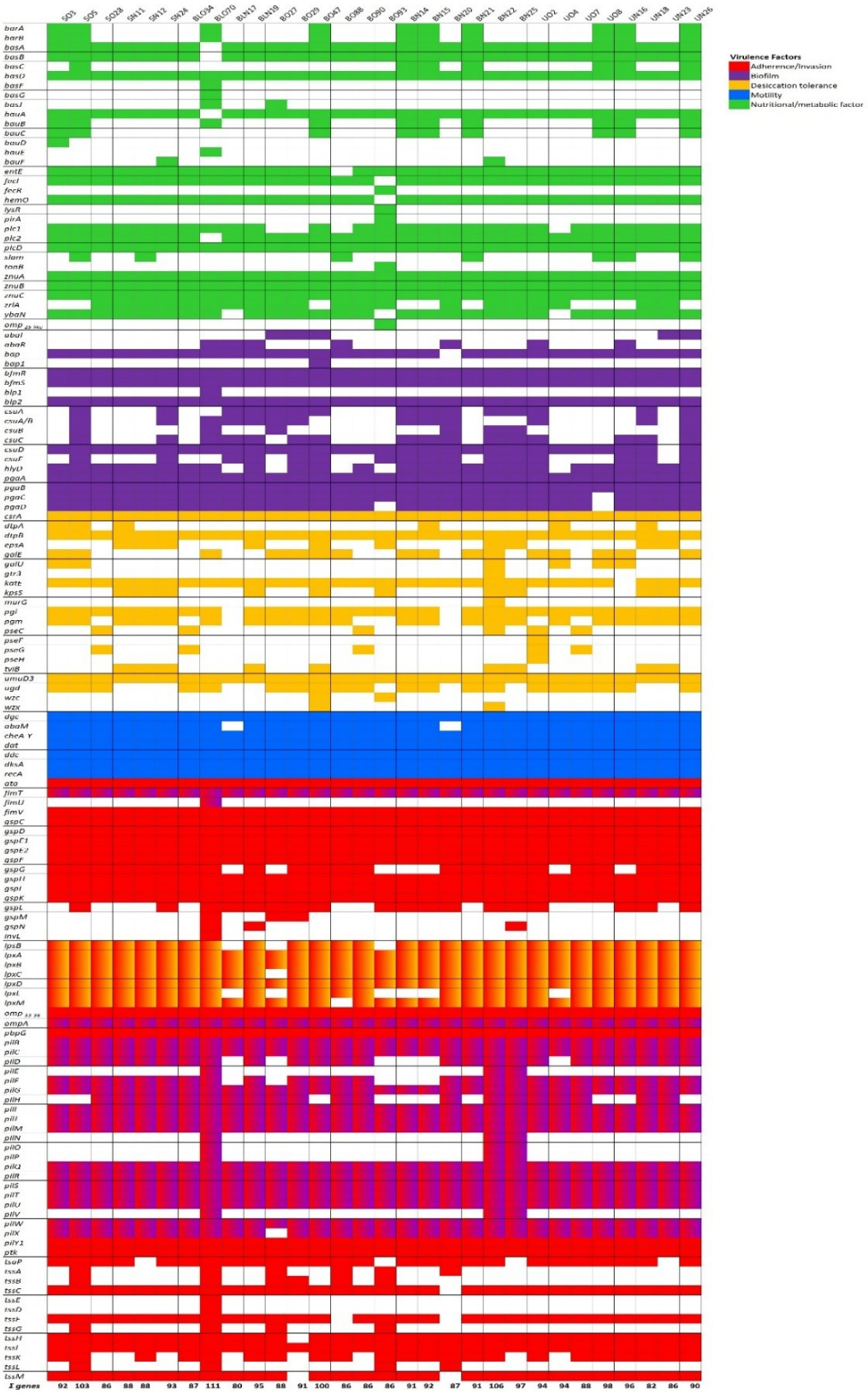

Figure 3.3. Genes directly and indirectly related to virulence detected in the isolate collection. Heat map of virulence genes identified using whole genome sequence analysis. Color-code represents genes involved in different aspects of virulence, adhesion, biofilm, secretion systems, exotoxins, immune modulation, and nutritional/metabolic factors, as indicated.

According to the biofilm results, the genes shared among all the strains displaying the strongest biofilm-forming ability were: *bap/blp2/bfmRS/csuD/pgaAB/fimTV/ompA/pilBCGIJlMlQRSTUWXY1* (9/9), with a prevalence of *hlyD*, *pgaCD* (8/9). Unexpectedly, the *abaIR* genes were found in a minority of strains, UN16, BLN17, BLN19, BLO70, and UO2, the latter only displaying a strong biofilm-forming activity (Figure 3.3). Conversely, the *abaR* gene, without *abaI*, was found only in BN20 and B088. Additionally, we found significant positive correlation between fast-growing and strong biofilm-forming isolates ($r = 0.42$, $P = 0.022$) (Supplementary Figure S2). Another critical feature for healthcare settings is *A. baumannii* desiccation tolerance since it allows long term survival, and therefore increases bacterial spread in the hospital environment [42,43]. Therefore, the tolerance to desiccation for 6 days was tested. Starting with an initial number of bacteria (approximately 10^8–10^9 CFU/ml/strain), the number of recovered bacteria varied (approximately 10^1–10^4 CFU/ml/strain) after six days of dryness and 25% of relative humidity. Seven isolates, SO3, BLN19, BN25, BO29, BO88, BO90, and UO8, displayed significant differences in their desiccation tolerance (Figure 3.4B). No reference strains were recovered. Among desiccation-tolerant strains, 57.1% (4/7) respiratory and 14.3% (1/7) urinary isolates, respectively, were retrieved before 2013. Genes directly and indirectly related to desiccation tolerance were searched, including *bfmRS, csrA* (carbon storage regulator A), *epsA* (exopolysaccharide), *katE* (catalase), *recA* (main recombinase), murG (*peptidoglycan*), *lpx/lpsB* (lipopolysaccharide), *wzc/wzx/gtr3/kpsS/pgm/pse* (capsule), *galU/ugd/pgi/pgm* (sugar precursors), *dtpAB* (hydrophilins), *umuCD* (error-prone DNA polymerase V), *adeABC* and *adeIJK* (efflux pumps*)* genes [44–46] (Figures 1, 3). Genes conserved in all isolates were *csrA, dtpB, umuD3, lpxABD, recA* and *adeG*, while prevalent *pgm, katE, lpxCM*, and *adeIJK*, (29/30, 97%) (Figure 3.3) [10,47]. According to the desiccation results, the most common genotype among the strains displaying the highest desiccation tolerance was: *bfmRS/csrA/katE/lpxABCD/pgi/dtpB/umuD3/adeAB/adeIJK.*

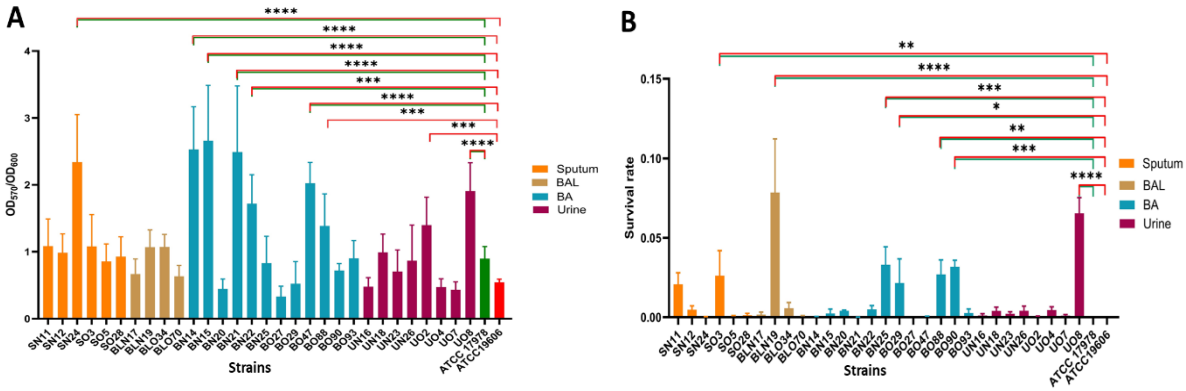

Figure 3.4. Ability of *A. baumannii* isolates to form biofilms and tolerate desiccation conditions. (A) *A. baumannii* strains were inoculated on polystyrene plates. Data are means ± standard deviation from at least three independent experiments, eight wells per strain (n=24). (B) Approximately 10^7–10^9 CFU/strain were inoculated in a 96 microplate. Plates were kept at 25°C with a relative humidity (RH) of 25 ± 3% for 6 days. Each isolate was recovered from three wells. Data are the ratio between the final and initial CFU/ml. Three independent experiments were performed in duplicate (n=6). Asterisks represent p values evaluated by one-way ANOVA in comparison to ATCC 17978 (green) and to ATCC 19606 (red); * P <0.05, ** P <0.01, *** P <0.001, **** P <0.0001.

3.3.4 Surface-associated motility and genomic content of related genes

A. baumannii can move via surface-associated motility, an appendage-independent kind of movement [48]. Hence, the surface-associated motility of isolates was tested on soft agar plates. Isolates SN11, SN12, UN23, and BN25 displayed a not motile phenotype, while UO4, UO7, BO47, and BO90 a very slow motility (Figure 5). Conversely, the other isolates displayed surface-associated motility characterized by peculiar shapes, including tentacle-like (37%, 11/30), root-shaped (20%, 6/30), halo-shaped (10%, 3/30), and multi-layered (2/30) (Figure 3.5). Notably, the different patterns of motility were equally distributed between past and current isolates. Several genes have been shown to be involved in surface-associated motility, including *ddc/dat* (production of 1,3-diaminopropane), *dgc* (diguanylate cyclase), *cheA/Y* (two component system), *dksA* (DnaK suppressor protein), *abaIRM*, *recA*, *ompA* [48]. Interestingly, all the aforementioned genes were conserved in all isolates with the exception of *abaM* gene that was not found in BNL17 and BN20 (28/30, 93%) (Figure 3.3). According to the surface-associated motility, the most common genotype of motile isolates was: *dgc, cheA-Y, dat, ddc, dksA* and *recA*.

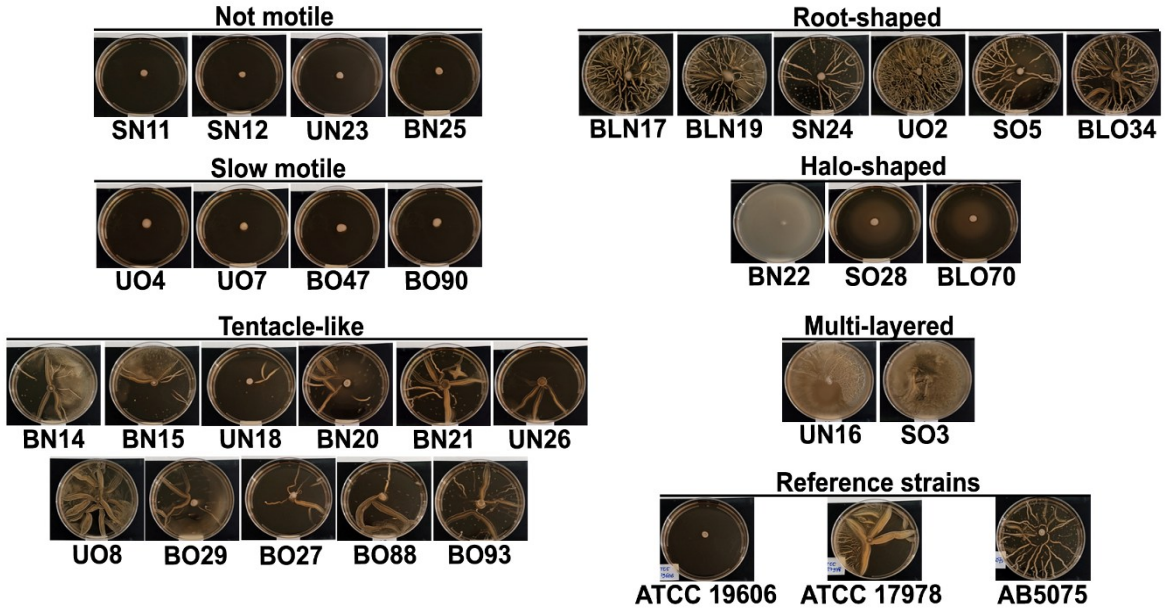

Figure 3.5. Surface-associated motility of clinical isolates. Each isolate was spotted on top of a soft agar plate. After 24 h of incubation at 37°C, plates were photographed. Three independent experiments were performed in duplicate (n=6). Representative images are shown. Reference strain AB5075 was included in the experiment for its different shape of surface-associated motility.

3.3.5 Host cell line invasiveness and genomic content of related genes

Some *A. baumannii* clinical isolates can enter epithelial cells to evade host immune responses and limit antibiotic accessibility [10,47]. Therefore, infection experiments using human lung and bladder epithelial cells were conducted to quantify the number of intracellular bacteria after 48 hours (Figure 3.6). Compared to the two reference strains, ATCC 17978 and ATCC 19606, a significantly higher invasive capacity in lung epithelial cells was observed in 23% (7/30) of the tested strains, most of which were retrieved from respiratory specimens (5/7, 71%), reaching values greater than 3×10^6 CFU/ml (Figure 3.6A). Additionally, the majority of these invasive strains were recently isolated (6/7, 86%). The same experiment with bladder epithelial cells revealed that 27% of the analyzed strains could invade this host cell line (8/30). In this experimental set, eight isolates demonstrated greater invasiveness compared to both reference strains, 75% (6/8) of these were old strains and 38% (3/8) were retrieved from the urinary tract (Figure 3.6B). Intriguingly, among invasive strains, SN11, and UO8 were able to invade both host epithelial models, suggesting a cell-type non-specific invasion phenotype (Figure 3.6). Genes directly and indirectly related to invasiveness were searched (Figure 3.3), including *ata* (*Acinetobacter* trimeric autotransporter), *gsp* (T2SS), *tss* (T6SS), *invL* (adhesin), *pbpG*, *lps*, *omp33-36/ompA*, *plc*, *pil* genes. According to the invasion experiments, the most common genotype displayed by invasive isolates was: *ata, fimTV, gspCDE1E2FHIK, lpsABCDM, omp33-36, ompA, pbpG, pilBCGIJMQRSTUWXY1, ptk*, and *tssCFHIM* (Figure 3.3).

Unexpectedly, *invL* was found only in BO70 (Figure 3.3). No major genetic differences between the cell-type non-specific invasion phenotypes and the other invasive isolates were found (Figure 3.3). Notably, significant negative correlations were found between urinary (r = -0.44, P = 0.014) and recent isolates (r = -0.36, P = 0.048) and the invasiveness of lung and bladder epithelial cells, respectively. Moreover, we found significant positive correlation (r = 0.40, P = 0.030) between strong biofilm-forming isolates and invasiveness of A549 cells (Supplementary Figure S2).

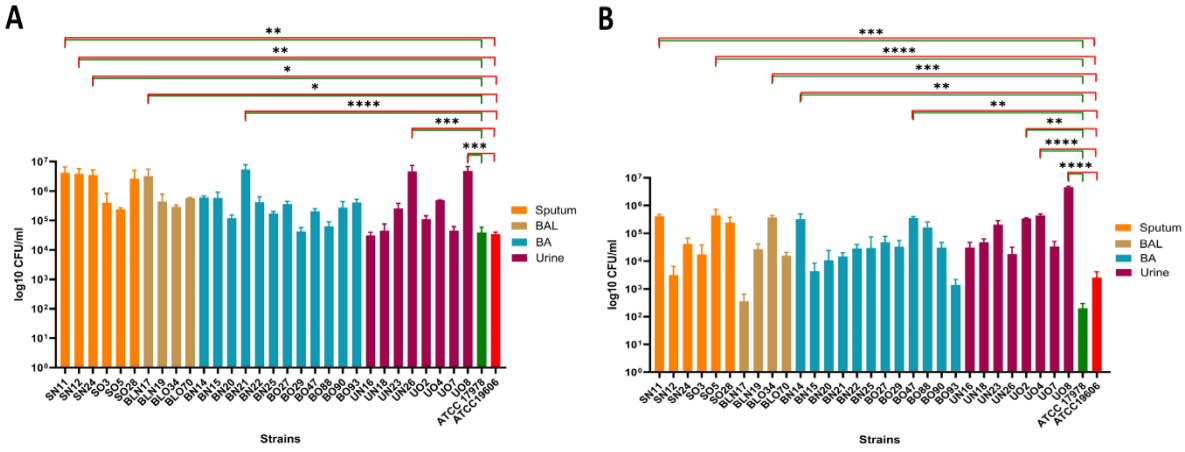

Figure 3.6. Ability of clinical isolates to be internalized in lung and bladder epithelial cells. Semi-confluent A549 (A) and HTB-9 (B) cell monolayers were infected with each isolate or ATCC 17978 or ATCC 19606 reference strains using a multiplicity of infection (MOI) of 10. Uninfected cells were used as control. After 2 h of adhesion, the medium was supplemented with colistin (10 µg/ml) to kill extracellular bacteria. Intracellular bacteria were enumerated after additional 48-h of incubation. Data (CFU/ml) are means ± standard deviation from at least five independent experiments, in duplicate (n=10). Asterisks represent p values evaluated by one-way ANOVA in comparison to ATCC 17978 (green) and to ATCC 19606 (red); * P <0.05, ** P <0.01, *** P <0.001, **** P <0.0001.

3.3.6 Proteolytic and hemolytic activities and genomic content of related genes

As an additional assay of virulence traits, protease and hemolytic activities were assayed on skim milk and blood agar plates, respectively. No proteolytic and hemolytic activities could be detected in the clinical isolates in comparison with *Pseudomonas aeruginosa* PAO1 and *Escherichia coli* H20P used as positive controls [23]. The *hlyD* gene, reported to be a putative hemolysis-related gene [49], was found in 83% (25/30) of the isolates (Figure 3.3). Additionally, among the *plc* genes [50], *plc1* was absent only in isolates BO29 and UO4, while *plc2* was absent only in BO70 (Figure 3.3). Conversely, *plcD* was common to all isolates (Figure 3.3). We noticed a high degree of heterogeneity among the clinical isolates in the shape of the macrocolonies [51]; in particular, four previously reported and one new macrocolony types (MTs) were identified [51] (Figure 3.7). This new macrocolony shape (MT G), shared by 50% of the strains (15/30), was characterized by a deep opaque center expanding to the round edge (Figure 3.7; Table 3.3). Interestingly, both *plc2* and *plcD* were shared among strains

displaying MT G (Figure 3.3). No morphology resembling types A and C was observed in any of our isolates [51]. The second prevalent MT was MT E, followed by MT F; only one isolate had a MT B (BN15), and one MT D (BN20) (Figure 3.7; Table 3.3). This MT pattern was homogeneously shared between past and recent isolates (8 and 7, respectively). Additionally, no correlation between MTs and surface-associated motility patterns was found (Figures 3.5, 3.7; Supplementary Figure S2) ($r = 0.080$, $P = 0.256$).

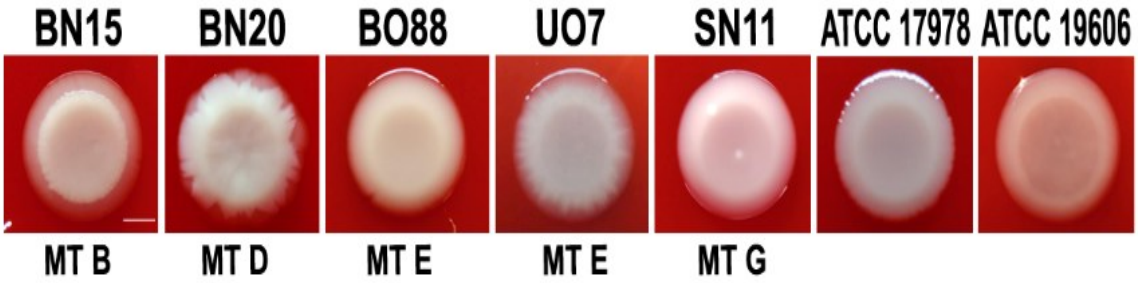

Figure 3.7. Macrocolony types (MTs) of clinical isolates on blood agar plates. One µl of each isolate was spotted on Columbia Agar with 5% sheep blood. After 24 h, macrocolonies were photographed. Representative images of one representative isolate per different MTs. Scale bar, 1 cm.

Table 3. Macrocolony types (MTs) (52).

MTs	Isolates
A	-
B	BN15
C	-
D	BN20
E	SO5, BLN17, BLO70, BO88, BN22, BO27, BN25, BO90, UO2, UN16, ATCC 17978
F	BN14, UO7, UN18
G	SO3, SO28, SN11, SN12, SN24, BLO34, BO47, BO93, BO29, BN21, BLN19, UN23, UO4, UO8, UN26, ATCC 19606

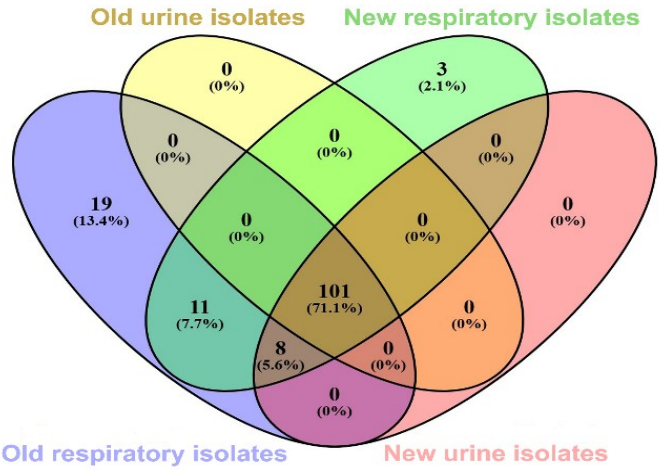

Figure 3.8. Venn diagram showing the number of common genes shared among the isolate collection. Each group is depicted by a different oval color, as indicated. Genes included are those reported in Figs. 1 and 3. Numbers in the non-overlapping regions show the number of genes unique to that strain group. The given percentage was calculated by considering the total number of genes (142) as 100%. The graph was generated using Venn 2.1. online software.

3.4 Discussion

From an evolutionary perspective, *A. baumannii* demonstrates remarkable adaptability, acquiring a wide range of virulence factors through high genomic plasticity. Understanding how this pathogen evolves to gain virulence and AR is critical for developing strategies to combat this public health threat. Thirty clinical isolates, 22 respiratory, and 8 urinary, were analyzed. The proportion of strains aligns with previous reports, where respiratory isolates dominate (39.5%) over uropathogenic isolates ranging from 6.1% to 29.3% [52]. In line with current reports, the ST2 was the most represented in our collection [17,19]. All the isolates displayed an XDR phenotype, with a high number of ARGs in each genome (Table 3.2; Figure 3.1). Among the 71 identified ARGs, old isolates have a higher gene content (> 30) with respect to recent ones (27 vs. 19 genes, respectively), particularly old respiratory isolates exhibited 12.5% increases in the average number of ARGs compared to recent urine isolates ($P = 0.02$) (Figure 3.1; Supplementary Figure S1A). Vice versa, recent respiratory isolates carried an overall higher content of resistance genes for beta-lactams, carbapenems, quinolones, and tetracyclines, compared with old ones (Figure 3.1). Increased resistance to quinolones and carbapenems is in accordance with the ECDC report of invasive strains (https://atlas.ecdc.europa.eu/public/index.aspx). Furthermore, the number of aminoglycoside resistance genes positively correlated with the MIC of gentamicin (r = 0.43, $P = 0.02$) and amikacin (r = 0.70, $P = 0.00002$), supporting their role in conferring resistance. Notably, recent respiratory isolates exhibited lower amikacin MICs, likely due to the reduced prevalence of aminoglycoside resistance genes (Table 3.2; Figure 3.1). In the past, the synergistic effects of combined treatment with aminoglycosides and carbapenems or colistin for *A. baumannii* infections were exploited [53]. Hence, the

lower prevalence of aminoglycoside resistance genes in our recent strains may reflect the decline in the use of this therapeutic approach, given its lack of significant improvement in clinical outcomes [54].

The lower content of macrolide resistance genes in recent isolates may be linked to the WHO's 2017 recommendation against macrolides (www.iris.who.int, Figure 3.1). The genetic adjustments made by recent isolates over old ones might be due to lower contacts with donor species and/or that global and local antibiotic guidelines changes for carbapenem-resistant *A. baumannii* [55]. Notably, all isolates remained susceptible to colistin; however, two isolates (SO5 and UO7) had MICs near the resistance breakpoint (EUCAST 2023), highlighting the presence of two colistin-heteroresistant strains. EUCAST clinical breakpoints were used for antibiotic susceptibility testing, as they are standard in Europe and facilitate interlaboratory comparisons; however, it is worth mentioning that, although EUCAST and CLSI breakpoints are aligned for carbapenem-resistant *A. baumannii*, notable discrepancies between the two methodologies exist for specific aminoglycoside and tetracycline subclasses, which should be duly considered [3,56–58]. Moreover, the content of genes encoding efflux pumps was stable among isolates. While the *adeE* gene, typically of *Acinetobacter nosocomialis*, was missing, the majority of isolates (25/30) carried the *adeB* gene, which was found shared among bacteria belonging to the *Acinetobacter* genus [59,60].

Distinctive traits of recent isolates include faster growth ($P < 0.0001$), a partial association with MT G (7/11), an average of 16.9 nutritionally-related genes, a strong biofilm-forming activity, and a lower desiccation tolerance than older ones (Figures 3.2–3.4A). These findings recall the behavior of multi-drug resistant (MDR) *A. baumannii* environmental isolates, in which this phenotype comes with a fitness cost that causes a significantly decrease in desiccation tolerance even with strong biofilm activity [61]. Being these clinical isolates, a possible explanation is that these strains experienced less desiccation stress pressures in their growth environment. Seven isolates, mostly from the past respiratory collection, survived six days of desiccation with an average survival rate of 3.44% (Figure 3.4B). Among the 21 desiccation-related genes identified, these isolates carried an average of 8.6 genes (Figure 3.3). Notably, the BfmR-dependent hydrophilin *dtpB* gene, involved in desiccation tolerance [46], was found in all strains (Figure 3.3). However, only two strains, BO88 and UO8, retained both biofilm-forming and desiccation tolerance abilities (Figures 3.3, 3.4). Desiccation tolerance was reported to be a typical characteristic of clinical *A. baumannii* strains [62]. However, from our data, it seems that the hospital environment may not exert desiccation pressure, offering enough water or humidity for bacterial survival and growth, potentially selecting mainly for stronger biofilm-forming strains.

The positive correlation found between growth rate and biofilm formation ($r = 0.42$, $P = 0.022$) corroborates previous findings that biofilm development depends on bacterial growth rates [56]. Conversely, urinary strains, while having the highest nutritionally-related gene content, were not proficient biofilm formers (Figure 3.4A). In dominant and non-dominant *A. baumannii* STs, despite a very similar content and expression patterns of biofilm-related genes, such as *adeFGH, bap, csu, pga/b/c/d, abaR*, and *abaI*, the actual biofilm-forming activity was not significantly different [63]. Strong biofilm-formers had an average of 12.3 biofilm genes (range: 8-15, Figure 3.3; Supplementary Figure 3.S1B), and it seems that at least 8 genes are sufficient for proficient biofilm formation. Moreover, the positive correlation between strong biofilm producers and invasion of lung epithelial cells ($r = 0.40$, $P = 0.030$) strengthen the notion that biofilm matrix can effectively shield bacteria, allowing persistence, and, eventually, invasion host cells [3].

Surface-associated motility was observed in 26 isolates, with variability from slow to hypermotile phenotypes (Figure 3.5). Variability in surface-associated morphotypes suggests that efflux pumps, quorum-sensing molecules and surfactant-like compounds and proteins may influence motility and phenotypic diversity [60,64,65]. Seven genes related to surface-associated motility were identified (Supplementary Figure 3.S1B) [48,66,67], but two isolates (BN20 and BLN17) lacked the *abaM* gene (Figure 3.3). The lack of surface-associated motility of isolate BLN17 could be due to the absence of genes encoding the AdeRS two-component system that regulates the RND efflux pump AdeABC, as previously described [68]. Chemotaxis in *E. coli* is subject to a behavioral variability and phenotypic diversity [69]; the pathogen swimming depends on external signal processing as well as the proton motif force and the levels of individual expression of the involved proteins, known as potential modulators of chemotactic variability [69]. Although *A. baumannii* lacks flagella, it is plausible that variability of surface-associated motility could be due to the to a combination of the activity of efflux pumps that, in turn, cause a variable secretion of surfactants, proteins or quorum sensing molecules [64,65,70].

Thirteen isolates demonstrated higher invasiveness into epithelial cells compared to reference strains (Figure 3.6). Recent respiratory isolates were more invasive in lung cells, while older isolates showed more invasiveness in bladder cells, with observed invasive colony numbers of 4×10^6 and 1×10^6, respectively (Figure 3.6). Interestingly, two strains, SN11 and UO8, exhibited a non-specific cell-type invasion phenotype, being capable of invading both cell lines (Figure 3.6). Overall, these results suggest a shift in recent respiratory strains toward lung tropism *in vitro*, reflecting their preferred colonization/infection site *in vivo* [52]. Several bacterial pathogens exhibit host cell tropism, dependent on specific surface appendages/proteins that ensure the interaction between pathogens and their respective hosts, like type 1 fimbriae for uropathogenic *E. coli* [71]. Among 63 conserved genes corresponded to invasiveness, 79% were across all isolates, encoding components of lipopolysaccharide (LPS), type II secretion system (T2SS), type IV secretion system (T4SS), and type VI secretion system (T6SS)

(Figure 3.3; Supplementary Figure 3.S1B). Several of these genes were shown to be involved in adhesion/invasion in *A. baumannii* [10,15,68]. Notably, the *invL* gene, encoding an invasin-like adhesin dependent on T2SS, involved in adhesion to urothelial cell cultures, was identified only strain BO47 [72] (Figure 3.3). Differently, the T2SS genes were found in all strains (*gspCDE1E2FHIK*), underlining the importance of this system for *A. baumannii* physiology and pathogenesis; indeed, T2SS contributes to *A. baumannii in vivo* fitness as well as protection to the human bactericidal activity [73,74]. Thus, other T2SS-dependent proteins might be involved in *A. baumannii* invasiveness; moreover, the high degree of conservation makes this an ideal target for innovative anti-*A. baumannii* therapeutics. It is worth mentioning that this study has some potential limitations, including a limited sample size, as well as geographical and time constraints. However, this study provides evidence of significant adaptations driven by clinical pressures. The findings herein reported could contribute to highlight key traits that could be targeted for improved infection control and treatment strategies.

In conclusion, significant genetic variability was observed between past and recent isolates, with 71.2% of identified genes distributed across all strains. Interestingly, 19 genes were unique to the old respiratory strains (Figure 3.8), mainly involved in adhesion and nutrient uptake (e.g. *fimU, gspM, tssBDEG, basFGJ, bauDE, bap1, wzc, pseG, lysR, fecR, pirA, tonB*, and *omp25-like*). The overlap between old and recent respiratory isolates was limited to 11 shared genes, including *pilE, pilNOPV, gspN, tssAL, tagX, pseC*, and *wzx*. Eight genes were conserved across recent urinary and respiratory strains (*tviB, kpsS, hemO, epsA, fecI, ybaN*, hlyD, and *slam*). Remarkably, no gene overlap was observed between past and recent urinary isolates, justifying the marked difference in the phenotypic traits. Old isolates were more desiccation-tolerant, and metabolically variable likely due to adaptation to broader nutrient sources and environmental conditions. In contrast, recent respiratory isolate exhibited increased growth, biofilm formation, and invasiveness, reflecting the dynamic evolution to clinical stress pressures. Overall, these findings support the genetic adaptation of *A. baumannii* in response to environmental pressures, including antibiotic use and host immune responses. Understanding these genetic changes will provide valuable insights for future therapeutic approaches and infection control strategies.

Supplementary materials

Figure 3.S1. Comparison of antibiotic-resistance and virulence genes among isolates. Each bar shows the average of the pooled number of genes encoding antibiotic resistance (A) and virulence (B), according to the type of isolate. Numbers at the top of the bar represents the total number of genes identified per functional category in all isolates. The graph was generated using Microsoft Excel.

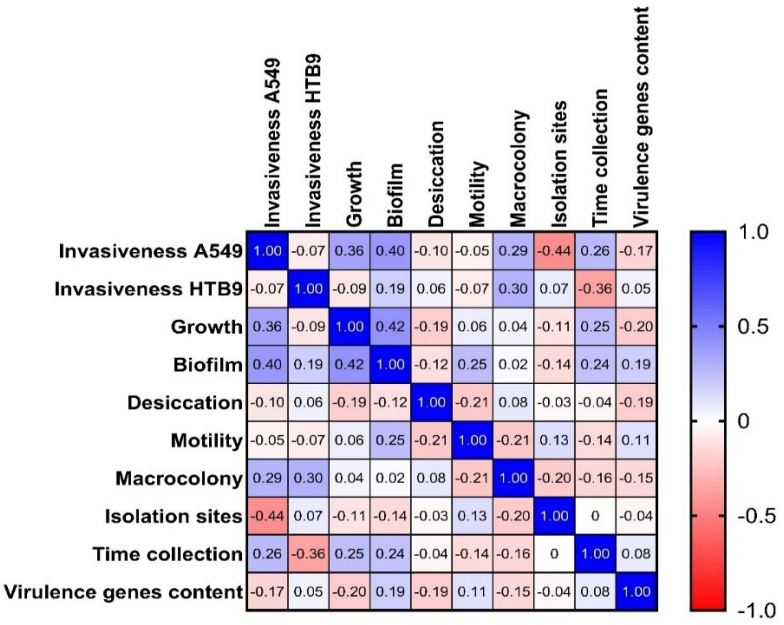

Figure 3.S2. Phenotypic and genotypic correlation matrix of major phenotypes. Parameters included in the analysis are reported. Data were transformed with the log(Y) function and analyzed using Pearson's correlation. The colors represent Pearson's correlation coefficient; its intensity depicts the coefficient's value (shades of blue are positive correlations and shades of red are negative correlations). The graph was generated using GraphPad Prism version 10.3.1.

References

1. Duan, Z. *et al.* Nosocomial surveillance of multidrug-resistant *Acinetobacter baumannii* : a genomic epidemiological study. *Microbiol. Spectr.* **12**, e02207-23 (2024).
2. Obenhuber, T. *et al.* An outbreak of multi-drug-resistant Acinetobacter baumannii on a burns ICU and its control with multi-faceted containment measures. *J. Hosp. Infect.* **146**, 102–108 (2024).
3. Yang, Z. *et al.* Characterization and genome annotation of a newly detected bacteriophage infecting multidrug-resistant Acinetobacter baumannii. *Arch. Virol.* **164**, 1527–1533 (2019).
4. Zeighami, H., Valadkhani, F., Shapouri, R., Samadi, E. & Haghi, F. Virulence characteristics of multidrug resistant biofilm forming Acinetobacter baumannii isolated from intensive care unit patients. *BMC Infect. Dis.* **19**, 629 (2019).
5. Valencia-Martín, R. *et al.* A multimodal intervention program to control a long-term Acinetobacter baumannii endemic in a tertiary care hospital. *Antimicrob. Resist. Infect. Control* **8**, 199 (2019).
6. Alrahmany, D., Omar, A. F., Alreesi, A., Harb, G. & Ghazi, I. M. Acinetobacter baumannii Infection-Related Mortality in Hospitalized Patients: Risk Factors and Potential Targets for Clinical and Antimicrobial Stewardship Interventions. *Antibiotics* **11**, 1086 (2022).
7. Murray, C. J. L. *et al.* Global burden of bacterial antimicrobial resistance in 2019: a systematic analysis. *The Lancet* **399**, 629–655 (2022).
8. Hu, Y. *et al.* Non-antibiotic prevention and treatment against Acinetobacter baumannii infection: Are vaccines and adjuvants effective strategies? *Front. Microbiol.* **14**, 1049917 (2023).
9. Ambrosi, C. *et al.* Acinetobacter baumannii Virulence Traits: A Comparative Study of a Novel Sequence Type with Other Italian Endemic International Clones. *Front. Microbiol.* **8**, 1977 (2017).
10. Ambrosi, C. *et al.* Acinetobacter baumannii Targets Human Carcinoembryonic Antigen-Related Cell Adhesion Molecules (CEACAMs) for Invasion of Pneumocytes. *mSystems* **5**, e00604-20 (2020).
11. Stracquadanio, S. *et al.* Acinetobacter baumannii and Cefiderocol, between Cidality and Adaptability. *Microbiol. Spectr.* **10**, e02347-22 (2022).
12. Scribano, D. *et al.* Acinetobacter baumannii OmpA-like porins: functional characterization of bacterial physiology, antibiotic-resistance, and virulence. *Commun. Biol.* **7**, 948 (2024).
13. Hamidian, M., Nigro, S. J. & Hall, R. M. Variants of the gentamicin and tobramycin resistance plasmid pRAY are widely distributed in Acinetobacter. *J. Antimicrob. Chemother.* **67**, 2833–2836 (2012).
14. Ambrose, S. J., Hamidian, M. & Hall, R. M. The extensively antibiotic resistant ST111 Acinetobacter baumannii isolate RBH2 carries an extensive mobile element complement of plasmids, transposons and insertion sequences. *Plasmid* **128**, 102707 (2023).
15. Sarshar, M., Behzadi, P., Scribano, D., Palamara, A. T. & Ambrosi, C. Acinetobacter baumannii: An Ancient Commensal with Weapons of a Pathogen. *Pathogens* **10**, 387 (2021).
16. Cain, A. K. & Hamidian, M. Portrait of a killer: Uncovering resistance mechanisms and global spread of Acinetobacter baumannii. *PLOS Pathog.* **19**, e1011520 (2023).
17. Hansen, F. *et al.* Characterisation of carbapenemase-producing Acinetobacter baumannii isolates from danish patients 2014–2021: detection of a new international clone – IC11. *Int. J. Antimicrob. Agents* **62**, 106866 (2023).
18. Karah, N. *et al.* Emergence of *Acinetobacter baumannii* International Clone 10 predominantly found in the Middle East. Preprint at https://doi.org/10.1101/2023.10.09.561570 (2023).

19. Müller, C. *et al.* A global view on carbapenem-resistant *Acinetobacter baumannii*. *mBio* **14**, e02260-23 (2023).

20. Holt, K. E. *et al.* Corrigendum: Five decades of genome evolution in the globally distributed, extensively antibiotic-resistant Acinetobacter baumannii global clone 1. *Microb. Genomics* **5**, (2019).

21. Penesyan, A., Nagy, S. S., Kjelleberg, S., Gillings, M. R. & Paulsen, I. T. Rapid microevolution of biofilm cells in response to antibiotics. *Npj Biofilms Microbiomes* **5**, 34 (2019).

22. Pompilio, A. *et al.* Gram-Negative Bacteria Holding Together in a Biofilm: The Acinetobacter baumannii Way. *Microorganisms* **9**, 1353 (2021).

23. Scribano, D. *et al.* Insights into the Periplasmic Proteins of Acinetobacter baumannii AB5075 and the Impact of Imipenem Exposure: A Proteomic Approach. *Int. J. Mol. Sci.* **20**, 3451 (2019).

24. Bolger, A. M., Lohse, M. & Usadel, B. Trimmomatic: a flexible trimmer for Illumina sequence data. *Bioinformatics* **30**, 2114–2120 (2014).

25. Bankevich, A. *et al.* SPAdes: A New Genome Assembly Algorithm and Its Applications to Single-Cell Sequencing. *J. Comput. Biol.* **19**, 455–477 (2012).

26. Ambrosi, C. *et al.* Molecular characterisation of extensively drug-resistant Acinetobacter baumannii: First report of a new sequence type in Italy. *J. Glob. Antimicrob. Resist.* **7**, 154–156 (2016).

27. Taguchi, A. *et al.* FtsW is a peptidoglycan polymerase that is functional only in complex with its cognate penicillin-binding protein. *Nat. Microbiol.* **4**, 587–594 (2019).

28. Warburton, P. J. *et al.* TetAB(46), a predicted heterodimeric ABC transporter conferring tetracycline resistance in Streptococcus australis isolated from the oral cavity. *J. Antimicrob. Chemother.* **68**, 17–22 (2013).

29. Huys, G. *et al.* Distribution of tetracycline resistance genes in genotypically related and unrelated multiresistant Acinetobacter baumannii strains from different European hospitals. *Res. Microbiol.* **156**, 348–355 (2005).

30. Sun, B. *et al.* New Mutations Involved in Colistin Resistance in Acinetobacter baumannii. *mSphere* **5**, e00895-19 (2020).

31. Hahm, C., Chung, H.-S. & Lee, M. Whole-genome sequencing for the characterization of resistance mechanisms and epidemiology of colistin-resistant Acinetobacter baumannii. *PLOS ONE* **17**, e0264335 (2022).

32. Liao, J. *et al.* Chloramphenicol Binding Sites of *Acinetobacter baumannii* Chloramphenicol Acetyltransferase CatB8. *ACS Infect. Dis.* **10**, 870–878 (2024).

33. Sharma, A., Sharma, R., Bhattacharyya, T., Bhando, T. & Pathania, R. Fosfomycin resistance in *Acinetobacter baumannii* is mediated by efflux through a major facilitator superfamily (MFS) transporter—AbaF. *J. Antimicrob. Chemother.* **72**, 68–74 (2017).

34. Short, F. L. *et al.* The Acinetobacter baumannii disinfectant resistance protein, AmvA, is a spermidine and spermine efflux pump. *Commun. Biol.* **4**, 1114 (2021).

35. Salehi, B., Ghalavand, Z., Yadegar, A. & Eslami, G. Characteristics and diversity of mutations in regulatory genes of resistance-nodulation-cell division efflux pumps in association with drug-resistant clinical isolates of Acinetobacter baumannii. *Antimicrob. Resist. Infect. Control* **10**, 53 (2021).

36. Marchand, I., Damier-Piolle, L., Courvalin, P. & Lambert, T. Expression of the RND-Type Efflux Pump AdeABC in *Acinetobacter baumannii* Is Regulated by the AdeRS Two-Component System. *Antimicrob. Agents Chemother.* **48**, 3298–3304 (2004).

37. Shafaati, M., Boroumand, M., Nowroozi, J., Amiri, P. & Kazemian, H. Correlation Between qacE and qacEΔ1 Efflux Pump Genes, Antibiotic and Disinfectant Resistant Among Clinical Isolates of E.coli. *Recent Patents Anti-Infect. Drug Disc.* **11**, 189–195 (2016).

38. Neidhöfer, C. *et al.* Exploring clonality and virulence gene associations in bloodstream infections using whole-genome sequencing and clinical data. *Front. Cell. Infect. Microbiol.* **13**, 1274573 (2023).

39. Sheldon, J. R. & Skaar, E. P. Acinetobacter baumannii can use multiple siderophores for iron acquisition, but only acinetobactin is required for virulence. *PLOS Pathog.* **16**, e1008995 (2020).

40. Bateman, T. J. *et al.* A Slam-dependent hemophore contributes to heme acquisition in the bacterial pathogen Acinetobacter baumannii. *Nat. Commun.* **12**, 6270 (2021).

41. Cook-Libin, S., Sykes, E. M. E., Kornelsen, V. & Kumar, A. Iron Acquisition Mechanisms and Their Role in the Virulence of Acinetobacter baumannii. *Infect. Immun.* **90**, e00223-22 (2022).

42. Farrow, J. M., Wells, G. & Pesci, E. C. Desiccation tolerance in Acinetobacter baumannii is mediated by the two-component response regulator BfmR. *PLOS ONE* **13**, e0205638 (2018).

43. Bashiri, S. *et al.* Growth Phase- and Desiccation-Dependent *Acinetobacter baumannii* Morphology: An Atomic Force Microscopy Investigation. *Langmuir* **37**, 1110–1119 (2021).

44. Tipton, K. A., Chin, C.-Y., Farokhyfar, M., Weiss, D. S. & Rather, P. N. Role of Capsule in Resistance to Disinfectants, Host Antimicrobials, and Desiccation in Acinetobacter baumannii. *Antimicrob. Agents Chemother.* **62**, e01188-18 (2018).

45. Singh, J. K., Adams, F. G. & Brown, M. H. Diversity and Function of Capsular Polysaccharide in Acinetobacter baumannii. *Front. Microbiol.* **9**, 3301 (2019).

46. Green, E. R. *et al.* Bacterial hydrophilins promote pathogen desiccation tolerance. *Cell Host Microbe* **30**, 975-987.e7 (2022).

47. Rubio, T. *et al.* Incidence of an Intracellular Multiplication Niche among Acinetobacter baumannii Clinical Isolates. *mSystems* **7**, e00488-21 (2022).

48. Jeong, G.-J., Khan, F., Tabassum, N. & Kim, Y.-M. Motility of Acinetobacter baumannii: regulatory systems and controlling strategies. *Appl. Microbiol. Biotechnol.* **108**, 3 (2024).

49. Schramm, S. T. J. *et al.* Genetic and Phenotypic Features of a Novel Acinetobacter Species, Strain A47, Isolated From the Clinical Setting. *Front. Microbiol.* **10**, 1375 (2019).

50. Fiester, S. E. *et al.* Iron-Regulated Phospholipase C Activity Contributes to the Cytolytic Activity and Virulence of Acinetobacter baumannii. *PLOS ONE* **11**, e0167068 (2016).

51. Valcek, A. *et al.* Phenotypic Characterization and Heterogeneity among Modern Clinical Isolates of Acinetobacter baumannii. *Microbiol. Spectr.* **11**, e03061-22 (2023).

52. Bagińska, N., Cieślik, M., Górski, A. & Jończyk-Matysiak, E. The Role of Antibiotic Resistant *A. baumannii* in the Pathogenesis of Urinary Tract Infection and the Potential of Its Treatment with the Use of Bacteriophage Therapy. *Antibiotics* **10**, 281 (2021).

53. Zhang, Y. *et al.* Insights into the epidemiology, risk factors, and clinical outcomes of carbapenem-resistant Acinetobacter baumannii infections in critically ill children. *Front. Public Health* **11**, 1282413 (2023).

54. Shields, R. K., Paterson, D. L. & Tamma, P. D. Navigating Available Treatment Options for Carbapenem-Resistant *Acinetobacter baumannii-calcoaceticus* Complex Infections. *Clin. Infect. Dis.* **76**, S179–S193 (2023).

55. Kim, M., Park, J. & Park, W. Genomic and phenotypic analyses of multidrug-resistant *Acinetobacter baumannii* NCCP 16007 isolated from a patient with a urinary tract infection. *Virulence* **12**, 150–164 (2021).

56. Farshadzadeh, Z. *et al.* Growth Rate and Biofilm Formation Ability of Clinical and Laboratory-Evolved Colistin-Resistant Strains of Acinetobacter baumannii. *Front. Microbiol.* **9**, 153 (2018).

57. Bulens, S. N. *et al.* Carbapenem-resistant Acinetobacter baumannii complex in the United States—An epidemiological and molecular description of isolates collected through the Emerging Infections Program, 2019. *Am. J. Infect. Control* **52**, 1035–1042 (2024).

58. Halim, J. *et al.* Combinations of Antibiotics Effective against Extensively- and Pandrug-Resistant Acinetobacter baumannii Patient Isolates. *Microorganisms* **12**, 1353 (2024).

59. Hou, P. F., Chen, X. Y., Yan, G. F., Wang, Y. P. & Ying, C. M. Study of the Correlation of Imipenem Resistance with Efflux Pumps AdeABC, AdeIJK, AdeDE and AbeM in Clinical Isolates of *Acinetobacter baumannii*. *Chemotherapy* **58**, 152–158 (2012).

60. Cosgaya, C. *et al.* In vitro and in vivo Virulence Potential of the Emergent Species of the Acinetobacter baumannii (Ab) Group. *Front. Microbiol.* **10**, 2429 (2019).

61. Greene, C., Vadlamudi, G., Newton, D., Foxman, B. & Xi, C. The influence of biofilm formation and multidrug resistance on environmental survival of clinical and environmental isolates of Acinetobacter baumannii. *Am. J. Infect. Control* **44**, e65–e71 (2016).

62. Hamidian, M. *et al.* Genomic and phenotypic analyses of diverse non-clinical Acinetobacter baumannii strains reveals strain-specific virulence and resistance capacity. *Microb. Genomics* **8**, (2022).

63. Kong, X. *et al.* Phenotypic and genomic comparison of dominant and nondominant sequence-type of Acinetobacter baumannii isolated in China. *Front. Cell. Infect. Microbiol.* **13**, 1118285 (2023).

64. Clemmer, K. M., Bonomo, R. A. & Rather, P. N. Genetic analysis of surface motility in Acinetobacter baumannii. *Microbiology* **157**, 2534–2544 (2011).

65. Pérez-Varela, M., Corral, J., Aranda, J. & Barbé, J. Roles of Efflux Pumps from Different Superfamilies in the Surface-Associated Motility and Virulence of *Acinetobacter baumannii* ATCC 17978. *Antimicrob. Agents Chemother.* **63**, e02190-18 (2019).

66. Blaschke, A. J. *et al.* Clindamycin-Resistant Group B Streptococcus and Failure of Intrapartum Prophylaxis to Prevent Early-Onset Disease. *J. Pediatr.* **156**, 501–503 (2010).

67. Corral, J. *et al.* Importance of twitching and surface-associated motility in the virulence of *Acinetobacter baumannii*. *Virulence* **12**, 2201–2213 (2021).

68. De Silva, P. M. & Kumar, A. Effect of Sodium Chloride on Surface-Associated Motility of Acinetobacter baumannii and the Role of AdeRS Two-Component System. *J. Membr. Biol.* **251**, 5–13 (2018).

69. Waite, A. J., Frankel, N. W. & Emonet, T. Behavioral Variability and Phenotypic Diversity in Bacterial Chemotaxis. *Annu. Rev. Biophys.* **47**, 595–616 (2018).

70. Gaona, M. *et al.* The novel MFS efflux pump SxtP, regulated by the LysR-type transcriptional activator SxtR, is involved in the susceptibility to sulfamethoxazole/trimethoprim (SXT) and the pathogenesis of *Acinetobacter baumannii*. *Antimicrob. Agents Chemother.* **68**, e00712-24 (2024).

71. Sarshar, M. *et al.* FimH and Anti-Adhesive Therapeutics: A Disarming Strategy Against Uropathogens. *Antibiotics* **9**, 397 (2020).

72. Jackson-Litteken, C. D. *et al.* InvL, an Invasin-Like Adhesin, Is a Type II Secretion System Substrate Required for Acinetobacter baumannii Uropathogenesis. *mBio* **13**, e00258-22 (2022).

73. Johnson, T. L., Waack, U., Smith, S., Mobley, H. & Sandkvist, M. Acinetobacter baumannii Is Dependent on the Type II Secretion System and Its Substrate LipA for Lipid Utilization and In Vivo Fitness. *J. Bacteriol.* **198**, 711–719 (2016).

74. Waack, U. *et al.* Targeting the Type II Secretion System: Development, Optimization, and Validation of a High-Throughput Screen for the Identification of Small Molecule Inhibitors. *Front. Cell. Infect. Microbiol.* **7**, 380 (2017).

Chapter 4. Goblet cell breakdown: transcriptomics reveals *Acinetobacter baumannii* early and robust inflammatory response in differentiated human bronchial epithelial cells

Daniela Scribano[a], Claudia Tito[b], Astri D. Tagueha[a], Martina Pasqua[c], Luciana De Angelis[b], Francesco Fazi[b], Dolores Limongi[d,e], Marta De Angelis[f,g], Lucia Nencioni[f], Anna Teresa Palamara[f,h], Cecilia Ambrosi[d,e*]

[a]*Department of Public Health and Infectious Diseases, Sapienza University of Rome, 00185 Rome, Italy;*
[b]*Department of Anatomical, Histological, Forensic & Orthopedic Sciences, Section of Histology & Medical Embryology, Sapienza University of Rome, 00161 Rome, Italy;*
[c]*Department of Biology and Biotechnologies "Charles Darwin", Institute Pasteur Italia, Sapienza University of Rome, 00185 Rome, Italy;*
[d]*Department of Promotion of Human Sciences and Quality of Life, San Raffaele Open University, 00166, Rome, Italy;*
[e]*Laboratory of Microbiology, IRCCS San Raffaele Roma, 00143, Rome, Italy;*
[f]*Department of Public Health and Infectious Diseases, Sapienza University of Rome, Laboratory Affiliated to Institute Pasteur Italia-Cenci Bolognetti Foundation, 00185 Rome, Italy;*
[g]*Laboratory of Virology, Department of Molecular Medicine, Sapienza University, Rome, Italy*
[h]*Department of Infectious Diseases, Istituto Superiore di Sanità, 00185 Rome, Italy.*

Published on 9 July 2025

Journal

Journal of Biomedical Science

IF (May 2026): 12.1

doi

https://doi.org/10.1186/s12929-025-01159-1

Abstract

The airway epithelium represents the first line of defense of the lungs, functioning both as a physical barrier as well as an active immune modulator. However, in the last years, pneumonia caused by the opportunistic pathogen *Acinetobacter baumannii* have become difficult to treat due to the increase of the number of extensively drug-resistant strains. In this study, we report for the first time the use of an *ex vivo* air–liquid interface (ALI) model of differentiated human bronchial epithelial cells to unravel the early response to *A. baumannii* infection. Epithelial integrity, tissue architecture, and goblet cell function were assessed through FITC-dextran permeability assays, hematoxylin and eosin staining, and indirect immunofluorescence. Transcriptomic profiling was performed to characterize host gene expression changes. Initial tissue damage began as early as at 4 h post-infection (hpi); at 24 hpi, goblet cell hypertrophy, reduced mucin secretion, and compromised epithelial integrity were highly evident. Transcriptomic data at 4 hpi revealed 668 differentially expressed genes (441 upregulated, 227 downregulated), mainly involved in a strong pro-inflammatory response and characterized by IL-8/CCL20-driven neutrophil recruitment and type 2 cytokine activation (IL-4, IL-13). Noteworthy, genes related to cytoskeletal organization, adhesion, and extracellular matrix remodeling were significantly altered, suggesting a bacterial mechanism to enhanced tissue dissemination. The PI3K-Akt survival pathway was inhibited, with downregulation of *PIK3R1* and *PIK3R2* genes, implying the induction of apoptosis/cell death and epithelial damage. Our findings are in agreement with previous *in vivo* studies, further strengthening the value of our ALI model in mimicking the early infection response of bronchial cells to *A. baumannii* infection. Our data highlight the early molecular mechanisms underlying *A. baumannii* pathogenesis and open new avenues for future investigations for therapeutic interventions.

4.1 Introduction

Acinetobacter baumannii is an opportunistic pathogen that causes severe infections in immunocompromised individuals, mainly pneumonia [1,2]. If untreated, *A. baumannii* infections can lead to high rates of morbidity and mortality [3] (Shields 2023). However, with the increase of the number of extensively drug resistant strains the therapeutic options to eradicate this pathogen are dramatically reduced [1–3]. The World Health Organization reports that carbapenem-resistant *A. baumannii* strains remain critical microorganisms urgently needing new therapeutic options (https://www.who.int/publications/i/item/9789240093461).

Adhesion is the first and most critical step for infection; *A. baumannii* strains have a plethora of appendages and adhesins allowing bacterial attachment to abiotic and biotic surfaces [4,5]. Key adhesion factors for the interaction with host epithelial cells include chaperone-usher pathway pili (Csu pili), the *Acinetobacter* trimeric autotransporter (Ata), the biofilm-associated protein (Bap), the filamentous hemagglutinin C (FhaC), the outer-membrane protein A (OmpA), the TonB-dependent outer membrane receptor (BauA), and

the ferrous iron transport protein FeoA, just to mention the most studied [2,6]. Transcriptome studies in *ex vivo* and *in vivo* models reveal upregulation of genes linked to antibiotic resistance, iron acquisition, and surface-associated properties, among different isolates [7,8]. Several modifications of *A. baumannii* transcriptome occur to improve its fitness and survival during infection within the host [9,10]. It also undergoes mucoid conversion over time during pulmonary infections to further enhance survival in this context by avoiding phagocytosis and pulmonary clearance [11]. However, few studies have analyzed the host response to colonization of *A. baumannii* [12]. One *in vivo* study shows that *A. baumannii* establishes an acute lethal pneumonia after 24 h, supported by high bacterial burdens, severe inflammatory cells infiltration and lung damage [13]. Understanding the interaction between *A. baumannii* and epithelia could reveal new diagnostic biomarkers and strategies to combat pneumonia caused by *A. baumannii*. Advanced *in vitro* infection models, such as air–liquid interface (ALI) culture models, replicate the human lung environment and can be exploited to dissect the different stages of microbial infections [14–17]. Indeed, these cells form a pseudostratified epithelium, including basal, ciliated, and mucus-secreting goblet cells, closely mimicking the native human airway epithelium [14–17]. Derived from 2D airway organoids or primary cells, these cultures have been used to study *Pseudomonas aeruginosa* infections and replicate important aspects of *in vivo* infection [18,19]. Therefore, the present study aimed to establish how human respiratory epithelia respond to *A. baumannii* colonization using advanced *in vitro* models that mimic host physiological conditions. By using for the first time differentiated primary human airway epithelial cells (2D ALI) derived from a healthy donor, we established how human bronchial cells respond to *A. baumannii* initial colonization steps by performing histological, immunofluorescence, and transcriptome sequencing (RNA-seq) analyses. Herein, we demonstrate that *A. baumannii* rapidly induces a robust pro-inflammatory transcriptomic response driven by chemokine signaling, coupled with early disruption of epithelial barrier integrity, goblet cell dysfunction, and increased permeability.

4.2 Materials and methods

4.2.1 Bacterial growth conditions and cell cultures

The *A. baumannii* AB5075-UW strain used in this study was provided by BEI Resources (Manassas, VA). Routine growth and plating were carried out in Luria–Bertani broth (LB) and 1.5% agar plates (Difco, Milan, Italy). A single opaque colony was inoculated in LB and grown at 37 °C with vigorous shaking (200 rpm) to the mid-exponential phase (optical density (OD) at 600 nm ≈ 0.8.

Normal human bronchial epithelial cells (NHBE) (CC-2540, Lonza, Italy, ID 45627) were seeded at a density of 1.7×10^5 cells in a T25 flask, following manufacturer's instructions. Expansion phase was achieved using PneumaCult™ ExPlus medium (STEMCELL Technologies, Italy). Once 50% confluent, cells were washed, and seeded onto 0.4 µm pore, PET 24 well Transwell® inserts (Greiner Bio-one, Italy) at a final density of

3.3×10^4/Transwell. After reaching confluency, the apical media were aspirated (air-lifted), and cells were allowed to differentiate in air liquid interface for 4 weeks in PneumaCult™ ALI differentiation media supplemented with 0.2% heparin, 5% hydrocortisone, and 0.2% Pen/strep and amphotericin B (all STEMCELL Technologies, Italy). The day before infection, Transwell inserts were washed twice, and the growth medium, depleted of antibiotics and antimycotics, was replaced in the basal chamber.

4.2.2 Infection of 2D ALI

2D ALI were washed twice with Dulbecco phosphate-buffered saline (PBS) to remove the produced mucus. The bacterial culture was washed twice in DMEM-F12, diluted, and 20 µl were used to infect the apical side of bronchial epithelia to reach a multiplicity of infection (MOI), as indicated. To estimate the number of cells on inserts, we referred to a previous published study, which adopted identical experimental conditions [20]. Infected and not infected 2D ALI were centrifuged at 200 × *g* for 10 min, and incubated at 37 °C with 5% CO_2 for 4 and 24 h. Four sets of infected and uninfected 2D ALI were assayed. Parallel uninfected cells exposed to 20 µl of DMEM-F12 served as negative controls.

4.2.3 Bacterial adherence

After 4 and 24 h of incubation, a set of 2D ALI were washed twice with PBS to remove unadherent bacteria; then, 200 µl of cold distilled water were added, incubated 5 min at room temperature (RT), and the transwell surface was scraped to recover bacteria. Serially diluted lysates were plated on LB agar plates to determine the colony forming units (CFU)/ml.

4.2.4 Hematoxylin–eosin (H&E) and periodic acid–Schiff (PAS) staining

The apical and basal chambers of a second set of 2D ALI was washed with PBS, and fixed with 10% buffered formalin overnight at 4 °C. Paraffin-embedding of ALI tissue, were sectioned (10 µm), and stained either with H&E or PAS, following a published protocol [21].

4.2.5 Immunofluorescence

A third set of 2D ALI was washed with PBS, and fixed with paraformadehyde 4% for 20 min at RT. After the washing steps, 2D ALI were permebilized with 0.5% Triton-X 100 for 25 min, blocked with 3% normal goat serum-1% bovine serum albumin (BSA), and incubated overnight with 1: 500 rabbit polyclonal anti-MUC5AC (Abcam AB198294), and 1:250 mouse monoclonal anti-Acetyl-tubulin antibodies (Santa Cruz SC-23950). In parallel, 2D ALI were stained with 1:100 rabbit polyclonal anti ZO-1 (Invitrogen PA5-28869), and 1:250 mouse monoclonal anti-*A. baumannii* antibodies (gift of Prof. B.B. Singer). Secondary anti-rabbit Alexa Fluor 488 (green) and anti-mouse Alexa Fluor 546 (red) antibodies were used 1:250, following manufacturer's instructions (Invitrogen, Italy). Finally, the nuclei were stained with Hoechst 33342 (Life Technologies) for 10 min in PBS, washed and mounted in VECTASHIELD antifade

mounting media (#H1000, Vector Laboratories). Images were acquired using a Zeiss LSM 900 confocal laser scanning microscope using ZEN software (Zeiss).

4.2.6 RNA isolation, RNA-seq and quantitative reverse-transcription PCR (qRT-PCR)

A fourth set of 2D ALI was used for RNA extraction. RNA was isolated at 4 h post-infection, using TRIzol reagent (Invitrogen, Italy) and Direct-zol RNA kit (Zymo Research, CA, USA), following manufacturer instructions. DNase I (Zymo Research, CA, USA) was used to remove genomic DNA. The quality and quantity of extracted RNA was evaluated by measuring the absorbance ratio A_{260}/A_{280} and 1.5% agarose gel electrophoresis, respectively. RNA integrity was measured using the Qubit 4.0 Fluorometer with the RNA IQ Assay kit following the corresponding manufacturers' standard protocols (Thermo Fisher Scientific, Italy). Frozen samples were sent for library preparation and RNA sequencing to BMR Genomics sequencing service (BMR Genomics srl, Padova, Italy). RNA integrity for library preparation was determined by analysis of extracted total RNA using a 2100 Bioanalyzer (Agilent Technologies) with RNA 6000 NanoChip. RNA concentrations were measured using Qubit RNA Assay Kit. Libraries were prepared from total RNA according to manufacturer instructions with Illumina Stranded mRNA Prep kit. Libraries quality was evaluated by size analysis on 2100 Bioanlyzer (Chip DNA HS) and concentrations were determined using Qubit DNA HS assay kit (Thermo Fisher). Sequencing was performed on Illumina Novaseq 6000 in the 150PE format. Expression of selected genes was determined by reverse transcriptase polymerase chain reaction (RT-PCR) to validate RNA-Seq results. RNA (1 µg) was converted to cDNA with the High-Capacity cDNA Reverse Transcription Kit (Applied Biosystems), following manufacturer's instructions. The RT-PCR analysis was performed using 2 µl of cDNA samples as template with primers reported in Table 4.S1. The expression of each target gene was normalized to *GAPDH* rRNA by using the $2^{-\Delta\Delta Ct}$ method [22]. The assay was conducted in triplicate; means and standard deviations were calculated for each group.

4.2.7 ALI permeability assay

The integrity of tight junctions of the pseudostratified cell culture was determined chemically by the use of 4 kDa fluorescein isothiocyanate (FITC)-dextran, corresponding to a molecular radius of 14 Angstrom (Sigma-Aldrich, Italy). Briefly, 200 µl of a solution containing 2 mg/ml of FITC-dextran in HBSS was added into the apical chamber, while 500 µl of HBSS was added to the basal chamber. ALI cultures were incubated at 37 °C and 5% CO_2 for 2 h. Samples from the basolateral medium for each insert were analyzed in triplicate by fluorescence measurement at 4 and 24 hpi, with excitation at 492 nm and emission at 520 nm, using a CLARIOStar microplate reader (BMG Labtech, Offenburg, Germany) in 96-well black microtiter. The Adjust Gain setting was calibrated using a 2 mg/ml solution to standardize all sample readings. Medium without FITC-dextran was used as a blank, while three empty Transwells served as controls for 100% permeability.

4.2.8 Bioinformatic analyses

Reads preprocessing was performed by using fastp v0.20.0 [23], applying specific parameters to keep only high quality data: qualified_quality_phred = 20, unqualified_percent_limit = 30, average_qual = 25, low_complexity_filter = True, complexity_threshold = 30. Mean value of uniquely mapped reads were 89%, unmapped reads 6% per sample. Passing filter reads were mapped to the genome reference (*Homo sapiens*) using STAR v2.7.9.a [24] with standard parameters, except for sjdbOverhang option set on read length. Genome and transcripts annotation provided as input were downloaded from v105 of Ensembl repository. Alignments were then elaborated by RSEM v1.3.3 [25], to estimate transcript and gene abundances. Subsequently, the sample-specific gene-level abundances were merged into a single raw expression matrix applying a dedicated RSEM command (rsem-generate-data-matrix). Genes with at least 10 counts in N samples were then selected, where N corresponds to the sample number in the smallest experimental group. Differential expression was computed by edgeR [26] from raw counts in each comparison. Multiple testing controlling procedure was applied and genes with a FDR ≤ 0.05 and logFC >|0.5| were considered differentially expressed. Annotation of differential expressed genes was performed using the bioMart package [27] into R 4.3, querying available Ensembl Gene IDs and retrieving Gene Names and Entrez gene IDs. In order to create the heatmap, the R library *(pheatmap)* with an unbiased hierarchical system was used. Obtained differentially expressed genes (DEGs) were used for GO analyses through the *clusterProfiler* library [28], and categorized into biological process (BP), molecular function (MF), and cellular component (CC). The same genes were used for pathway enrichment analyses in the Reactome database using the *ReactomePA* library [29]. Metapathway was generated using genes selected from enrichment pathways describing inflammation, apoptosis, and cell–cell interaction, and processed in STRING to extract experimentally validated and database interactions. Cytoscape [30] was used to visualize the corresponding network graphs for each process.

4.2.9 Video microscopy

A Video of the differentiated epithelia was recordered under a light microscope (Motik AE21 microscopy, Italy) at 10 × magnification at 30 frames per second with a resolution of up to 1920 × 1080 pixels (Samsung Galaxy S20 FE).

4.2.10 Statistical analysis

A total of four independent experiments were performed (n = 4). Normal distribution was determined with the Shapiro–Wilk test. Statistical significance was determined using the unpaired Student's t test using Prism software v. 8.0.2 (GraphPad, USA). *P* values < 0.05 were taken as being statistically significant. The comparison of gene expression data by RT-PCR and RNA-seq showed a significant Pearson correlation coefficient between the results of the two approaches ($P < 0{,}0001$, R squared = 0,9771).

4.2.11 Shi Data availability

The RNA-seq data of this study have been deposited in NCBI underBioProject No. PRJNA1219108.

4.3 Results

4.3.1 Establishment of air–liquid interface (ALI) cultures to study *A. baumannii* Pathogenesis Mechanisms

We aimed to investigate the interaction between *A. baumannii* and the airway epithelium during early and late infection. To achieve this, we established ALI cultures using Normal Human Bronchial Epithelial (NHBE) cells derived from a healthy human donor. The cells were cultured on Transwell inserts and allowed to differentiate for 28 days, as detailed in the Materials and Methods section. Immunofluorescence staining of NHBE cells on Transwell inserts confirmed the expression of key markers: acetylated tubulin for ciliated cells and mucin-5 subtype AC (MUC5AC) for goblet cells (Figure 4.1A and 1B). H&E staining of tangential sections of ALI culture highlighted the presence of apical cells mostly columnar in shape, featured with multiple cilia (Figure 4.1C), while PAS staining detailed a physiological distribution of mucus-secreting goblet cells (Figure 4.1D). Video 1 shows the fully functional pseudostratified tissues, with highly active cilia on their surface, which coordinately beat and move secreted mucus layer. Tightness of the pseudostratified epithelium was tested by measuring the passage of 4 kDa FITC-dextran. The flux of dextran from the upper into the lower compartment, was significantly reduced by the four week-ALI-matured epithelial layer in comparison to the cell-free synthetic Transwell membrane. These findings confirm the successful differentiation of a functional pseudostratified airway epithelium that closely resembles the native human bronchial epithelium, making it well-suited for studying host–pathogen interactions.

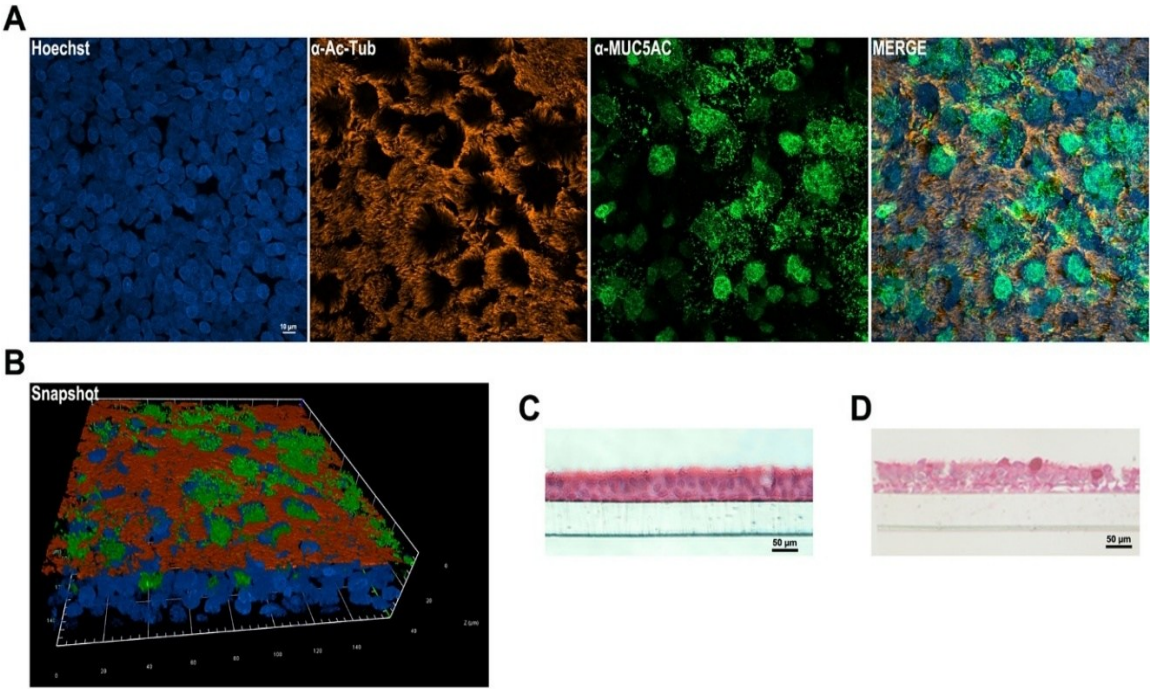

Figure 4.1. Characterization of differentiated NHBE cells cultured at the air–liquid interface (ALI). 2D ALI cultures were grown for 28 days, before being analyzed. **A** After 28 days of air exposure, the pseudostratified epithelium was stained with specific antibodies to visualize ciliated cells with well-developed apical projections (acetylated tubulin, red), and sparse goblet cells secreting mucin-5 subtype AC- (MUC5AC, green). Nuclei were counterstained with Hoechst 33342 (blue). **B** An image illustrating the spatial organization and differentiation of ciliated and goblet cells within the epithelium. **C**, **D** Representative histological image of tangential sections of the epithelium stained with H&E and PAS, respectively. Three independent experiments using cells from the same donor were performed. Scale bar sizes are indicated in the images.

4.3.2 *A. baumannii* induces swelling in goblet cells

The differentiated ALI culture was employed to examine the temporal progression of colonization and the cellular responses of the epithelium during early infection. Thus, 2D bronchial epithelium was apically infected with *A. baumannii* AB5075 at a multiplicity of infection (MOI) of 100. A preliminary time-course infection experiment was performed to evaluate histological changes in the ALI culture following *A. baumannii* infection. Based on these observations, 4 hpi was selected for transcriptomic analysis as early epithelial alterations were detectable at this stage, while 24 hpi was selected to investigate the progression of infection and tissue damage over time. At 4 and 24 h post-infection, the adherent bacteria were assessed by measuring the number of colony forming units (CFU)/ml recovered from the ALI culture. A 2-log reduction in the bacterial count compared to the initial inoculum was recorded, which remained stable over time. Thus, no significant replication of *A. baumannii* was observed at either time point. In accordance with the membrane size (0.4 µm), no bacteria could be recovered from the basal chamber. The histological staining of tangential ALI sections with H&E at 4 hpi revealed that goblet cells appeared lightly swollen, grainy, and irregular in infected

cultures compared to non-infected counterparts (Figure 4.2A). These changes became more evident and intense at 24 hpi, exibiting a swollen and hypertrophic phenotype (Figure 4.2B). The same effect was shown with ALI culture infected with MOI 2 and 5 (Supplementary material Figure 4.S1). Moreover, Giemsa staining showed that during the first 4 h, the majority of bacteria were closer to goblet cells than to ciliated cells (Figure 4.2C). By 24 h, most bacteria remained near goblet cells, although some were observed near ciliated cells, potentially due to the extent of damage to the pseudostratified epithelium (Figure 4.2D). Thus, *A. baumannii* caused severe disruption of goblet cells, impacting the overall architecture of ALI cultures.

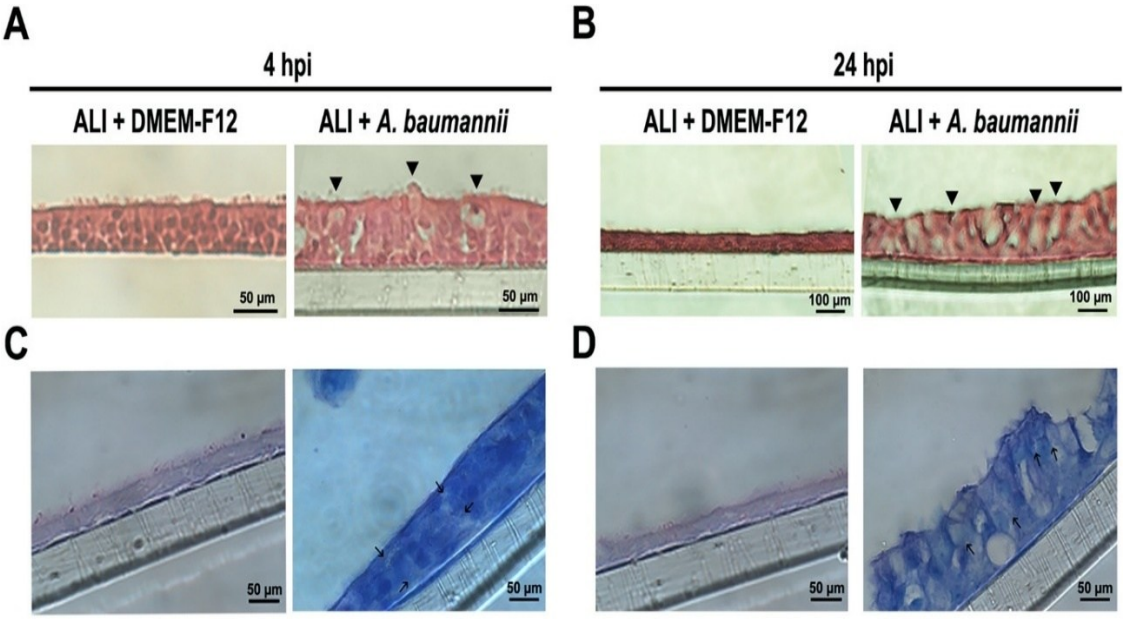

Figure 4.2. Histology of ALI infected with *A. baumannii*. A total of 20 µl of bacteria resuspended in DMEM-F12 was used for infection. Non-infected ALI cultures were treated with an equivalent volume of DMEM-F12 as a negative control. **A**, **B** Representative images of infected and unifected ALI cultures stained with H&E at 4 h post-infection (hpi) and 24 hpi, respectively, as indicated. **C**, **D** Representative images of the same sections shown in panels (**A** and **B)**, stained with Giemsa. Three independent experiments using cells from the same donor were performed. Scale bar sizes are indicated in the images.

Immunofluorescence (IF) staining was used to characterize specific interactions between the bacteria and epithelial cells. No clear co-localization was observed under our experimental conditions between bacteria and secreted mucin glycoproteins MUC5AC or the regulator of barrier function, zonulin (ZO-1). IF showed that *A. baumannii*-infected ALI exhibited a less defined pattern of ZO-1 immunostaining, particularly at 24 h post-infection when compared to uninfected cells, indicating a less polarization state of the epithelial cells (Figure 4.3 and Figure 4.S2). Interestingly, a reduced amount of excreted mucin was detected at 24 hpi, in accordance with their swollen and hypertrophic phenotype (Figure 4.2B and D and Figure 4.3B).

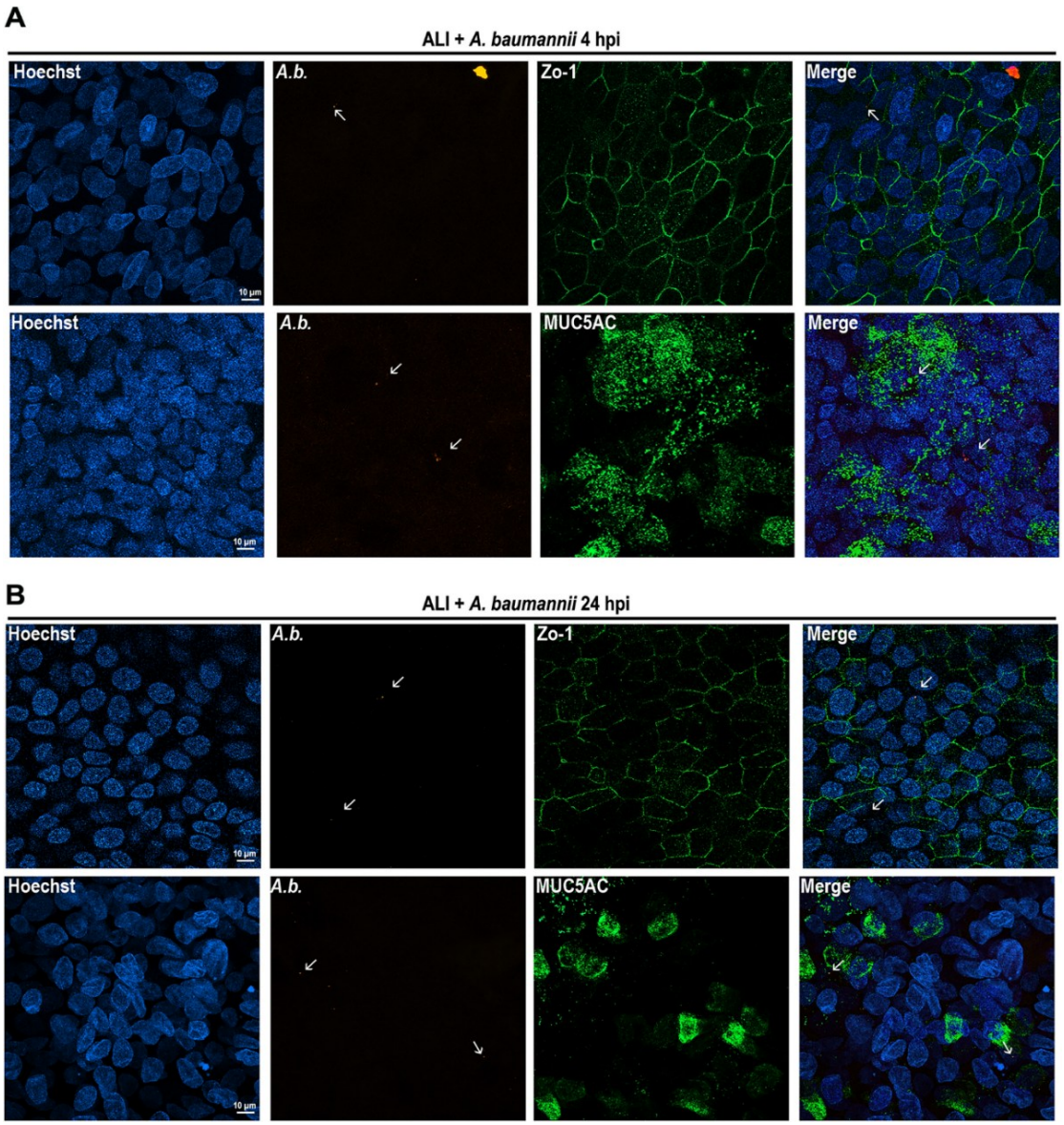

Figure 4.3. Immunofluorescence of ALI infected with *A. baumannii*. Representative images of infected ALI cultures stained with antibodies against *A. baumannii* (*A.b.*, red) and either MUC5AC (green) or ZO-1 (green) at 4 and 24 h post-infection (hpi). Nuclei were counterstained with Hoechst 33342 (blue). Non-infected ALI cultures were treated with an equivalent volume of DMEM-F12 as a negative control. Three independent experiments were performed. Scale bar sizes are indicated in the images.

4.3.3 *A. baumannii* infection induces airway epithelial barrier disruption

To monitor the functional integrity of epithelial barrier, the paracellular FITC-dextran flux assays of infected and uninfected ALI cultures were performed at 4 and 24 hpi. Pairwise comparison indicated significant differences ($P = 0.0013$) between ALI cultures at 24 hpi (Figure 4.4), indicating altered expression and/or redistribution of tight junction proteins and perturbations of the actin cytoskeleton and increased paracellular permeability in ALI infected cultures.

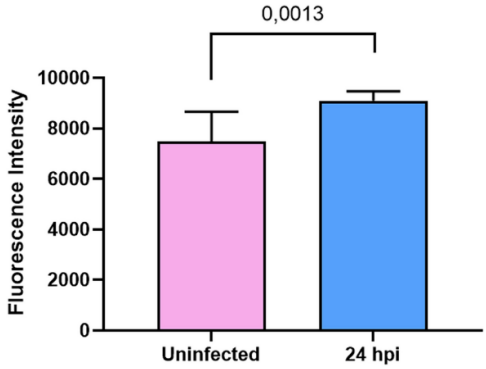

Figure 4.4. *A. baumannii* infection increases paracellular permeability in ALI cultures. Differentiated 2D ALI bronchial epithelial cultures were infected apically with strain AB507. At 24 h post-infection (hpi), barrier integrity was assessed by measuring the paracellular flux of 2 mg/ml of FITC-dextran (4 kDa) from the apical to the basolateral compartment. After 2 h of further incubation at 37 °C and 5% CO2, fluorescence measurement (excitation at 492 nm and emission at 520 nm) were recorded using a CLARIOStar microplate reader (BMG Labtech, Offenburg, Germany) in a 96-well black microtiter. The Adjust Gain setting was calibrated using a 2 mg/ml solution to standardize all sample readings. Data are expressed as mean ± standard deviation of three independent experiments. Statistical analysis was performed using Student's t-test.

4.3.4 *A. baumannii* infection triggers a high inflammation response in ALI cultures

To investigate gene expression in ALI cultures following *A. baumannii* infection, we compared the transcriptional profiles of infected and non-infected bronchial cells using RNA-seq at 4 hpi, a time point when histological changes begin to emerge. The clear separation between the groups in the Principal-component analysis (PCA) plotting revealed high intra-group similarity and strong inter-group divergence (Figure 4.5A). The analysis identified 1,099 statistically significant differentially expressed genes (DEGs) (P value ≤ 0.05), with 584 upregulated and 515 downregulated. The clustered heatmap of all DEGs is presented in Figure 4.5B, and the complete DEG list is available in Table 4.S2. When considering DEGs with a False Discovery Rate (FDR) ≤ 0.05, 441 genes were upregulated, and 227 were downregulated. The Gene Ontology (GO) enrichment analysis was conducted to elucidate the biological functions of DEGs upon bacterial exposure. The enriched GO terms in biological process included pathways related to inflammation and its regulation, immune response, cell–cell interaction, along with cell cycle progression, apoptosis, cellular stress, and metabolism (Figure 4.5C and 5D). A strong immune response was evident, with differential expression of genes involved in interleukin-10 (IL-10), interleukin-4 (IL-4), interleukin-13 (IL-13), and interleukin-17 (IL-17) signaling, indicating a dynamic regulation of pro- and anti-inflammatory responses (*SOCS3, IL17C, IL1RN, IL4R*, *PTAFR*). Additionally, interleukin-1 (IL-1) processing and RIP-TRAF6-mediated NF-κB activation suggest a strong inflammatory response. Notably, the long non-coding RNA (lncRNA) MIR3142HG was also upregulated, potentially contributing to immune modulation in response to *A. baumannii* infection. Pathways involved in chemokine receptor signaling were also significantly enriched, highlighting the recruitment of immune cells to the site of infection (*NFKBIA, NFKBIB, NFKBIE, NFKBIZ, TNFAIP3, REL, BCL3*). TP53 downregulation,

along with altered expression of death receptor-related genes, suggests apoptosis suppression or a shift toward survival mechanisms in response to bacterial infection. PI3K signaling dysregulation was observed, with downregulation of *PIK3R1, PIK3R2*, and *PTGS2*, and upregulation of *IRS1*/2, affecting cell survival and immune responses. Upregulation of *RND1, RND3, RHOB*, and *RHOBTB2* in the RAC1 GTPase cycle suggests cytoskeletal disruption, potentially weakening cell junctions and barrier integrity in bronchial epithelial cells. Additionally, *FGFR2* ligand binding (*FGFR2*), and ERK inactivation (*DUSP1, DUSP5, DUSP6*) were also detected (Figure 4.5C and 5D). Furthermore, Figure 4.5E illustrates the robust proinflammatory response to bacterial lipopolysaccharide and related molecules, with GO term connections representing shared genes. Notably, volcano plot analysis highlighted significantly altered genes in infected ALI cultures (Figure 4.5F). Additionally, *IFITM2* and *IFNGR1*were induced, further amplifying the inflammatory cascade. Upregulation of *CSF3, ICAM1, MMP13, PLAU, PTGS2, VCL*, and *FERMT2* suggests active epithelial remodeling and barrier modulation. Conversely, downregulation of *PIK3R1, PIK3R2, GSTA2, TRIM25*, and *MAP3K1*, involved in oxidative stress defense and cytoskeletal regulation, may compromise epithelial resilience. To validate this result, we performed reverse transcriptase quantitative PCR (RT-qPCR) assays to assess the RNA transcript levels of genes representing crucial hubs in the three pathways (Table 4.S1 and Figure 4.S3). Expression of those genes was in agreement with data from RNA-seq (R squared = 0,9771).

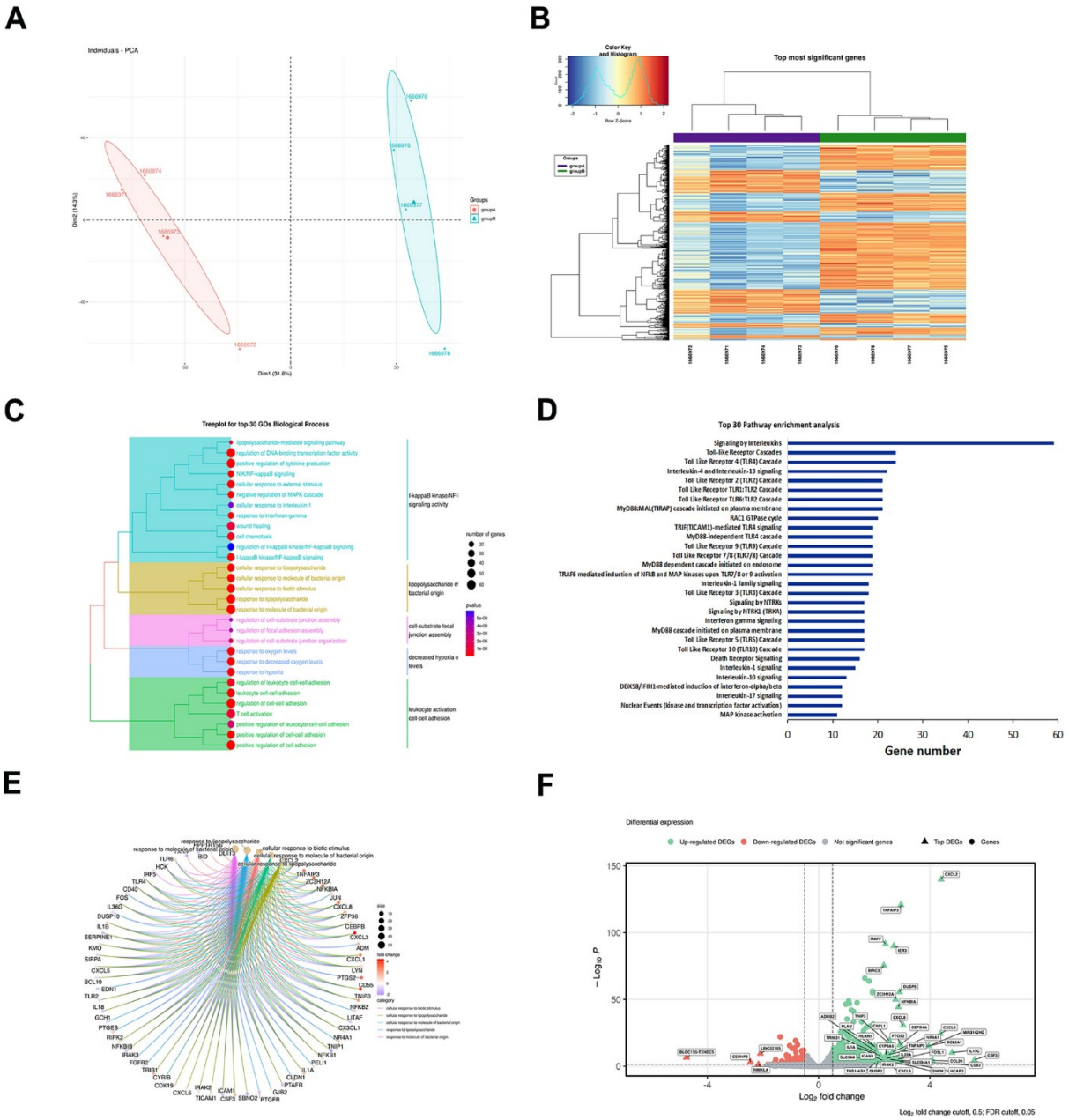

Figure 4.5. Global transcriptiomic response of bronchial epithelium to *A. baumannii* AB5075 infection at 4 hpi. **A** Principal Component Analysis (PCA) plot illustrating the clustering of unexposed (group A) and *A. baumannii*-exposed (group B) bronchial cells based on transcriptomic profiles. **B** Heatmap and hierarchical clustering dendrogram of the top differentially expressed genes (DEGs) in unexposed and exposed bronchial cells (FDR *P* value < 0.05). Warmer colors indicate upregulated genes, while cooler colors indicate downregulated genes. **C** Tree plot of the top 30 Gene Ontology (GO) terms related to the biological process of DEGs. The size of each node represents the level of enrichment significance, and the hierarchical arrangement reflects functional similarities between terms. **D** Description of the top 30 pathway enrichment analysis within the DEGs list, obtained through the use of a hypergeometric model. **E** Chord diagram illustrating the $\log_2$ fold changes of genes involved in the selected GO terms. **F** Volcano plot depicting the distribution of DEGs, with the most significantly upregulated (green) and downregulated (red) genes highlighted. The x-axis represents log2 fold change, and the y-axis represents -log10 (FDR *P* value), with a threshold of FDR < 0.05 used to identify significant DEGs.

To better understand the triggered pathways, the protein–protein interaction (PPI) network of DEGs was constructed by the STRING database and displayed via the Reactome FI Cytoscape Plugin. Three main modules were retrieved, each containing 35 to 39 nodes (Figure 4.6). Interestingly, *PIK3R1* and *PIK3R2* emerged as key hubs in all modules; these phosphoinositide-3-kinases(PI3Ks) genes encode the regulatory subunits (p85α and p85β, respectively) of Class IA PI3Ks, which are ubiquitously expressed in the body and play crucial roles in signal transductions of cytoskeletal regulation, apoptosis, and immune responses [31]. The Insulin receptor substrate 2 (IRS2) was also present in all modules (Figure 4.6). Module 1 highlights pro-inflammatory genes involved in cytokine signaling, and immune regulation, including *CXCL2, CXCL8, CCL20, IL18, IL23A,* and *LIF*, suggesting a robust pro-inflammatory response, through NF-κB (*NFKB1, NFKB2,* and *NFKBIB*) and JAK-STAT pathways. Moreover, Toll-Like Receptor (TLR) activation (*TLR2, TICAM1*, and *RIPK2*) suggests strong pattern recognition receptor (PRR) activation, leading to cytokine production and antimicrobial responses. Expression of *CSF3* (colony-stimulating factor 3) links immune activation, epithelial integrity, and cell survival during infection, playing a dual role in both host defense and tissue damage modulation. IRF1 and IFNGR1 support interferon signaling for antiviral and antibacterial defense. Expression of NF-κB regulators, *TNFAIP3* (A20) and *CYLD,* suggest a mechanism to prevent excessive inflammation and tissue damage, while *TXNIP* downregulation may reflect metabolic stress adaptation. The downregulation of *PI3K*-related genes (*MAP3K1, PIK3R1, PIK3R2, TRIM25*, and *TXNIP*) indicates PI3K-Akt inhibition, potentially shifting cellular priorities toward immune activation over cellular proliferation or survival. Module 2 focused on epithelial barrier function and growth factor signaling, identified *EREG, FGFR2,* and *MET* as central hubs, alongside *AREG* and *HBEGF*, which support epithelial repair and regeneration after infection-induced damage. Cytoskeletal remodeling and cell adhesion changes were indicated by upregulation of *RHOB, RND1, DLC1, RHOV, FERMT2, SDC4*, and downregulation of *ARHGEF6* and *ARHGEF19*. Interactions among *CXCL8, NFKB2, NFKBIA, SOCS3, ATF3, ATF4,* and *JUNB* suggest inflammation-induced epithelial damage. Module 3, related to cell survival and apoptosis, links *SQSTM1* (p62) to autophagy and inflammatory signaling. Apoptotic signals are supported by *BIRC3* and *CASP10*, while *TNFRSF10A* (TRAIL-R1) and *TNFRSF12A* indicate death receptor-mediated apoptosis. Expression of *BBC3* (PUMA), *BID*, and *PMAIP1* (NOXA) suggests activation of intrinsic and extrinsic apoptotic pathways. Downregulation of *ATM* and *TP53INP1*, critical for DNA damage repair, may indicate genomic instability and reduced cell viability. However, *BCL2* expression may counteract apoptosis, promoting cell survival. Growth factors *FGFR2, MET, AREG, EREG,* and *HBEGF* could support tissue repair, counterbalancing apoptosis with tissue repair and regeneration.

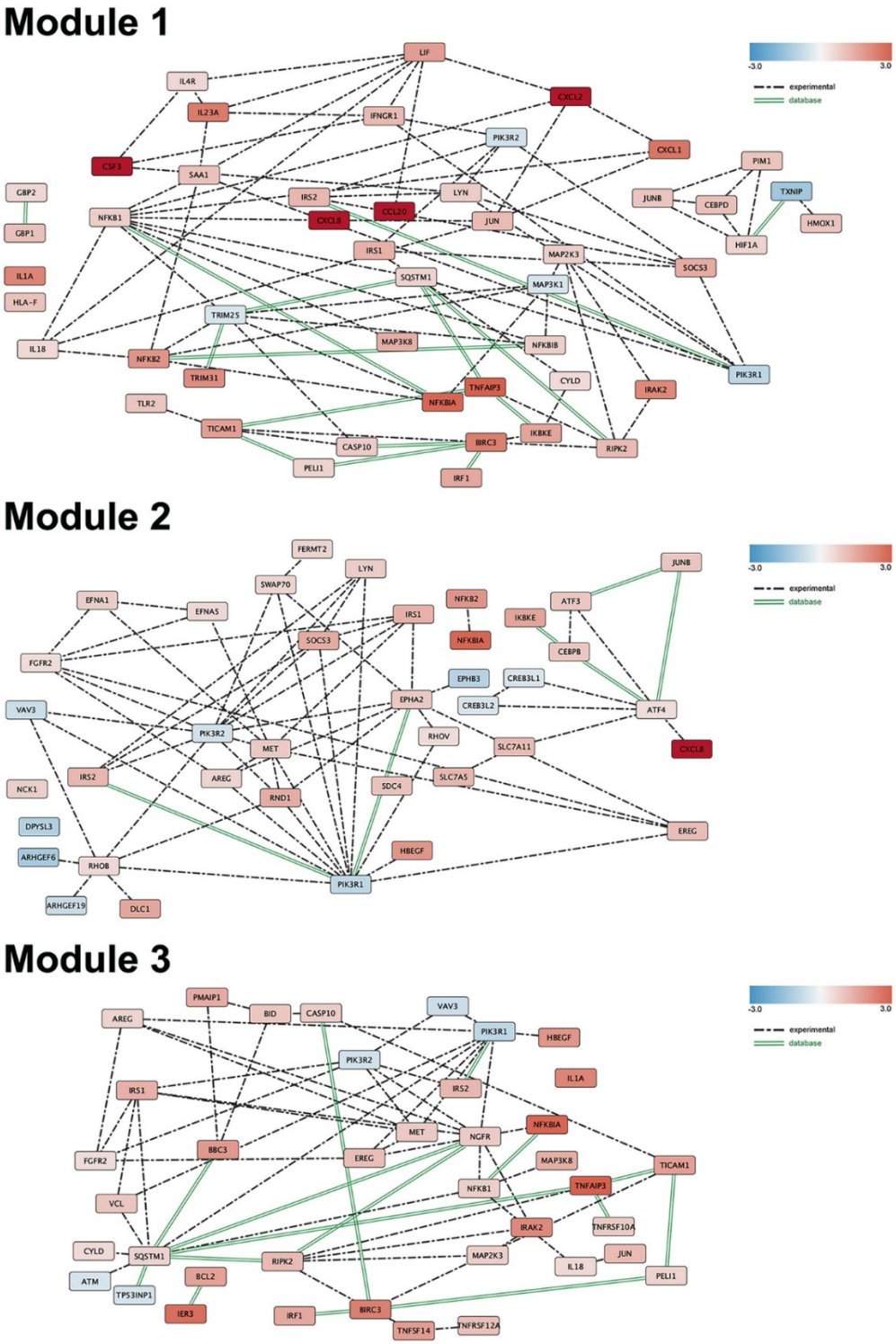

Figure 4.6. Protein–protein interaction network. The three modules represent the protein–protein interaction in the main pathways idendified constructed by Reactome functional interactions Cytoscape Plugin. Module 1, DEGs involved in inflammation and signaling regulation, module 2 DEGs involved in cell–cell interaction, module 3 DEGs in cell stress, survival and apoptosis. The color code indicates up or downregulation. Dotted lines report experimentally demonstrated interactions, solid green lines interactions reported in the databases.

Integrating these data with the KEGG pathway and STRING database allowed us to generate a working model of the three main triggers elicited by *A. baumannii* during the exposure of bronchial epithelium (Figure 4.7).

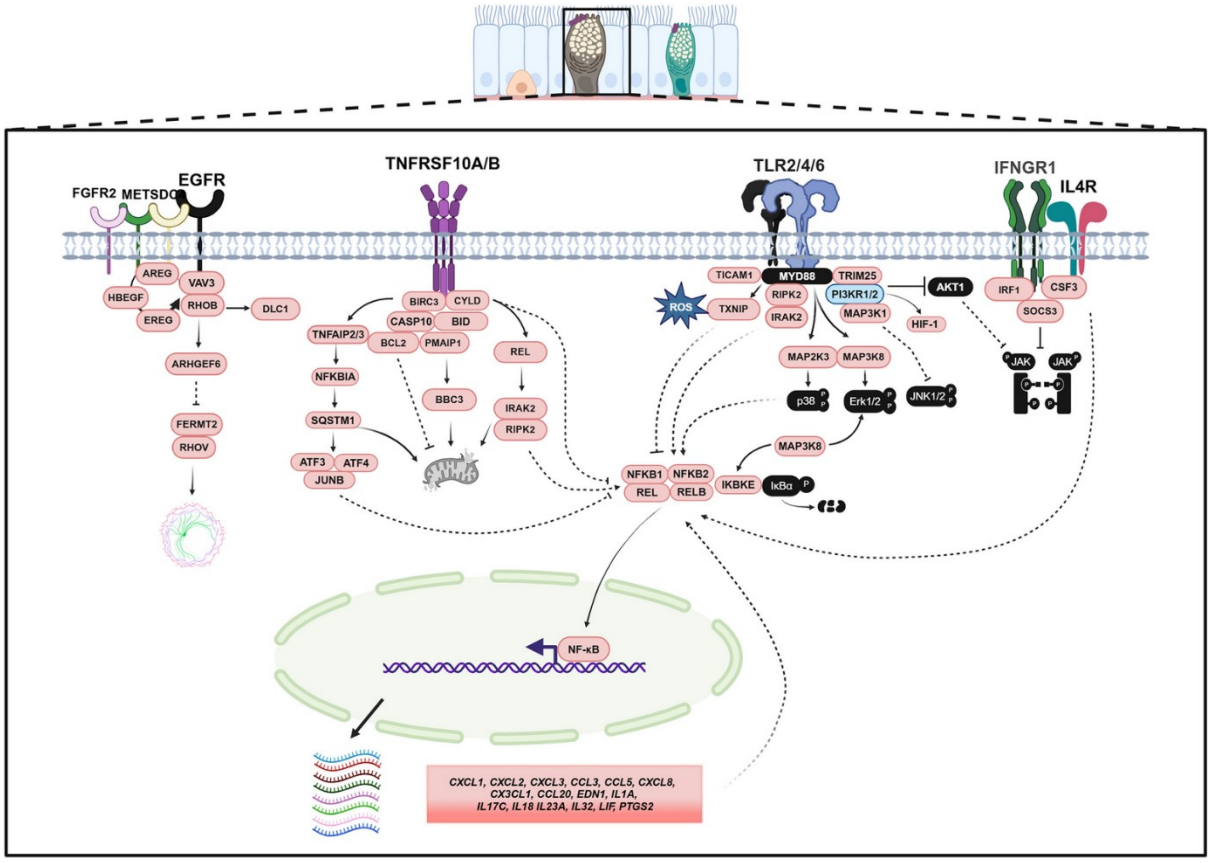

Figure 4.7. Proposed regulatory networks of human bronchial epithelium upon exposure to *A. baumannii*. Based on the results of this study, three main pathways highly interconnected were triggered by bacteria: inflammation and signaling regulation, cell–cell interaction, and autophagy/cell death. Black-filled proteins were not found among DEGs. Orange and light blue proteins represent upregulated and downregulated genes, respectively. Solid lines indicate previously demonstrated interactions, while dotted lines refer to missing interactors. Additional details are provided in the main text. The figure was created with BioRender.com

4.4 Discussion

The airway epithelium serves as the first line of defense in the lungs, acting as a physical barrier against inhaled pathogens while also recruiting and activating effector cells to eliminate invaders. The bronchial epithelium is a pseudostratified structure primarily composed of columnar multiciliated, secretory (goblet), and undifferentiated cells that overlay smaller basal cells with self-renewal capacity, along with rarer cell types such as neuroendocrine and brush (tuft) cells [32]. In this study, we investigated the response of human bronchial epithelial cells to exposure to the opportunistic pathogen *A. baumannii*. To the best of our knowledge, this is the first study addressing this issue using a fully

differentiated and functional human epithelium of the lower respiratory tract, serving as an ex vivo organotypic model (Figure 4.1). As early as 4 hpi, mucus-secreting goblet cells appeared hypertrophic and secreted less mucin, the ZO-1 immunostaining pattern became less defined, and the epithelial barrier was compromised (Figures 4.2 and 4.3). These changes progressively intensified in infected ALI cultures, becoming more pronounced at 24 hpi (Figures 4.2 and 4.3), and were associated with increased permeability to FITC-dextran compared to uninfected ALI cultures ($P = 0.0013$) (Figure 4.4). This recalls the goblet cell death and epithelial rupture reported for *P. aeruginosa* in an identical *in vitro* model, via the Type III Secretion System (T3SS) [20]; however, since *A. baumannii* lacks this virulence mechanism, it is likely that other secretion systems (*e.g*. the T6SS) or virulence factors are responsible for the epithelial damage observed in our study. In addition, the altered ZO-1 fluorescence pattern highlighted the different strategy used by *A. baumannii* compared to *Burkholderia cenocepacia*, which disrupts the cell-to-cell junctions at the occluding level, leaving ZO-1 unaffected [33]. Interestingly, we did not observe alterations in ciliated cells or the overexpression of Spondin 2 (SPON2), a pattern recognition receptor (PRR) molecule, known to be upregulated upon bronchial epithelial interaction with nontypeable *Haemophilus influenzae* [34]. Taken together, these findings indicate that *A. baumannii* adopts unique strategies to disrupt the airway epithelial integrity, underlining the importance of pathogen-specific studies and reliable *in vitro* models for accurately dissecting airway infection dynamics and host–pathogen interactions.

At the transcriptomic level, RNA sequencing and bioinformatics analyses identified 668 DEGs, with 441 upregulated and 227 downregulated in infected versus uninfected ALI cultures at 4 hpi. Three main pathways were detected (Figure 4.6). Most upregulated genes were involved in the production and release of pro-inflammatory cytokines, chemokines, and immune mediators that facilitate immune cell recruitment, particularly neutrophils and macrophages, as previously reported [13]. This response is critical for pathogen clearance through phagocytosis and eventual bacterial killing. Several DEGs identified in this study overlapped with those reported in a previous study where human nasal epithelial cells were exposed to lipopolysaccharide (LPS) from *Escherichia coli* O55:B5 [35]. Common genes included *CSF3, CXCL1, CXCL8, CCL20, SAA1, BIRC3, IRAK2, NFKBIZ, ZC3H12A, RELB, IL1A*, and *JUN*, which are involved in chemokine-related pathways, such as the IL-17, TNF signaling pathways (Figures 4.5, 4.6, and Table 4.S2). Despite the structural differences between the lipooligosaccharide (LOS) of *A. baumannii* and the LPS of *E. coli* [35,36], both bacteria appear to elicit a similar chemokine-driven immune response. In addition, in our study, TLR signaling plays a key role in pathogen recognition, detecting other bacterial-related structures, such as porin proteins, peptidoglycan, lipoproteins, and CpG DNA motifs (Figures 4.6, and 4.7) [2,4,37]. The upregulation of the lncRNA MIR3142HG in response to *A. baumannii* LOS exposure further sustains the strong inflammation response observed, consistent with previous findings [38]. Studies in human pulmonary

microvascular endothelial cells have shown that this lncRNA induces the release of inflammatory mediators, enhances apoptosis, and contributes to endothelial barrier disruption [38]. In agreement with the three main pathways identified in our study, the upregulation of MIR3142HG shows how deeply these host responses are interconnected. Additionally, among the upregulated genes directly and indirectly encoding macrophage and neutrophil chemoattractant proteins, we identified *CXCL1, CXCL2, CXCL3, CXCL5, CXCL6, CXCL8, CCL20, CX3CL1, CXCL16, CSF3, SAA1*, and *SAA2* (Table 4.S2). These results are in agreement with those obtained from a mouse *in vivo* model, further supporting the strong host inflammatory response during *A. baumannii* infection [13]. Macrophages play a dual role in bacterial infections by directly defending against pathogens and promoting neutrophil recruitment [2,4,39]. Neutrophils are particularly critical in respiratory infections [2,4,40]. Upon infection, neutrophils are recruited to the site as early as 4 h, with infiltration peaking at 24 h post-infection. Notably, the strong upregulation of CXCL8 (IL-8) observed in this study is consistent with previous findings in lung cell lines [41,42], further supporting its key role in recruiting neutrophils and monocytes during *A. baumannii* infection. While neutrophil influx is particularly needed for pathogen clearance, inflammation must be finely controlled to avoid tissue damage, and to allow effective repair and rebuilding of the tissue. Accordingly, our pathway enrichment analysis indicates that intact and viable *A. baumannii* cells trigger the expression of genes directly and indirectly involved in the production of type 2 cytokines, IL-4, and IL-13 (Figure 4.5, and Table 4.S2). In contrast to type 1 immune responses, type 2 immunity plays a dual role, being anti-inflammatory to prevent excessive tissue damage caused by inflammation, and tissue-reparative, to promote tissue repair [43]. Matrix metalloproteases (MMPs) play an essential role in the normal tissue repair process by degrading almost every component of the extracellular matrix components [43]. Research has shown that IL-13 and, to some extent, IL-4 can induce the expression and activity of MMP7 and MMP13 in airway epithelial cells [43–45]. These MMP-inducers were also found to facilitate recruitment of neutrophils to the sites of infection [43–45]. Interestingly, in an *in vivo* model of *A. baumannii* pneumonia, MMP9 and MMP14 were upregulated, whereas the Gram-negative bacterium *Francisella tularensis* induces the expression of MMP9 only *in vivo*; these proteins could be responsible for bacterial spread, severe lung damage due to neutrophil accumulation, and increased mortality [13,46]. Furthermore, the opportunistic pathogen *P. aeruginosa* induces increased expression levels of MMP7 in human lung epithelial cells as early as 3 hpi, via flagellin signaling; the MMP7 upregulation may contribute to tissue damage and facilitate *P. aeruginosa* dissemination within injured tissues [47] (Lopez 2001). In addition, it has been reported that in *P. aeruginosa* infected differentiated human bronchial epithelial cell cultures, Th2 cytokines attenuates hBD-2 mRNA upregulation [43]. Conversely, in our experimental conditions, a net increase in defensin beta 4A (DEFB4A) mRNA was observed (Table 4.S2), suggesting a different behavior of *A. baumannii* with respect to *P. aeruginosa*. The Th2 cytokine pathway could synergize with the upregulated and downregulated expression of 68 and 22 genes, respectively, that affect directly and

indirectly epithelial barrier integrity, adhesion molecules, and cytoskeletal reorganization (Table 4.S2). Genes like *ICAM1, SDC4, VCL, CLDN1, LAMB3, LAMC2, FERMT2, RND1, RND3, RHOV, RHOB, ARHGEF6, ARHGEF19, DLC1, DOCK4, PALLD, ITGB8, KRT6B, KRT17,* and *SEPTIN11* regulate cytoskeletal organization, cell junctions, and adhesion. Together with the downregulation of *KRT15, VPS13D,* and *SRGAP3*, these data suggest epithelial barrier dysfunction, reduced cytoskeletal stability, and increased permeability, facilitating bacterial invasion and dissemination. These results are in agreement with the goblet cells appearance as swollen, grainy, and irregular shape, and corroborate the severe impact of *A. baumannii* on the overall architecture of ALI cultures (Figures 4.2, 4.6 and 4.7). Moreover, the upregulation of *MMP7, MMP13* as well as *MET, EPHA2, EFNA1, EFNA5, HBEGF, FGFBP1, TNS1, TNS4, PLAUR,* and *PTGES* as well as the downregulation of *PIK3R2, MAP3K1, CREB3L1, CREB3L2,* and *IRX5* could participate to extracellular matrix degradation. Noteworthy, these latter genes could also impair pro-survival and regenerative pathways [48]. Interestingly, also *PI3KR1* and *PIK3R2* were downregulated in our experimental conditions (Figures 4.6, 4.7 and Table 4.S2), in agreement with previous finding on *A. baumannii* infection *in vivo* [13]. Both genes encode regulatory subunits of Class IA phosphoinositide 3-kinases (PI3Ks), that mediates the synthesis of phosphatidylinositol (3,4,5)-trisphosphate (PIP_3) within cells. This lipid second messenger activates the PI3K-Akt pathway, a major survival signaling cascade. Among other effects, inhibition of this pathway can induce apoptosis [48,49]. This pathway is subverted by several human pathogens for their advantage. For instance, *Salmonella* and *Listeria monocytogenes* hijack the PI3K-Akt pathway to prevent host cell apoptosis, creating a protected intracellular niche for their survival [50–52]. In a human lung tissue explant model, Sohail et al. suggested that activation of the PI3K-Akt pathway could be modulated by *P. aeruginosa*-derived microRNAs targeting host mRNAs, thereby contributing to a rapid pro-inflammatory response, early epithelial barrier disruption, and activation of tissue damage-associated pathways [53]. Conversely, enteropathogenic *E. coli* [54], *Streptococcus pneumoniae* [55], *Klebsiella pneumoniae* [56], and *Bacillus anthracis* [57] inhibit the PI3K-Akt pathway to enhance bacterial survival and dissemination by promoting autophagy/cell death and disruption of epithelial barriers. This finding is consistent with previous studies demonstrating that *A. baumannii* infection induced apoptosis, pyroptosis, and necroptosis across different cell models, regardless of the strain used [58–62]. However, unlike a previous *in vivo* study [13], we did not observe JAK-STAT pathway activation. This discrepancy may be due to the earlier time point of our RNA-seq analysis (4 hpi vs. 24 hpi in the previous study), as JAK-STAT activation could be a later event in the host response. A limitation of our model is the lack of immune cells that are key producers of JAK-STAT-activating cytokines, which may further contribute to the absence of its activation. Finally, it is important to note differences from our previous studies using carcinogenic human lung epithelial cells, emphasizing the distinct host response observed in a more physiologically relevant model [42,63]. At the same time, our findings reinforce the reliability of ALI cultures in

dissecting the complex interplay between *A. baumannii* and the host. Despite some limitations (a single donor and one bacterial strain), a major strength of this study is the early analysis of the host response, which closely aligns with *in vivo* studies and provides crucial insights into the initial stages of infection.

4.5 Conclusion

This study highlights the early host response to *A. baumannii* using a physiologically relevant air–liquid interface (ALI) bronchial epithelium model. Within 4 hpi, *A. baumannii* triggered a strong inflammation, induced apoptosis/cell death, compromised cytoskeletal organization, leading to increased permeability and early tissue damage. By 24 hpi, goblet cell hypertrophy, reduced mucin secretion, and compromised epithelial integrity were highly evident. RNA sequencing revealed 668 DEGs across inflammation, epithelial barrier disruption, and apoptosis/cell death pathways, with a strong expression of pro-inflammatory chemokines (IL-8/CCL20) and type 2 cytokines (IL-4, IL-13), indicating that *A. baumannii* infection triggers both innate immune recruitment and broader inflammatory signalling. Significant alterations in cell adhesion and extracellular matrix genes suggest bacterial dissemination, while PI3K-Akt pathway inhibition aligns with other pathogens promoting cell death and barrier dysfunction. This work establishes a strong foundation for further investigations into *A. baumannii*-host interactions using a robust and reproducible human *in vitro* model. However, future studies including innate immune cells and focusing on cellular pathway herein described will be essential to fully elucidate the mechanisms underlying *A. baumannii* pathogenesis.

Supplementary information

Supplementary Material 1: Figure 4.S1. Histology of ALI infected with *A. baumannii*. A total of 20 µl of bacteria resuspended in DMEM-F12 was used for infection at an MOI of 2 and 5. Non-infected ALI cultures were treated with an equivalent volume of DMEM-F12 as a negative control. (A, B) Representative images of infected and uninfected ALI cultures stained with H&E at 4 hours post-infection (hpi) and (C, D) at 24 hpi, respectively.

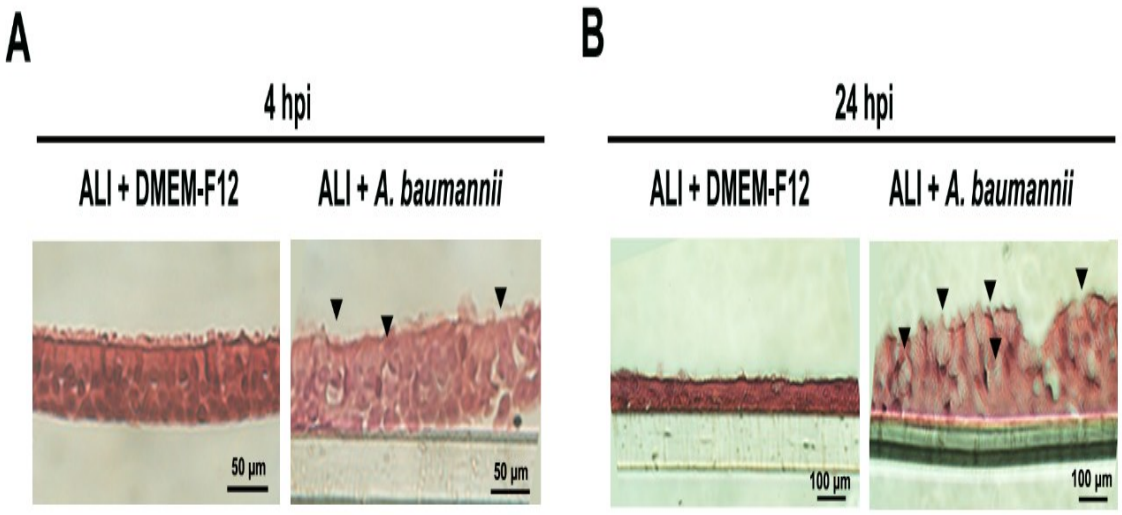

Supplementary Material 2: Figure 4.S2. Immunofluorescence of uninfected ALI cultures. ALI cultures were treated with 20 µl of DMEM-F12, and stained with antibodies against *A. baumannii* (*A.b.*) and either MUC5AC (green) or ZO-1 (green) at 24 h. Nuclei were counterstained with Hoechst 33342 (blue). Three independent experiments were performed. Scale bar sizes are indicated in the images.

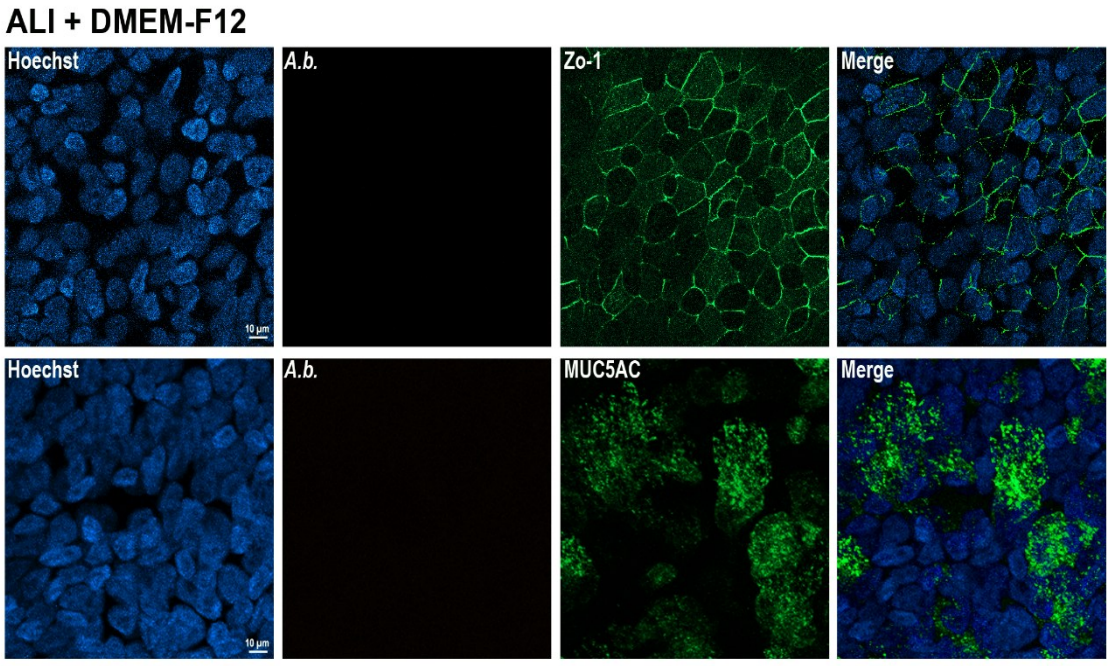

Supplementary Material 3: Figure 4.S3. Comparison of RNA-seq and RT-qPCR data. RT-PCR analysis of *PIK3R1, PIK3R2, NFKBIA, CXCL8, MAP3K1, SWAP70, RHOB, CASP10, IRAK2*, and *SOC3* in infected and uninfected ALI cultures of human bronchial epithelial cells. GAPDH was used as a reference gene. Each group contained three biological sample repeats, and each sample contained four technical repeats of qRT-PCR. A Pearson correlation coefficient of 0.9771 was observed between the RNA-seq and RT-qPCR data expressed as $\log_2$ fold change.

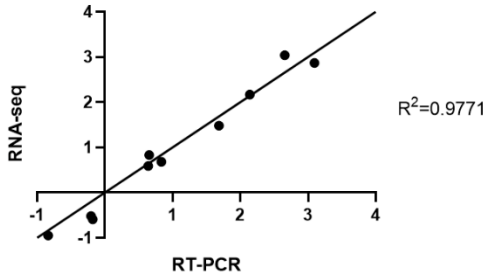

Table S1. Primers used to validate RNA-seq data by qRT-PCR analysis.

ID*	SYMBOL	Module 1	Module 2	Module 3	Primer 5'→3'
ENSG00000145675	PIK3R1	☒	☒	☒	FW CTCTCTGAAAGAACTGGTGCTACATT RV AACGACTCCCTCAATGTCACACTA
ENSG00000105647	PIK3R2	☒	☒	☒	FW CCCGGCAGAAGAAAATCAAC RV TCTTGCCCACGTACCAAGTG
ENSG00000100906	NFKBIA	☒	☒	☒	FW GCTGAAGAAGGAGCGGCTACT RV TCGTACTCCTCGTCTTTCATGGA
ENSG00000169429	CXCL8	☒			FW ACCGGAAGGAACCATCTCACT RV ATCAGGAAGGCTGCCAAGAG
ENSG00000095015	MAP3K1	☒			FW AATCACACCACCCCGAAGAG RV AACACGGCGGTTTGTTTCC
ENSG00000133789	SWAP70	☒	☒	☒	FW CAGCCCTCCACCACACAAA RV TGTCGCTCCAGTTCCTCTTGTT
ENSG00000143878	RHOB		☒		FW GACTCCCGCCCAAGCAT RV CCCCAAGTCAGTTGCAAATGT
ENSG00000003400	CASP10			☒	FW CTGGCAGAACTCCTCTATATCATACG RV CGTAGAGCAGGTTTCTAAACAGAGAA
ENSG00000134070	IRAK2	☒		☒	FW CCCCAGCAGATTCCATTACCT RV TGCTATGGCATTGCAGAACTG
ENSG00000184557	SOC3		☒		FW TGGGACGATAGCAACCACAA RV CGAAGTGTCCCCTGTTTGGA

*Up and downregulated genes are reported in green and red, respectively.

References

1. Cain, A. K. & Hamidian, M. Portrait of a killer: Uncovering resistance mechanisms and global spread of Acinetobacter baumannii. *PLOS Pathog.* **19**, e1011520 (2023).
2. Sarshar, M., Behzadi, P., Scribano, D., Palamara, A. T. & Ambrosi, C. Acinetobacter baumannii: An Ancient Commensal with Weapons of a Pathogen. *Pathogens* **10**, 387 (2021).
3. Shields, R. K., Paterson, D. L. & Tamma, P. D. Navigating Available Treatment Options for Carbapenem-Resistant *Acinetobacter baumannii-calcoaceticus* Complex Infections. *Clin. Infect. Dis.* **76**, S179–S193 (2023).
4. Shadan, A., Pathak, A., Ma, Y., Pathania, R. & Singh, R. P. Deciphering the virulence factors, regulation, and immune response to Acinetobacter baumannii infection. *Front. Cell. Infect. Microbiol.* **13**, 1053968 (2023).
5. Pompilio, A. *et al.* Cell-free supernatants from Lactobacillus strains exert antibacterial, antibiofilm, and antivirulence activity against Pseudomonas aeruginosa from cystic fibrosis patients. *Microbes Infect.* **26**, 105301 (2024).
6. Maure, A., Robino, E. & Van Der Henst, C. The intracellular life of Acinetobacter baumannii. *Trends Microbiol.* **31**, 1238–1250 (2023).
7. Wright, M. S., Jacobs, M. R., Bonomo, R. A. & Adams, M. D. Transcriptome Remodeling of *Acinetobacter baumannii* during Infection and Treatment. *mBio* **8**, e02193-16 (2017).
8. Martínez-Guitián, M. *et al.* Global Transcriptomic Analysis During Murine Pneumonia Infection Reveals New Virulence Factors in *Acinetobacter baumannii*. *J. Infect. Dis.* **223**, 1356–1366 (2021).
9. Allen, J. L., Tomlinson, B. R., Casella, L. G. & Shaw, L. N. Regulatory networks important for survival of Acinetobacter baumannii within the host. *Curr. Opin. Microbiol.* **55**, 74–80 (2020).
10. Méndez, J. A. *et al.* Quantitative proteomic analysis of host—pathogen interactions: a study of Acinetobacter baumannii responses to host airways. *BMC Genomics* **16**, 422 (2015).
11. Zhang, W. *et al.* Interactions between host epithelial cells and *Acinetobacter baumannii* promote the emergence of highly antibiotic resistant and highly mucoid strains. *Emerg. Microbes Infect.* **11**, 2556–2569 (2022).
12. Feng, Z. *et al.* Epithelial Innate Immune Response to Acinetobacter baumannii Challenge. *Infect. Immun.* **82**, 4458–4465 (2014).
13. Zeng, X. *et al.* Transcriptome Profiling of Lung Innate Immune Responses Potentially Associated With the Pathogenesis of Acinetobacter baumannii Acute Lethal Pneumonia. *Front. Immunol.* **11**, 708 (2020).
14. Baldassi, D., Gabold, B. & Merkel, O. M. Air−Liquid Interface Cultures of the Healthy and Diseased Human Respiratory Tract: Promises, Challenges, and Future Directions. *Adv. NanoBiomed Res.* **1**, 2000111 (2021).
15. BéruBé, K., Prytherch, Z., Job, C. & Hughes, T. Human primary bronchial lung cell constructs: The new respiratory models. *Toxicology* **278**, 311–318 (2010).
16. Prytherch, Z. *et al.* Tissue-Specific Stem Cell Differentiation in an in vitro Airway Model. *Macromol. Biosci.* **11**, 1467–1477 (2011).
17. Dvorak, A., Tilley, A. E., Shaykhiev, R., Wang, R. & Crystal, R. G. Do Airway Epithelium Air–Liquid Cultures Represent the *In Vivo* Airway Epithelium Transcriptome? *Am. J. Respir. Cell Mol. Biol.* **44**, 465–473 (2011).
18. Pleguezuelos-Manzano, C. *et al.* Establishment and characterization of a new *Pseudomonas aeruginosa* infection model using 2D airway organoids and dual RNA sequencing. Preprint at https://doi.org/10.1101/2023.03.11.532178 (2023).
19. Tang, M. *et al.* Evaluating Bacterial Pathogenesis Using a Model of Human Airway Organoids Infected with Pseudomonas aeruginosa Biofilms. *Microbiol. Spectr.* **10**, e02408-22 (2022).

20. Swart, A. L. *et al.* Pseudomonas aeruginosa breaches respiratory epithelia through goblet cell invasion in a microtissue model. *Nat. Microbiol.* **9**, 1725–1737 (2024).

21. Manna, V. & Caradonna, S. Isolation, expansion, differentiation, and histological processing of human nasal epithelial cells. *STAR Protoc.* **2**, 100782 (2021).

22. Sarshar, M. *et al.* Adaptive strategies of uropathogenic Escherichia coli CFT073: from growth in lab media to virulence during host cell adhesion. *Int. Microbiol.* **25**, 481–494 (2022).

23. Chen, S., Zhou, Y., Chen, Y. & Gu, J. fastp: an ultra-fast all-in-one FASTQ preprocessor. *Bioinformatics* **34**, i884–i890 (2018).

24. Dobin, A. *et al.* STAR: ultrafast universal RNA-seq aligner. *Bioinformatics* **29**, 15–21 (2013).

25. Li, B. & Dewey, C. N. RSEM: accurate transcript quantification from RNA-Seq data with or without a reference genome. *BMC Bioinformatics* **12**, 323 (2011).

26. McCarthy, D. J., Chen, Y. & Smyth, G. K. Differential expression analysis of multifactor RNA-Seq experiments with respect to biological variation. *Nucleic Acids Res.* **40**, 4288–4297 (2012).

27. Durinck, S., Spellman, P. T., Birney, E. & Huber, W. Mapping identifiers for the integration of genomic datasets with the R/Bioconductor package biomaRt. *Nat. Protoc.* **4**, 1184–1191 (2009).

28. Yu, G. Thirteen years of clusterProfiler. *The Innovation* **5**, 100722 (2024).

29. Yu, G. & He, Q.-Y. ReactomePA: an R/Bioconductor package for reactome pathway analysis and visualization. *Mol. Biosyst.* **12**, 477–479 (2015).

30. Shannon, P. *et al.* Cytoscape: A Software Environment for Integrated Models of Biomolecular Interaction Networks. *Genome Res.* **13**, 2498–2504 (2003).

31. Engelman, J. A., Luo, J. & Cantley, L. C. The evolution of phosphatidylinositol 3-kinases as regulators of growth and metabolism. *Nat. Rev. Genet.* **7**, 606–619 (2006).

32. Davis, J. D. & Wypych, T. P. Cellular and functional heterogeneity of the airway epithelium. *Mucosal Immunol.* **14**, 978–990 (2021).

33. Kim, J. Y., Sajjan, U. S., Krasan, G. P. & LiPuma, J. J. Disruption of Tight Junctions during Traversal of the Respiratory Epithelium by *Burkholderia cenocepacia*. *Infect. Immun.* **73**, 7107–7112 (2005).

34. Baddal, B. *et al.* Dual RNA-seq of Nontypeable Haemophilus influenzae and Host Cell Transcriptomes Reveals Novel Insights into Host-Pathogen Cross Talk. *mBio* **6**, e01765-15 (2015).

35. Tan, S. *et al.* Insights from bioinformatics analysis reveal that lipopolysaccharide induces activation of chemokine-related signaling pathways in human nasal epithelial cells. *Sci. Rep.* **14**, 7672 (2024).

36. Rodriguez-Loureiro, I., Latza, V. M., Fragneto, G. & Schneck, E. Conformation of Single and Interacting Lipopolysaccharide Surfaces Bearing O-Side Chains. *Biophys. J.* **114**, 1624–1635 (2018).

37. Noto, M. J. *et al.* Toll-Like Receptor 9 Contributes to Defense against Acinetobacter baumannii Infection. *Infect. Immun.* **83**, 4134–4141 (2015).

38. Gong, X. *et al.* MIR3142HG promotes lipopolysaccharide-induced acute lung injury by regulating miR-450b-5p/HMGB1 axis. *Mol. Cell. Biochem.* **476**, 4205–4215 (2021).

39. Qiu, H. *et al.* Role of Macrophages in Early Host Resistance to Respiratory Acinetobacter baumannii Infection. *PLoS ONE* **7**, e40019 (2012).

40. Van Faassen, H. *et al.* Neutrophils Play an Important Role in Host Resistance to Respiratory Infection with *Acinetobacter baumannii* in Mice. *Infect. Immun.* **75**, 5597–5608 (2007).

41. March, C. *et al.* Dissection of Host Cell Signal Transduction during Acinetobacter baumannii – Triggered Inflammatory Response. *PLoS ONE* **5**, e10033 (2010).

42. Ambrosi, C. *et al.* Acinetobacter baumannii Targets Human Carcinoembryonic Antigen-Related Cell Adhesion Molecules (CEACAMs) for Invasion of Pneumocytes. *mSystems* **5**, e00604-20 (2020).

43. Allen, J. E. IL-4 and IL-13: Regulators and Effectors of Wound Repair. *Annu. Rev. Immunol.* **41**, 229–254 (2023).

44. Wadsworth, S. J. *et al.* IL-13 and TH2 cytokine exposure triggers matrix metalloproteinase 7–mediated Fas ligand cleavage from bronchial epithelial cells. *J. Allergy Clin. Immunol.* **126**, 366-374.e8 (2010).

45. Lee, H. S. & Kim, W. J. The Role of Matrix Metalloproteinase in Inflammation with a Focus on Infectious Diseases. *Int. J. Mol. Sci.* **23**, 10546 (2022).

46. Malik, M. *et al.* Matrix Metalloproteinase 9 Activity Enhances Host Susceptibility to Pulmonary Infection with Type A and B Strains of *Francisella tularensis*. *J. Immunol.* **178**, 1013–1020 (2007).

47. López-Boado, Y. S., Wilson, C. L. & Parks, W. C. Regulation of Matrilysin Expression in Airway Epithelial Cells by Pseudomonas aeruginosa Flagellin. *J. Biol. Chem.* **276**, 41417–41423 (2001).

48. Hoxhaj, G. & Manning, B. D. The PI3K–AKT network at the interface of oncogenic signalling and cancer metabolism. *Nat. Rev. Cancer* **20**, 74–88 (2020).

49. Hemmings, B. A. & Restuccia, D. F. PI3K-PKB/Akt Pathway. *Cold Spring Harb. Perspect. Biol.* **4**, a011189–a011189 (2012).

50. Gessain, G. *et al.* PI3-kinase activation is critical for host barrier permissiveness to *Listeria monocytogenes*. *J. Exp. Med.* **212**, 165–183 (2015).

51. Ireton, K. *et al.* A Role for Phosphoinositide 3-Kinase in Bacterial Invasion. *Science* **274**, 780–782 (1996).

52. Steele-Mortimer, O. *et al.* Activation of Akt/Protein Kinase B in Epithelial Cells by theSalmonella typhimurium Effector SigD. *J. Biol. Chem.* **275**, 37718–37724 (2000).

53. Sohail, A. *et al.* Differential transcriptomic host responses in the early phase of viral and bacterial infections in human lung tissue explants ex vivo. *Respir. Res.* **25**, 369 (2024).

54. Celli, J., Olivier, M. & Finlay, B. B. Enteropathogenic Escherichia coli mediates antiphagocytosis through the inhibition of PI 3-kinase-dependent pathways. *EMBO J.* **20**, 1245–1258 (2001).

55. Li, P. *et al.* Streptococcus pneumoniae Induces Autophagy through the Inhibition of the PI3K-I/Akt/mTOR Pathway and ROS Hypergeneration in A549 Cells. *PLOS ONE* **10**, e0122753 (2015).

56. Kamaladevi, A. & Balamurugan, K. Global Proteomics Revealed Klebsiella pneumoniae Induced Autophagy and Oxidative Stress in Caenorhabditis elegans by Inhibiting PI3K/AKT/mTOR Pathway during Infection. *Front. Cell. Infect. Microbiol.* **7**, 393 (2017).

57. Popova, T. *et al.* Anthrax infection inhibits the AKT signaling involved in the E-cadherin-mediated adhesion of lung epithelial cells. *FEMS Immunol. Med. Microbiol.* **56**, 129–142 (2009).

58. Gaddy, J. A., Tomaras, A. P. & Actis, L. A. The *Acinetobacter baumannii* 19606 OmpA Protein Plays a Role in Biofilm Formation on Abiotic Surfaces and in the Interaction of This Pathogen with Eukaryotic Cells. *Infect. Immun.* **77**, 3150–3160 (2009).

59. Kang, M., Jo, S., Kim, D. & Park, J. NLRP 3 inflammasome mediates interleukin-1 β production in immune cells in response to *Acinetobacter baumannii* and contributes to pulmonary inflammation in mice. *Immunology* **150**, 495–505 (2017).

60. Pires, S. & Parker, D. Innate Immune Responses to *Acinetobacter baumannii* in the Airway. *J. Interferon Cytokine Res.* **39**, 441–449 (2019).

61. Li, Y. *et al.* Type I IFN operates pyroptosis and necroptosis during multidrug-resistant *A. baumannii* infection. *Cell Death Differ.* **25**, 1304–1318 (2018).

62. Lee, J. S., Choi, C. H., Kim, J. W. & Lee, J. C. *Acinetobacter baumannii* outer membrane protein a induces dendritic cell death through mitochondrial targeting. *J. Microbiol.* **48**, 387–392 (2010).

63. Ambrosi, C. *et al.* A*cinetobacter baumannii* Virulence Traits: A Comparative Study of a Novel Sequence Type with Other Italian Endemic International Clones. *Front. Microbiol.* **8**, 1977 (2017).

Chapter 5. Third-Generation Cephalosporin-Resistant Uropathogenic *Escherichia coli* From Community- and Hospital-Acquired Infections Show High Level of Antibiotic Resistance and Specific Virulence Traits

Amina Bougouizi[1], Astri Dwyanti Tagueha[2], Daniela Scribano[2], Zohra Chekroud[1], Zahrat el Imen Lamraoui[3]; Lucia Nencioni[2], Cecilia Ambrosi[4,5], and Hamza Rahab[6]

[1]Research Laboratory of Interactions, Biodiversity, Ecosystems and Biotechnology, Department of Nature and Life Sciences, Faculty of Sciences, University 20 August 1955 Skikda, Skikda 21000, Algeria; [2]Department of Public Health and Infectious Diseases, Sapienza University of Rome, Rome 00185, Italy; [3]Biotechnology's Laboratory of the Bioactive Molecules and the Cellular Physiopathology, Department of Biology of Organisms, Faculty of Natural and Life Sciences, University of Batna2, Batna, Algeria; [4]Department of Promotion of Human Sciences and Quality of Life, San Rafaele University, Rome, Italy; [5]Laboratory of Microbiology of Chronic-Neurodegenerative Diseases, IRCCS San Rafaele Roma, Rome, Italy; [6]Biotechnology Research Center - C.R.Bt Constantine, El Khroub, Algeria.

Published on 5 May 2025

Journal

Canadian Journal of Infectious Diseases and Medical Microbiology

IF (May 2026): 2.6

doi

https://doi.org/10.1155/cjid/9021465

Abstract

Escherichia coli is a leading cause of both community-acquired and nosocomial infections. In particular, *E. coli* is responsible for 90% of all uncomplicated urinary tract infections (UTIs) and 65% of complicated UTIs. Among complicated UTIs, those caused by third-generation cephalosporin (3GC)–resistant *E. coli* strains, expressing extended-spectrum beta-lactamases (ESBLs), are on the rise. These strains show often a multidrug-resistant (MDR) phenotype, limiting the therapeutic options and the increasing incidence of MDR *E. coli* in Algeria is concerning. This study aims to compare the antibiotic resistance rates and profiles as well as the virulence traits between 3CG-resistant *E. coli* isolates, collected from Algerian inpatients (IPs) and outpatients (OPs). Our analyses include phenotypic and genotypic resistance factor detection, strains classification by genotyping and phylogrouping, as well as genotypic and phenotypic virulence factor evaluation. Among 42 *E. coli* isolates, 76.20% caused UTIs. ESBL producers ($n = 35$) carried all the $bla_{\text{CTX–M}}$, while bla_{TEM} was found in 69.04% of isolates. All isolates were MDR, and no significant differences in type and rate of antibiotic resistance were observed between IP- and OP-isolates. OP-isolates demonstrated greater virulence, exhibiting higher motility and biofilm production, compared to IP-isolates. Moreover, pathogenic Phylogroup B2 was prevalent among OP-isolates, while IP-isolates belonged predominantly to Phylogroup A. Our data suggest a uniform spreading of antibiotic-resistant genes within hospitals and communities. However, hospital environment selects for less virulent strains with increasing level of resistance; differently, communities host more virulent strains. This study highlights the urgent need to implement the surveillance of 3CG-resistant *E. coli* and to adopt the One Health approach to monitor the antimicrobial resistance (AMR) in the country.

5.1 Introduction

Escherichia coli, the principal facultative anaerobe found in the intestinal microbiota of humans and warm-blooded animals, exhibits a remarkable adaptability and genomic diversity [1]. While the majority of *E. coli* strains are commensal, certain strains have evolved pathogenic mechanisms capable of causing severe diseases [1,2]. *E. coli* strains can be categorized into different phylogroups-A, B1, B2, C, D, E, and, F-indicating their animal or human origin as well as their virulent potential [3]. Indeed, pathogenic *E. coli* strains primarily belong to Phylogroups B2 and D, whereas commensal strains are predominantly found within Phylogroups A and B1 [4]. However, commensal phylogroups often display heightened resistance profiles while expressing a more limited array of virulence genes compared to pathogenic phylogroups [4,5].

E. coli can be classified based on its capacity to cause infections either within the gastrointestinal tract due to intestinal pathogenic *E. coli* pathotypes (IPEC), or outside due to extraintestinal pathogenic *E. coli* strains (ExPEC) [1,6]. The latter group can cause a variety of infections, particularly urinary tract infections (UTIs), pneumonia, bacteremia, soft tissue infections (surgical wounds), bloodstream infections, lower respiratory tract infections, and neonatal meningitis [1,7]. Virulence genes encoding

various functions crucial for adhesion, colonization, invasion, and evasion of host defenses are common features of pathogenic *E. coli* strains. These genes are often clustered in chromosomal blocks, plasmids, or phages, making transfer between different *E. coli* strains easy and contributing to the dynamic nature of their pathogenicity [1].

Uropathogenic *E. coli* (UPEC) strains are the most common pathogens responsible for approximately 90% of all uncomplicated UTIs and 65% of complicated UTIs [8]. Cystitis, a single episode of pyelonephritis, and some cases of recurrent cystitis can be classified as uncomplicated UTIs, as they are eradicated with first-line antibiotics and they result in no long-term complications. Any UTI that does not meet the above criteria or clinical management is considered a complicated UTI. Examples are UTIs in males, in immunocompromised subjects, recurrent UTIs caused by resistant strains, and hospital-acquired UTIs (HA-UTI) [9]. Risk factors of HA-UTI include catheterization, bladder dysfunction, long-term hospitalization, previous UTI history, age, and comorbidities, including diabetes, hypertension, and stroke [10]. Among HA-UTI, UPEC strains account for about 50% of total cases and the most frequently isolated from catheters [11]. Major pandemic ExPEC lineages responsible for UTIs include sequence types (ST) ST131, ST73, ST69, and ST95. However, ST131, characterized by high level of antibiotic resistance, is the predominant one in hospital settings [12]. Although there are no genomic signatures defining UPEC strains, the presence of specific urovirulence factors can support their identifications. These factors include redundant iron acquisition systems, several pili associated with specific adhesins, hemolysins, and/or cytotoxins and biofilm forming ability [13]. Accordingly, the majority of studies characterizing UPEC isolates include the analysis of urovirulence factors [13].

The management of uncomplicated UTIs is based on the use of first line antibiotic such as nitrofurantoin, sulfamethoxazole/trimethoprim, fosfomycin, and first-generation cephalosporins [14]. Differently, in complicated UTIs, the co-administration of amoxicillin plus an aminoglycoside, a second-generation cephalosporin plus an aminoglycoside, and a third-generation cephalosporin (3GC), mainly as an empirical treatment, are recommended [9].

3GC-resistant *E. coli* isolates show an increasing trend worldwide. The most critical geographical areas include African and Asian countries with percentages of 3GC-resistant isolates reaching 90% in Burkina Fasu and Bangladesh [15]. In Algeria, 3GCs are extensively prescribed for treating various infections acquired both in hospital and community settings [16,17]. According to Algerian Antibiotic Resistance Surveillance Network (AARN) report, *E. coli* was identified as the predominant pathogen responsible for UTIs in both hospitalized and outpatient (OP) populations, accounting for 52.72% and 61.00% of isolates, respectively. Resistance to 3GC was reported in 27.84% of hospital isolates and 14.84% OP-isolates, respectively, leading to an overall resistance rate of 21.14% [18].

The widespread use of 3CGs, compounded by factors such as inadequate infection control measures and inappropriate antibiotic use, has led to a concerning rise in resistance to these agents, particularly due to the emergence of extended-spectrum β-lactamases (ESBLs) [14,19,20]. ESBLs are versatile enzymes responsible for the hydrolysis of beta-lactam antibiotics including penicillins and first to 3GC, and they are categorized molecularly and functionally according to Ambler and Bush Jacoby-Medeiros classifications [21,22]. *Escherichia coli* species mainly expresses three different ESBL types, including Cefotaximase-Munich (CTX-M), Temoniera (TEM), and sulfhydryl variable (SHV) enzymes [23]. These three ESBL types are classified in the Ambler class A and Bush Jacoby-Medeiros Group 2. In *E. coli*, the CTX-M type is the most widespread and includes 270 variants, whose genes are hosted within plasmids, transposons and integrons. They are responsible for the hydrolysis of cefotaxime, and they are found in the most resistant *E. coli* strains worldwide [23].

TEM enzymes were among the first beta-lactamases discovered, originally conferring resistance to penicillin and to the first-generation cephalosporins. Subsequently, the progressive accumulation of mutations resulted in the evolution of 202 variants with the capability to hydrolyze a broader spectrum of beta-lactams, including 3GC [24]. Moreover, TEM enzymes are also not susceptible to beta-lactamase inhibitors such as clavulanic acid and sulbactam making *E. coli* isolates resistant to amoxicillin-clavulanic acid and ampicillin-sulbactam, commonly used in community and hospitals [24]. The SHV type was initially identified in *Klebsiella pneumoniae* and showed a narrow spectrum of activity. Overtime, the 232 *E. coli* variants gained the capability to hydrolyze cephalosporins and monobactams [23]. In *E. coli*, the most represented type is CTX-M. Moreover, $bla_{\text{CTX–M15}}$ gene was found to be positively associated with multidrug-resistant (MDR) *E. coli* strains. Indeed, these isolates show co-resistance to aminoglycosides and fluoroquinolones. It was suggested that the plasmidic co-carriage of plasmid-mediated quinolone resistance (PMQR) genes (i.e., *qnr* genes), and aminoglycoside methylases genes could favor the $bla_{\text{CTX–M15}}$ maintenance and spreading [25]. This antibiotic-resistant gene content aligns with the alarmingly high rate of MDR *E. coli* isolates in Algeria; indeed, recent findings reported that about the 70% of clinical isolates shows an MDR phenotype. [26,27]. Moreover, antimicrobial resistance (AMR) extends beyond hospitalized patients, affecting animals, food, the environment, and nonhospitalized populations in Algeria. Several reports highlighted the presence of about 40% of MDR *E. coli* in healthy and diseased livestock [28,29]. The spread of ESBL-producing *E. coli* is driven by excessive antibiotic use in human and veterinary medicine [30], inadequate infection control measures, and international travels [31], which facilitates their dissemination from high-prevalence regions. Additionally, the genetic adaptability of certain lineages to the host, as ST131, causes a prolonged intestinal carriage, further expanding its transmission [32]. Carbapenems were and are the last resort antibiotics for treating ESBL-producing strains; however, their widespread use has promoted the emergence and dissemination of carbapenem-resistant strains, in several types of bacteria

including [33–35]. Although the rate of carbapenem-resistant *E. coli* strains in Algeria is still low, the identification of bla_{OXA48} as well as bla_{NDM} genes, coding for enzymes capable to hydrolyze carbapenems, is becoming a great concern [35,36].

In light of this emerging trend, this study aims to compare the antibiotic resistance rates and profiles as well as the virulence traits between 3CG-resistant ExPEC isolates collected from Algerian inpatients (IPs) and OPs. Our analyses include phenotypic and genotypic resistance factor detection, strains classification by genotyping and phylogrouping, as well as genotypic and phenotypic virulence factor (VF) evaluation. This comprehensive investigation will increase our knowledge on 3CG-resistant *E. coli* in order to identify appropriate strategies to control their spread and to develop innovative therapeutic as well as antivirulence approaches.

5.2 Materials and Methods

5.2.1 Clinical Isolates Collection

Clinical isolates belonging to *Enterobacterales* were collected between October 2020 and June 2022 from both the public Abderrezek Bouhara Hospital and several private clinical laboratories, selected for their large catchment area in Skikda city, Algeria. To select isolates responsible for extraintestinal infections, urine, pus, blood, and cerebrospinal fluid were screened. Isolates identified as cefotaxime-resistant based on antibiogram results provided by the clinical microbiology laboratories were included in the study. Using the formula $4PQ/L^2$ [37], the initial sample size was determined to be 29 isolates based on a 95% confidence level, 10% error margin, and 8% prevalence of *Entrobacterales* ESBL producers in Algerian clinical centers, as reported in a previous study [38]. To minimize the error margins, the sample size was expanded to 82 isolates. The work chart of sample collection and treatments is shown in Figure 5.1.

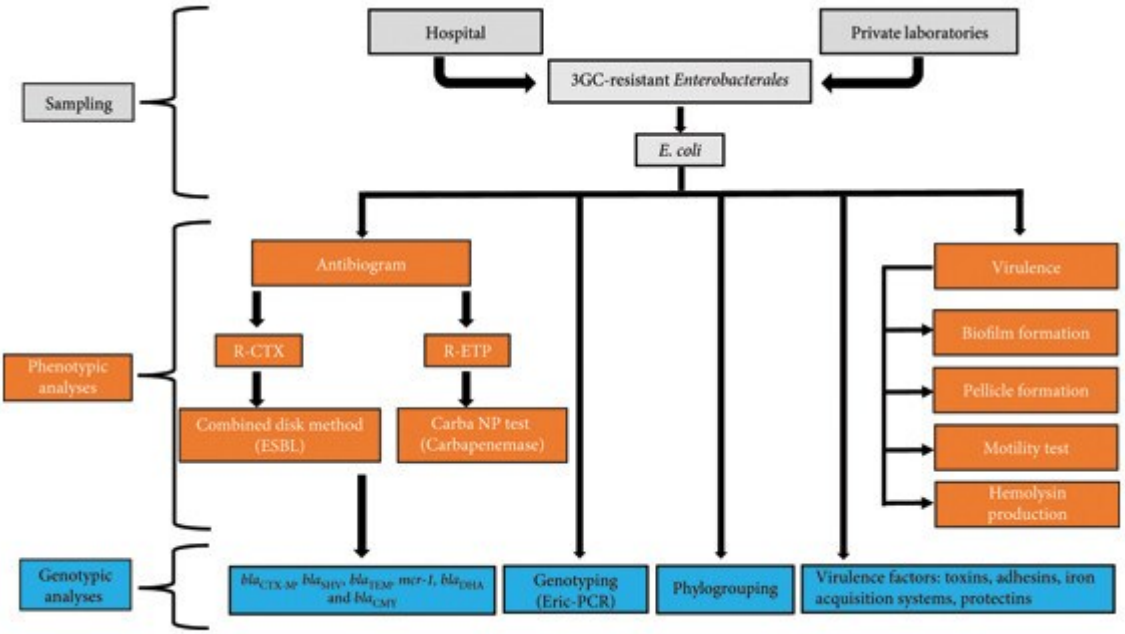

Figure 5.1. Flowchart of sample collection and genotypic and phenotypic analyses. Clinical isolates belonging to *Enterobacterales* were collected from both the public Abderrezek Bouhara Hospital and several private clinical laboratories. After testing for the resistance to 3GC, isolates belonging to *Escherichia coli* species were selected for genotypic and phenotypic analyses as described in the main text.

5.2.2 Clinical Isolates Identification and Antibiotic Susceptibility Testing

Procedures for collection, transport, and clinical isolate identification followed the clinical microbiology procedures described by Leber [39]. Clinical samples were cultured on blood agar and MacConkey agar plates (BioMérieux, France) and incubated for 24 h at 37°C. The CHROMAgar™ Orientation (DMED, Alger, Algeria) medium was also used, as previously described [35]. Isolated colonies were identified using the automated VITEK® 2 Compact 15 system (BioMérieux) and stocked in tryptic soy broth (TSB) containing 15% of glycerol at −70°C. For each experiment, isolates were freshly plated onto Lennox broth (LB) agar plates (LA, Difco, Milan, Italy) and cultured for 16 h at 37°C. VITEK 2 was also employed for antibiotic susceptibility testing. Tested antibiotics included, ampicillin (AMP), amoxicillin/clavulanic acid (AMC), piperacillin/tazobactam (TZP), cefazolin (CZ), cefoxitin (FOX), cefotaxime (CTX), ceftazidime (CAZ), imipenem (IMP), ertapenem (ETP), amikacin (AK), gentamicin (GEN), ciprofloxacin (CIP), fosfomycin (FOS), chloramphenicol (CHL), sulfamethoxazole/trimethoprim (SXT), and nitrofurantoin (NIT). The obtained minimal inhibitory concentration (MIC) values were interpreted by comparison with the standard set by Clinical Laboratory Standard Institute (CLSI 2020, Version of M02 M07 M11, 30th ed). *E. coli* strain ATCC 25922 served as the reference strain for the analysis. Additionally, the broth microdilution method was employed to ascertain the colistin MIC values following CLSI guidelines.

Bacteria were classified as MDR when resistant to at least one antibiotic in three or more antibiotic categories [40].

5.2.3 Phenotypic Characterization of ESBL and Carbapenemase Production

ESBL production among isolates was evaluated through the combined disk method [41]. The production of carbapenem-hydrolyzing enzymes was assessed using the modified Carba-NP test [42].

5.2.4 Detection of Beta-Lactamase and mcr-1 Genes

DNA extraction was carried out using the boiling lysis method [35]. Briefly, isolated colonies were resuspended in 100 µL of nuclease-free water and incubated at 95°C for 10 min. After centrifugation at 10.000 × g for 10 min, supernatants were retrieved and stored at −20°C before use. DNA purity and concentration were assessed using a NanoDrop 8000 spectrophotometer (Thermo Fisher Scientific, Waltham, MA, USA). Conventional PCR was utilized to screen for the presence of the three most frequent beta-lactamase-encoding genes (*bla*$_{CTX-M}$, *bla*$_{TEM}$, and *bla*$_{SHV}$), as previously described Bougouzi [35]. Additionally, for isolates demonstrating resistance to cefoxitin, two *ampC*-encoding genes (*bla*$_{DHA}$ and *bla*$_{CMY}$) were targeted, as previously described [43,44]. Nuclease-free water was used as negative control in each reaction. Each PCR reaction was prepared according to the manufacturer's instruction, with a total volume of 15 µL, including 7.5 µL of Master Mix (Thermo Fisher Scientific), 0.2 µL of each primer pairs (forward and reverse primer solution), 1 µL of DNA template, and 6.1 µL of nuclease-free water to reach the final volume. In addition to beta-lactamase-encoding genes, the presence of *mcr*-1 gene, coding for the resistance to colistin, was screened, as previously described [45]. The primer sequences and amplicon sizes are summarized in Table 4.1. The PCR products were separated by electrophoresis on a 1.5% agarose gel, stained with Sybr Green, and visualized under a UV transilluminator.

5.2.5 Genotyping, Phylogrouping, and Detection of Virulence Genes

Isolates belonging to *E. coli* species were selected for genotyping and phylogrouping analyses. Isolates were genotyped using *Enterobacterial* Repetitive Intergenic Consensus sequence (ERIC)-PCR profiles as previously described [46]. Phylogenetic grouping was performed by quadruplex PCR [5,46,47]. Primers are reported in Table 5.1. Isolates not belonging to any phylogroup were excluded from further analyses. The presence of virulence genes was assessed by multiplex as well as single PCR assays as previously described [47,48]. The banding patterns generated from ERIC-PCR were examined using TotalLab TL120 Trace Version 2006 (nonlinear dynamics) with a position tolerance set at 1.5%. Following the calculation of the Dice coefficient of similarity, cluster analysis was carried out in XLstat 7.5 (Addinsoft, USA), using the unweighted pair group method with arithmetic averages (UPGMA). To distinguish clonally distinct groups, the percentage of similarity was established at 60%.

E. coli isolates were tested for the presence of 24 virulence genes via a standard PCR assay. The virulence genes targeted included adhesins: *sfa/focDE* (S fimbriae or F1C fimbriae), *papC* (P fimbriae major subunit), *papG* (P fimbriae adhesin), *tsh* (temperature-sensitive hemagglutinin), *yadN* (outer membrane protein), *papAH* (P fimbriae assembly protein); toxins: *usp* (uropathogenic specific protein), *sat* (secreted autotransporter toxin), *traT* (transfer protein T), *vat* (vacuolating autotransporter toxin), *hlyA* (hemolysin A), *malX* (MalX regulator), *cnf1* (cytotoxic necrotizing factor 1), *ibeA* (invasion of brain endothelium A), *clbN* (colibactin N), *clbB* (colibactin B), siderophores: *feoB* (ferrous iron transport protein B), *iroN* (iron transport protein N), *iutA* (ferric aerobactin receptor), *fyuA* (ferric yersiniabactin receptor), *chuA* (hemin receptor), *irp2* (iron-repressible protein 2), and protectins: *kpsMT II* (capsular polysaccharide export inner-membrane protein) and *ompT* (outer membrane protease T) (Table 5.S3). The UPEC reference strain CFT073 and strains B10P, I12P, and H20P, previously isolated from colonic adenoma, were used as positive controls [47,48]. Nuclease-free water was included as negative control. Each isolate was assigned an arbitrary VF score [47].

Table 5.1. List of primer sequences used in the PCR reactions for detection of resistance genes and for phylogenetic grouping.

Primer Function	Target	Primer sequence	Amplicon size (bp)	Reference
beta-lactamase genes	bla_{CTX-M}	F-TTTGCGATGTGCAGTACCAGTAA	500	35
		R-CGATATCGTTGGTGGTGCCATA		
	bla_{TEM}	F-ATGAGTATTCAACATTTCCG	840	35
		R-CCAATGCTTAATCAGTGAGG		
	bla_{SHV}	F-TTTATGGCGTTACCTTTGACC	1051	35
		R-ATTTGTCGCTTCTTTACTCGC		
	bla_{CMY}	F-ATGATGAAAAAATCGTTATGC	1200	43
		R-TTGCAGCTTTTCAAGAATGCGC		
	bla_{DHA}	F-TGATGGCACAGCAGGATATTC	997	44
		R-GCTTTGACTCTTTCGGTATTCG		
Colistin-resistance gene	*mrc-1*	F-AGTCCGTTTGTTCTTGTGGC	320	45
		R-AGATCCTTGGTCTCGGCTTG		
Phylotyping	*chuA*	F-ATGGTACCGGACGAACCAAC	288	5
		R-TGCCGCCAGTACCAAAGACA		
	yjaA	F-CAAACGTGAAGTGTCAGGAG	211	5
		R-AATGCGTTCCTCAACCTGTG		
	TspE4.C2	F-CACTATTCGTAAGGTCATCC	152	5
		R-AGTTTATCGCTGCGGGTCGC		
	arpA	F-AACGCTATTCGCCAGCTTGC	400	5
		R-TCTCCCCATACCGTACGCTA		
	Group E	F-GATTCCATCTTGTCAAAATATGCC	301	5
		R-GAAAAGAAAAAGAATTCCCAAGAG		
	Group C	F-AGTTTTATGCCCAGTGCGAG	219	5
		R-TCTGCGCCGGTCACGCCC		
	Internal control	F-CGGCGATAAAGACATCTTCAC	489	5
		R-GCAACGCGGCCTGGCGGAAG		

5.2.6 Phenotypic Assays

Production of hemolysin(s) was assessed using blood agar plates (bioMérieux, Milan, Italy), whereas motility using 0.3% agar plates (Difco, Milan, Italy). Plates were incubated at 20°C for 16 h and motility zones (mm) were evaluated using ImageJ software, as previously described [49]. Biofilm formation was measured as previously reported [47]. Briefly, overnight cultures were diluted 1:10 in fresh LB (Difco, Milan, Italy) and used to inoculate three replicate wells per microtiter plate (200 µL per well). Negative controls consisted of uninoculated wells containing sterile medium only and the *E. coli* strain D4C was used as positive control [47,50]. After reading the absorbance at 600 nm (OD_{600}), plates were washed three times with phosphate-buffer saline (PBS) solution, fixed with methanol for 20 min at room temperature, and stained with 0.1% crystal violet solution (Sigma, SIAL, Italy) for 15 min. After four additional washes with water, the surface-associated dye was solubilized with 200 µL of 33% acetic acid and the OD_{570} was recorded. Results were reported as the OD_{570}/OD_{600} ratio to normalize the amount of biofilm formed to the total bacterial content. The pellicle formation was assayed as previously described [50]. Ten microliters of overnight cultures were transferred into test tubes containing 3 mL of fresh LB. Tubes were incubated for 24 h at 37°C in static condition. Pellicles were photographed with a Xiaomi MI 10T phone. Sedimentation assay was performed as previously described [51]. Briefly, overnight cultures were diluted 1:100 in fresh LB (total volume 5 mL) and incubated statically at 37°C for 24 h. One hundred microliter samples were taken from the middle of the cultures, and the OD_{600} was measured using a 1-cm cuvette in a total volume of 1 mL. The OD_{600} value of 0.8 was chosen as a cut-off to distinguish nonaggregative and aggregative cells. Representative images were acquired with a Xiaomi MI 10T phone.

5.2.7 Statistical Analysis

The nonparametric data category was assigned to both the antibiotic effectiveness and the presence of virulence genes. Therefore, Wilcoxon matched-pairs signed rank test was used to determine the different distribution of these two variables among OP- and IP-isolates. Regarding the impact of virulence genes in multiple antibiotic susceptibility/resistance patterns, the binary logistic regression analysis was conducted to evaluate an association. The coefficient regression represents the likelihood (odds ratio = OR); therefore, VF genes with significant OR were recognized as predictors of susceptibility or resistance to antibiotic agents. Additionally, a permutational multivariate analysis of variance (PERMANOVA) test with 9999 permutations was performed to evaluate the differences in phenotypic characteristics among phylogroups and origins, followed by a sequential Bonferroni post hoc test. p values less than 0.05 were considered statistically significant. Nonparametric and logistic regression analyses were performed using IBM SPSS Statistics, Version 23.0 (IBM Corporation, Cary, NC, USA), and PERMANOVA test was executed using Past software Version 4.11 (Oslo, Norway).

5.3 Results

5.3.1 3GC-Resistant *E. coli* Isolates Collected From OPs and IPs Belong to Different Phylogroups

A total of 82 isolates belonging to *Enterobacterales* and resistant to 3GC were collected, with 37 from IPs and 45 from OPs. The identification results showed that the highest proportion of isolates were *E. coli* ($n = 47$; 57.32%), followed by *K. pneumoniae* (34.00%). Four isolates (4.90%), including *Enterobacter cloacae* and *Proteus mirabilis*, *Serratia marcescens*, and *Salmonella* spp., were individually found in distinct specimens.

Focusing on *E. coli*, we found 22 isolates collected from urine specimens, representing 100% of *E. coli* collected from patients admitted to private laboratories (OP-isolates, $n = 22$); differently, we found 10 isolates from urine, nine from pus and one from blood specimens, representing the 50%, 45%, and 5% of isolates collected from hospitalized patients (IP-isolates, $n = 20$), respectively. ERIC-PCR genotyping generated bands ranging in size from about 100 bp to 3000 bp, with the majority ranging from about 400 bp to 1000 bp (Figure 5.2a). The analysis of the dendrogram (60% of genetic similarity) showed 7 clusters comprising more than 1 isolate (Figure 5.2b) and 5 singletons (C34, C22, H16, H25, H24), indicating isolates with unique profiles. IP- and OP-*E. coli* were homogenously distributed within the identified clusters. The analysis of phylogroup distribution showed a high prevalence of B2 isolates among OP-isolates (9 out of 22; 41%), followed by Phylogroup E (6 out of 22; 27.30%), while, IP-isolates belonged mainly to Phylogroup A (10 out of 20; 50.00%), followed by B2 (6 isolates), as reported in Table 5.2.

Table 5.2. Distribution of phylogroups among IP- and OP-*Escherichia coli* isolates.

Isolates	**Phylogroups n (%)**					
	B2 (n=15)	**D (n=2)**	**A (n=12)**	**B1 (n=3)**	**E (n=7)**	**F (n=3)**
IPs-*E. coli* (n=20)	6 (30%)	1(5%)	10 (50%)	2 (10%)	1 (5%)	0 (0%)
OPs-*E. coli* (n=22)	9 (40,9%)	1 (4,6%)	2 (9,1%)	1 (4,6%)	6 (27,3%)	3 (13,6%)

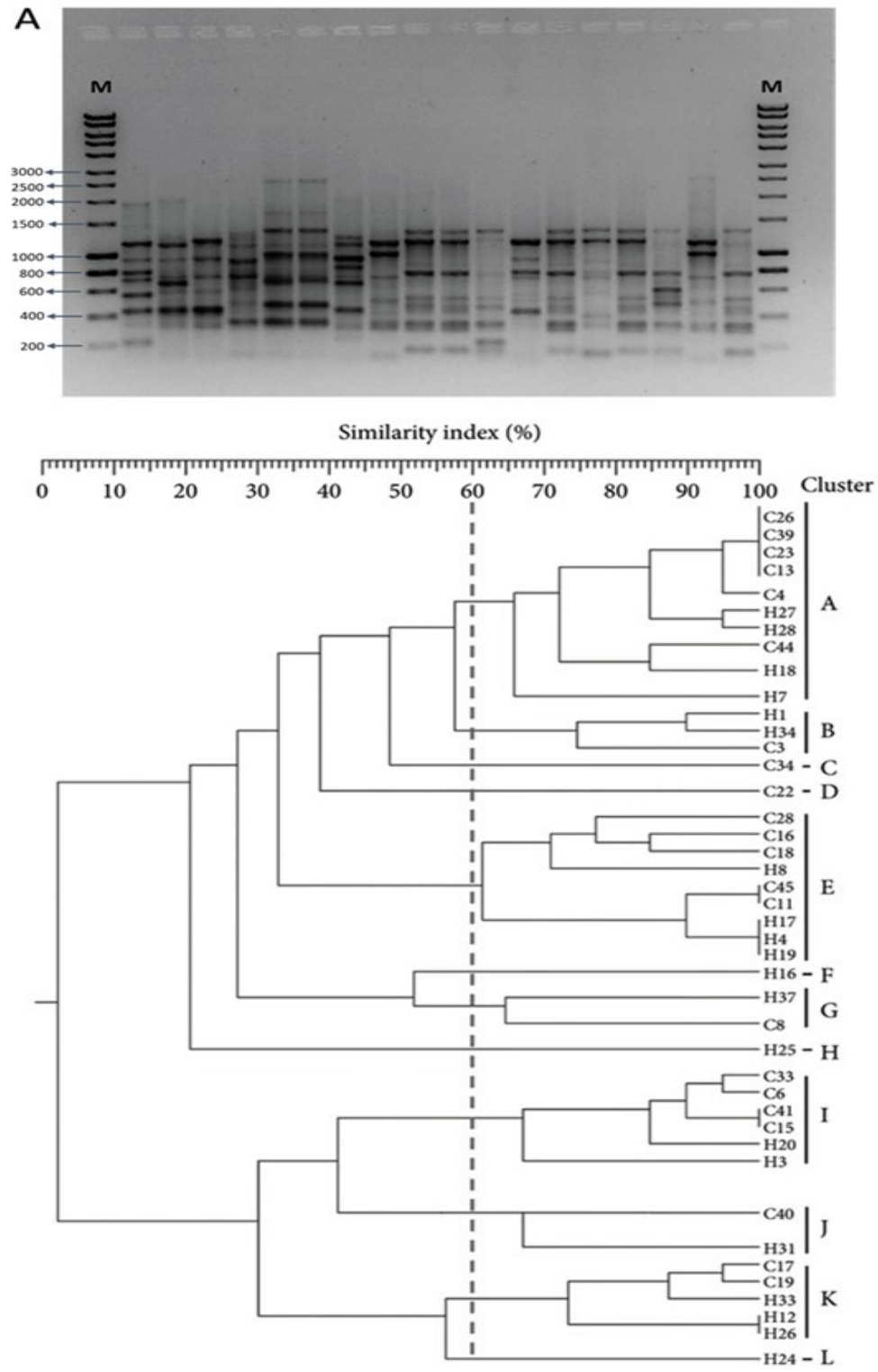

Figure 5.2. RIC-PCR profiles and dendrogram of IP- and OP-isolates. Representative image of ERIC-PCR profiles on agarose gel. (a) Genetic similarity among isolates was based on the Dice Similarity Index as the numeric coefficient and the unweighted pair group mathematical average (UPGMA) clustering algorithm. Similarity percentage cutoff of 60% was set to differentiate cluster profiles (b) M: 1 Kb DNA marker.

5.3.2 OP- and IP-*E. coli* Isolates Share Similar Antibiotic Resistance Profiles

OP- and IP-isolates showed similar profiles of antibiotic resistance, with no statistically significant differences. All isolates were resistant to ampicillin, cefazolin, and cefotaxime (MIC ≥ 32 and 64 respectively). Moreover, 68.18% of OPs and 90.00% of IPs showed co-resistance to ceftazidime (MIC ≥ 32). IPs exhibited higher rates of resistance to amoxicillin/clavulanic acid (70.00% vs. 59.10%, MIC ≥ 32), piperacillin/tazobactam (50.00% vs. 36.40%, MIC ≥ 64), and ciprofloxacin (90.00% vs. 72.73%, MIC ≥ 4). In addition, a higher percentage of IP-isolates showed increased MIC values compared to OP-isolates for ceftazidime (44.44% vs. 33.33%, MIC ≥ 64). Conversely, isolates from OPs showed higher resistance rates to gentamicin (45.50% vs. 30.00%, MIC ≥ 16) and chloramphenicol (27.27% vs. 5.00%, MIC ≥ 64). Additionally, the resistance rates to trimethoprim/sulfamethoxazole were high in both groups, but higher in OP-isolates (90.90% vs. 80.00%, MIC ≥ 320). Both groups had similar resistance rates to nitrofurantoin and fosfomycin (5.00% of IPs vs. 4.60% of OPs, MIC ≥ 128 and MIC ≥ 256, respectively) as well as to amikacin (30.00% of IPs vs. 36.40% of OPs, MIC ≥ 16). Carbapenems remained effective against all OP-isolates but one, whereas 25.00% and 15.00% of the IP-isolates showed nonsusceptibility to ertapenem and imipenem, respectively. The detailed MIC results are provided in Table 5.S1.

OP- and IP-isolates were all MDR. In particular, 19.00% of isolates were resistant to one agent in three different antibiotic categories, while the 81.00% showed resistance to one agent in more than four different categories (Table 5.S2). OP-isolates belonging to Phylogroup B2 accounted for the highest resistance rates against the majority of tested antibiotics, while, among IPs, isolates from Phylogroup A showed the greater resistance rates (Table 5.S2).

5.3.3 *bla*$_{\text{CTX–M}}$ Is the Dominant β-lactamase Gene Type Among IP- and OP-Isolates

Among the 3GC-resistant *E. coli* isolates, 35 (83.30%) were identified as ESBL producers, including 15 isolates from IPs and 20 isolates from OPs. Additionally, 6 *E. coli* were found to be carbapenemase producers, including 5 from IPs and one from OPs. The *bla*$_{\text{CTX–M}}$ gene was the most prevalent, being found in all, but two, ESBL-producing isolates, followed by the *bla*$_{\text{TEM}}$ gene, found in 69.04% of the isolates. The less represented genes were *bla*$_{\text{CMY}}$, *bla*$_{\text{DHA}}$, and *bla*$_{\text{SHV}}$ found in 4, 2, and 2 isolates, respectively (Table 5.S1).

5.3.4 Specific Virulence Genes Characterize OP and IP Isolates

It is known that ExPEC isolates possess a high carriage of virulence genes [1]. Results showed a significant difference of virulence gene content between OP- and IP-isolates ($p = 0.0025$). Moreover, OP- and IP-isolates belonging to the Phylogroup B2 showed the highest VF score compared to isolates belonging to other phylogroups (B2 vs. other phylogroups of OP-isolates, $p < 0.001$; B2 vs. other phylogroups of IP-isolates, $p < 0.001$). The most prevalent genes in both groups were those encoding for iron acquisition systems, such as *fyuA*, detected in 38 isolates (90.50%), followed by *feoB* in

35 isolates (83.30%) and *irp2* in 33 isolates (78.60%); conversely, the least represented was *iroN* (4.60% of OP-isolates and 15.00% of IP-isolates, respectively). *fyuA* was significantly associated with IP-isolates (100% from IPs vs. 81.80% from OP, $p = 0.045$) (Table 5.3); vice versa *chuA* gene was associated with OP-isolates (86.40% from OPs vs. 40.00% from IPs, $p = 0.002$). Among the analyzed toxin-encoding genes, *usp*, *sat*, *malX*, and *cnf1* genes were more frequently found in OP-isolates compared to IP-isolates, with the most notable difference for the *cnf1* gene (22.70% vs. 5.00%), followed by *malX* (36.40% vs. 25.00%), *sat* (40.90% vs. 30.00%), and *usp* (36.40% vs. 30.00%) (Table 4.3). However, these differences were not statistically significant ($p > 0.05$). In contrast, *traT* gene was more prevalent among hospital isolates (80.00% of IPs vs. 63.60% of OPs). The least frequent genes found in both groups were *vat* (4.60% from OPs vs. 5.00% from IPs), *hlyA* (4.60% vs. 0.00%), *clbB* (4.60% vs. 5.00%), and *clbN* (9.10% vs. 5.00%). The *ibeA* virulence gene was absent in both *E. coli* groups.

Table 5.3. Prevalence of virulence genes (VGs) in IP- and OP-*Escherichia coli* isolates.

Gene categories	VGs	OP-*E. coli* (n=22), n(%)	IP-*E. coli* (n=20), n(%)	*p* value
Toxins	*usp*	8 (36,4%)	6 (30%)	0,662
	sat	9 (40,9%)	6 (30%)	0,461
	traT	14 (63,6%)	16 (80%)	0,241
	vat	1 (4,6%)	1 (5%)	0,945
	malX	8 (36,4%)	5 (25%)	0,426
	hlyA	1 (4,6%)	0 (0%)	0,335
	cnf1	5 (22,7%)	1 (5%)	0,101
	ibeA	0 (0%)	0 (0%)	-
	clbN	2 (9,1%)	1 (5%)	0,607
	clbB	1 (4,6%)	1 (5%)	0,945
Adhesins	*sfa/focDE*	1 (4,6%)	0 (0%)	0,335
	papC	10 (45,5%)	8 (40%)	0,721
	papG	11 (50%)	7 (35%)	0,327
	tsh	2 (9,1%)	2 (10%)	0,920
	yadN	20 (90,9%)	10 (50%)	**0,003**
	papAH	11 (50%)	9 (45%)	0,516
Iron acquisition system	*feoB*	18 (81,8%)	17 (85%)	0,782
	ironN	1 (4,6%)	3 (15%)	0,249
	iutA	15 (68,2%)	13 (65%)	0,827
	fyuA	18 (81,8%)	20 (100%)	**0,045**
	chuA	19 (86,4%)	8 (40%)	**0,002**
	irp2	17 (77,3%)	16 (80%)	0,830
Protectins	*kpsMT II*	13 (59,1%)	7 (35%)	0,118
	ompT	13 (59,1%)	11 (55%)	0,789

Note: Numbers in bold indicate statistically significant *p* values.

Genes encoding fimbriae-associated factors, such as *papC*, *papG*, and *papAH,* were more frequently detected in OP-isolates, although this association did not reach statistical significance ($p > 0.05$). Interestingly, the presence of the *yadN* gene was significantly higher in OP- compared to IP-isolates (90.90% vs. 50.00%, $p = 0.003$) (Table 3). Differently, *tsh* and *sfa* genes were barely detected in both *E. coli* groups. The protectin-encoding genes, *kpsMT* II (59.10% vs. 35.00%) and *ompT* (59.10% vs. 55.00%), were both more common in *E. coli* from OPs than from IPs. However, the differences in prevalence for both genes were not statistically significant ($p > 0.05$) (Table 5.3). The prevalence of virulence genes and the relative VF scores for each isolate are reported in Figure 5.3.

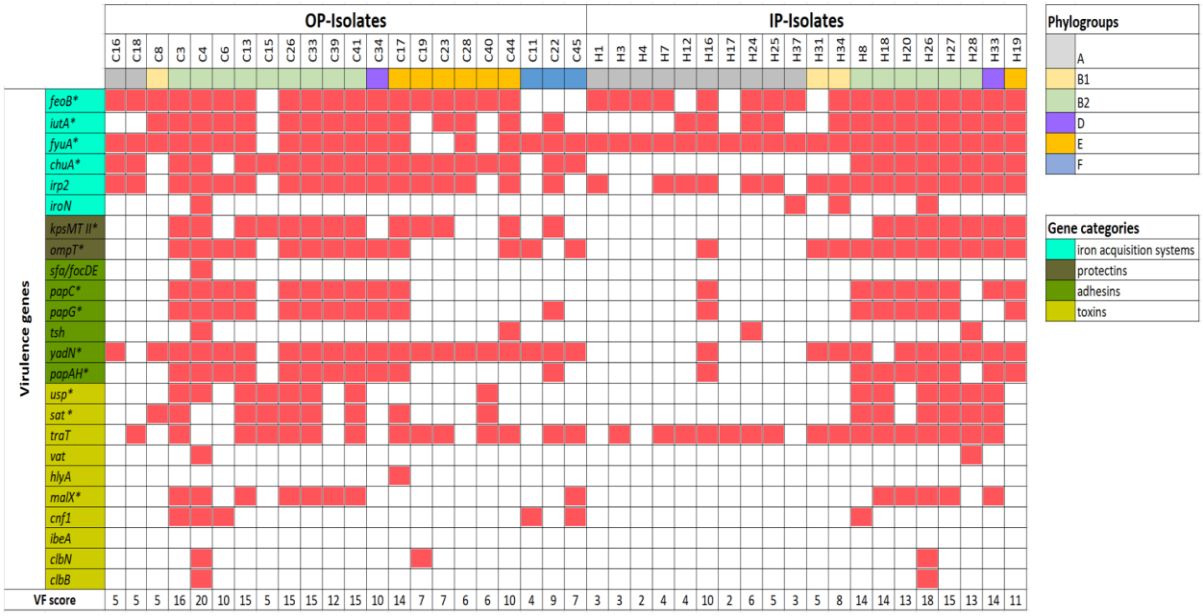

Figure 5.3. Distribution of virulence genes among *Escherichia coli* isolates from outpatients (OP-isolates) and inpatients (IP-isolates). The presence/absence of genes is indicated by filled and empty boxes, respectively. Phylogroups and gene categories are indicated by colored boxes. Asterisks underline genes significantly associated with resistance/susceptibility to ertapenem, gentamicin, and ciprofloxacin antibiotics. The virulence factor (VF) score is also reported.

5.3.5 Specific Association Between Virulence Genes and Resistance Phenotype to Commonly Used Antibiotics

According to the binary logistic regression analysis, significant associations were identified between certain virulence genes and resistance or susceptibility to three antibiotics: ertapenem, ciprofloxacin, and gentamicin (Table 5.4). The *pap* genes (*papC* and *papG*: OR = 0.500, $p = 0.022$; *papAH*: OR = 0.472, $p = 0.016$), along with *sat* (OR = 0.583, $p = 0.049$) and *chuA* (OR = 0.077, $p = 0.009$), are associated with susceptibility to ertapenem, with no VFs showing an inverse association (Table 4.4). In contrast, resistance to gentamicin is predicted by several virulence genes, including *pap* genes and *ompT* that showed the strongest association

(OR > 10, $p < 0.001$), followed by *yadN* (OR = 9.625, $p = 0.019$), *malX* (OR = 8.625, $p = 0.002$), *chuA* (OR = 6.036, $p = 0.024$), *kpsMTII* (OR = 5.500, $p = 0.013$), *sat* (OR = 5.250, $p = 0.014$), *usp* (OR = 4, $p = 0.040$), and *iutA* (OR = 2.481, $p = 0.001$) (Table 4.4). Additionally, resistance to ciprofloxacin is also associated with several virulence genes, including sthe two *pap* genes (*papC*: OR = 2.125, $p = 0.006$; *papAH*: OR = 7.875, $p = 0.039$), *malX* (OR = 1.619, $p = 0.035$), *fyuA* (OR = 19.800, $p = 0.003$), and *ompT* (OR = 14.636, $p = 0.005$). The only VF significantly associated with gentamicin sensitivity is *feoB* (OR = 0.741, $p = 0.031$). The predictor role of selected virulence genes for resistance to gentamicin and ciprofloxacin was confirmed by the MIC values.

Table 5.4. Binary logistic regression analysis of virulence-associated genes as predictors of resistance to antibiotics.

VGs	Resistance to antibiotic agents					
	ertapenem		gentamicin		ciprofloxacin	
	OR	*p*	OR	*p*	OR	*p*
usp	-	> 0,05	**4**	**0,040**	-	> 0,05
sat	**0,583**	**0,049**	**5,250**	**0,014**	-	> 0,05
malX	-	> 0,05	**8,625**	**0,002**	**1,619**	**0,035**
papC	**0,500**	**0,022**	**80,500**	**< 0,001**	**2,125**	**0,006**
papG	**0,500**	**0,022**	**80,500**	**< 0,001**	-	> 0,05
yadN	-	> 0,05	**9,625**	**0,019**	-	> 0,05
papAH	**0,472**	**0,016**	**61,600**	**< 0,001**	**7,875**	**0,039**
feoB	-	> 0,05	**0,741**	**0,031**	-	> 0,05
iutA	-	> 0,05	**2,481**	**0,001**	-	> 0,05
fyuA	-	> 0,05	-	> 0,05	**19,800**	**0,003**
chuA	**0,077**	**0,009**	**6,036**	**0,024**	-	> 0,05
kpsMT II	-	> 0,05	**5,500**	**0,013**	-	> 0,05
ompT	-	> 0,05	**23,800**	**< 0,001**	**14,636**	**0,005**

Note: A significant association ($p \leq 0.05$) was identified by the binary logistic regression analysis. When $p \leq 0.05$ and OR > 1, the virulence-associated gene is a predictor of resistance to the antibiotic agent. However, when OR < 1, the virulence-associated gene is a predictor of susceptibility to the antibiotic agent. Numbers in bold indicate statistically significant values.

5.3.6 Isolates Collected From OPs Show High Biofilm-Forming Activity and Motility

Biofilm represents one of the common strategies used by *E. coli* to establish infections; therefore, the biofilm-forming ability of each isolate was measured. Results demonstrated that OP-isolates produced higher amounts of biofilm than IP-isolates which showed mainly weak biofilm-forming activity ($p < 0.0001$), and this phenotype was not phylogroup-dependent (Figure 5.4a). The capability to form air–liquid interface pellicle was also evaluated. Results showed that the 33.40% of isolates produced pellicle; however, no significant difference in the distribution of pellicle-positive or -negative isolates between OP- and IP-isolates was found (Figure 5.4b). Interestingly, the majority

of pellicle-positive isolates were weak biofilm producers (8/14, 57.00%). Furthermore, the sedimentation assay showed that the 69.00% of isolates showed OD_{600} values higher than 0.8, which was the selected cut-off to distinguish aggregative and non-aggregative cells, independently from the isolation source (Figure 5.4c). Nonaggregative phenotype was mainly associated to isolates showing weak biofilm forming activity (22/29).

In *E. coli,* motility is considered a VF, especially associated to ExPEC strains. Hence, the extent of motility for each isolate was tested. Results showed that OP-isolates were more motile compared to IP-isolates ($p < 0.018$). This phenotype was mainly associated to B2 ($p = 0.0004$) and D ($p = 0.0463$) (Figure 5.4d). Isolates belonging to Phylogroup A were almost not motile, whereas OP-isolates of Phylogroup F were highly motile ($p = 0.0035$).

5.3.7 OP- and IP-*E. coli* Isolates Show Low Hemolytic Activity

Commonly, ExPEC isolates are characterized by the presence of toxins [1]. Each isolate was tested for the production of hemolysins on blood agar plates. Few isolates showed hemolysis ($n = 6$; 14.30%), with 4 (18.20%) from OPs and 2 (10.00%) from IPs. Among hemolytic isolates, 50.00% belonged to Phylogroup B2, while the remainder belong to Phylogroups A and B1 (Figure 5.4e). However, none of the six hemolytic isolates possessed the *hlyA* gene, suggesting the involvement of other cytolytic toxins.

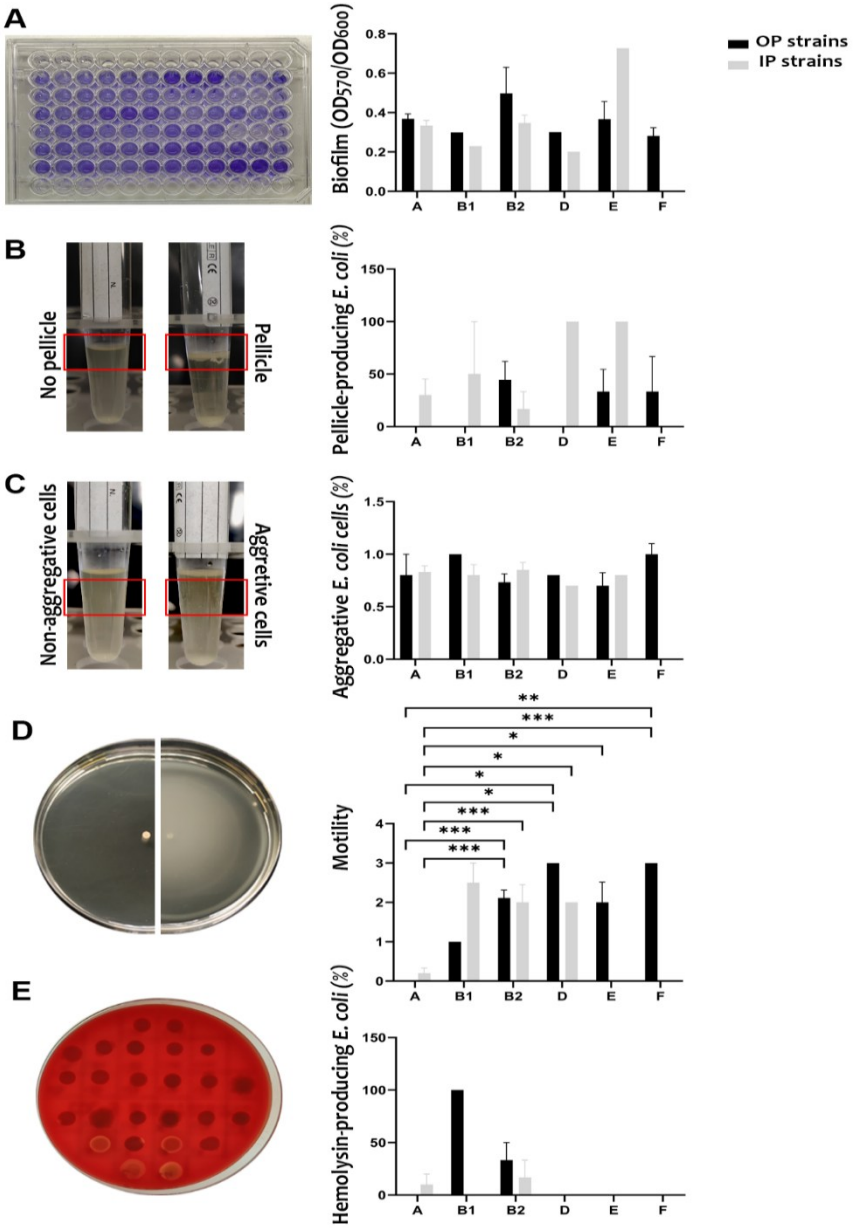

Figure 5.4a-e. Phenotypic traits of IP- and OP-*Escherichia coli* isolates. (a) Representative image of the crystal violet stained biofilm on a 96-well tissue culture plate (left panel) and relative distribution of isolates according to the phylogroups (right panel). Isolates were grouped based on A_{570}/A_{600} values: no production ($0 < OD < 0.2$), weak production ($0.2 < OD < 0.4$), moderate production ($0.4 < OD < 0.6$), and strong production ($OD > 0.6$). (b) Representative images of non- and pellicle-forming isolates (left panel) and relative distribution of isolates according to the phylogroups (right panel). (c) Representative images of nonaggregative and aggregative *E. coli* isolates (left panel) and relative distribution of isolates according to the phylogroups (right panel). (d) Representative images of *E. coli* motility on a soft agar plate (left panel) and relative distribution of isolates according to the phylogroups (right panel). Isolates were grouped based on the diameter size of swim zones: 0, nonmotile (< 10 mm); 1, low motile (10–20 mm); 2, motile (20–40 mm), and 3, hypermotile (> 40 mm). (e) Representative image of hemolysin-producing *E. coli* isolates on blood agar plates (left panel) and relative distribution of isolates according to the phylogroups (right panel) and the source (right). Black and gray bars indicate OP-isolates and IP-isolates, respectively.

5.4 Discussion

3GC-resistant *Enterobacterales* are categorized in the critical group of the WHO bacterial priority pathogens list [52]. In this two-year study, a total of 82 3GC-resistant *Enterobacterales* isolates from IPs and OPs were collected in Skikda, Algeria. Among these, *E. coli* predominated, accounting for 57.10% of the isolates. This finding aligns with numerous studies highlighting *E. coli* as the most prevalent species in both hospital- and community-acquired enterobacterial infections [53,54]. Among these, 76.20% of isolates were recovered from urine samples of both IPs and OPs, confirming their major involvement in both community- and hospital-acquired UTIs [55,56]. An in-depth phenotypic and genotypic characterization of 3GC-resistant *E. coli* collected from IPs and OPs was performed.

Unlike many studies reporting higher resistance rates among isolates from IPs compared to those from OPs [57,58], our study found that isolates from IPs and OPs exhibited nonstatistically significant differences in resistance rates to the majority of tested antibiotics. This finding corroborates results from Milano et al. and suggests comparable selective pressures from antibiotic use in both hospital and community settings [55].

The majority of 3GC-resistant *E. coli* isolates were identified as ESBL producers, consistent with findings from North Africa and other regions [16]. In Algeria, studies have reported a high prevalence of 3GC resistance, predominantly linked to $bla_{\text{CTX–M}}$ genes [29,59]. Similar studies in Tunisia and Morocco have also identified $bla_{\text{CTX–M–15}}$ as the predominant variant, often coexisting with bla_{TEM} and bla_{SHV} [60,61]. In accordance, our study showed that all ESBL-producing *E. coli,* but two, carried the $bla_{\text{CTX–M}}$ gene, confirming its primary involvement in cefotaxime inactivation. Moreover, a significant percentage harbored also bla_{TEM}, while only two isolates showed the bla_{SHV} indicating that the distribution of this latter gene is still limited, as previously observed [60,61]. Interestingly, 35.00% of isolates retained the susceptibility to the cefoxitin, a non-ESBL susceptible antibiotic; however, the *ampC*-type encoding genes bla_{CMY} and bla_{DHA} were detected in 26.66% and 13.33% of cefoxitin-resistant *E. coli*, respectively. This result suggests that bla_{CMY} and bla_{DHA} could be involved in cefoxitin inactivation and encourages the monitoring of the spread of these genes. We observed a higher prevalence of carbapenem-resistant isolates among IP-isolates compared to OP-isolates. Although this difference did not reach a statistical significance, probably due to the low number of identified isolates, this result is in line with previous observations on the low rate of carbapenem-resistant strains collected from OPs [35,62,63]. The limited occurrence outside hospital settings is likely due to the reserved use of carbapenems as last-line antibiotics for treating severe infections in hospitals[62]. Among, ertapenem-resistant isolates, the *NDM-5* gene was found, highlighting its predominant role in carbapenem resistance in *E. coli* isolates [62–64]. However, variations in carbapenemase distribution have been reported across different regions, influenced by differences in antimicrobial prescribing practices, infection control measures, and surveillance strategies. In Algeria, most studies have focused on hospital settings, where OXA-48- and NDM-5-

producing *E. coli* have been predominantly reported [36]. However, sporadic cases in community-acquired infections have also been documented [36,62] suggesting the possible circulation of these resistant strains outside hospitals. Studies from North Africa and neighboring regions have documented the presence of carbapenemase-producing *E. coli* in both hospital and community settings, with some reports indicating an increasing detection of these resistance determinants outside healthcare environments [65–67]. The problem of carbapenem-resistant *Enterobacteriaceae* (CRE) in Africa is aggravated by factors such as high infection rates, poor diagnostic tools, sub-optimal disease surveillance, and misuse of antibiotics [67].

Our findings highlighted high resistance levels to fluoroquinolones and sulfamethoxazole/trimethoprim in both groups of isolates, in agreement with previous reports showing resistance rates exceeding 50% to these agents among resistance to 3GC enterobacteria in Tunisia [60,64]. Similar patterns were observed in 3GC-resistant *E. coli* isolates from both IPs and OPs in Ushuaia, *Argentina*, with resistance rates up to 75% for ciprofloxacin and 65% for sulfamethoxazole/trimethoprim [59,60]. This observation may be attributed to the easy availability and widespread, uncontrolled use of these antibiotics in these countries, as in Algeria, and strengthens the correlation between resistance to 3GC and resistance to other antibiotic classes due to shared resistance mechanisms or cross-resistance.

The susceptibility of both groups to amikacin and fosfomycin, along with low resistance to chloramphenicol and nitrofurantoin, is supported by previous reports [68,69]. These antibiotics may be effective alternatives for treating 3GC-resistant infections in both hospital and community settings. The observed susceptibility of all isolates to colistin may be due to its limited use in human therapy in Algeria, where it is more commonly used in veterinary medicine for growth promotion or the prevention and treatment of *Enterobacterales* infections in animals [70]. These findings are consistent with the fact that resistance to colistin among clinical *Enterobacterales* in humans has been documented in only few studies in Algeria [38,71–73].

Results from genotyping revealed a genetic relatedness among IP- and OP-isolates, suggesting cross-contaminations between hospital and community settings. Accordingly, only 12.00% of isolates showed unique genotypic profiles. This could justify the similar resistance rates and profiles found in both groups of isolates. The expansion of successful clusters combined with the intrinsic genetic variability of *E. coli* underscores the complexity of dissemination dynamics and genetic evolution of this species, aligning with the observations of Saeki et al. [74]. Accordingly, a low level of genotypic differences was observed among *E. coli* sharing the same profile of antibiotic resistance and, in particular, among ESBL-producing *E. coli* [75]. Differently, we found a significant difference in the distribution of phylogroups among IP and OP-*E. coli* isolates; IP-*E. coli* mainly belonged to Phylogroups A and B1, whereas the pathogenic Phylogroups B2 and E were more prevalent in OP-isolates. This distribution has been consistently reported

in other studies [76,77]. Indeed, it is interesting to note that carbapenem-resistant isolates found in this study belonged to Phylogroups A and B1, further supporting the hypothesis that commensal *E. coli* strains, upon acquiring high levels of antibiotic resistance, are primarily responsible for nosocomial infections. On the other hand, the high prevalence of the pathogenic Phylogroups B2 and E in OPs suggests that community settings may favor the persistence of more virulent strains. Indeed, we found that OP-*E. coli* isolates exhibited a significant higher virulence gene content compared to IP-isolates. Among the genes tested, *yadN* and *chuA* were statistically significantly associated with OP-isolates, while *fyuA* was mainly present in IP-isolates. *yadN* encodes for the major subunit of the Yad fimbriae expressed by UPEC during bladder–cell adhesion and biofilm formation [78,79]. Accordingly, OP-isolates showed a higher biofilm-forming activity compared to IP-isolates. *chuA* mediates direct heme uptake, instead *fyuA* is the receptor for yersiniabactin uptake [79,80]. Although functional redundancy exists in the iron acquisition systems of *E. coli*, *chuA* and *fyuA* are two receptors that contribute the most during infections and in particular during UTIs. The *chuA* gene showed higher prevalence in B2 and E isolates in comparison to A and B1 isolates [81]. Moreover, the prevalence of *chuA* among OP-*E. coli* was already reported in previous studies [27,53,81]. This indicates that the heme receptor better copes with the limiting-iron conditions experienced by community-associated *E. coli*. This finding highlights the adaptability of *E. coli*, and suggests that the heme receptor is crucial for bacterial survival and pathogenicity under iron-limiting conditions [82]. Conversely, the higher prevalence of *fyuA* in isolates from hospitalized patients was already reported [83,84]. Moreover, a significant association between this gene and the resistance to ceftazidime and cefotaxime was also noted [83,84] confirming the contribution of commensal *E. coli* to nosocomial infections. It can be concluded that bacteria preferentially retain the most efficient iron acquisition systems in their genome to adapt to diverse environmental conditions. Although iron acquisition is not directly involved in antibiotic resistance, it enhances bacterial pathogenicity by providing a competitive edge, enabling them to survive and persist under antibiotic exposure and immune challenges.

The binary regression analysis identified a positive association between several virulence genes and the resistance to antibiotics commonly used in therapy. Specifically, the presence of *pap* genes, *malX*, and *ompT* strongly correlates with resistance to ciprofloxacin and gentamicin. This aligns with findings from previous studies reporting similar associations [85,86] (Mahdi 2023, Yazdanpour 2020). Yazdanpour et al. noted a significant association between *malX* and increased resistance to ciprofloxacin and gentamicin, as well as 3GC [86], which supports our results. *malX* is located in a UPEC pathogenetic island and its role is still not well characterized [87]. Recently, it has been shown that this gene correlates with UTIs and the phylogenetic group B2, which includes mainly ExPEC such as UPEC strains [88]. Furthermore, it was suggested that this gene could increase *E. coli* fitness in urine, being involved in the uptake of different carbohydrates [88]. Hence, it can be hypothesized that antibiotic-resistant UPEC strains

harboring *malX* may be more proficient in urinary tract colonization, driven by an enhanced capacity for nutrient uptake within the bladder environment. Furthermore, Monroy-Pérez et al. observed that *ompT* and *pap* genes were frequently present in strains resistant to ciprofloxacin and gentamicin [89]. *pap* genes significantly contribute to UTIs, by aiding resistant UPEC strains to adhere to the urothelium. Moreover, it has been recently reported that OmpT and OmpT-like proteases, strongly associated to UPEC strains, could degrade antimicrobial peptides in the urinary tract, thereby conferring resistance to innate immunity [90]. Overall, it can be speculated that the energetic cost of resistance mechanisms may be compensated by virulence genes, collectively enhancing the fitness and persistence of UPEC strains. However, a study conducted by Adegoke et al. on cefotaxime-resistant *E. coli* isolated from a wastewater treatment plant showed a correlation between *pap* genes, *malX*, and *ompT* with resistance to ciprofloxacin and gentamicin [91]. The potential combined carriage of these genes in numerous isolates raises the possibility that specific virulence and antibiotic-resistant genes may co-localize on similar genetic elements, such as plasmids or integrons [92].

The phenotypic screening showed that OP-isolates were biofilm-formers and motile, while IP-isolates were characterized by weak biofilm activity and lower level of motility. In *E. coli,* biofilm represents a relevant VF of UPEC strains since it helps the establishment of UTIs [93]. Furthermore, it was shown that biofilm-forming activity is a feature that outlines *E. coli* strains undergoing pathogenic adaptation [47]. Hence, in line with several reports, community-associated *E. coli* isolates must enhance the expression of specific virulence traits to cause infections, such as biofilm-forming activity and motility [27,53]. Accordingly, successful hospital-associated *E. coli* are primarily forced at acquiring antibiotic resistance mechanisms, rather than virulence traits, thereby retaining the typical features of commensal *E. coli* [94].

The dissemination of 3GC-resistant *E. coli* in both hospital and community settings underscores the need for reinforced surveillance programs and optimized antibiotic therapy in Algeria. Infection control strategies should be adapted to limit the spread of resistant strains, particularly in OPs where we found more virulent isolates. Therefore, strengthening antimicrobial stewardship programs by extending preventive measures beyond healthcare facilities is essential to mitigate the public health impact of these infections. With this aim, the WHO recently developed the “Tricycle” protocol within the One Health approach, to highlight the concept of simultaneously addressing three aspects of bacterial resistance, human health, food chain (animals), and the environment. The unique bioindicator, or sentinel, analyzed in the tricycle protocol is represented by ESBL-producing *E. coli* strains due to (i) their variable colonization rates in and among countries, and prevalence trends in humans, in farm animals, and in the environment; (ii) interventions leading to a decreased exposure to antibiotics in animals or humans have been followed by a decrease in ESBL *E. coli* occurrence rates; (iii) ESBLs confer resistance to critically important antimicrobial drugs, including the current rise of carbapenem as well as colistin-resistant ESBL-producing *E. coli* strains. Hence, ESBL *E.*

coli is a relevant and representative proxy for the magnitude and trends of the global AMR problem. Based on the tricycle protocol, data on ESBL-producing *E. coli* strains offer the opportunity to explore the prevalence and to track the dissemination of AMR [95].

This study presents some limitations. The sample size was relatively small, and isolates were collected from a single region, which may not fully represent the national epidemiological situation. Additionally, whole-genome sequencing was not performed, which could have provided a more comprehensive understanding of the genetic background of resistance and VFs as well as the dissemination of variants. Future studies should expand the sample size and use advanced molecular techniques to further elucidate the mechanisms driving resistance and pathogenicity in 3GC-resistant *E. coli*.

5.5 Conclusion

Results described here reported a high level and homogeneous distribution of resistance rates among 3CG-resistant *E. coli* isolated from community- and hospital-acquired infections in Algeria. Interestingly, IP- and OP-isolates belonged to different phylogroups and were characterized by the presence of specific virulence genes and by the expression of particular virulence traits. It can be hypothesized that the success of OP-isolates is mainly associated with their capability to form biofilm and to express motility, while IP-isolates rely mainly on the expression of antibiotic-resistant genes. This study highlights the urgent need to implement the surveillance of 3CG-resistant *E. coli* and to adopt the One Health approach to monitor AMR in the country. Ultimately, integrating genomic and phenotypic data is essential to develop innovative therapeutic solutions, new antibacterial molecules, phage-based therapies, and antivirulence strategies, to combat these MDR strains and to optimize AMR control policies.

Supplementary materials

Table 5.S1: Antibiotic resistance and the distribution of genes encoding β-lactamase rate of IP- and OP-*E. coli* strains

SAMPLE ID	MIC values (µg/ml)																β-lactamase encoding genes
	AMP	AMC	TZP	CZ	FOX	CTX	CAZ	ETP	IMP	AK	GEN	CIP	FOS	NIT	CHL	SXT	
C3	≥32 (R)	≥32 (R)	64 (R)	≥64 (R)	16	≥64 (R)	32 (R)	0,25	≤0,25	16 (R)	≥16 (R)	≥4 (R)	≤16	32	16	≥320 (R)	*blaCTX-M*
C4	≥32 (R)	16	64 (R)	≥64 (R)	32 (R)	≥64 (R)	≥64 (R)	0,25	≤0,25	≤2	≥16 (R)	≥4 (R)	≤16	≤16	≥64 (R)	≥320 (R)	*blaCTX-M- blaTEM*
C6	≥32 (R)	16	8	≥64 (R)	16	≥64 (R)	32 (R)	≤ 0,12	≤0,25	16 (R)	≥16 (R)	≥4 (R)	≤16	32	16	≥320 (R)	*blaCTX-M*
C8	≥32 (R)	4	≤4	≥64 (R)	≤4	≥64 (R)	8	≤ 0,12	≤0,25	≤2	≥16 (R)	≥4 (R)	≤16	≤16	≥64 (R)	≥320 (R)	*blaCTX-M- blaTEM*
C11	≥32 (R)	4	≤4	≥64 (R)	16	≥64 (R)	8	≤ 0,12	≤0,25	≤2	≤1	≥4 (R)	≤16	≤16	≥64 (R)	≤20	*blaCTX-M*
C13	≥32 (R)	≥32 (R)	64 (R)	≥64 (R)	≥64 (R)	≥64 (R)	≥64 (R)	≤ 0,12	≤0,25	16 (R)	≥16 (R)	≥4 (R)	≤16	64	16	≥320 (R)	*blaCTX-M*
C15	≥32 (R)	≥32 (R)	≥128 (R)	≥64 (R)	≤4	≥64 (R)	1	≤ 0,12	≤0,25	16 (R)	≤1	≥4 (R)	≤16	≤16	4	≥320 (R)	*blaCTX-M- blaTEM*
C16	≥32 (R)	≥32 (R)	≥128 (R)	≥64 (R)	8	≥64 (R)	8	≤ 0,12	≤0,25	≤2	≤1	≤0,25	≤16	32	8	≥320 (R)	*blaCTX-M- blaTEM*
C17	≥32 (R)	16	64 (R)	≥64 (R)	32 (R)	≥64 (R)	≥64 (R)	0,25	≤0,25	8	≥16 (R)	≥4 (R)	≤16	≤16	16	≥320 (R)	*blaCTX-M- blaTEM*
C18	≥32 (R)	≥32 (R)	≥128 (R)	≥64 (R)	≤4	≥64 (R)	32 (R)	0,25	2	≤2	≤1	≥4 (R)	≤16	≤16	16	≤20	*blaCTX-M*
C19	≥32 (R)	≥32 (R)	≥128 (R)	≥64 (R)	8	≥64 (R)	32 (R)	≤ 0,12	≤0,25	≤2	≤1	≤0,25	≤16	64	8	≥320 (R)	*blaCTX-M- blaTEM*
C22	≥32 (R)	≥32 (R)	≤4	≥64 (R)	≥64 (R)	≥64 (R)	32 (R)	≤ 0,12	≤0,25	≤2	≤1	≤0,25	≤16	≤16	8	≥320 (R)	*blaCTX-M*
C23	≥32 (R)	4	≤4	≥64 (R)	8	≥64 (R)	8	≤ 0,12	≤0,25	≤2	≤1	≤0,25	≤16	64	4	≥320 (R)	*blaCTX-M*
C26	≥32 (R)	≥32 (R)	8	≥64 (R)	≤4	≥64 (R)	32 (R)	≤ 0,12	≤0,25	16 (R)	≥16 (R)	≥4 (R)	≤16	≤16	≤2	≥320 (R)	*blaCTX-M- blaTEM*
C28	≥32 (R)	16	≤4	≥64 (R)	32 (R)	≥64 (R)	32 (R)	≤ 0,12	≤0,25	≤2	≤1	≥4 (R)	≤16	32	≥64 (R)	≥320 (R)	*blaCTX-M- blaTEM*
C33	≥32 (R)	16	8	≥64 (R)	≤4	≥64 (R)	32 (R)	≤ 0,12	≤0,25	8	≤1	≥4 (R)	≤16	≤16	4	≥320 (R)	*blaCTX-M*
C34	≥32 (R)	≥32 (R)	≥128 (R)	≥64 (R)	≤4	≥64 (R)	≥64 (R)	≤ 0,12	≤0,25	16 (R)	≥16 (R)	≥4 (R)	≤16	≤16	4	≥320 (R)	*blaCTX-M- blaTEM*
C39	≥32 (R)	≥32 (R)	64 (R)	≥64 (R)	≥64 (R)	≥64 (R)	32 (R)	≤ 0,12	≤0,25	16 (R)	≥16 (R)	≥4 (R)	≤16	≤16	4	≥320 (R)	*blaCTX-M- blaTEM- blaDHA*
C40	≥32 (R)	8	≤4	≥64 (R)	≤4	≥64 (R)	8	≤ 0,12	≤0,25	≤2	≤1	≤0,25	≤16	≤16	≥64 (R)	≥320 (R)	*blaCTX-M- blaTEM*
C41	≥32 (R)	≥32 (R)	≥128 (R)	≥64 (R)	≥64 (R)	≥64 (R)	≥64 (R)	≤ 0,12	2	16 (R)	≥16 (R)	≥4 (R)	≤16	>128 (R)	8	≥320 (R)	*blaCTX-M- blaTEM*

C44	≥32 (R)	≥32 (R)	≥128 (R)	≥64 (R)	≤4	≥64 (R)	4	2 (R)	2	≤2	≤1	≤0,25	≤16	≤16	4	≥320 (R)	*blaTEM- blaOXA-48*
C45	≥32 (R)	≥32 (R)	≥128 (R)	≥64 (R)	≥64 (R)	≥64 (R)	32 (R)	0,25	≤0,25	≤2	≤1	≥4 (R)	≥256 (R)	≤16	≥64 (R)	≥320 (R)	*blaTEM-blaSHV- blaCMY*
H1	≥32 (R)	16	≤4	≥64 (R)	≤4	≥64 (R)	32 (R)	≤ 0,12	≤0,25	≤2	≤1	≤0,25	≤16	≤16	16	≥320 (R)	*blaCTX-M-blaTEM-blaSHV*
H3	≥32 (R)	≥32 (R)	≥128 (R)	≥64 (R)	≥64 (R)	≥64 (R)	≥64 (R)	≥8 (R)	2	≤2	≤1	≥4 (R)	≤16	≤16	16	≥320 (R)	*blaTEM-blaCMY- blaNDM-5*
H4	≥32 (R)	≥32 (R)	≥128 (R)	≥64 (R)	≥64 (R)	≥64 (R)	≥64 (R)	≥8 (R)	≥16 (R)	≤2	≤1	≥4 (R)	≤16	≤16	16	≥320 (R)	*blaTEM-blaCMY- blaNDM-5*
H7	≥32 (R)	4	≤4	≥64 (R)	16	≥64 (R)	32 (R)	≤ 0,12	≤0,25	≤2	≤1	≤0,25	≤16	>128 (R)	4	≤20	*blaCTX-M*
H8	≥32 (R)	16	32	≥64 (R)	16	≥64 (R)	≥64 (R)	≤ 0,12	≤0,25	16 (R)	≥16 (R)	≥4 (R)	≤16	64	16	≥320 (R)	*blaCTX-M*
H12	≥32 (R)	≥32 (R)	≥128 (R)	≥64 (R)	≤4	≥64 (R)	32 (R)	≤ 0,12	≤0,25	≤2	≤1	≥4 (R)	≤16	≤16	16	≥320 (R)	*blaCTX-M- blaTEM*
H16	≥32 (R)	≥32 (R)	≥128 (R)	≥64 (R)	8	≥64 (R)	32 (R)	0,25	1	≤2	≤1	≥4 (R)	≤16	≤16	16	≤20	*blaCTX-M*
H17	≥32 (R)	≥32 (R)	≥128 (R)	≥64 (R)	≥64 (R)	≥64 (R)	≥64 (R)	≥8 (R)	2	≤2	≤1	≥4 (R)	≤16	≤16	16	≥320 (R)	*blaTEM-blaCMY- blaNDM-5*
H18	≥32 (R)	≥32 (R)	16	≥64 (R)	16	≥64 (R)	≥64 (R)	≤ 0,12	≤0,25	16 (R)	≥16 (R)	≥4 (R)	≥256 (R)	32	16	≥320 (R)	*blaCTX-M- blaTEM*
H19	≥32 (R)	≥32 (R)	64 (R)	≥64 (R)	≤4	≥64 (R)	32 (R)	≤ 0,12	≤0,25	16 (R)	≥16 (R)	≥4 (R)	≤16	≤16	4	≥320 (R)	*blaCTX-M- blaTEM*
H20	≥32 (R)	16	8	≥64 (R)	≤4	≥64 (R)	32 (R)	≤ 0,12	≤0,25	8	≥16 (R)	≥4 (R)	≤16	≤16	4	≥320 (R)	*blaCTX-M- blaTEM*
H24	≥32 (R)	≥32 (R)	64 (R)	≥64 (R)	≥64 (R)	≥64 (R)	≥64 (R)	≤ 0,12	≤0,25	16 (R)	≤1	≥4 (R)	≤16	≤16	16	≥320 (R)	*blaCTX-M- blaTEM*
H25	≥32 (R)	≥32 (R)	≥128 (R)	≥64 (R)	≤4	≥64 (R)	32 (R)	≤ 0,12	≤0,25	≤2	≤1	≥4 (R)	≤16	≤16	16	≥320 (R)	*blaCTX-M- blaTEM*
H26	≥32 (R)	≥32 (R)	≥128 (R)	≥64 (R)	≤4	≥64 (R)	32 (R)	≤ 0,12	≤0,25	16 (R)	≥16 (R)	≥4 (R)	≤16	≤16	8	≥320 (R)	*blaCTX-M*
H27	≥32 (R)	≥32 (R)	≥128 (R)	≥64 (R)	≤4	≥64 (R)	32 (R)	≤ 0,12	≤0,25	8	≥16 (R)	≥4 (R)	≤16	≤16	4	≥320 (R)	*blaCTX-M- blaTEM*
H28	≥32 (R)	8	≤4	≥64 (R)	≤4	≥64 (R)	4	≤ 0,12	≤0,25	4	≤1	≥4 (R)	≤16	≤16	4	≥320 (R)	*blaCTX-M- blaTEM*
H31	≥32 (R)	≥32 (R)	≥128 (R)	≥64 (R)	≥64 (R)	≥64 (R)	≥64 (R)	≥8 (R)	≥16 (R)	16 (R)	≤1	≥4 (R)	≤16	≤16	4	≥320 (R)	*blaCTX-M- blaTEM- blaNDM-5*
H33	≥32 (R)	≥32 (R)	≤4	≥64 (R)	32 (R)	≥64 (R)	32 (R)	≤ 0,12	≤0,25	≤2	≤1	≥4 (R)	≤16	≤16	16	≤20	*blaCTX-M- blaDHA*
H34	≥32 (R)	≥32 (R)	≥128 (R)	≥64 (R)	≥64 (R)	≥64 (R)	≥64 (R)	2 (R)	≥16 (R)	8	≤1	≥4 (R)	≤16	≤16	4	≤20	*blaCTX-M- blaTEM- blaNDM-5*
H37	≥32 (R)	4	≤4	≥64 (R)	≤4	≥64 (R)	1	≤ 0,12	≤0,25	≤2	≤1	≥4 (R)	≤16	≤16	≥64 (R)	≥320 (R)	*blaCTX-M- blaTEM*

AMP, ampicillin; AMC, amoxicillin/clavulanic acid; TZP, piperacillin/tazobactam; CZ, cefazolin; FOX, cefoxitin; CTX, cefotaxime; CAZ, ceftazidime; IMP, imipenem; ETP, ertapenem; AK, amikacin; GEN, gentamicin; CIP, ciprofloxacin; FOS, fosfomycin; CHL, chloramphenicol; SXT, sulfamethoxazole/trimethoprim; NIT, nitrofurantoin.

Table 5.S2: Prevalence and phylogenetic distribution of antibiotic-resistant IP- and OP- *E. coli* strains

Antibiotics	OP-*E. coli* (n=22)						IP-*E. coli* (n=20)				
	B2 (n=9); n(%)	**A (n=2); n(%)**	**B1 (n=1); n(%)**	**D (n=1); n(%)**	**E (n=6); n(%)**	**F (n=3); n(%)**	**B2 (n=6); n(%)**	**A (n=10); n(%)**	**B1 (n=2); n(%)**	**D (n=1); n(%)**	**E (n=1); n(%)**
AMP	9 (100%)	2 (100%)	1 (100%)	1 (100%)	6 (100%)	3 (100%)	6 (100%)	10 (100%)	2 (100%)	1 (100%)	1 (100%)
AMC	6 (66,67%)	2 (100%)	0 (0%)	1 (100%)	2 (33,33%)	2 (66,67%)	3 (50%)	7 (70%)	2 (100%)	1 (100%)	1 (100%)
TZP	2 (22,22%)	2 (100%)	0 (0%)	1 (100%)	2 (33,33%)	1 (33,33%)	2 (33,33%)	6 (60%)	2 (100%)	0 (0%)	0 (0%)
CZ	9 (100%)	2 (100%)	1 (100%)	1 (100%)	6 (100%)	3 (100%)	6 (100%)	10 (100%)	2 (100%)	1 (100%)	1 (100%)
FOX	4 (44,44%)	0 (0%)	0 (0%)	0 (0%)	2 (33,33%)	2 (66,67%)	0 (0%)	4 (40%)	2 (100%)	1 (100%)	0 (0%)
CTX	9 (100%)	2 (100%)	1 (100%)	1 (100%)	6 (100%)	3 (100%)	6 (100%)	10 (100%)	2 (100%)	1 (100%)	1 (100%)
CAZ	8 (88,89%)	1 (50%)	0 (0%)	1 (100%)	3 (50%)	2 (66,67%)	5 (88,33%)	9 (90%)	2 (100%)	1 (100%)	1 (100%)
ETP	0 (0%)	0 (0%)	0 (0%)	0 (0%)	1 (16,67%)	0 (0%)	0 (0%)	3 (30%)	2 (100%)	0 (0%)	0 (0%)
IMP	0 (0%)	0 (0%)	0 (0%)	0 (0%)	0 (0%)	0 (0%)	0 (0%)	1 (10%)	2 (100%)	0 (0%)	0 (0%)
AK	0 (0%)	0 (0%)	0 (0%)	0 (0%)	0 (0%)	0 (0%)	0 (0%)	0 (0%)	0 (0%)	0 (0%)	0 (0%)
GEN	7 (77,78%)	0 (0%)	1 (100%)	1 (100%)	1 (16,67%)	0 (0%)	5 (83,33%)	0 (0%)	0 (0%)	0 (0%)	1 (100%)
CIP	9 (100%)	1 (50%)	1 (100%)	1 (100%)	2 (33,33%)	2 (66,67%)	6 (100%)	8 (80%)	2 (100%)	1 (100%)	1 (100%)
FOS	1 (11,11%)	0 (0%)	0 (0%)	0 (0%)	0 (0%)	0 (0%)	0 (0%)	0 (0%)	1 (50%)	0 (0%)	0 (0%)
NIT	1 (11,11%)	0 (0%)	0 (0%)	0 (0%)	0 (0%)	0 (0%)	0 (0%)	1 (10%)	0 (0%)	0 (0%)	0 (0%)
CHL	0 (0%)	1 (50%)	1 (100%)	0 (0%)	2 (33,33%)	2 (66,67%)	0 (0%)	1 (10%)	0 (0%)	0 (0%)	0 (0%)
SXT	9 (100%)	1 (50%)	1 (100%)	1 (100%)	6 (100%)	2 (66,67%)	6 (100%)	8 (80%)	1 (100%)	0 (0%)	1 (100%)

*Color code indicates antibiotic categories: Penicillins, Cephalosporins, Carbapenems, Aminoglycosides, Fluoroquinolones, Fosfomycin, Nitrofurantoin, Chloramphenicol, Trimethroprim-sulfamethoxazole.

Table 5.S3. List of primer sequences used for virulence genes detection

Functional category	Target	Primer sequence	Amplicon size (bp)
Adhesion	*sfa/focDE*	F-CTCCGGAGAACTGGGTGCATCTTAC	410
		R-CGGAGGAGTAATTACAAACCTGGCA	
	tsh	F-GTCAGGTCAGTAACGAGCAC	289
		R-AGAGACGAGACTGTATTTGC	
	papG	F-GGGATGAGCGGGCCTTTGAT	190
		R-CGGGCCCCCAAGTAACTCG	
	papAH	F-ATGGCAGTGGTGTCTTTTGGTG	720
		R-CGTCCCACCATACGTGCTCTTC	
	papC	F-GTGGCAGTATGAGTAATGACCGTTA	203
		R-GTGGCAGTATGAGTAATGACCGTTA	
	yadN	F-CCACTGTTAATGGCGGTGTA	125
		R-TTTAGCCAGGCGAGAAGAAC	
Protectins	*kpsMTII*	F-GCGCATTTGCTGATACTGTTG	272
		R-CATCCAGACGATAAGCATGAGCA	
	ompT	F-ATCTAGCCGAAGAAGGAGGC	559
		R-CCCGGGTCATAGTGTTCATC	
Toxins	*vat*	F-TACCGTAACCAGCTCATCAACAG	131
		R- CATACCCACCTGTTACCCAATGT	
	hlyA	F-AACAAGGATAAGCACTGTTCTGGCT	1177
		R-ACCATATAAGCGGTCATTCCCGTCA	
	traT	F-GGTGTGGTGCGATGAGCACAG	290
		R-CACGGTTCAGCCATCCCTGAG	
	cnf1	F-AAGATGGAGTTTCCTATGCAGGAG	498
		R-CATTCAGAGTCCTGCCCTCATTATT	
	sat	F-CTACAGCTTGATCACCTATGGC	410
		R-CTCCCTGGTATTTCTTTGTGG	
	usp	F-ACATTCACGGCAAGCCTCAG	440
		R-AGCGAGTTCCTGGTGAAAGC	
	malX	F-GGACATCCTGTTACAGCGCGCA	930
		R-GGACATCCTGTTACAGCGCGCA	
	clbB	F-GATTTGGATACTGGCGATAACCG	579
		R-CAGTTCGGGTATGTGTGGAAG	
	clbN	F-GTTTTGCTCGCCAGATAGTCATTC	733
		R-CAGTTCGGGTATGTGTGGAAGG	
	ibeA	F-AGGCAGGTGTGCGCCGCGTAC	170
		R-TGGTGCTCCGGCAAACCATGC	
Iron acquisition system	*iroN*	F-AAGTCAAAGCAGGGGTTGCCCG	668
		R-GACGCCGACATTAAGACGCAG	
	irp2	F-AAGGATTCGCTGTTACCGGAC	413
		R-AACTCCTGATACAGGTGGC	
	chuA	F-AGCGTGTTGAGATTGTTCGC	124
		R-AAACCACTGCTTTGTCCTTCCTGC	
	iutA	F-AAAGAGCTGAAAGACGCACTGG	145
		R-TGTCGGAACGTGAAGAGTTGAG	
	fhuA	F-ACGGCCAAAGCCAGAATAAC	133
		R-TTACCGTAAAGCACGGAAACCG	
	feoB	F-GCACTCTTTGTGCATGGTATTC	111
		R-GGCAGCACGGTGTTAAT	
	fyuA	F-ATGCCTATGTGGGATGGAATG	128
		R-CCAGTCATCGGTGGTGTATTT	

References

1. Sora, V. M. *et al.* Extraintestinal Pathogenic Escherichia coli: Virulence Factors and Antibiotic Resistance. *Pathogens* **10**, 1355 (2021).
2. Ramos, S. *et al.* Escherichia coli as Commensal and Pathogenic Bacteria among Food-Producing Animals: Health Implications of Extended Spectrum β-Lactamase (ESBL) Production. *Animals* **10**, 2239 (2020).
3. Aguirre-Sánchez, J. R. *et al.* Phylogenetic group and virulence profile classification in Escherichia coli from distinct isolation sources in Mexico. *Infect. Genet. Evol.* **106**, 105380 (2022).
4. Picard, B. *et al.* The Link between Phylogeny and Virulence in *Escherichia coli* Extraintestinal Infection. *Infect. Immun.* **67**, 546–553 (1999).
5. Clermont, O., Christenson, J. K., Denamur, E. & Gordon, D. M. The Escherichia coli phylo-typing method revisited: improvement of specificity and detection of new phylo-groups. *Environ. Microbiol. Rep.* **5**, 58–65 (2013).
6. Riley, L. W. Distinguishing Pathovars from Nonpathovars: Escherichia coli. *Microbiol. Spectr.* **8**, 8.4.1 (2020).
7. Mueller, M. & Tainter, C. Escherichia coli Infection. (2021).
8. Timm, M. R., Russell, S. K. & Hultgren, S. J. Urinary tract infections: pathogenesis, host susceptibility and emerging therapeutics. *Nat. Rev. Microbiol.* **23**, 72–86 (2025).
9. Sabih, A. & Leslie, S. W. Complicated urinary tract infections. (2017).
10. King, C. *et al.* Risk factors for healthcare-associated urinary tract infection and their applications in surveillance using hospital administrative data: a systematic review. *J. Hosp. Infect.* **82**, 219–226 (2012).
11. Zou, Z. *et al.* E. coli catheter-associated urinary tract infections are associated with distinctive virulence and biofilm gene determinants. *JCI Insight* **8**, e161461 (2023).
12. Riley, L. W. Pandemic lineages of extraintestinal pathogenic Escherichia coli. *Clin. Microbiol. Infect.* **20**, 380–390 (2014).
13. Campos, A. C. C. *et al.* Corrigendum: Comprehensive Molecular Characterization of Escherichia coli Isolates from Urine Samples of Hospitalized Patients in Rio de Janeiro, Brazil. *Front. Microbiol.* **11**, 599031 (2020).
14. Bono, M. J. & Leslie, S. W. Uncomplicated urinary tract infections. in *StatPearls [Internet]* (StatPearls Publishing, 2025).
15. WHO. *Bloodstream Infections Due to Selected Antimicrobial-Resistant Organisms*. https://www.who.int/data/gho/data/indicators/indicator-details/GHO/sdg-3.d.2--proportion-of-bloodstream-infections-due-to-selected-antimicrobial-resistant-organisms--median-(-) (2025).
16. Asogwa, I. Third-Generation Cephalosporin-Resistant Enterobacteriaceae in Africa. *Arch. Pharm. Pract.* **0**, 0 (2018).
17. Dramowski, A. *et al.* Mortality attributable to third-generation cephalosporin resistance in Gram-negative bloodstream infections in African hospitals: a multi-site retrospective study. *JAC-Antimicrob. Resist.* **3**, dlaa130 (2021).
18. AARN. *Surveillance de La Résistance Des Bactéries Aux Antibiotiques*. https://aarn.pasteur.dz/ (2023).
19. Baba Ahmed-Kazi Tani, Z. & Arlet, G. Actualité de la résistance aux antibiotiques chez les bacilles à Gram négatif en Algérie. *Pathol. Biol.* **62**, 169–178 (2014).
20. Oteo, J., Pérez-Vázquez, M. & Campos, J. Extended-spectrum β-lactamase producing Escherichia coli: changing epidemiology and clinical impact. *Curr. Opin. Infect. Dis.* **23**, 320–326 (2010).
21. Ambler, R. P. The structure of β-lactamases. *Philos. Trans. R. Soc. Lond. B Biol. Sci.* **289**, 321–331 (1980).

22. Bush, K., Jacoby, G. A. & Medeiros, A. A. A functional classification scheme for beta-lactamases and its correlation with molecular structure. *Antimicrob. Agents Chemother.* **39**, 1211–1233 (1995).

23. Aljohni, M. S., Harun-Ur-Rashid, M. & Selim, S. Emerging threats: Antimicrobial resistance in extended-spectrum beta-lactamase and carbapenem-resistant Escherichia coli. *Microb. Pathog.* **200**, 107275 (2025).

24. Bajaj, P., Singh, N. S. & Virdi, J. S. Escherichia coli β-Lactamases: What Really Matters. *Front. Microbiol.* **7**, (2016).

25. Cantón, R., González-Alba, J. M. & Galán, J. C. CTX-M Enzymes: Origin and Diffusion. *Front. Microbiol.* **3**, (2012).

26. Kara, A., Massaro, C., Giammanco, G. M., Alduina, R. & Boussoualim, N. Phylogenetic Diversity, Antibiotic Resistance, and Virulence of Escherichia coli Strains from Urinary Tract Infections in Algeria. *Antibiotics* **13**, 773 (2024).

27. Yahiaoui, M. *et al.* Antibiotic Resistance, Virulence, and Genetic Background of Community-Acquired Uropathogenic *Escherichia coli* from Algeria. *Microb. Drug Resist.* **21**, 516–526 (2015).

28. Tahar, S. *et al.* Molecular Characterization of Multidrug-Resistant Escherichia coli Isolated from Milk of Dairy Cows with Clinical Mastitis in Algeria. *J. Food Prot.* **83**, 2173–2178 (2020).

29. Sadi, M. *et al.* Antimicrobial Resistance of Escherichia coli Involved in Algerian Bovine Carriage, ESBL Detection, Integron Characterization and Genetic Lineages. *Kafkas Univ. Vet. Fak. Derg.* https://doi.org/10.9775/kvfd.2023.30670 (2024) doi:10.9775/kvfd.2023.30670.

30. Mandujano-Hernández, A. *et al.* The Global Rise of ESBL-Producing Escherichia coli in the Livestock Sector: A Five-Year Overview. *Animals* **14**, 2490 (2024).

31. Raffelsberger, N. *et al.* Community carriage of ESBL-producing *Escherichia coli* and *Klebsiella pneumoniae* : a cross-sectional study of risk factors and comparative genomics of carriage and clinical isolates. *mSphere* **8**, e00025-23 (2023).

32. Van Der Putten, B. C. L. *et al.* Extra-intestinal pathogenic lineages of extended-spectrum β-lactamase (ESBL)-producing Escherichia coli are associated with prolonged ESBL gene carriage. *Access Microbiol.* **6**, (2024).

33. Nordmann, P., Dortet, L. & Poirel, L. Carbapenem resistance in Enterobacteriaceae: here is the storm! *Trends Mol. Med.* **18**, 263–272 (2012).

34. Wang, Z. Exploring the role of PilY1 family proteins in natural transformation. (Simon Fraser Universiy, 2022).

35. Bougouizi, A., Chekroud, Z., Rahab, H., Boumegoura, A. & Touati, A. Prevalence and characterization of Carbapenem-Resistant Enterobacterales among inpatients and outpatients in Skikda, Algeria. *J. Infect. Dev. Ctries.* **18**, 383–390 (2024).

36. Abderrahim, A. *et al.* Dissemination of OXA-48- and NDM-1-Producing Enterobacterales Isolates in an Algerian Hospital. *Antibiotics* **11**, 750 (2022).

37. Cochran, W. G. *Sampling Techniques*. (John Wiley & Sons, USA, 1977).

38. Nabti, L. Z. *et al.* High Prevalence of Multidrug-Resistant *Escherichia coli* in Urine Samples from Inpatients and Outpatients at a Tertiary Care Hospital in Sétif, Algeria. *Microb. Drug Resist.* **25**, 386–393 (2019).

39. Leber, A. L. *Clinical Microbiology Procedures Handbook*. (John Wiley & Sons, 2020).

40. Magiorakos, A.-P. *et al.* Multidrug-resistant, extensively drug-resistant and pandrug-resistant bacteria: an international expert proposal for interim standard definitions for acquired resistance. *Clin. Microbiol. Infect.* **18**, 268–281 (2012).

41. Jarlier, V., Nicolas, M.-H., Fournier, G. & Philippon, A. Extended Broad-Spectrum -Lactamases Conferring Transferable Resistance to Newer -Lactam Agents in Enterobacteriaceae: Hospital Prevalence and Susceptibility Patterns. *Clin. Infect. Dis.* **10**, 867–878 (1988).

42. Bakour, S. *et al.* Rapid identification of carbapenemase-producing Enterobacteriaceae, Pseudomonas aeruginosa and *Acinetobacter baumannii* using a modified Carba NP test. *New Microbes New Infect.* **7**, 89–93 (2015).

43. Kiiru, J., Kariuki, S., Goddeeris, B. M. & Butaye, P. Analysis of β-lactamase phenotypes and carriage of selected β-lactamase genes among Escherichia coli strains obtained from Kenyan patients during an 18-year period. *BMC Microbiol.* **12**, 155 (2012).

44. Dallenne, C., Da Costa, A., Decré, D., Favier, C. & Arlet, G. Development of a set of multiplex PCR assays for the detection of genes encoding important β-lactamases in Enterobacteriaceae. *J. Antimicrob. Chemother.* **65**, 490–495 (2010).

45. Rebelo, A. R. *et al.* Multiplex PCR for detection of plasmid-mediated colistin resistance determinants, mcr-1, mcr-2, mcr-3, mcr-4 and mcr-5 for surveillance purposes. *Eurosurveillance* **23**, (2018).

46. Sarshar, M. *et al.* Genetic diversity, phylogroup distribution and virulence gene profile of pks positive Escherichia coli colonizing human intestinal polyps. *Microb. Pathog.* **112**, 274–278 (2017).

47. Ambrosi, C. *et al.* Colonic adenoma-associated Escherichia coli express specific phenotypes. *Microbes Infect.* **21**, 305–312 (2019).

48. Sarshar, M. *et al.* Adaptive strategies of uropathogenic Escherichia coli CFT073: from growth in lab media to virulence during host cell adhesion. *Int. Microbiol.* **25**, 481–494 (2022).

49. Perruzza, L. *et al.* The Shigella flexneri virulence factor apyrase is released inside eukaryotic cells to hijack host cell fate. *Microbiol. Spectr.* **11**, e00775-23 (2023).

50. Weiss-Muszkat, M. *et al.* Biofilm Formation by and Multicellular Behavior of *Escherichia coli* O55:H7, an Atypical Enteropathogenic Strain. *Appl. Environ. Microbiol.* **76**, 1545–1554 (2010).

51. Montero, D. A. *et al.* Locus of Adhesion and Autoaggregation (LAA), a pathogenicity island present in emerging Shiga Toxin–producing Escherichia coli strains. *Sci. Rep.* **7**, 7011 (2017).

52. WHO. *WHO Bacterial Priority Pathogens List 2024: Bacterial Pathogens of Public Health Importance, to Guide Research, Development, and Strategies to Prevent and Control Antimicrobial Resistance*. (World Health Organization, Geneva, 2024).

53. Radera, S., Srivastava, S. & Agarwal, J. Virulence Genotyping and Multidrug Resistance Pattern of Escherichia coli Isolated From Community-Acquired and Hospital-Acquired Urinary Tract Infections. *Cureus* https://doi.org/10.7759/cureus.29404 (2022) doi:10.7759/cureus.29404.

54. Satán, C. *et al.* Epidemiology of antimicrobial resistance in bacteria isolated from inpatient and outpatient samples, Ecuador, 2018. *Rev. Panam. Salud Pública* **47**, 1 (2023).

55. Milano, A. *et al.* Antimicrobial Resistance Trends of *Escherichia coli* Isolates from Outpatient and Inpatient Urinary Infections over a 20-Year Period. *Microb. Drug Resist.* **28**, 63–72 (2022).

56. Gramundi, I. *et al.* Characterization of third generation cephalosporin-resistant Escherichia coli clinical isolates from Ushuaia, Argentina. *Rev. Argent. Microbiol.* **55**, 43–48 (2023).

57. Lubwama, M. *et al.* CTX-M, TEM, and SHV Genes in Escherichia coli, Klebsiella pneumoniae, and Enterobacter spp Isolated from Hematologic Cancer Patients with Bacteremia in Uganda. *Infect. Drug Resist.* **Volume 17**, 641–653 (2024).

58. Nachimuthu, R. *et al.* CTX-M-type ESBL-mediated resistance to third-generation cephalosporins and conjugative transfer of resistance in Gram-negative bacteria isolated from hospitals in Tamil Nadu, India. *Access Microbiol.* **3**, (2021).

59. Benbrahim, C., Barka, M. S., Benmahdi, L., Zatout, A. & Khadir, A. Klebsiella pneumoniae producing extended spectrum β-lactamase in Regional Military University Hospital of Oran, Algeria: antibiotic

resistance, biofilm formation, and detection of blaCTX-M and blaTEM genes. *Afr. J. Clin. Exp. Microbiol.* **22**, 28–37 (2021).

60. Dziri, R. *et al.* Huge Diversity of TEM and SHV β-Lactamases Types Among CTX-M-15-Producing Enterobacteriaceae Species in Tunisia. *Microb. Drug Resist.* **25**, 1149–1154 (2019).
61. Barguigua, A. *et al.* Prevalence and genotypic analysis of plasmid-mediated β-lactamases among urinary Klebsiella pneumoniae isolates in Moroccan community. *J. Antibiot. (Tokyo)* **66**, 11–16 (2013).
62. Bourafa, N. *et al.* Molecular characterization of carbapenem-resistant Gram-negative bacilli clinical isolates in Algeria. *Infect. Drug Resist.* **Volume 11**, 735–742 (2018).
63. Loucif, L. *et al.* First detection of OXA-48-producing Klebsiella pneumoniae in community-acquired urinary tract infection in Algeria. *J. Glob. Antimicrob. Resist.* **12**, 115–116 (2018).
64. Sallem, N. *et al.* Extended-spectrum beta-lactamase- and carbapenemase-producing Escherichia coli isolates causing hospital- and community-acquired infections in Tunisia (2001–2019): expansion of CTX-M-15-C2 and CTX-M-27-C1 ST131 subclades. *Microbiol. Spectr.* **12**, e01471-24 (2024).
65. BENZAARATE, I. *et al.* Prevalence of Enterobacteriaceae producing carbapenemase (OXA-48) responsible for urinary tract infections in Casablanca. *Moroc. J. Public Heath* **3**, (2022).
66. Manenzhe, R. I., Zar, H. J., Nicol, M. P. & Kaba, M. The spread of carbapenemase-producing bacteria in Africa: a systematic review. *J. Antimicrob. Chemother.* **70**, 23–40 (2015).
67. Gulumbe, B. H. & Ajibola, O. Carbapenem Resistant Enterobacteriaceae in Africa. *Borneo J. Pharm.* **3**, 71–78 (2020).
68. Graf, F. E. *et al.* Molecular mechanisms of re-emerging chloramphenicol susceptibility in extended-spectrum beta-lactamase-producing Enterobacterales. *Nat. Commun.* **15**, 9019 (2024).
69. Park, K.-S. *et al.* Susceptibility to Fosfomycin and Nitrofurantoin of ESBL-Positive *Escherichia coli* and *Klebsiella pneumoniae* Isolated From Urine of Pediatric Patients. *J. Korean Med. Sci.* **38**, e361 (2023).
70. Kempf, M. *et al.* Detection of *Acinetobacter baumannii* in human head and body lice from Ethiopia and identification of new genotypes. *Int. J. Infect. Dis.* **16**, e680–e683 (2012).
71. Belbel, Z. *et al.* First report of colistin resistance in an OXA-48- and a CTX-M-15 producing Klebsiella pneumoniae clinical isolate in Algeria due to PmrB protein modification and mgrB inactivation. *J. Glob. Antimicrob. Resist.* **14**, 158–160 (2018).
72. Touati, A. & Mairi, A. Plasmid-Determined Colistin Resistance in the North African Countries: A Systematic Review. *Microb. Drug Resist.* **27**, 121–133 (2021).
73. Yanat, B. *et al.* First report of the plasmid-mediated colistin resistance gene mcr-1 in a clinical Escherichia coli isolate in Algeria. *Int. J. Antimicrob. Agents* **48**, 760–761 (2016).
74. Saeki, M. *et al.* Clonality investigation of clinical Escherichia coli isolates by polymerase chain reaction-based open-reading frame typing method. *J. Infect. Chemother.* **26**, 38–42 (2020).
75. Tanko, N. *et al.* Genetic relatedness in extended-spectrum beta-lactamase-producing Escherichia coli from clinical isolates using enterobacterial repetitive intergenic consensus polymerase chain reaction. *Int. J. Health Sci.* **15**, 18 (2021).
76. Gatya Al-Mayahie, S. M., Al-Guranie, D. R. T., Hussein, A. A. & Bachai, Z. A. Prevalence of common carbapenemase genes and multidrug resistance among uropathogenic Escherichia coli phylogroup B2 isolates from outpatients in Wasit Province/ Iraq. *PLOS ONE* **17**, e0262984 (2022).
77. Mojaz-Dalfardi, N., Kalantar-Neyestanaki, D., Hashemizadeh, Z. & Mansouri, S. Comparison of virulence genes and phylogenetic groups of Escherichia coli isolates from urinary tract infections and normal fecal flora. *Gene Rep.* **20**, 100709 (2020).
78. Spurbeck, R. R. *et al.* Fimbrial Profiles Predict Virulence of Uropathogenic Escherichia coli Strains: Contribution of Ygi and Yad Fimbriae. *Infect. Immun.* **79**, 4753–4763 (2011).

79. Chen, Y. *et al.* Attenuation of Yersinia pestis fyuA Mutants Caused by Iron Uptake Inhibition and Decreased Survivability in Macrophages. *Front. Cell. Infect. Microbiol.* **12**, 874773 (2022).

80. Torres, A. G., Redford, P., Welch, R. A. & Payne, S. M. TonB-Dependent Systems of Uropathogenic *Escherichia coli* : Aerobactin and Heme Transport and TonB Are Required for Virulence in the Mouse. *Infect. Immun.* **69**, 6179–6185 (2001).

81. Shahid, S. S. & Yousif, M. G. Prevalence of chuA gene virulence factor in Escherichia Coli isolated from clinical samples in AL-Diwaniyah province. *Int. J. Health Sci.* 2610–2618 (2022) doi:10.53730/ijhs.v6nS5.10489.

82. Paterson, J. R., Wadsworth, J. M., Hu, P. & Sharples, G. J. A critical role for iron and zinc homeostatic systems in the evolutionary adaptation of Escherichia coli to metal restriction. *Microb. Genomics* **9**, (2023).

83. Karam, M. R. A., Habibi, M. & Bouzari, S. Relationships between Virulence Factors and Antimicrobial Resistance among Escherichia coli Isolated from Urinary Tract Infections and Commensal Isolates in Tehran, Iran. *Osong Public Health Res. Perspect.* **9**, 217–224 (2018).

84. Fonseca-Martínez, S. A., Martínez-Vega, R. A., Farfán-García, A. E., González Rugeles, C. I. & Criado-Guerrero, L. Y. Association Between Uropathogenic Escherichia coli Virulence Genes and Severity of Infection and Resistance to Antibiotics. *Infect. Drug Resist.* **Volume 16**, 3707–3718 (2023).

85. Mahdi, S. M., Yahya, H. A., Yasir, M. K., Naser, R. N. & Jaber, K. A. K. Investigation of papA, papC, and papG virulence genes revealed their association with antimicrobial resistance among uropathogenic Escherichia coli strains isolated from patients in Thi-Qar province, Iraq. *Tex. J. Med. Sci.* **25**, 1–21 (2023).

86. Yazdanpour, Z., Tadjrobehkar, O. & Shahkhah, M. Significant association between genes encoding virulence factors with antibiotic resistance and phylogenetic groups in community acquired uropathogenic Escherichia coli isolates. *BMC Microbiol.* **20**, 241 (2020).

87. Johnson, J. R., Owens, K., Gajewski, A. & Kuskowski, M. A. Bacterial Characteristics in Relation to Clinical Source of *Escherichia coli* Isolates from Women with Acute Cystitis or Pyelonephritis and Uninfected Women. *J. Clin. Microbiol.* **43**, 6064–6072 (2005).

88. Petter, A., Hogins, J., Zimmern, P. E. & Reitzer, L. MP77-14 malx as virulence factor in Uropathogenic Escherichia col: Correlation with urinary tract infections and analysis of its function. *J. Urol.* **203**, (2020).

89. Monroy-Pérez, E. *et al.* Virulence gene transcription, phylogroups, and antibiotic resistance of cervico-vaginal pathogenic E. coli in Mexico. *PLOS ONE* **15**, e0234730 (2020).

90. Desloges, I. *et al.* Identification and characterization of OmpT-like proteases in uropathogenic *Escherichia coli* clinical isolates. *MicrobiologyOpen* **8**, e915 (2019).

91. Adegoke, A. A., Madu, C. E., Aiyegoro, O. A., Stenström, T. A. & Okoh, A. I. Antibiogram and beta-lactamase genes among cefotaxime resistant E. coli from wastewater treatment plant. *Antimicrob. Resist. Infect. Control* **9**, 46 (2020).

92. Tabasi, M. Genotypic Characterization of Virulence Factors in Escherichia coli Isolated from Patients with Acute Cystitis, Pyelonephritis and Asymptomatic Bacteriuria. *J. Clin. Diagn. Res.* https://doi.org/10.7860/JCDR/2016/21379.9009 (2016) doi:10.7860/JCDR/2016/21379.9009.

93. Nhu, N. T. K. *et al.* Discovery of New Genes Involved in Curli Production by a Uropathogenic Escherichia coli Strain from the Highly Virulent O45:K1:H7 Lineage. *mBio* **9**, e01462-18 (2018).

94. Cooke, N. M., Smith, S. G., Kelleher, M. & Rogers, T. R. Major Differences Exist in Frequencies of Virulence Factors and Multidrug Resistance between Community and Nosocomial *Escherichia coli* Bloodstream Isolates. *J. Clin. Microbiol.* **48**, 1099–1104 (2010).

95. WHO. *WHO Integrated Global Surveillance on ESBL-Producing E. Coli Using a "One Health" Approach: Implementation and Opportunities*. https://www.who.int/publications/i/item/9789240021402 (2021).

Chapter 6. Facing Antimicrobial Resistance and Virulence in *Streptococcus agalactiae* during Late Pregnancy: Evaluation of *Lactobacilli* as a Supportive Approach

Manuscript in submission

Astri D. Tagueha[1], Giulia Radocchia[2], Daniela Scribano[1], Matteo Lo Scalzo[3], Giacinto Panella[4], Serena Schippa[1], Giovanni Gherardi[5], Roberta Creti[5], Ilaria Marani[5], Giovanna Alfarone[5], Monica Imperi[5], Massimiliano Marazzato[1], Lucia Nencioni[6], Paola Checconi[3,7], Dolores Limongi[3,7], Anna Teresa Palamara[5,6], and Cecilia Ambrosi[3,7*]

[1]Department of Public Health and Infectious Diseases, Sapienza University of Rome, 00185, Rome, Italy; [2] Department of Life Science, Health, and Health Professions, Link Campus University, 00166, Rome, Italy; [3]Department of Human Sciences and Promotion of the Quality of Life, San Raffaele Open University, 00166, Rome, Italy; [4]U.O.C Patologia Clinica, Ospedale Fabrizio Spaziani, 03100 Frosinone, Italy; [5]Department of Infectious Diseases, Istituto Superiore di Sanità, 00185, Rome, Italy; [6]Department of Public Health and Infectious Diseases, Sapienza University of Rome, Laboratory Affiliated to Institute Pasteur Italia-Cenci Bolognetti Foundation, 00185, Rome, Italy; [7]Laboratory of Microbiology, IRCCS San Raffaele Roma, 00166, Rome, Italy.

Abstract

Streptococcus agalactiae (Group B streptococcus, GBS) remains a major cause of neonatal sepsis and meningitis, despite the success of intrapartum antibiotic prophylaxis. However, the rising trend of antimicrobial resistance and the emergence of hypervirulent lineages highlight the need for complementary, innovative prophylactic strategies. In this study, we performed an integrated phenotypic, genotypic, and functional analysis of 31 clinical *S. agalactiae* isolates collected during routine pre-partum screening. We identified strains exhibiting multidrug resistance (MDR), inducible clindamycin resistance, high-level gentamicin resistance, and hypervirulent ST-17 lineages. Notably, approximately 23% of the isolates displayed MDR profile against tetracycline, erythromycin, and clindamycin. Furthermore, the isolate set displayed marked phenotypic heterogeneity in β-hemolytic activity and aggregation capacity, which correlated with specific capsular serotypes, pilus island profiles, and virulence gene repertoires. A non-antibiotic prophylactic strategy was investigated, based on the antagonistic potential of individual or combined *Lactobacillus* spp. strains under experimental conditions designed to mimic the vaginal niche (human cervical carcinoma HeLa cells). *Lactobacillus* spp. exerted strong, strain-dependent inhibitory activity against our *S. agalactiae* isolates, reducing bacterial survival in co-culture, preserving epithelial cell viability, and impairing pathogen adhesion by up to 98%. Importantly, the multi-strain *Lactobacillus* combination was more effective than individual strains, through a synergistic antimicrobial, protective, and antagonistic mechanism, which affected also MDR, inducible-clindamycin resistant, hypervirulent ST-17, and strongly hemolytic GBS strains. Overall, our findings suggest the topical use of multi-strain *Lactobacillus* preparations to reduce maternal colonization by MDR and hypervirulent *S. agalactiae* lineages, thereby reducing the risk of vertical transmission and neonatal disease.

6.1 Introduction

Streptococcus agalactiae (Group B Streptococcus, GBS) are Gram-positive, β-hemolytic bacteria that represent one of the leading causes of neonatal morbidity and mortality worldwide [1]. Indeed, GBS can asymptomatically colonize the maternal gastrointestinal or genitourinary systems, thereby spreading from mother to child during labour and delivery [2]. It was reported that in 2020, 19.7 million pregnant women were positive for *S. agalactiae* in the recto-vaginal region, determining an estimated 58,300 infant deaths, 46,200 stillbirths, and 518,000 GBS-associated preterm births globally [3]. Furthermore, 390,000 infants developed early- or late-onset *S. agalactiae* disease, with around 40,000 survivors affected by long-term neurological sequelae [4]. *S. agalactiae* harbours several virulence factors that enhance its ability to colonize mucosal surfaces, adhere to host tissues, evade immune defences, allowing the development of invasive GBS disease. These include genes encoding proteins involved in adhesion (*fbsA/B*, and *lmb*), in hemolysis (*cylB* and *hylB*), in immune evasion (*scpB*, and *bac*), and surface anchored alpha-like proteins (*alpha-C* or *bca*, *epsilon or alp1*, *alp2*/3, and *alp4*). Together, these virulence factors drive the colonization capacity and invasive potential of clinical strains [5–7]. Notably, hypervirulent strains, carrying specific surface factors, such as HvgA and Srr2, are strongly associated with

neonatal meningitis; some GBS lineages also developed high-level gentamicin resistance (HLGR), an antibiotic widely used as therapy in neonatal sepsis and meningitis [8]. Many of these hypervirulent isolates belong to the clonal complex 17 (CC17), particularly sequence type 17 (ST17), a lineage widely recognized as highly adapted to neonatal infection and associated with increased invasive potential and central nervous system tropism (Lamy *et al.,* 2006; Hsu *et al.*, 2023). In the USA and several European countries, recto-vaginal screening at 35–37 weeks of gestation was introduced to reduce the burden of neonatal *S. agalactiae* infections, followed by intrapartum antibiotic prophylaxis (IAP) for colonized mothers [9,10]. While this strategy has significantly reduced the incidence of neonatal early-onset sepsis, it may be a major driver for the general increase in antibiotic resistance among *S. agalactiae* strains and does not guarantee prevention of *S. agalactiae*-related abortions, stillbirths, preterm births, and late-onset disease [11,12]. In addition, extensive IAP exposure may hamper the establishment and development of the neonatal microbiota, with potential long-term health implications, including the predominance of pathogenic bacteria [13]. In light of these concerns, there is growing interest in identifying alternative or complementary strategies to control maternal *S. agalactiae* colonization during pregnancy. Among the most promising candidates are probiotic *Lactobacillus* spp. strains, which may exert antimicrobial effects through competitive exclusion, production of inhibitory substances, and modulation of the local immune response [14–17]. Thus, the aim of this study was to characterize a collection of *S. agalactiae* clinical isolates, by assessing their antimicrobial susceptibility, hemolytic activity, and virulence gene profiles, and to evaluate the ability of selected commercial *Lactobacillus* spp. strains to inhibit *S. agalactiae* growth, both under co-culture conditions and in an *in vitro* cervical epithelial cell adhesion model. Our findings demonstrated the strong inhibitory potential of combined *Lactobacillus* spp. strains against currently circulating GBS isolates, supporting the further development of strain-specific probiotic approaches as alternative or complementary options to current antibiotic protocols.

6.2 Materials and Methods

6.2.1 Clinical isolates collection

Thirty-one clinical *S. agalactiae* isolates were collected between January and March 2025 as part of a screening for pathogen colonization of pregnant women at the end of the third trimester of gestation (35-37 weeks), from uro-vaginal-rectal swabs (n=26), and urine (n=5). Species identification was conducted using matrix-assisted laser desorption ionization-time of flight mass spectrometry (MALDI-TOF MS). Samples were preserved at −80°C in glycerol stocks in Todd Hewitt broth. For experiments, isolates were routinely cultured in Brain Heart Infusion (BHI) medium, unless differently specified.

6.2.2 Antibiogram profiles

The antimicrobial susceptibility profiles of *S. agalactiae* clinical isolates were determined using the VITEK®2 system (bioMérieux, Italia S.p.A, Grassina, Italy). Interpretation was performed according to the European Committee on Antimicrobial Susceptibility Testing (EUCAST) guidelines (v14.0, 2024), using the corresponding minimum inhibitory concentration (MIC)

breakpoints for each antibiotic class. For specific antibiotics, such as tetracycline, clindamycin, and erythromycin, susceptibilities were initially assessed by MIC and then verified with disk diffusion tests. The detection of inducible clindamycin resistance was performed using the D-test method, according to the EUCAST guidelines, as previously described (Imperi *et al.,* 2024). Erythromycin resistance phenotypes were classified as expressing the inducible (IR), constitutive (CR), M, and S phenotype as previously described [18]. HLGR was assessed at the recommended concentration (500 µg/ml). The presence of associated antibiotic resistance genes (*ermA, ermB, mef, tet(M), tet(O),* and *aac(6')-Ie-aph(2")-Ia* was assessed as previously described [19–21]. MDR was defined as resistance to at least three different classes of antibiotics [22].

6.2.3 Hemolytic test

A single colony of each *S. agalactiae* clinical isolate from a freshly streaked BHI agar plate was inoculated into 3 ml of BHI broth and incubated at 37°C for 18-24 h under aerobic conditions. Subsequently, 10 µl of the culture were spotted onto Columbia blood agar plates (Becton Dickinson, Milan, Italy) and incubated under identical conditions. Following incubation, the bacterial spots were inspected to determine the presence and type of hemolysis. The β-hemolytic phenotype was classified into four categories: non-haemolytic; weak, characterized by a narrow, faint, or poorly defined zone of clearance; moderate, exhibiting a medium-sized zone with less distinct edges and a yellowish translucency under transmitted light; and strong, displaying a clear and transparent zone.

6.2.4 Aggregation test

The ability of *S. agalactiae* clinical isolates to auto-aggregate was assessed, as previously described [17], with minor modifications. In brief, overnight cultures were harvested by centrifugation at 10,000 x g for 10 min, washed twice with phosphate-buffered saline (PBS), and resuspended in PBS to an initial OD_{600} (referred to as A_0) of 0.5. The bacterial suspensions were then incubated overnight at room temperature without agitation, and the OD_{600} (A_t) was measured. The percentage of auto-aggregation was calculated according to the following formula:

$$Aggregation\ (\%) = 1 - \frac{A_t}{A_0} x\ 100$$

The aggregation percentage was then converted to z-scores to define aggregation categories to avoids arbitrary percentage cut-offs, using following formula:

$$z\ score = \frac{Aggregation - mean\ all\ values}{standard\ deviation}$$

Based on z score, *S. agalactiae* clinical isolates were further classified into four categories: non-aggregating ($z \leq -1$), weak aggregating ($-1 < z < 0$), moderate aggregating ($0 \leq z < 1$), and strong aggregating ($z \geq 1$).

6.2.5 Serotyping, detection of pilus island, virulence genes, and hypervirulent ST-17

Serotyping of *S. agalactiae* clinical isolates was performed using the commercial latex agglutination test ImmuLexTM StrepB-Kit (SSI Diagnostica, Hillerød, Denmark) [23,24]. Molecular typing by multiplex-Polymerase Chain Reaction (PCR) was further applied in case of not-typeable strains and to confirm the results of the agglutination test, as previously reported [20]. The presence of pilus islands (PI-1, PI-2a, and PI-2b) and virulence genes (*fbsA, fbsB, lmb, cylB, hylB, scpB, bac, alp2/3, alp4, alpha-C*, epsilon, and *rib)* was detected by multiplex PCR, as previously described [5,25,26]. In addition, a singleplex PCR was used to detect the *hvgA* gene as a marker of the hypervirulent ST-17 lineage [27]. The resulting amplicons were separated on 2% agarose gels stained with SafeView^{Tm} Classic (abm, Canada) and visualized using a ChemiDoc Imaging System (Bio-Rad, USA). All the primers used in this study are listed in Table S3.

6.2.6 Evaluation of antagonistic activity of *Lactobacilli* against *S. agalactiae*

Four *Lactobacillus* spp. strains belonging to four different species, *Lactobacillus plantarum* strain NCIMB 30437, *Lactobacillus paracasei* strain NCIMB 30439, *Lactobacillus rhamnosus* strain CRL1505 (DSM 29673), and *Lactobacillus reuteri* strain NCIMB 30242 (referred to as *L. plantarum*, *L. paracasei*, *L. rhamnosus*, and *L. reuteri* throughout the whole text) were selected for this study. The inhibitory activity of the *Lactobacillus* spp. strains against clinical *S. agalactiae* isolates was first qualitatively evaluated using a co-plating assay and then quantified through co-culture experiments in BHI broth. For the co-plating assay, single colonies of each *Lactobacillus* and *S. agalactiae* strain were individually inoculated into BHI broth and incubated aerobically at 37°C for 24–48 h. Next, 150 µL of each *Lactobacillus* culture was spread onto BHI agar, and 10 µL of each *S. agalactiae* culture was spotted onto the surface. Plates were incubated at 37°C for 24-48 h. Growth inhibition, defined as the presence of a clear zone around the *S. agalactiae* spots, was interpreted as a positive for antagonistic activity. *S. agalactiae* isolates susceptible to *Lactobacillus* inhibition were selected for further co-culture experiments. For the co-culture assay, a freshly streaked single colony of each *Lactobacillus* strain and *S. agalactiae* isolate were co-inoculated into 3 ml of BHI broth and incubated under the same conditions; corresponding monocultures were included as growth controls. Following incubation, co-culture and monoculture suspensions were serially diluted in PBS and plated onto MRS agar (for *Lactobacilli*) and BHI agar (for *S. agalactiae*) to determine colony-forming units (CFUs)/ml. The mortality rate and competition index (CI) were calculated using the following formulas:

$$\text{Mortality rate} = \frac{\text{CFU monoculture} - \text{CFU co} - \text{culture}}{\text{CFU monoculture}} \text{ x } 100\%$$

$$\text{Competition index} = \frac{\left(\text{CFU } \textit{Lactobacilli} \text{ co} - \text{culture} / \text{CFU } \textit{S. agalactiae} \text{ co} - \text{culture}\right)}{\left(\text{CFU } \textit{Lactobacilli} \text{ monoculture} / \text{CFU } \textit{S. agalactiae} \text{ monoculture}\right)}$$

6.2.7 Cytotoxicity of *Lactobacillus* spp. and *S. agalactiae* isolates on host cells

The cytotoxicity of selected *Lactobacillus* spp. strains and of *S. agalactiae* was individually evaluated on human cervical carcinoma HeLa (CCL-2™) cell monolayers cultured in Dulbecco's Modified Eagle Medium (DMEM) supplemented with 10% fetal bovine serum (FBS), 1% glutamine, 1% penicillin-streptomycin, and 50 µg/ml gentamicin. HeLa cells (2.5 x 10^5 per well) were seeded onto 24-well plates (Corning®) and incubated overnight to reach > 70% confluency. *Lactobacillus* cultures were harvested by centrifugation at 4,000 x g for 15 min and resuspended in antibiotic-free DMEM containing 5% FBS. After washing with PBS, HeLa cell monolayers were exposed either to individual *Lactobacillus* spp. strains or to a mixture of the four strains, using a multiplicity of infection (MOI) of 1,000. Cells were incubated at 37°C with 5% CO_2 for 1.5 and 3 h. After five washes with PBS, cytotoxicity was assessed using an MTT assay, as previously reported [28]. Briefly, 300 µl of the MTT solution (0.5 mg/ml in DMEM without phenol red; Sigma-Aldrich) was added to each well and allowed to incubate for 3 h. Subsequently, 500 µL of 0.1 N HCl in isopropanol was added to solubilize the formazan crystals, and plates were incubated for 1 h before measuring absorbance at 570 nm using a microplate reader (BioTek). To evaluate the combined cytotoxic effects of *S. agalactiae* and *Lactobacillus* spp. strains, HeLa cell monolayers were first infected with *S. agalactiae* at an MOI of 10 for 30 min. Then, the medium was removed and replaced with the mixture of *Lactobacillus* at an MOI of 1,000, followed by incubation for 1.5 or 3 h before performing the MTT assay. Untreated cells were used as controls. Cell viability was calculated with the following formula:

$$Viability\ (\%) = \frac{Mean\ OD_{treated}}{Mean\ OD_{control}}\ x\ 100\%$$

Optical microscopic images were acquired using a 20× objective on an Optika microscope (Optika Microscopes, Italy) equipped with a Tucsen MIchrome 20 camera.

6.2.8 *Lactobacilli* host cell protection assay against *S. agalactiae*

To assess the ability of *Lactobacillus* spp. strains to displace adherent *S. agalactiae* isolates, HeLa cell monolayers were first infected with *S. agalactiae* and then exposed to the mixture of the four *Lactobacillus* spp. strains, as described above. After 3 h of incubation, cell monolayers were extensively washed with PBS to remove loosely adherent bacteria and then lysed with 1 ml of 0.1% Triton X-100 to recover adherent bacteria. Lysates were serially diluted and plated onto BHI (for *S. agalactiae*) and MRS agar (for *Lactobacillus* spp.) to determine colony-forming units (CFU)/ml. Untreated cells, as well as cells individually infected with *S. agalactiae*, or *Lactobacillus* spp. strains were included as controls. The percentage inhibition index of *S. agalactiae* was calculated using the following formula:

$$\%\ \text{Inhibition} = 1 - \frac{\text{CFU co} - \text{culture}}{\text{CFU monoculture}}\ \text{x}\ 100\%$$

Optical microscopic images of methanol-fixed, Giemsa-stained monolayers were acquired as described above.

6.2.9 Statistical analysis

Statistical analyses were performed using GraphPad Prism Software (version 11). Continuous data from aggregation assays are presented as z-scores. For the MTT assay, differences in cell viability among multiple treatment groups were analysed using one-way ANOVA. Dunnett's post hoc test was subsequently applied to compare each treatment group to the control. Differences in bacterial adherence on HeLa cells between treated cells and control conditions were assessed using two-tailed paired t-test. Associations between genotypic and phenotypic characteristics were evaluated using Spearman's rank correlation. P values < 0.05 were taken as being statistically significant.

6.3 Results

6.3.1 *S. agalactiae* clinical isolates showed different hemolytic patterns

To classify the hemolytic properties of our *S. agalactiae* isolate collection, strains were spotted onto Columbia blood agar plates (Figure 6.1). Overall, the intensity and appearance of a β-hemolytic varied among clinical isolates. Strains 3 and 21 (6%, 2/31) showed the strongest β-hemolysis, while moderate hemolysis was observed in strains 1, 2, 4, 5, 6, 8, 9, 12, 17, 20, and 25 (35%, 11/31) (Figure 6.1). The majority of the remaining isolates (55%, 17/31) exhibited weak β-hemolysis. Notably, only strain 22 showed no visible clearing zone, suggesting a γ -hemolytic phenotype (Figure 6.1).

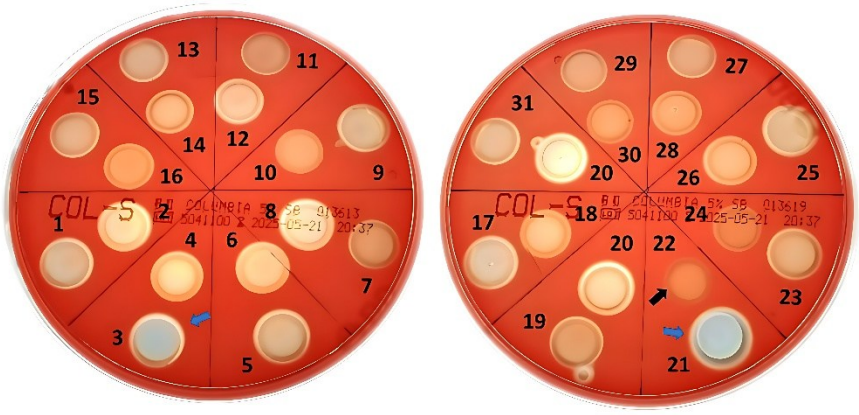

Figure 6.1. *S. agalactiae* hemolytic activity. Ten microliters of the overnight cultures were spotted onto Columbia blood agar plates and incubated for 18-24 h in aerobic condition. Strong β-hemolytic isolates are indicated by blue arrows, whereas the γ-hemolytic strain is indicated by a black arrow. Numbers represent strain IDs. Images were acquired with a resolution up to 3616 x 1732 pixels (Infinix X6817).

6.3.2 *S. agalactiae* clinical isolates showed variable aggregation capacity, serotype and pilus island profiles

Since autoaggregation is considered a key factor contributing to bacterial persistence and colonization in *S. agalactiae*, we evaluated this phenotype across our strain collection. Overall, our clinical isolates exhibited marked variability in their aggregation capacity, in that 42% (13/31) were classified as weak aggregators, 29% (9/31) as moderate, and 16% (5/31) as strong aggregators, whereas 13% (4/31) exhibited no detectable aggregation under the tested condition (Figure 6.2). Next, capsular serotypes and pilus island (PI) profiles were characterized. Among the ten well-characterized *S. agalactiae* serotypes, our clinical isolates belonged to six groups, with serotype III being the most prevalent (35.5%, 11/31), followed by serotype II and V (19.3% each, 6/31), and IV (12.9%, 4/31), and Ia and VI (6.4%, 2/31) (Table 6.1). Notably, the most prevalent serotypes were associated with diverse PI profiles. PI-1+2b combination was exclusively detected in the majority of serotype III (8/11, 72.7%). PI-1+2a occurred in all serotypes but one, with the highest proportion observed in serotype V (4/6, 66.7%). The PI-2a profile was detected in three serotypes, Ia, II and V. In contrast, the less frequent PI-2b profile was restricted to serotype III and IV (Table 6.1). Collectively, these findings highlight the marked genetic diversity of surface structures within our clinical *S. agalactiae* collection.

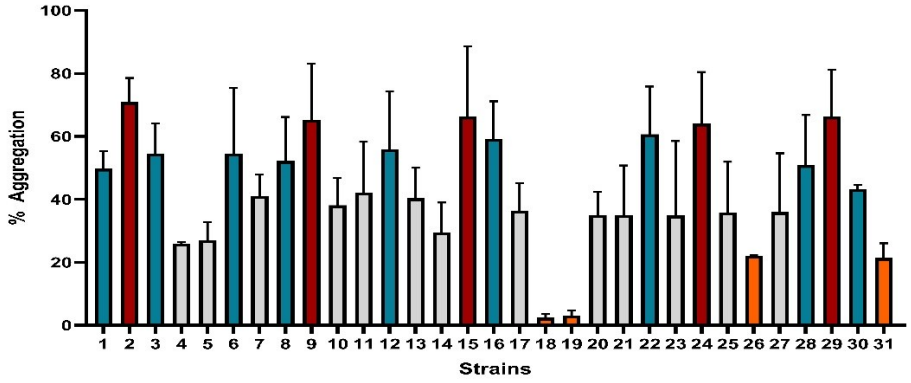

Figure 6.2. Aggregation ability of *S. agalactiae* clinical isolates. Aggregation profiles, expressed as the percentage of aggregated cells after overnight incubation. Bars represent the mean ± standard deviation (SD) from three independent experiments (n = 6). Based on z-scores, isolates were classified into four categories, indicated by color codes: non-aggregating (orange), weak (grey), moderate (green), and strong (red) aggregators.

Table 6.1. Microbiological characteristics of 31 studied GBS clinical isolates

Serotype (n. isolates)	Alpha-like protein genes (n. isolates)	Pilus island (PI) (n. isolates)	*hvg*A gene (ST-17) (n. isolates)	Erythromycin phenotype/ genotype (n. isolates)	Tetracyline phenotype/ genotype (n. isolates)	HLGR[a], n. isolates	MDR[c]
Ia (2)	epsilon (1), alp2/3 (1)	PI-2a (2)	neg (2)	IR/*erm*A (1), M/*mef*A (1)	R/*tet*M (2)	0	1
II (6)	rib (5), neg (1)[b]	PI-1+2a (3), PI-2a (3)	neg (6)	IR/neg (1)[b], S (5)	R/*tet*M (3), R/*tet*O (2), S (1)	1	1
III (11)	rib (11)	PI-1+2b (8), PI-1+2a (2), PI-2b (1)	pos (9), neg (2)	CR/*erm*B (1), S (10)	R/*tet*M (7), R/*tet*O (2), S (2)	0	1
IV (4)	alpha-C (3), rib (1)	PI-1+2a (2), PI-2b (2)	pos (3), neg (1)	S (4)	R/*tet*M (1), S (3)	2	0
V (6)	alp2/3 (4), alpha-C (2)	PI-1+2a (4), PI-2a (2)	neg (6)	CR/*erm*B (4), S (2)	R/*tet*M (6)	0	4
VI (2)	alpha-C (2)	PI-1+2a (2)	neg (2)	S (2)	S (2)	0	0

Abbreviations. CR, erythromycin resistance with constitutive clindamycin resistance; IR, erythromycin resistance with inducible clindamycin resistance; M, erythromycin resistance and clindamycin susceptibility; S, erythromycin and clindamycin susceptibility; HLGR, high-level gentamycin resistance. [a]All HLGR isolates carried the *aac(6')-Ie-aph(2")-Ia* resistance gene. [b]One serotype II isolate was negative for all alpha-like surface protein genes tested (epsilon, rib, alpha-C, alp2/3, and alp4) and showed IR phenotype with no erythromycin resistance genes detected. [c]MDR, multidrug-resistant isolates, contemporarily resistant to at least 3 classes of antibiotics (erythromycin, clindamycin and tetracycline).

6.3.3 *S. agalactiae* clinical isolates showed a high prevalence of key virulence associated-genes

To assess the presence and distribution of virulence determinants, known virulence-associated genes were analyzed using a combination of monoplex and multiplex PCR assays (Figure 3). The genes *fbsA, fbsB* and *lmb,* encoding adhesion-related proteins involved in fibrinogen and laminin binding, were highly prevalent, being identified in 100% of isolates for *fbsA, fbsB,* and 90% (28/31) for *lmb*. The *cylB* and *hylB* genes, essential for cytolysin/hemolysin production, were detected in the vast majority of isolates (30/31, 97%), consistent with the predominant β-hemolytic phenotype observed (Figures 1 and 3). The *scpB* gene, encoding the C5a peptidase involved in immune evasion, was identified in the entire strain collection but one (30/31, 97%), whereas the gene encoding the surface Cβ protein (*bac*), which binds IgA and complement factor H, was rare, and detected in only one strain (1/31, 3%). Among the genes encoding surface proteins, *rib* was the most prevalent (17/31, 54.8%), typically associated with serotypes III and II, followed by *alpha-C* (7/31, 22%). *alp2/3* was frequent in serotype V (4/6, 66.7%), and *epsilon* (1/31, 3%) only identified in serotype Ia, while the *alp4* gene was not detected in any strain (Table 6.1). Noteworthy, strain 10 lacked any alpha-protein-like genes. The hypervirulence-associated gene

hvgA, highly specific for the ST-17 lineage, was detected in 12 of 31 isolates (39%), and mainly associated with serotype III (9/12, 75%) and serotype IV (3/12, 25%) (Table 6.1 and Figure 6.3).

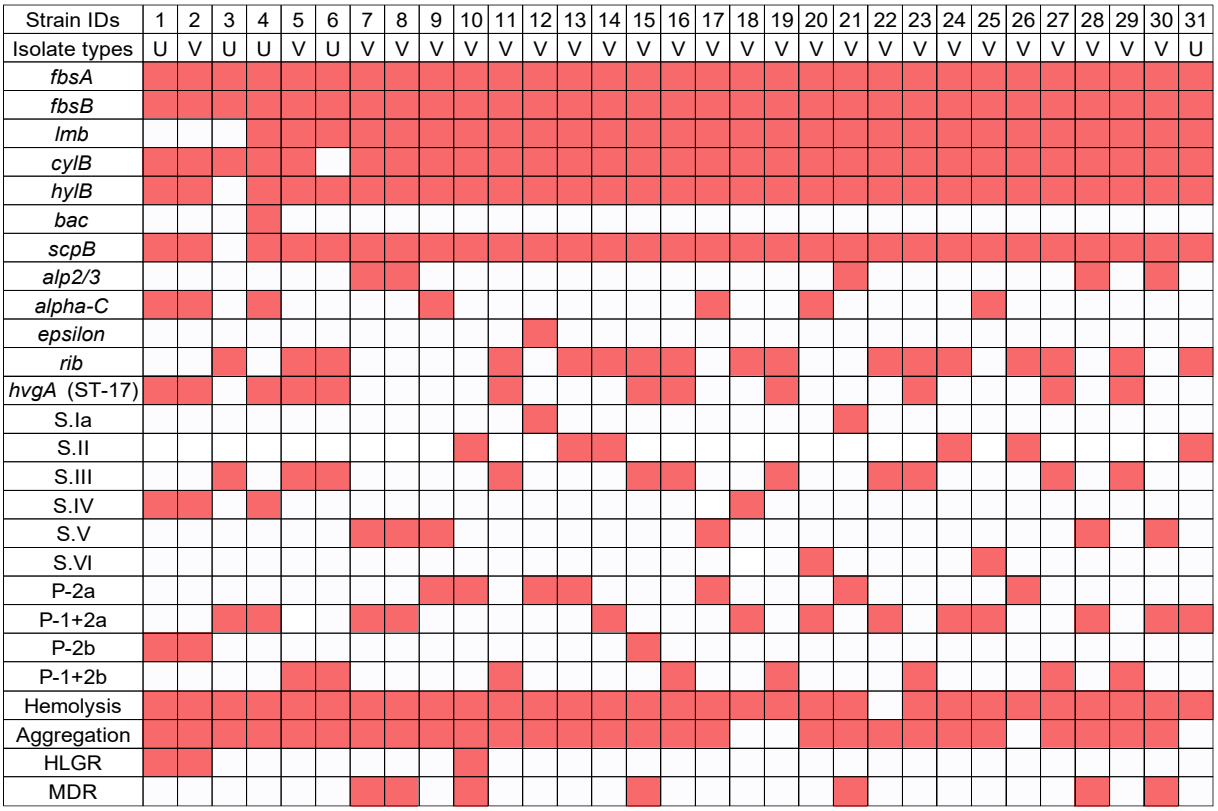

Figure 3. Distribution of virulence genes and phenotypic traits among *S. agalactiae* clinical isolates. The presence/absence of genes is indicated by filled and empty boxes, respectively. Isolate sources indicated by symbol, U for urine and V for vagina.

Interestingly, most *hvgA*-positive isolates were recovered from vaginal specimens (9/12, 75%). All these isolates carried the adhesin and invasion genes *fbsA, fbsB, cylB,* and *scpB,* and many harbored *rib* genes. Nearly all *hvgA*-positive isolates were β-hemolytic and displayed an aggregation phenotype. The predominant PI profile among hypervirulent isolates was PI-1+2b (8/12, 67%), followed by PI-2b (3/12, 25%), and the PI-1+2a (1/12, 8%) (Figure 6.3). Additionally, more than half of the *hvgA*-positive isolates exhibited resistance to tetracycline and rifampicin (58%, 7/12 each), and two showed HLGR phenotype (17%, 2/12). Despite this mosaic resistance pattern, only one hypervirulent ST-17 isolate displayed a MDR profile with CR phenotype (Table 6.1).

6.3.4 Emerging rifampicin resistant *S. agalactiae* isolates

All *S. agalactiae* isolates were susceptible to penicillin, linezolid, moxifloxacin, teicoplanin, tigecycline, trimethoprim/sulfamethoxazole, and vancomycin (Table 6.S1). In contrast, resistance was observed to tetracycline (74.2%, 23/31), rifampicin (71%, 22/31), erythromycin (25.8%, 8/31), clindamycin (22.6%, 7/31), and levofloxacin (3.2%, 1/31) (Table 6.S1). Five isolates identified as erythromycin-clindamycin-resistant (CR phenotype) isolates, four of serotype V and

one of serotype III harbored the *ermB* gene (16%, 5/31) (Table 6.1 and Table 6.S1). Two erythromycin-resistant isolates with inducible IR phenotype were detected: one serotype Ia isolate carrying the *ermA* gene, while the other was a serotype II negative for all tested resistance genes (Table 6.1). In addition, one erythromycin-resistant and clindamycin-susceptible isolate (M phenotype) of serotype Ia carried the *mef* gene (Table 6.1). All erythromycin- and clindamycin-susceptible isolates (S phenotype, 74.2%, 23/31) lacked resistance genes (Table 6.1 and Table 6.S2). Among 23 tetracycline-resistant isolates, all carried at least one resistance gene, with *tetM* being the most prevalent (82.6%, 19/23), followed by *tetO* (17.4%, 4/23). MDR phenotype was observed in 22.6% (7/31) of isolates, involving combined resistance to tetracycline-erythromycin-clindamycin (Table 6.1 and Table 6.S1). MDR isolates belonged to serotype V (four isolates), Ia, II, and III (one isolate each) (Table 6.1). Overall, three isolates (9.7%), two of serotype IV and one serotype II, exhibited HLGR and carried the *aac(6')-Ie-aph(2")-Ia* gene (Table 6.S2).

6.3.5 *Lactobacillus* spp. exhibit inhibitory activity against clinical *S. agalactiae* isolates

Given the growing need of alternative or complementary strategies to limit *S. agalactiae* colonization, we set up a qualitative co-plating assay to evaluate the antagonistic potential of selected *Lactobacillus* spp. strains against our *S. agalactiae* clinical isolates. Although the majority of *S. agalactiae* isolates were not markedly inhibited by selected *Lactobacillus* spp. strains, this initial screening revealed thin partial-to-clear areas surrounding the *S. agalactiae* spot zones, suggesting some degree of inhibition (Figure 6.4). In particular, 14 isolates were identified as species-specific sensitive isolates (3, 4, 10, 12, 13, 14, 18, 21, 23, 26, 27, 29, 30, and 31). Among this subset of clinical isolates, 64% (9/14) were inhibited by *L. plantarum* and *L. paracasei*, 71% by *L. rhamnosus*, and 86% by *L. reuteri* (Figure 6.4).

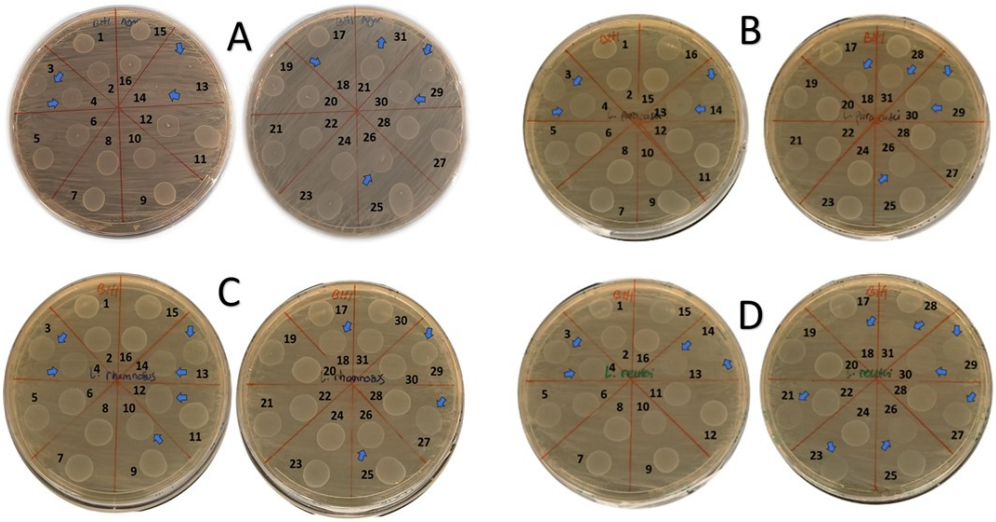

Figure 6.4. Inhibitory effects of *Lactobacillus* spp. on *S. agalactiae* clinical isolates. Plates were seeded with (A) *L. plantarum*, (B) *L. paracasei*, (C) *L. rhamnosus*, and (D) *L. reuteri* as a bacterial lawn, and 10 µL of all *S. agalactiae* isolates were spotted on top. Sensitive strains showing partial to clear zone are indicated by blue arrows. Two independent experiments were performed in duplicate (n=4). Representative images are shown.

To quantify the extent of *S. agalactiae-Lactobacillus* growth inhibition, broth co-culture assays were performed using different strain combinations (Figure 6.5). For most combinations, *Lactobacillus* spp. strains induced substantial killing of plate-sensitive *S. agalactiae* isolates, with mortality values approaching 100% across all *Lactobacillus* strains (Figure 6.5A, 6.5C, 56.E, 6.5G), including three MDR isolated tested (strains 10, 21, and 30). In contrast, strain 31 was the only one displaying a survival advantage when co-cultured with *L. paracasei,* as indicated by a relative overgrowth of 1.92-fold higher than those observed in its corresponding monoculture control (Figure 6.5C). Overall, these data indicate that, despite some strain-specific differences, the *Lactobacillus* panel exerted a robust inhibitory effect on almost all tested *S. agalactiae* isolates.

To achieve a deeper understanding of the interaction between *S. agalactiae* isolates and *Lactobacillus* spp., the competition index (CI) was calculated by combining the survival outcomes of both species and expressing the results as $\log_{10}$ values. The CI profiles showed that *Lactobacillus* strains generally exerted moderate to strong inhibition of *S. agalactiae* isolates, although the interaction patterns were both isolate- and species/strain-dependent (Figure 6.5B, 6.5D, 6.5F, 6.5H). Moderately to strongly inhibited *S. agalactiae* isolates accounted for 78% (7/9) in the interaction with *L. plantarum*, and 67% (6/9) with *L. paracasei*, while *L. rhamnosus*, and *L. reuteri* showed inhibitory activity against 40% (4/10), and 33% (4/12) of *S. agalactiae* isolates, respectively. Weakly inhibited isolates were more frequent in co-cultures with *L. rhamnosus* (5/10, 50%) and *L. reuteri* (5/12, 58%). Non-inhibited phenotypes ($\log_{10}$CI<0) were clearly evident only for isolate 31 in combination with *L. paracasei*, consistent with the survival advantage previously observed for this pair (Figure 6.5C).

Noteworthy, some sensitive isolates, such as strains 10 and 21, displayed high mortality under co-culture conditions (Figure 6.5E and 6.5G), but did not appear inhibited according to their CI values (Figure 6.5F and 6.5H). This apparent discrepancy can occur because the CI measures a relative ratio, and therefore it can hide high mortality if the surviving pathogen multiplies fast enough to balance or exceed *Lactobacillus* growth. In particular, strain 21 antagonized *L. reuteri*, yielding a negative CI that reflects a relative overgrowth of pathogen (1.1-fold higher) compared to the probiotic strain. In addition, the interaction between strain 10 and *L. rhamnosus* resulted in a CI close to zero, consistent with a balanced co-culture in which neither species clearly dominates. These findings suggest that some *S. agalactiae* lineages may partially resist or even counteract the inhibitory potential of individual probiotic strains, as observed for strains 10 and 21, both displaying an MDR phenotype.

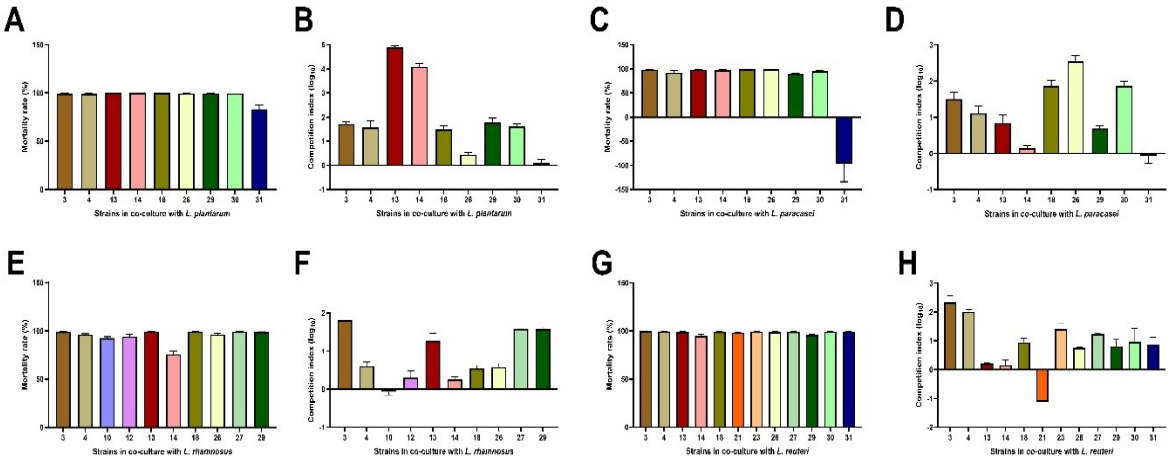

Figure 6.5. Inhibitory activity of *Lactobacillus* spp. against *S. agalactiae* in broth co-culture. Previously, S. *agalactiae* isolates identified as plate-sensitive were tested in broth co-culture assays with (A and B) *L. plantarum*, (C and D) *L. paracasei*, (E and F) *L. rhamnosus*, and (G and H) *L. reuteri*. Inhibitory effects were evaluated by determining *S. agalactiae* mortality rates (A, C, E, G), and by calculating the competition index (CI), expressed as $\log_{10}$-transformed values (B, D, F, H). Based on $\log_{10}$CI values, *S. agalactiae* isolates were classified as non-inhibited ($\log_{10}CI < 0$), weakly inhibited ($0 < \log_{10}CI < 1$), moderately inhibited ($1 < \log_{10}CI < 2$), or strongly inhibited ($\log_{10}CI \geq 2$). Data are presented as mean ± SD from three independent experiments (n=6). Only *S. agalactiae* isolates showing susceptibility in the co-culture assay are reported.

6.3.6 *Lactobacillus spp.* protect HeLa cells from S. agalactiae-induced cytotoxicity and reduce adhesion

To assess the safety of *Lactobacillus* spp. strains on human cells at high dosage, their cytotoxicity, either individually or as a combination, was evaluated using an MTT assay on HeLa cell monolayers exposed to an MOI of 1,000 for 1.5 and 3 h (Figure 6.6). After 1.5 h of exposure, HeLa cell viability was equal to or higher than that of control cells, with significant increases observed for cells treated with *L. plantarum*, *L. paracasei*, and *L. rhamnosus* (Figure 6.6A). This beneficial profile persisted at 3 h, as all *Lactobacillus* strains preserved cell viability. Only cells exposed to *L. reuteri* alone or to the *Lactobacillus* combination showed a small further increase in cell viability compared with 1.5 h, although this difference did not reach statistical significance (Figure 6.6B). Next, the cytotoxicity potential of *S. agalactiae* isolates on HeLa cell monolayers was assessed, using an MOI of 10 for 1.5 and 3 h (Figure 6.6C and 6.6D). A panel of *S. agalactiae* strains (3, 6, 12, 18, 20, 21, 22, and 30) was chosen to represent different characteristics, including *Lactobacillus*-sensitive and -resistant isolates, MDR and non-MDR profiles, CR/IR/M phenotypes, hemolytic and non-hemolytic isolates, aggregating and non-aggregating phenotypes, carrying diverse alpha-like protein genes, PI profiles, and the ST-17 lineage. Interestingly, the impact of *S. agalactiae* on cell viability was both strain- and time-dependent (Figure 6.6C and 6.6D). Indeed, after 1.5 h of infection, all strains induced only minimal and non-significant reductions in cell viability, accounting for less than 5% (Figure 6.6C). Conversely, after 3 h of

infection, *S. agalactiae* isolates caused a statistically significant decrease in cell viability, ranging from approximately 71 to 85% compared with the control cells (Figure 6.6D). Finally, to assess the protective role of *Lactobacillus* spp. strains in counteracting *S. agalactiae*-induced cytotoxicity and preventing pathogen adhesion to epithelial cells, a co-infection assay was performed. HeLa cell monolayers were first infected with representative *S. agalactiae* isolates at an MOI of 10 for 30 min, followed by the addition of the *Lactobacillus* combination at an MOI of 1,000 for 1.5 and 3 h (Figure 6.6E and 6.6F). No differences in cell viability were observed at 1.5 h post-infection (hpi) (Figure 6.6E). Conversely, at 3 hpi, cell viability remained above 90% for all *S. agalactiae* isolates tested, with the exception of strain 3, which reduced cell viability to values slightly but significantly below the control cells (Figure 6.6F).

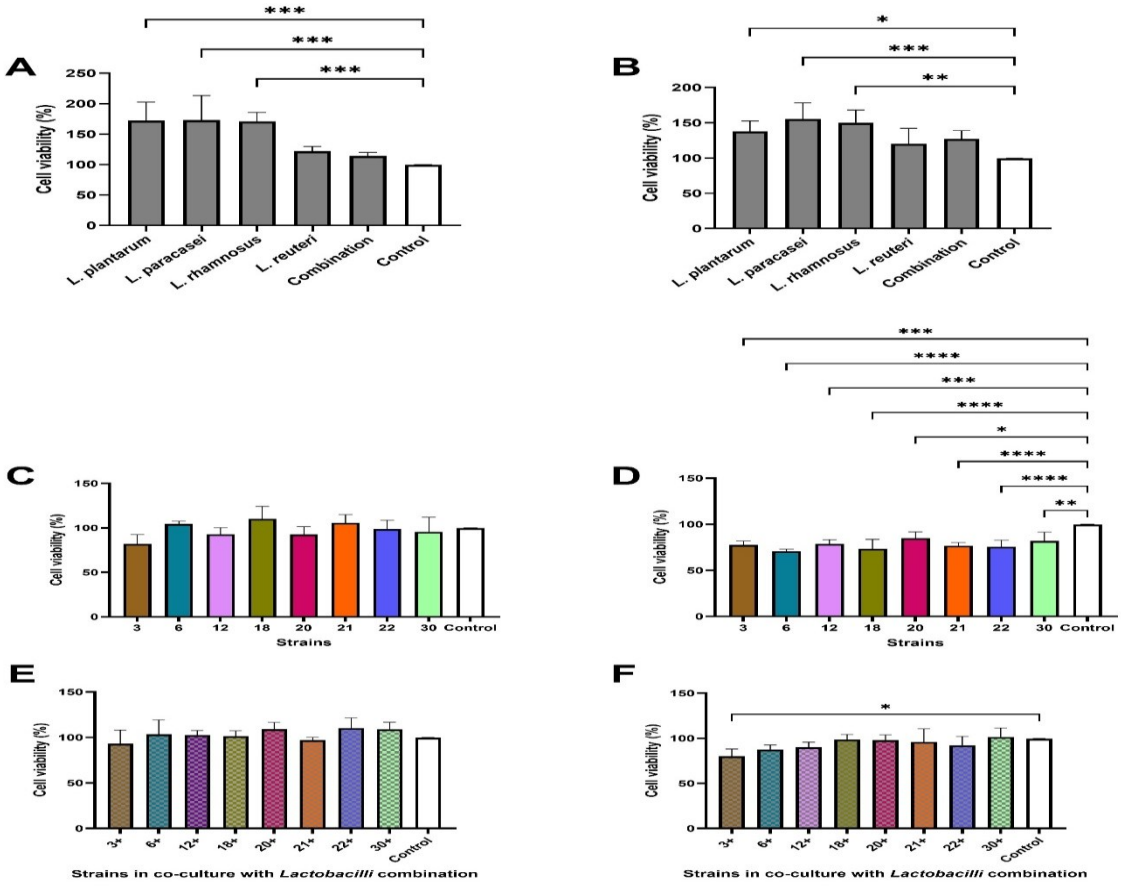

Figure 6.6. Viability of HeLa cells following exposure to *Lactobacillus* spp. strains, *S. agalactiae*, or their combination. Cell viability of confluent HeLa cell monolayers was determined at fixed time points using the MTT assay. (A, B) Exposure to individual *Lactobacillus* strains or to their four-strain combination at an MOI of 1,000 for 1.5 and 3 h, respectively. (C, D) Infection of selected *S. agalactiae* isolates at an MOI 10 for 1.5 and 3 h, respectively. (E, F) Sequential co-infection (first with *S. agalactiae* for 30 min and then with the *Lactobacillus* combination) at the above indicated MOIs for 1.5 and 3 hpi, respectively. Data are expressed as percentages relative to uninfected control cells (mean ± SD from at least three independent experiments; n=6).). Statistical significance was assessed using one-way ANOVA; * $P < 0.05$, ** $P < 0.01$, *** $P < 0.001$, **** $P < 0.0001$.

The same experimental setting was used to quantify the ability of the *Lactobacillus* strain combination to reduce/inhibit the adhesion of *S. agalactiae* isolates at 3 hpi (Figure 6.7), corresponding to the time point showing maximal cytotoxicity (Figure 6.6D). The presence of the *Lactobacillus* combination significantly reduced host cell adhesion for almost all *S. agalactiae* isolates, with inhibition values ranging from approximately 0.2- to 1.7- fold relative to the corresponding control without *Lactobacillus* (Figure 6.7A and 6.7B). The strongest effects were observed for strains 22, 18, and 3, which showed inhibition levels of about 98%, 93%, and 93%, respectively (Figure 6.7B). A weaker inhibition was observed for strain 30, accounting for approximately 40%, whereas strain 21 showed a non-statistically significant reduction of 36% (Figure 6.7B). CI analysis further highlighted these differences (Figure 6.7C), ranking the extent of adhesion inhibition as follows: 22>18>3>12>6>20>30>21 (Figure 6.7C).

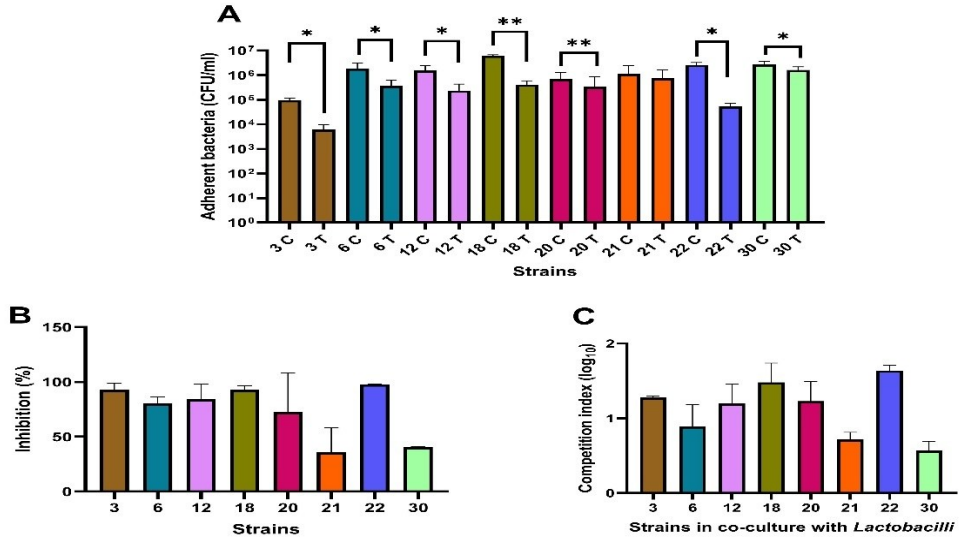

Figure 6.7. *Lactobacillus* combination-mediated inhibition of *S. agalactiae* adherence to HeLa cells. Confluent HeLa cell monolayers were first infected with representative *S. agalactiae* isolates at an MOI of 10 for 30 min, followed by the addition of the *Lactobacillus* combination at an MOI of 1,000 for 3 h. (A) Number of adherent *S. agalactiae* cells recovered from HeLa cell monolayers in the absence (C, controls) or presence (T, treated) of the *Lactobacillus* combination, expressed as CFU/ml. (B) Percentage of inhibition of *S. agalactiae* adherence, calculated from CFU counts. (C) Corresponding CI values. Data are presented as mean ± SD from at least three independent experiments (n=6). Statistical significance of adherent bacteria was assessed using two-tailed paired t-test; * $P < 0.05$, ** $P < 0.01$.

6.4 Discussion

S. agalactiae is still a leading cause of neonatal sepsis and meningitis worldwide, representing a major public health concern [1]. Historically, this pathogen was responsible for nearly 50% of neonatal infection before the intrapartum antibiotic prophylaxis (IAP) strategy [29]. The implementation of universal screening programs and IAP has significantly reduced the incidence of early-onset disease and its associated mortality [10]. However, the increasing prevalence of MDR resistance strongly highlights the need to develop alternative and/or supportive therapeutic approaches, while awaiting an effective vaccine for maternal immunization [3,11,12,30]. Despite the limited size of our clinical isolate collection, two distinct resistance patterns were observed among the the seven MDR strains: resistance to rifampicin-tetracyclines-erythromycin-clindamycin or to tetracyclines-erythromycin-clindamycin (Table 6.1 and Table 6.S1). All erythromycin-resistant GBS isolates carried one of the resistance gene tested *ermA*, *mef*, and *ermB,* while all tetracycline resistant strains harbored either *tetM* or *tetO* (Table 6.S2). The strong alignment between disk diffusion test results and the presence of *tetM*/*tetO* genes for tetracycline resistance and *ermA*/*ermB*/*mef* genes for macrolides–lincosamides resistance in our isolates supports the integration of phenotypic and genotypic data to obtain a more robust definition of resistance [21,31]. The HLGR phenotype detected in three isolates was consistent with the presence of *aac(6')-Ie-aph(2")-Ia* gene, with one HLGR isolate being MDR. This suggests that high-level gentamicin resistance may be co-selected with other resistance determinants, possibly through mobile genetic elements carrying clustered resistance genes [32,33]. Importantly, HGLR strains further narrow therapeutic options by compromising the synergistic ampicillin-gentamicin regimen widely used for neonatal sepsis and meningitis management [8,11].

Beyond antimicrobial resistance, the β-hemolysin/cytolysin is a key virulence factor of *S. agalactiae* that triggers inflammation, disrupts host barriers, and promotes systemic dissemination, ultimately leading to severe neonatal infections [34,35]. In our strain collection, most isolates displayed a β-hemolytic phenotype, but with varying halo intensities (Figure 6.1) from weak to moderate hemolysis more frequently observed among vaginal isolates (r=-0.36, p=0.045) (Figure S1). Despite *S. agalactiae* from animal strains are generally considered to exhibit more variable β-hemolysis activities than human isolates, considerable heterogeneity has also been reported among human pathogenic strains [36,37]. This phenotypic heterogeneity could be linked to regulatory mutations, such as single-point mutations in the promoter region of the *covR* gene, which belongs to the CovR-CovS two-component regulatory system known to modulate the bacterial hemolytic activity [38]. Alternatively, this variability could be related to mutations within the *cyl* operon, which is essential for the biosynthesis, transport, and secretion of both β-hemolysin and pigment production [39,40]. These phenotypic traits are closely interconnected, as non-hemolytic strains are typically non-pigmented; additionally, shifts in regulatory or environmental conditions may modulate their expression levels, ultimately varying the hemolytic halo intensity from strong to moderate or weak [35,40]. Moreover, the small proportion of γ-hemolytic isolates observed in our study is consistent with a previous report describing this phenotype infrequent, but recognized among *S. agalactiae* clinical isolates [41]. Notably, our γ-hemolytic isolate carried both

cylB and *hylB*; thus, the absence of hemolytic activity may related to altered gene expression or additional regulatory or structural defects rather than the absence of hemolysin-associated genes [36,37].

Bacterial aggregation in static condition reflects an initial step of microcolony formation, preceeding biofilm formation, since this allows *S. agalactiae* cells to progressively settle and form thick, adhesive matrix over time [42]. The varying intensities of aggregation observed in our clinical isolates (Figure 6.2) could be associated with strain-specific differences in surface proteins and regulatory networks, as supported by the intermediate positive correlation detected between aggregation and PI-2b (r=0.412, p=0.021, Figure 6.S1), and in agreement with previous evidence suggesting that aggregation is primarily linked to the expression of a key adhesin [43–45].

The predominance of serotype III across all PI profiles in our clinical collection (Figure 6.2), and the strong positive correlation with PI-1+2b (r=0.80, p<0.0001, Figure S1) align with previous Italian and international studies on neonatal disease and maternal colonization [6,9,21,46]. Interestingly, we also found serotypes Ia and VI (6% each), the latter being rarely reported in humans and sharing genetic traits with isolates retrieved from animals [47]. Two out of four serotype IV strains were HLGR and *hvgA*-positive, reflecting characteristics previously report among clinical GBS isolates [48]. The serotype-pilus association suggests that specific capsule-pilus genotypes may confer a fitness advantage, enhancing the ability of the pathogen to persist in the vagina and cause ascending infections [49]. However, the identification of less common pilus arrangements and serotypes may indicate an ongoing adaptation of endemic strains to immune pressure, antibiotic exposure or microenvironmental differences in the genital tract, as previously suggested [50,51]. Alternatively, these differences could be due to the introduction into our local setting of new strains by human mobility from different geographic locations and ethnic diversities [52,53].

The virulence gene repertoire identified in our collection supports our first hypothesis that traits previously associated with invasive *S. agalactiae* are now common in colonizing strains (Table 6.1 and Figure 6.3). Adhesion/invasion and immune evasion genes (*fbsA*, *fbsB lmb*, and *scpB*), as well as *cylB* and *hylB* were widely distributed in our isolates collection (Figure 6.3), highlighting their key role in the vaginal and rectal colonization and in pathogenicity [5,6,40]. Within the alpha-like protein family, *rib* and *alpha-C* were the most common genes in our collection. Rib protein was predominant in serotypes III and II isolates, while alpha-C in serotypes IV, V, and VI, supporting their contribution to host-pathogen interactions within these lineage [6]. Regarding hemolytic phenotype, *alpha-C* showed positive correlation (r = 0.54, p = 0.002), whereas *rib* was negatively correlated (r=-0.51, p=0.003). This opposing pattern, together with lack of co-occurrence (r=-0.60, p<0.0001) (Figure 6.3 and Figure 6.S1), suggests mutually exclusive evolutionary strategies. In addition, the association between *rib* and the PI-1+2b (r=0.54, p=0.002) found in serotype III isolates points to a preferential linkage of virulence determinants that may synergistically promote colonization and tissue invasion [54–56]. Notably, strain 10, an MDR isolate with inducible clindamycin resistance, lacked all type of alpha-like protein genes, a rare profile that may reflect

an unusual evolutionary path involving both resistance acquisition and alteration of the surface protein repertoire [57,58]. The low prevalence of *alp2/3*, the rarity of *bac* and *epsilon*, and the absence of *alp4* genes, are in line with previous studies describing the restricted distribution of some alpha-like protein genes among particular serotypes or clonal complexes [6,7].

While *hvgA*-positive strains are historically associated with neonatal meningitis, their increasing detection even in non-pregnant adults, and healthy carriers suggests silent dissemination in the community [32,59]. In our study, one-fourth of *hvgA*-positive strains were recovered from urine (25%, 9/12) indicating their expansion beyond the vaginal niche and supporting the notion that urinary and fecal areas specimens can be additional reservoirs of hypervirulent *S. agalactiae*, both in symptomatic infections and asymptomatic carriage [60–63]. Furthermore, *hvgA*-positive strains were strongly associated with serotype III ($r=0.66$, $p<0.0001$), and with pilus island combinations PI-2b ($r=0.41$, $p=0.021$) and PI-1+2b ($r=0.74$, $p<0.0001$) (Figure 6.S1), mirroring the well-described serotype III-PI-2b combination [59,64]. The *hvgA*-positive HLGR strains with the serotype IV/PI-2b/*alpha-C* virulence profile (17%) resemble the emergent hypervirulent clone currently expanding in Italian healthcare settings [48]. The presence of PI-2b within this lineage may increase the risk of epithelial colonization and central nervous system invasion [49]. Altogether, this overlap between enhanced virulence traits, resistance determinants and maternal colonization fits with emerging descriptions of "dual-threat" ST17-related clones and reinforces the need for both rigorous antibiotic stewardship and alternative preventive strategies, including vaccines and probiotic approaches. In this context, we evaluated *Lactobacillus* spp. strains for their potential antagonistic effect against representative *S. agalactiae* isolates from our collection. Experimental conditions were designed to closely mimic the vaginal niche, with high *Lactobacillus* dosage, reflecting their dominance in healthy microbiota and low *S. agalactiae* infection dose. Under these conditions, *Lactobacillus* spp. strains did not affect epithelial viability (Figure 6.S3), while *S. agalactiae* induced detectable epithelial damage within only 3 h. Probiotic strains exerted strain-dependent growth inhibition, preservation of epithelial viability, and marked impairment of pathogen adhesion (Figures 6.4-6.7). Co-culture experiments confirmed strong antagonistic activity of selected *Lactobacillus* [60–63] strains against *S. agalactiae*, with mortality rates approaching 100% for most *S. agalactiae* isolates (Figure 6.5). However, the magnitude of inhibition varied depending on both probiotic and pathogen genotypes and phenotypes. Spearman's correlation analysis supported these findings, revealing an increased susceptibility of serotype II to probiotic activity, whereas *L. rhamnosus* showed strain-specific inhibition pattern activity against MDR strains ($r=-0.37$, $p=0.039$). In contrast, inhibition by *L. plantarum* and *L. paracasei* was positively correlated with the presence of PI-1+2a ($r=0.39$, $p=0.035$) (Figure 6.S2), while no significant correlation was observed for *L. reuteri*. These results underscore that *S. agalactiae* susceptibility to probiotic inhibition reflects a complex interplay between bacterial capsule composition, resistance profile, as well as the metabolic and antimicrobial properties of individual *Lactobacillus* species [16,17]. Thus, to overcome strain-specific variability, a combination of multiple *Lactobacillus* strains with complementary inhibition profiles was tested under the same experimental conditions, using a panel of *S. agalactiae* strains representing diverse

virulence and resistance profiles. The *Lactobacillus* combination most effectively reduced adhesion of non-hemolytic, highly aggregative *rib*-positive strains from diverse serotype and pilus profiles, whereas protection was less pronounced against *hvgA*-positive, MDR, inducible clindamycin resistance, or strongly hemolytic strains (Figures 6.5-6.7). Notably, the strong hemolytic strains lacking MDR or hypervirulent lineage markers were more susceptible than isolates combining these virulence traits, suggesting that adhesins, toxins, resistance-associated adaptations may impact on *Lactobacillus* competition at epithelial surfaces. The enhanced performance of the *Lactobacillus* mixture likely reflects the convergence of multiple complementary and synergistic mechanisms, including competitive exclusion at epithelial binding sites, modulation of host receptors, production of inhibitory metabolites such as organic acids, and interference with early aggregation or biofilm initiation [16,17]. Several studies highlighted the potential of vaginal lactobacilli as alternative or complementary strategies to IAP for the control of *S. agalactiae* [14–17]. For instance, early clinical and translational investigations demonstrated that *Lactobacillus salivarius* can significantly reduce recto-vaginal *S. agalactiae* carriage during pregnancy, thereby decreasing the proportion of women requiring IAP at delivery [16]. Additionally, *Lactobacillus fermentum* and *L. rhamnosus* limit *in vitro* pathogen attachment via exclusion, competition, and displacement by their strong adhesion to epithelial cells [15]. Furthermore, purified and secreted bacteriocin-like molecules were shown to inhibit the growth of the majority of tested *S. agalactiae* clinical isolates, [14]. Therefore, our results align with prior findings on the efficacy of selected *Lactobacillus* spp. against *S. agalactiae*, and extend this knowledge by demonstrating that multi-strain *Lactobacillus* combinations can offer a broader and more effective protection, even against emerging ST-17 hypervirulent or multidrug-resistant *S. agalactiae* lineages. From a translational standpoint, such combined probiotic strategies could represent a valuable alternative or complementary approach to standard antibiotic prophylaxis, particularly in settings where hypervirulent or MDR *S. agalactiae* lineages circulate in the maternal vaginal reservoir. When used topically, appropriately formulated *Lactobacillus* spp. mixtures have the promising ability to effectively constrain both typical and dual-threat *S. agalactiae* lineages in the vaginal niche, thereby reducing the risk of vertical transmission and neonatal disease.

Supplementary Material

Table 6.S1. Susceptibility profiles of *S. agalactiae* clinical isolates based on MIC and disk diffusion test for selected antibiotics.

Strain IDs	BZP	LVX	LNZ	MXF	RIM	TEC	TGC	T/S	VAN	TET	EM	CLN	GENT	Category
1	0.12	0.5	≤2	0.12	0.25	≤0.12	≤0.06	≤ 10	0.5	27	25	21	0	
2	≤0.06	0.5	≤2	0.25	0.25	≤0.12	≤0.06	≤ 10	0.5	26	25	24	0	
3	≤0.06	0.5	≤2	0.12	0.25	≤0.12	≤0.06	≤ 10	0.5	16	27	25	16	
4	≤0.06	1	≤2	0.12	≤0.06	≤0.12	≤0.06	≤ 10	0.5	27	24	21	15	
5	≤0.06	1	≤2	0.12	0.12	≤0.12	≤0.06	≤ 10	0.5	27	25	22	16	
6	≤0.06	0.5	≤2	0.25	≤0.06	≤0.12	≤0.06	≤ 10	0.5	27	26	24	16	
7	≤0.06	1	≤2	0.25	0.25	≤0.12	≤0.06	≤ 10	0.5	16	0	0	17	**MDR**
8	0.12	1	≤2	0.12	0.12	≤0.12	≤0.06	≤ 10	0.5	16	0	0	17	**MDR**
9	0.12	0.5	≤2	0.12	0.12	≤0.12	≤0.06	≤ 10	0.5	16	25	23	16	
10	≤0.06	0.5	≤2	0.12	≤0.06	≤0.12	≤0.06	≤ 10	0.5	18	0	22/0*	0	**MDR**
11	≤0.06	1	≤2	0.12	≤0.06	≤0.12	≤0.06	≤ 10	0.5	16	26	24	18	
12	0.12	1	≤2	0.12	0.25	≤0.12	≤0.06	≤ 10	0.5	17	13	22	17	
13	≤0.06	1	≤2	0.12	≤0.06	≤0.12	≤0.06	≤ 10	0.25	16	25	24	14	
14	≤0.06	1	≤2	0.12	0.12	≤0.12	≤0.06	≤ 10	0.5	16	25	25	15	
15	≤0.06	1	≤2	0.12	≤0.06	≤0.12	≤0.06	≤ 10	0.25	15	0	0	16	**MDR**
16	0.12	1	≤2	0.25	0.12	≤0.12	≤0.06	≤ 10	0.5	16	24	22	17	
17	0.12	1	≤2	0.25	0.25	≤0.12	≤0.06	≤ 10	1	16	25	22	16	
18	0.12	0.5	≤2	0.12	0.12	≤0.12	≤0.06	≤ 10	0.5	16	26	26	17	
19	≤0.06	1	≤2	0.25	0.25	≤0.12	≤0.06	≤ 10	0.5	15	26	23	17	
20	≤0.06	1	≤2	0.25	≤0.06	≤0.12	≤0.06	≤ 10	0.5	26	26	24	16	
21	≤0.06	1	≤2	0.25	0.25	≤0.12	≤0.06	≤ 10	0.5	15	0	22/0*	16	**MDR**
22	≤0.06	0.5	≤2	0.12	0.12	≤0.12	≤0.06	≤ 10	0.5	16	27	25	14	
23	≤0.06	0.5	≤2	0.12	0.12	≤0.12	≤0.06	≤ 10	0.25	16	24	23	16	
24	≤0.06	0.5	≤2	0.12	0.12	≤0.12	≤0.06	≤ 10	0.5	27	25	23	18	
25	≤0.06	1	≤2	0.25	0.12	≤0.12	≤0.06	≤ 10	0.5	28	25	24	15	
26	≤0.06	1	≤2	0.25	0.12	≤0.12	≤0.06	≤ 10	0.5	15	25	23	15	
27	≤0.06	1	≤2	0.25	0.25	≤0.12	≤0.06	≤ 10	1	15	25	23	19	
28	≤0.06	≥16	≤2	0.25	0.12	≤0.12	≤0.06	≤ 10	0.5	14	0	0	17	**MDR**
29	≤0.06	0.5	≤2	0.12	≤0.06	≤0.12	≤0.06	≤ 10	0.5	22	28	28	19	
30	≤0.06	0.5	≤2	0.12	≤0.06	≤0.12	≤0.06	≤ 10	0.5	15	0	0	17	**MDR**
31	≤0.06	0.5	≤2	0.12	0.12	≤0.12	≤0.06	≤ 10	0.5	15	25	23	17	

MICs for BZP, Benzylpenicillin (R>0.125), LVX, Levofloxacin (R>2), LNZ, Linezolid (R>2), MXF, Moxifloxacin (R>0.5), RIM, Rifampicin (R>0.06), TEC, Teicoplanin (R>2), TGC, Tigecycline (R>0.12), T/S, Trimethoprim/Sulfamethoxazole (R>20), and VAN, Vancomycin (R>2), TET, Tetracycline (R>1); EM, Erythromycin (R>0.25), and CLN, Clindamycin (R>0.5) were determined using the VITEK® 2 system and interpreted according to EUCAST clinical breakpoints (v15.0). Resistance to TET,

Tetracycline (R<23), EM, Erythromycin (R=0), CLN, Clindamycin (R<20), and GENT, Gentamicin (R=0) was assessed by disk diffusion (30 µg TET, 15 µg EM, 2 µg CLN, and 500 µg GENT). Inducible clindamycin resistance was specifically detected using the D-test method. An asterisk (*) indicates inducible clindamycin resistance. MDR, multidrug resistant.

Table 6.S2. Concordance between disk test and resistance genes for tetracycline, erythromycin, clindamycin, and gentamicin in *S. agalactiae* isolates.

Strain IDs	**TET**	**TET pheno-type**	***tetM* gene**	***tetO* gene**	**EM**	**CLN**	**CR/IR/M pheno-type**	***ermA* gene**	***mef* gene**	***ermB* gene**	**GENT**	**HLGR**	***aac(6')-Ie-aph(2")-Ia* gene**
1	27	S	-	-	25	21	S	-	-	-	0	R	+
2	26	S	-	-	25	24	S	-	-	-	0	R	+
3	16	R	+	-	27	25	S	-	-	-	16	S	-
4	27	S	-	-	24	21	S	-	-	-	15	S	-
5	27	S	-	-	25	22	S	-	-	-	16	S	-
6	27	S	-	-	26	24	S	-	-	-	16	S	-
7	16	R	+	-	0	0	CR	-	-	+	17	S	-
8	16	R	+	-	0	0	CR	-	-	+	17	S	-
9	16	R	+	-	25	23	S	-	-	-	16	S	-
10	18	R	+	-	0	22/0*	IR	-	-	-	0	R	+
11	16	R	+	-	26	24	S	-	-	-	18	S	-
12	17	R	+	-	13	22	M	-	+	-	17	S	-
13	16	R	-	+	25	24	S	-	-	-	14	S	-
14	16	R	+	-	25	25	S	-	-	-	15	S	-
15	15	R	-	+	0	0	CR	-	-	+	16	S	-
16	16	R	+	-	24	22	S	-	-	-	17	S	-
17	16	R	+	-	25	22	S	-	-	-	16	S	-
18	16	R	+	-	26	26	S	-	-	-	17	S	-
19	15	R	+	-	26	23	S	-	-	-	17	S	-
20	26	S	-	-	26	24	S	-	-	-	16	S	-
21	15	R	+	-	0	22/0*	IR	+	-	-	16	S	-
22	16	R	-	+	27	25	S	-	-	-	14	S	-
23	16	R	+	-	24	23	S	-	-	-	16	S	-
24	27	S	-	-	25	23	S	-	-	-	18	S	-
25	28	S	-	-	25	24	S	-	-	-	15	S	-
26	15	R	-	+	25	23	S	-	-	-	15	S	-
27	15	R	+	-	25	23	S	-	-	-	19	S	-
28	14	R	+	-	0	0	CR	-	-	+	17	S	-
29	22	R	+	-	28	28	S	-	-	-	19	S	-
30	15	R	+	-	0	0	CR	-	-	+	17	S	-
31	15	R	+	-	25	23	S	-	-	-	17	S	-

Tetracycline (TET), Erythromycin (EM), Clindamycin (CLN), and GENT (Gentamycin) phenotype were assessed by disk diffusion test. CR, clindamycin resistance (CLN-R/EM-R); IR, inducible clindamycin resistance (EM-R/CLN-S with D-shaped inhibition); M, M-phenotype (EM-R/CLN-S without flattening); R, resistant; and S, susceptible. HLGR was defined by reduced inhibition around high-content gentamicin and correlated with *aac(6')-Ie-aph(2")-Ia*. The D-test phenotypes showed the consistent presence of macrolide–lincosamide resistance genes (*ermA, ermB, mef*), except for strain 10.

Table 6.S3. Primer sequences used in this study.

Category	*Genes*	Primers (5'-3')	References
Serotypes	cpsI-Ia-6-7-F	GAATTGATAACTTTTGTGGATTGCGATGA	[20]
	cpsI-6-R	CAATTCTGTCGGACTATCCTGATG	
	cpsI-7-R	TGTCGCTTCCACACTGAGTGTTGA	
	cpsI-7-9-F	CTGTAATTGGAGGAATGTGGATCG	
	cpsI-9-R	AATCATCTTCATAATTTATCTCCCATT	
	cpsL-F	CAATCCTAAGTATTTTCGGTTCATT	
	cpsL-R	TAGGAACATGTTCATTAACATAGC	
	cpsG-F	ACATGAACAGCAGTTCAACCGT	
	CpsG-R	ATGCTCTCCAAACTGTTCTTGT	
	CpsG-2-3-6-R	TCCATCTACATCTTCAATCCAAGC	
	CpsN-5-F	ATGCAACCAAGTGATTATCATGTA	
	CpsN-5-R	CTCTTCACTCTTTAGTGTAGGTAT	
	CpsJ-8-F	TATTTGGGAGGTAATCAAGAGACA	
	CpsJ-8-R	GTTTGGAGCATTCAAGATAACTCT	
	cpsJ-2-4-F	CATTTATTGATTCAGACGATTACATTGA	
	cpsJ-2-R	CCTCTTTCTCTAAAATATTCCAACC	
	cpsJ-4-R	CCTCAGGATATTTACGAATTCTGTA	
	cpsJ-Ib-F	GCAATTCTTAACAGAATATTCAGTTG	
	cpsJ-Ib-R	GCGTTTCTTTATCACATACTCTTG	
Pilus Island	adhP_F162	ACGCATTTTGGGTCACGA	[26]
	adhP_R944	GTATCCACAGGCACTTTTTCAAC	
	SAG647_F496	CTACCAACGGCCAAGCTATTTACC	
	SAG647_R889	TAGCCGCTTTTTCATTCTTTCTCC	
	SAG1406_F356	AACTCCCTATATTTGCAGGTTCAA	
	SAG1406_R598	CGGGTGTAACGACTTTTATCTGAT	
	SAN1517_F57	GGGGGTAGGCTTAATGGCTTAT	
	SAN1517_R575	TCCGGTTTAACTGTTCTGATTTGAT	
Virulence genes	*fbsA*	F-TGTAGCTAATGGACCGATGTT R-TTTTCATTGCGTCTCAAACC	[5]
	fbsA	F-TGTAGCTAATGGACCGATGTT R-TTTTCATTGCGTCTCAAACC	
	fbsB	F-ACAACTGCGGAAATGACCTC R-ACGAGCGACGTTGAATTCTT	
	lmb	F-GACGCAACACACGGCAT R-TGATAGAGCACTTCCAAATTTG	
	cylB	F-GGGCTGCAGGTATTATCGAA R-ATTTCCACCAAAAGCAAACG	
	hylB	F-TTATCATCCAGCGCCTCCTAG R-GTGGTGATAACTGACTTCTTGGGA	

scpB	F-AGCCATATGCTGCGATCTCT R-GGGTTGAACCAAGTGTGCTT	
bac	F-TGTAAAGGACGATAGTGTGAAGAC R-CATTTGTGATTCCCTTTTGC	
rib	F-CAGGAAGTGCTGTTACGTTAAAC R-CGTCCCATTTAGGGTCTTCC	
*hvgA*_(ST-17S)	ATACAAATTCTGCTGACTACCG	[27]
hvgA_ST-17AS	TTAAATCCTTCCTGACCATTCC	
Universal-F	TGATACTTCACAGACGAAACAACG	[25]
AlphaC-R	TACATGTGGTAGTCCATCTTCACC	
Epsilon-R	CCAGATACATTTTTTACTAAAGCGG	
Alp2/3-R	CACTCGGATTACTATAATATTTAGCAC	
Alp4-R	TTAATTTGCACCGGATTAACACCAC	

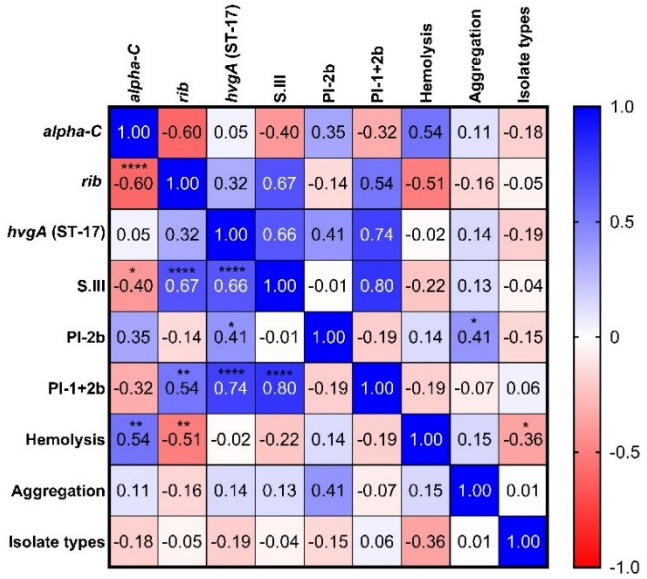

Figure 6.S1. Correlation matrix of phenotypes and genotypes traits. Parameters included in the analysis are reported. Data were analyzed using Spearman's correlation. The colors represent correlation coefficient; its intensity depicts the coefficient's value (shades of blue are positive correlations and shades of red are negative correlations). The graph was generated using GraphPad Prism version 11. * $P < 0.05$, ** $P < 0.01$, *** $P < 0.001$, **** $P < 0.0001$.

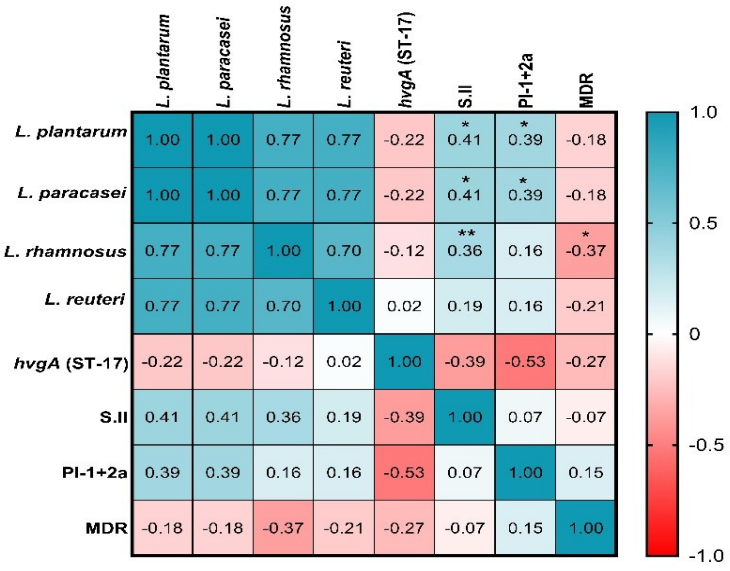

Figure 6.S2. *Lactobacillus* inhibition in broth co-culture with *S. agalactiae* isolates displaying phenotype and genotype traits. Parameters included in the analysis are reported. Data were analyzed using Spearman's correlation. The colors represent correlation coefficient; its intensity depicts the coefficient's value (shades of green are positive correlations and shades of red are negative correlations). The graph was generated using GraphPad Prism version 11. *P < 0.05, ** P < 0.01.

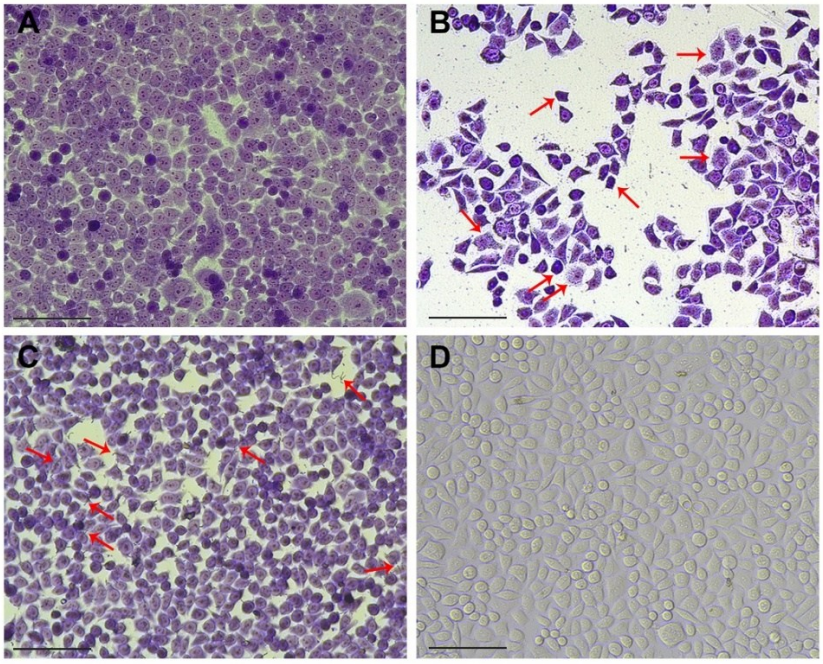

Figure 6.S3. Representative images of HeLa cell monolayers under *S. agalactiae* and *Lactobacilli* treatments. (A) Uninfected HeLa cell monolayer. (B) HeLa cells infected with *S. agalactiae*; the red arrow points to a dying cell with cytopathic changes. (C) HeLa cells co-infected with *S. agalactiae* and the *Lactobacillus* combination; the red arrow points to *Lactobacillus* cells. (D) Phase-contrast image of HeLa cells treated with the *Lactobacillus* combination after five washing steps before the MTT assay.

References

1. Oliveira, L. M. A. *et al.* WHO defeating meningitis symposium, 3rd international symposium on Streptococcus agalactiae disease (ISSAD) in Rio de Janeiro, Brazil: State-of-the-art overview of S. agalactiae meningitis. *Vaccine* **52**, 126895 (2025).
2. Furuta, A. *et al.* Bacterial and Host Determinants of Group B Streptococcal Infection of the Neonate and Infant. *Front. Microbiol.* **13**, 820365 (2022).
3. Gonçalves, B. P. *et al.* Group B streptococcus infection during pregnancy and infancy: estimates of regional and global burden. *Lancet Glob. Health* **10**, e807–e819 (2022).
4. Paul, P., Gonçalves, B. P., Le Doare, K. & Lawn, J. E. 20 million pregnant women with group B streptococcus carriage: consequences, challenges, and opportunities for prevention. *Curr. Opin. Pediatr.* **35**, 223–230 (2023).
5. Bobadilla, F. J., Novosak, M. G., Cortese, I. J., Delgado, O. D. & Laczeski, M. E. Prevalence, serotypes and virulence genes of Streptococcus agalactiae isolated from pregnant women with 35–37 weeks of gestation. *BMC Infect. Dis.* **21**, 73 (2021).
6. EL-Lakany, R. R., Abdelmaged, E. S., Shams, M., Hassan, R. & Rizk, D. E. Incidence of virulence determinants among *Streptococcus agalactiae* isolated from pregnant women and association with their serotypes. *Egypt. J. Basic Appl. Sci.* **10**, 650–670 (2023).
7. Zeng, Z. *et al.* Strain-level genomic analysis of serotype, genotype and virulence gene composition of group B streptococcus. *Front. Cell. Infect. Microbiol.* **14**, 1396762 (2024).
8. Creti, R., Imperi, M., Berardi, A., Angeletti, S. & Gherardi, G. Laboratory breakpoints for assessing high level gentamicin resistance in Streptococcus agalactiae: it is the time for a consensus. *Clin. Microbiol. Infect.* **28**, 1050–1052 (2022).
9. Lohrmann, F. *et al.* Maternal Streptococcus agalactiae colonization in Europe: data from the multi-center DEVANI study. *Infection* **53**, 373–381 (2025).
10. Panneflek, T. J. R. *et al.* Intrapartum antibiotic prophylaxis to prevent Group B streptococcal infections in newborn infants: a systematic review and meta-analysis comparing various strategies. *eClinicalMedicine* **74**, 102748 (2024).
11. Bostanghadiri, N. *et al.* Global Antimicrobial Resistance Trends in Group B *Streptococcus* Isolates From Pregnant Women: Systematic Review and Meta-Analysis. *MicrobiologyOpen* **14**, e70087 (2025).
12. Hsu, C.-Y. *et al.* Global patterns of antibiotic resistance in group B Streptococcus: a systematic review and meta-analysis. *Front. Microbiol.* **16**, 1541524 (2025).
13. Iqbal, F. *et al.* Influence of perinatal antibiotic on neonatal gut microbiota: a prospective cohort study. *BMC Pediatr.* **25**, 560 (2025).
14. Ruíz, F. O. *et al.* Synergistic Effect Between Two Bacteriocin-like Inhibitory Substances Produced by Lactobacilli Strains with Inhibitory Activity for Streptococcus agalactiae. *Curr. Microbiol.* **64**, 349–356 (2012).
15. Ortiz, L., Ruiz, F., Pascual, L. & Barberis, L. Effect of Two Probiotic Strains of Lactobacillus on In Vitro Adherence of Listeria monocytogenes, Streptococcus agalactiae, and Staphylococcus aureus to Vaginal Epithelial Cells. *Curr. Microbiol.* **68**, 679–684 (2014).
16. Martín, V. *et al.* Rectal and Vaginal Eradication of Streptococcus agalactiae (GBS) in Pregnant Women by Using Lactobacillus salivarius CECT 9145, A Target-specific Probiotic Strain. *Nutrients* **11**, 810 (2019).
17. Marziali, G., Foschi, C., Parolin, C., Vitali, B. & Marangoni, A. In-vitro effect of vaginal lactobacilli against group B Streptococcus. *Microb. Pathog.* **136**, 103692 (2019).
18. Kamińska, D. *et al.* Macrolide and lincosamide resistance of Streptococcus agalactiae in pregnant women in Poland. *Sci. Rep.* **14**, 3877 (2024).

19. Vakulenko, S. B. *et al.* Multiplex PCR for Detection of Aminoglycoside Resistance Genes in Enterococci. *Antimicrob. Agents Chemother.* **47**, 1423–1426 (2003).

20. Imperi, M. *et al.* A multiplex PCR assay for the direct identification of the capsular type (Ia to IX) of Streptococcus agalactiae. *J. Microbiol. Methods* **80**, 212–214 (2010).

21. Creti, R. *et al.* Invasive Group B Streptococcal Disease in Neonates and Infants, Italy, Years 2015–2019. *Microorganisms* **9**, 2579 (2021).

22. Magiorakos, A.-P. *et al.* Multidrug-resistant, extensively drug-resistant and pandrug-resistant bacteria: an international expert proposal for interim standard definitions for acquired resistance. *Clin. Microbiol. Infect.* **18**, 268–281 (2012).

23. Afshar, B. *et al.* International External Quality Assurance for Laboratory Identification and Typing of Streptococcus agalactiae (Group B Streptococci). *J. Clin. Microbiol.* **49**, 1475–1482 (2011).

24. Slotved, H.-C. & Hoffmann, S. Evaluation of procedures for typing of group B *Streptococcus* : a retrospective study. *PeerJ* **5**, e3105 (2017).

25. Creti, R., Fabretti, F., Orefici, G. & Von Hunolstein, C. Multiplex PCR Assay for Direct Identification of Group B Streptococcal Alpha-Protein-Like Protein Genes. *J. Clin. Microbiol.* **42**, 1326–1329 (2004).

26. Springman, A. C. *et al.* Pilus distribution among lineages of group b streptococcus: an evolutionary and clinical perspective. *BMC Microbiol.* **14**, 159 (2014).

27. Lamy, M.-C. *et al.* Rapid detection of the “highly virulent” group B streptococcus ST-17 clone. *Microbes Infect.* **8**, 1714–1722 (2006).

28. Scribano, D. *et al.* d-Mannose Treatment neither Affects Uropathogenic Escherichia coli Properties nor Induces Stable FimH Modifications. *Molecules* **25**, 316 (2020).

29. Koenig, J. M. & Keenan, W. J. Group B Streptococcus and Early-Onset Sepsis in the Era of Maternal Prophylaxis. *Pediatr. Clin. North Am.* **56**, 689–708 (2009).

30. Thorn, N., Karampatsas, K., Le Doare, K. & Heath, P. T. Progress towards a Group B streptococcal vaccine – where are we now? *Vaccine* **62**, 127575 (2025).

31. Zakerifar, M., Kaboosi, H., Goli, H. R., Rahmani, Z. & Peyravii Ghadikolaii, F. Antibiotic resistance genes and molecular typing of Streptococcus agalactiae isolated from pregnant women. *BMC Pregnancy Childbirth* **23**, 43 (2023).

32. Gong, X. *et al.* Genomic characterization and resistance features of Streptococcus agalactiae isolated from non-pregnant adults in Shandong, China. *J. Glob. Antimicrob. Resist.* **38**, 146–153 (2024).

33. McGee, L. *et al.* Multistate, Population-Based Distributions of Candidate Vaccine Targets, Clonal Complexes, and Resistance Features of Invasive Group B Streptococci Within the United States, 2015–2017. *Clin. Infect. Dis.* **72**, 1004–1013 (2021).

34. Sagar, A. *et al.* The β-Hemolysin and Intracellular Survival of Streptococcus agalactiae in Human Macrophages. *PLoS ONE* **8**, e60160 (2013).

35. Whidbey, C. *et al.* A hemolytic pigment of Group B Streptococcus allows bacterial penetration of human placenta. *J. Exp. Med.* **210**, 1265–1281 (2013).

36. Mosabi, J. M., Arimi, S. M. & Kang’Ethe, E. K. Isolation and characterization of group B streptococci from human and bovine sources within and around Nairobi. *Epidemiol. Infect.* **118**, 215–220 (1997).

37. Lupo, A., Ruppen, C., Hemphill, A., Spellerberg, B. & Sendi, P. Phenotypic and molecular characterization of hyperpigmented group B Streptococci. *Int. J. Med. Microbiol.* **304**, 717–724 (2014).

38. Zhu, L. *et al.* Genetic Basis Underlying the Hyperhemolytic Phenotype of Streptococcus agalactiae Strain CNCTC10/84. *J. Bacteriol.* **202**, (2020).

39. Nizet, V. Streptococcal β-hemolysins: genetics and role in disease pathogenesis. *Trends Microbiol.* **10**, 575–580 (2002).

40. Rosa-Fraile, M., Dramsi, S. & Spellerberg, B. Group B streptococcal haemolysin and pigment, a tale of twins. *FEMS Microbiol. Rev.* **38**, 932–946 (2014).

41. Zastempowska, E., Twarużek, M., Grajewski, J. & Lassa, H. Virulence Factor Genes and Cytotoxicity of *Streptococcus agalactiae* Isolated from Bovine Mastitis in Poland. *Microbiol. Spectr.* **10**, e02224-21 (2022).

42. Miranda, P. S. D. *et al.* Biofilm formation on different pH conditions by *Streptococcus agalactiae* isolated from bovine mastitic milk. *Lett. Appl. Microbiol.* **67**, 235–243 (2018).

43. Pietrocola, G. *et al.* FbsA, a fibrinogen-binding protein from Streptococcus agalactiae, mediates platelet aggregation. *Blood* **105**, 1052–1059 (2005).

44. Konto-Ghiorghi, Y. *et al.* Dual Role for Pilus in Adherence to Epithelial Cells and Biofilm Formation in Streptococcus agalactiae. *PLoS Pathog.* **5**, e1000422 (2009).

45. Thomas, L. S. & Cook, L. C. A Novel Conserved Protein in Streptococcus agalactiae, BvaP, Is Important for Vaginal Colonization and Biofilm Formation. *mSphere* **7**, e00421-22 (2022).

46. Creti, R. *et al.* Group B Streptococcus (GBS) Carriage in Pregnant Women: Possible Emergence of Rare Serotypes and Antibiotic Resistance in Neonatal Disease. *Microorganisms* **13**, 1496 (2025).

47. He, E.-M. *et al.* The genome of serotype VI Streptococcus agalactiae serotype VI and comparative analysis. *Gene* **597**, 59–65 (2017).

48. Creti, R. *et al.* Emergence of High-Level Gentamicin Resistance in Streptococcus agalactiae Hypervirulent Serotype IV ST1010 (CC452) Strains by Acquisition of a Novel Integrative and Conjugative Element. *Antibiotics* **13**, 491 (2024).

49. Kaminska, D., Ratajczak, M., Nowicka, W., Dlugaszewska, J. & Gajecka, M. New Strategies for Preventing Perinatal Group B Streptococcus (GBS) Infections. *Pathogens* **15**, 22 (2025).

50. Khodaei, F. *et al.* Pilus–encoding islets in S. agalactiae and its association with antibacterial resistance and serotype distribution. *Microb. Pathog.* **116**, 189–194 (2018).

51. Lopes, E. *et al.* Increasing macrolide resistance among Streptococcus agalactiae causing invasive disease in non-pregnant adults was driven by a single capsular-transformed lineage, Portugal, 2009 to 2015. *Eurosurveillance* **23**, (2018).

52. Russell, N. J. *et al.* Maternal Colonization With Group B Streptococcus and Serotype Distribution Worldwide: Systematic Review and Meta-analyses. *Clin. Infect. Dis.* **65**, S100–S111 (2017).

53. Jamrozy, D. *et al.* Population genetics of group B Streptococcus from maternal carriage in an ethnically diverse community in London. *Front. Microbiol.* **14**, 1185753 (2023).

54. Sharma, P. *et al.* Role of Pilus Proteins in Adherence and Invasion of Streptococcus agalactiae to the Lung and Cervical Epithelial Cells. *J. Biol. Chem.* **288**, 4023–4034 (2013).

55. Lazzarin, M. *et al.* Contribution of pilus type 2b to invasive disease caused by a Streptococcus agalactiae ST-17 strain. *BMC Microbiol.* **17**, 148 (2017).

56. Tsai, I.-A., Su, Y., Wang, Y.-H. & Chu, C. Alterations in Genes rib, scpB and Pilus Island Decrease the Prevalence of Predominant Serotype V, Not III and VI, of Streptococcus agalactiae from 2008 to 2012. *Pathogens* **11**, 1145 (2022).

57. Maeland, J. A., Afset, J. E., Lyng, R. V. & Radtke, A. Survey of Immunological Features of the Alpha-Like Proteins of Streptococcus agalactiae. *Clin. Vaccine Immunol.* **22**, 153–159 (2015).

58. Bianchi-Jassir, F. *et al.* Systematic review of Group B Streptococcal capsular types, sequence types and surface proteins as potential vaccine candidates. *Vaccine* **38**, 6682–6694 (2020).

59. Imperi, M., Gherardi, G., Alfarone, G. & Creti, R. Group B Streptococcus Infections in Non-Pregnant Adults, Italy, 2015–2019. *Pathogens* **13**, 807 (2024).

60. WHO. *WHO Recommendation on Screening of Pregnant Women for Intrapartum Antibiotic Prophylaxis for the Prevention of Early Onset Group B Streptococcus Disease in Newborns*. (World Health Organization, Human Reproduction Programme, Geneva, 2024).

61. Abgral, M. *et al.* Impact of combined vaginal group B Streptococcus screening (culture and rapid PCR) in pregnant women on neonatal morbidity and mortality. *J. Infect. Public Health* **18**, 102883 (2025).

62. Piccinelli, G. *et al.* Emergence of the First Levofloxacin-Resistant Strains of Streptococcus agalactiae Isolated in Italy. *Antimicrob. Agents Chemother.* **59**, 2466–2469 (2015).

63. Motallebirad, T. *et al.* Molecular Characterization of Hospital- and Community-Acquired Streptococcus agalactiae Isolates among Nonpregnant Adults in Isfahan, Iran. *Adv. Biomed. Res.* **9**, (2020).

64. Hsu, J.-F. *et al.* The Clinical and Genetic Characteristics of Streptococcus agalactiae Meningitis in Neonates. *Int. J. Mol. Sci.* **24**, 15387 (2023).

Chapter 7. The Promise and Challenges of Serine-Based Gemini Nanoparticles as Antibacterial Compounds

Manuscript in preparation

This study is a part of project collaboration between Prof. Cecilia Ambrosi and Prof. Marina Pinheiro from Universidade do Minho, Braga, Portugal.

Abstract

Serine-based gemini nanoparticles are bio-inspired surfactants derived from serine, an amino acid naturally occurring in biological systems. Their spacer and headgroup composition can markedly influence self-assembly and antimicrobial activity. This study was designed to determine the biological effects of different serine-based gemini nanoparticle formulations by varying ester versus amide headgroup–spacer chemistry and the co-lipid molecules. Ten formulations incorporating $(12Ser)_2COO12$ or $(12Ser)_2CON12$ with 8-8Ser, DMPG or DMPC were tested against various bacterial pathogens and their toxicity was assessed in A549 lung epithelial cells. The results showed that ester and amide derivates containing the monomer 8-8Ser or DMPG revealed the promising bactericidal effect, significantly inhibiting *Staphylococcus aureus* ATCC 6538 over a broad concentration range, while only partially inhibited of *Escherichia coli* MG1655 and *Acinetobacter baumannii* ATCC 17978, and showed limited activity against *Pseudomonas aeruginosa* PAO1. A clear dose-dependent NPs bactericidal effect was observed among the tested microorganisms. Notably, these effects were observed only by viable count method, because high intrinsic turbidity of culture-mixed nanoparticles hindered absorbance readings in microdilution assay, thereby restricting standard MIC evaluation. In addition, the safety profile of selected formulation was limited by substantial cytotoxicity at minimal bactericidal concentrations. Overall, these findings support serine-based gemini nanoparticles as a promising antimicrobial treatment, especially against Gram-positive pathogens, while underscoring the need for future optimization to improve selectivity and reduce host-cell toxicity.

7.1 Introduction

Nanoparticles (NPs) are widely explored for diagnostics, drug delivery, and antimicrobial therapies because their ability to improve drug loading, controlled release and enhanced interaction with biological interfaces [1–3]. However, the application of NPs in complex biological highlights potential toxicity. When introduced into complex media (such as blood or cellular fluid), NPs interact with proteins to form biomolecular corona (a coating of protein), altering cells to recognize NPs and trigger the immune response or cellular toxicity [1,3]. To address these challenges, surfactants or referred as surface-active agents, have become versatile tools in nanotechnology, which serve as essential stabilizers that coat the NP surface. Through steric hindrance or electrostatic repulsion, surfactants prevent the NPs from aggregating (clumping) during synthesis and maintain their stability within hostile biological environments, thereby preserving their intended therapeutic function [4,5].

Among various surfactant-based designs, gemini surfactants are particularly promising. Deriving their name from the mythological twins, these amphiphilic molecules forming unique dimeric architecture: two hydrophobic tails and two polar headgroups covalently linked by a spacer group. Consequently, this structure gives the ability to self-assemble into aggregates (micelles) at significantly lower concentrations, a property known as a lower Critical Micelle Concentration (CMC), allows them to solubilize drugs or disrupt bacterial membranes at much lower doses,

potentially reducing the total chemical load required for treatment [6–8]. Many cationic gemini surfactant, particularly bis-quaternary ammonium types, display broad-spectrum antibacterial and antifungal activity [8–10]. However, they high chemical stability and poor biodegradability raise significant environmental and safety concerns [11,12], therefore novel gemini structures incorporating cleavable ester or amide linkages have been develop to improve biocompatibility and biodegradability and at the same time maintaining high surface activity and antimicrobial potency [11,13].

Serine-based cationic gemini surfactants represent a prominent class of bio-inspired amphiphiles. By utilizing the amino acid serine as the polar headgroup, these molecules are designed to combine enhanced interfacial properties with low cytotoxicity, making them highly suitable for biological and pharmaceutical applications. Structurally, these surfactants consist of two N-acyl-serine units linked to form amphiphiles with cleavable amide or ester connections. A recent study demonstrated that two such serine-derived gemini surfactants: the ester $(12Ser)_2COO12$ and the amide $(12Ser)_2CON12$, exhibit very low minimum inhibitory concentrations (MIC), as low as 5 μM, against MDR *E. coli* and Methicillin-resistant *Staphylococcus aureus* (MRSA), while preventing hemolytic of human red blood cells at relevant doses. Their selective interaction with anionic phosphatidylglycerol-rich model membranes (DPPG) versus zwitterionic phosphatidylcholine bilayers (DPPC) further highlights their specialization in perturbing bacterial envelopes. In addition, these serine geminis can self-assemble into liposomal nanostructures and provide dual action as antimicrobial agents and potential carriers for co-loaded antibiotics [14].

The chemical nature of the spacer and headgroup region give significant impact on both self-assembly and antimicrobial activity. For serine-based geminis, the specific linkage chemistry appears to modulate selectivity; amide derivative has been reported to produce broad-spectrum bactericidal effects against MRSA and MDR *E. coli*, whereas the ester analogue can show stronger specificity towards MRSA. This suggest that the more rigid, hydrogen-bonding amide linkage may promote stronger interactions with certain bacterial membranes [14]. Studies on other ester-based cationic gemini surfactants similarly show that variations in hydrophobic chain length and type of spacer (amine, ether, or additional cationic groups) possibly modulate CMC, micellization efficiency, and antimicrobial behavior. In general, derivatives with optimized hydrophobic chain lengths and additional cationic charges display higher antimicrobial potency, while the incorporation of ester bonds specifically confers improved biodegradability [7,10,13,15]. Moreover, other type of peptidic geminis with different amide-type spacer (such as L-lysine amide vs L-cystine diamide) demonstrate a trade-off: more hydrophobic and rigid amide spacers tend to enhance antimicrobial and antibiofilm activity at the cost of increased cytotoxicity, whereas less hydrophobic spacers improve biocompatibility but may reduce antimicrobial performance [16].

In this context, the present study aimed to determine the biological effect of different serine-based gemini NPs formulations. By varying ester versus amide headgroup-spacer chemistry and the co-lipid molecules, this study assessed how these formulations differ in bactericidal activity against Gram-positive and Gram-negative bacteria and in cytotoxicity toward A549 lung epithelial cells.

7.2 Materials and methods

7.2.1 Nanoparticles (NPs) formulation and detail composition

Two families of serine-based surfactant were used to generate antibacterial nanoparticle formulation: an ester-linked gemini surfactant $(12Ser)_2COO12$ and amine-linked gemini $(12Ser)_2CON12$, and monomeric serine surfactatn 8-8Ser (Figure 7.1). The formulations were developed and kindly provided by Prof. Marina Pinheiro from Universidade do Minho.

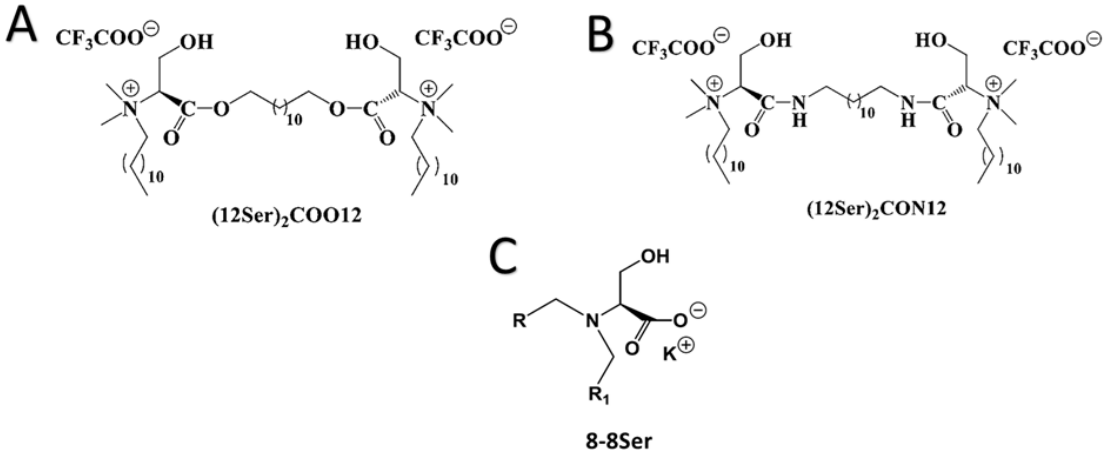

Figure 7.1. The molecular structure of serine-based surfactant. The serine-based gemini surfactant were classified as ester (A) and amine derivate (B) according to the spacer or headgroup connection. Another formulation is serine-based monomeric or single headgroup (C).

To modulate surface charge and membrane-mimicking properties, the cationic gemini surfactants were combined with either the anionic serine-based surfactant 8-8Ser, the anionic phospholipid 1,2-fimyristoyl-sn-glycero-3-phospho-rac- (1-glycerol) sodium salt (DMPG), or the zwitterionic phospholipid 1,2-dimyristoyl-sn-glycero-3-phosphocholine (DMPC). Different molar ratio (1:2, 2:1, and 4:1) are expressed as the number of gemini molecules per co-lipid molecule and define the composition of each NPs formulation (Table 7.1).

Table 7.1. Detail composition of serine-based nanoparticles

System	Composition	Molar fraction
D1	$(12Ser)_2COO12$:8-8Ser	2:1
D2	$(12Ser)_2COO12$:DMPC	2:1
D3_1	$(12Ser)_2COO12$:DMPG	1:2
D3_2	$(12Ser)_2COO12$:DMPG	2:1
D3_3	$(12Ser)_2COO12$:DMPG	4:1
E1_1	$(12Ser)_2CON12$:8-8Ser	1:2
E1_2	$(12Ser)_2CON12$:8-8Ser	2:1
E2_1	$(12Ser)_2CON12$:DMPC	1:2
E2_2	$(12Ser)_2CON12$:DMPC	2:1
E3	$(12Ser)_2CON12$:DMPG	4:1

7.2.2 Evaluation of antibacterial properties

Staphylococcus aureus ATCC 6538, *Escherichia coli* MG 1655, *Acinetobacter baumannii* ATCC 17978, and *Pseudomonas aeruginosa* PAO1 were used to evaluate the antibacterial activity of the serin-based NPs formulations by microdilution and viable count methods.

For microdilution method, a single colony from a freshly streaked tryptic soy agar (TSA; Condalab) was inoculated into tryptic soy broth (TSB; Condalab) and grown overnight at 37ºC with vigorous shaking. Cultures were adjusted to an optical at density at 600 nm (OD_{600}) of 0.1 and dispensed into 96-well microtiter plates containing each formulation at final concentration ranges of 15.6 – 500 µM. Plates were incubated overnight at 37°C under static condition, after which OD_{600} was recorded. Uninoculated TSB (blank) served as a negative control while untreated inoculated cultures as control positive. OD_{600} values were normalised using the following equation:

$$OD_{600}\ \text{normalization} = OD_{600}\ \text{treated} - (\text{mean of blank} + 3\ \text{SD})$$

Active formulations were then tested in viable-count experiments. Overnight cultures were diluted 1:100 (starting $OD_{600} \approx 0.1$) in TSB containing each formulation preheated at 50^0C for 1 h. Cultures were incubated overnight at 37°C with vigorous shaking. After incubation, bacterial suspensions were serially diluted in phosphate-buffered saline (PBS) and plated onto LB agar to determine viable cell counts (CFU/ml).

7.2.3 Cell cytotoxicity

The cytotoxic effects of tested molecules were assessed using the 3-(4,5-dimethylthiazol-2-yl)-2, 5-diphenyltetrazolium bromide (MTT; Sigma-Aldrich) assay using the human A549 lung epithelial cell line type II (ATCC CCL185). Briefly, A549 cells were seeded into 24-well plates (Costar, Corning Inc.) at a density of 6×10^4 cells per well in 1000 µL of DMEM supplemented with 10% fetal bovine serum and 1% glutamine, and incubated overnight at 37°C in a 5% CO_2. The following day, cells were exposed to the different NPs formulations, at final concentrations equivalent to their MIC. Untreated cells served as controls. After 48 h of incubation, 300 µL of MTT solution (0.5 mg/mL in DMEM without phenol red) was added to each well, followed by a further incubation of 3–4 h at 37°C. Next, 500 µL isopropanol HCl (0.1N) was added to the medium, and plates were incubated for additional 1-2 h. Absorbance was measured at 570 nm using a microplate reader (BioTek), and cell viability was calculated with the following formula:

$$Viability\ (\%) = \frac{Mean\ OD_{treated}}{Mean\ OD_{control}}\ x\ 100$$

Optical microscopic images were acquired using the 20X objective of a Motic AE21 microscope, connected with a ZZCAT digital camera.

7.2.4 Statistical analysis

Statistical analyses were conducted using GraphPad Prism Software (version 11). Data were analyzed using one-way ANOVA followed by Dunnet's post hoc tests for multiple comparison, with statistically significance set at a threshold of $P < 0.05$.

7.3 Results

7.3.1 Preliminary antibacterial screening of serine-based nanoparticles formulations

7.3.2 Microdilution method

Ten serine-based NPs formulations were initially screened for antibacterial activity at various concentration against four reference strains (Figure 7.2). Across all concentrations, OD_{600} values for all pathogens were higher than or similar to untreated positive controls. However, these reading alone could not discriminate between true bacterial growth and intrinsic turbidity arising from the physical properties of the formulations, which could interfere with the optical measurements.

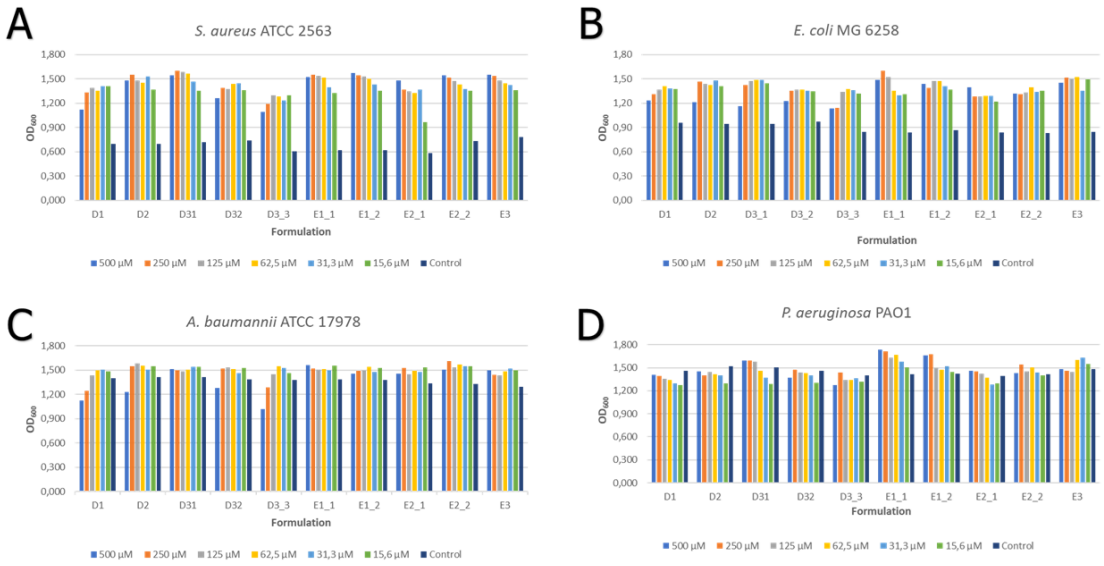

Figure 7.2. Microdilution assay to determine the NPs formulation against the growth of four bacterial species. Bars show mean OD_{600} ± variability from one experiment with four replicates per condition. Given the single-experiment design, these data are interpreted as descriptive screening results only.

Therefore, three conditions were tested: TSB supplemented with each NPs formulation at 500 µM (no preheating), and TSB contain the same formulations preheated at either 25°C or *50*°C for 1 h. All media were separately inoculated with all tested strains, incubated overnight with vigorous shaking, and OD_{600} was measured at following day. Several formulations, particularly those containing DMPG and DMPC, showed higher OD_{600} values than the control condition (Table 7.2). Preheating at 50°C did not significantly reduce turbidity compared to other two conditions ($p = 0.06$), as shown in Figure 7.4. Since the inherent turbidity of the formulations interfered with optical density readouts regardless of pre-treatment, CFU-based enumeration was employed as a more accurate method to evaluate their antimicrobial efficacy.

Table 7.2. Turbidity measurements of of bacterial cultures cultured in the presence of serine-based NP under different pre-treating conditions.

	OD_{600}		
Molecules	No preheating	Pre-heated at 25°C	Pre-heated at 50°C
D1	0.756	0.948	0.977
D2	1.096	1.723	1.604
D3_1	1.186	1.343	1.397
D3_2	1.230	1.206	1.167
D3_3	1.975	1.682	1.667
E1_1	0.797	1.740	1.745
E1_2	1.488	2.089	2.073
E2_1	1.278	1.926	1.904
E2_2	1.932	2.151	2.206
E3	1.548	2.136	2.165

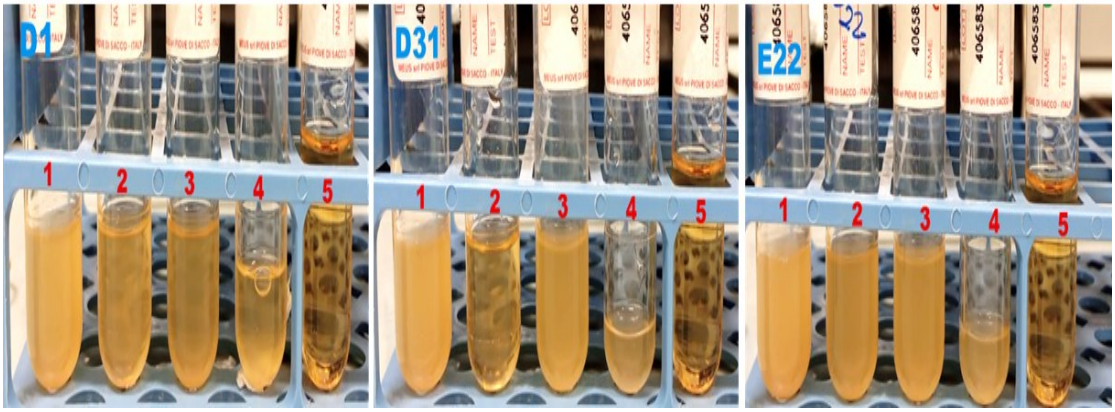

Figure 7.3. Visual inspection of bacterial cultures exposed to selected serine-based NPs formulations at 500 µM. Tubes contain D1 (left panel), D3_1 (middle), and E2_2 (right) after overnight incubation. The numbers correspond to: (1) *P. aeruginosa* PAO1, (2) *S. aureus* 6538, (3) *A. baumannii* ATCC 17978, (4) uninoculated TSB with NPs, and (5) TSB only.

7.3.3 Viable-count assay

Viable counts of four bacterial species cultured in the presence of all ten formulations at 500 µM were determined (Figure 7.4). All formulations significantly reduced CFU/ml compared with untreated cultures, although the magnitude of viability reduction was formulation- and species-dependent. *S. aureus* was consistently the most susceptible microorganism, with undetectable colony counts in all tested formulations, indicating a high bactericidal effect (Figure 7.4). Exposure of *E. coli*, to D1, D3_2 and D3_3 induced growth decreases up to approximately 5-fold reduction compared to the untreated control, whereas other formulations had more modest effects (Figure 7.4). Various effects were observed for *A. baumannii*, complete inhibition was achieved for D1 and D2, while only moderate decrease in CFU/ml was observed for D3_2, D3_3, E1_2, E2_2 and E3 (Figure 7.4). On the contrary, *P. aeruginosa* showed the highest tolerance, as most formulations resulted in lower minimal CFU reductions compared with the control, indicating only limited susceptibility even at higher concentration (Figure 7.4).

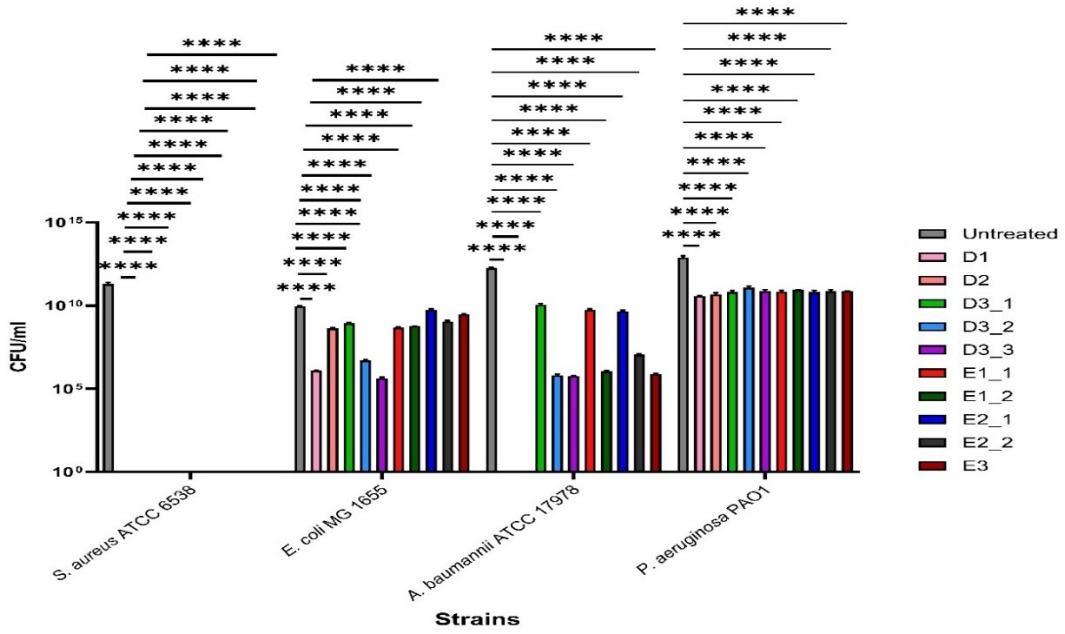

Figure 7.4. Viable-count screening of serine-based NPs for antibacterial activity against the four reference strains. The y axis represents colony-forming units (CFU/ml) after incubation in tryptic soy broth (TSB) with 500 µM of the ten serine-based NPs. All compounds were preheated at 50°C prior to use. Untreated, untreated cultures used as controls. Data are presented as mean ± SD, from at least two independent experiments; statistical significance was assessed using ANOVA; ****$p < 0.0001$.

7.3.4 Selection of four representative formulations

Based on the preliminary screening presented in Figure 7.4, the four formulations: D1, D3_3, E1_2, and E3 were selected as representative for further characterization, these formulations represented both ester- and amide- linked gemini surfactants, and covered distinct co-lipid combinations (8-8Ser vs DMPG) and gemini:co-lipid ratios. Specifically, D1 and E1_2 are formulations containing the serine-based monomer 8-8Ser at 2:1 molar ratios, whereas D3_3 and E3 are DMPG-containing formulations with a 4:1 gemini:DMPG ratio.

7.3.5 Dose-dependent antibacterial activity of selected serin-based NPs formulations

The antibacterial effects of the four selected formulations were assayed through detailed dose-response analyses. All formulations caused a marked growth inhibition of *S. aureus* ATCC 6538 across the entire concentration range, with complete inhibition observed at ≥ 250 μM (Figure 7.5A). D3_3 was the most potent formulation, causing a total growth inhibition at 31.25 μM. Conversely, the other formulation required higher concentrations to achieve a comparable effect: D1 and E1_2 exhibited complete inhibition at 125 μM and reduced CFU/ml by approximately eight-fold at 62.5 μM, while E3 showed a weaker effect at the same concentration. The ability of D1, E1_2, and E_3 to suppress CFU/ml at sub-inhibitory doses (15.6–62.5 μM) indicates that these formulations still exert measurable bactericidal effects against *S. aureus*, although they are less active than D3_3. In contrast, the Gram-negative strains were less susceptible to these formulations. For *E. coli* MG1655, statistically significant reductions in CFU/ml were detected mainly at 250 and 500 μM, with D1 and D3_3 exerting the strongest effects, while E1_2 and E3 caused more modest decreases (Figure 7.5B). A similar pattern was observed for *A. baumannii* ATCC 17978, which showed a significant but moderate CFU/ml reduction, particularly in the presence of D3_3, E1_2 and E3, whereas D1 was able to suppress growth to undetectable levels at the highest concentration tested (Figure 7.5C). All formulations were less effective against *P. aeruginosa* PAO1, as shown by the higher number of survival colonies at both 250 and 500 *μM*; nevertheless, D3_3 reduced the growth of this pathogen by approximately five-fold compared with the untreated culture (Figure 7.5D).

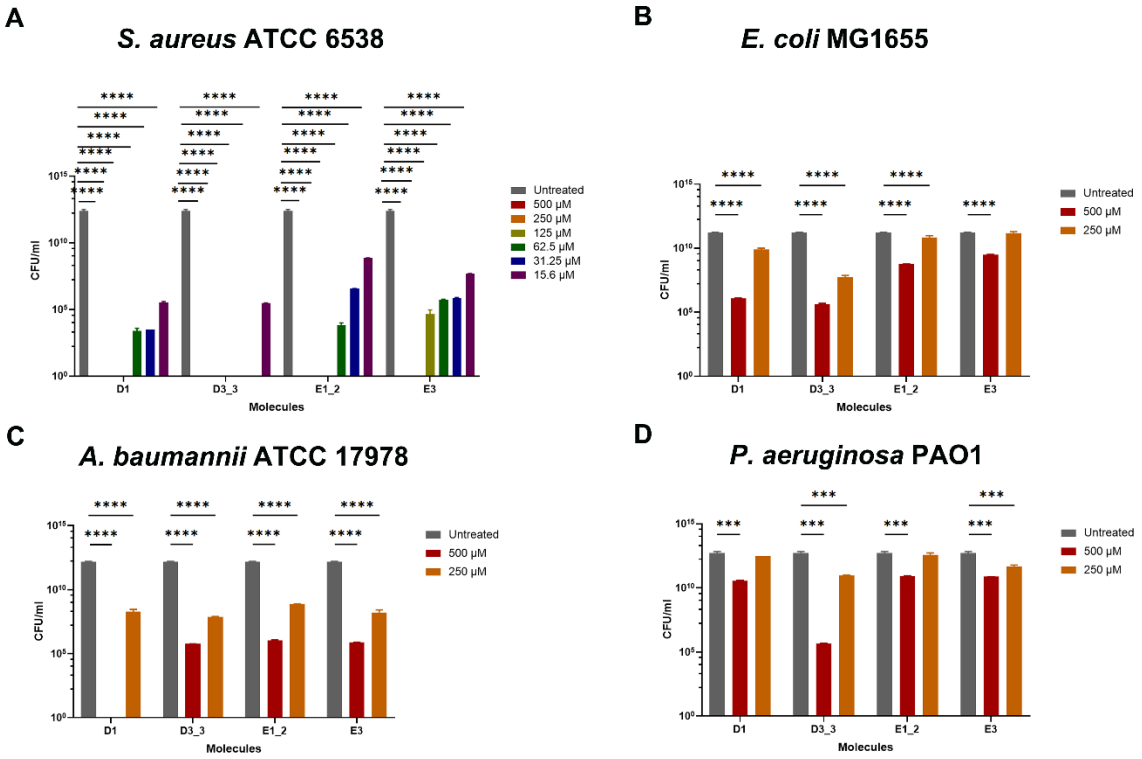

Figure 7.5. Dose-dependent antibacterial activity of four selected NPs-based molecules. These molecules at the indicated final concentrations were tested against *S. aureus* ATCC 6538 (A), *E. coli* MG 1655 (B), *A. baumannii* ATCC 17978 (C), and *P. aeruginosa* PAO1 (D); antibacterial activity was measured by determining the CFU/mL. Untreated cultures, grown under the same experimental conditions were used as controls. Data are presented as mean ± SD, from at least three independent experiments; statistical significance was assessed using ANOVA; ****$P < 0.0001$, ***$P < 0.001$.

7.3.6 Exposure to serine-based NPs significantly influences the viability of host cells

The toxicity of the four selected serin-based formulations was evaluated using the human epithelial lung cell line A549. These representative formulations were tested at concentrations corresponding to their bactericidal level, especially those effective against *S. aureus*. The results showed that all three treatments (D1, D3_3, and E1_2) caused a significant reduction in the cell viability compared with untreated controls. At 125 µM, D1 reduced viability to approximately 39% of the control, whereas D3_3 at 31.25 µM resulted in a cells viability about 43%, indicating substantial cytotoxicity even at concentrations close to the lowest effective antibacterial dose. E1_2 at 125 µM reduced cell viability by approximately 50% (Figure 7.6A). Surprisingly, the apparent viability values for E3 at 250 µM were higher than those of untreated cells; however, this increase is most likely an optical artifact due to strong turbidity arising from the aggregation or precipitation of the formulation, which also interfered with OD_{570} readings in a similar manner to that observed in the MIC assays. As a consequence, the true proportion of viable cells after E3 exposure cannot be reliably determined from the MTT data alone. Microscopic inspection supported the cytotoxic profile of all four formulations; in contrast to the confluent and spread morphology of untreated monolayers, treated cells displayed clear signs of damage, including rounding, shrinkage,

increased refractility and detachment from the surface. In the case of E3, clearly visible cell detachment was observed despite the turbidity of the medium (Figure 7.6B). These findings indicate that the serine-based NPs formulations compromise A549 cell integrity at concentrations that overlap with their therapeutic antibacterial range.

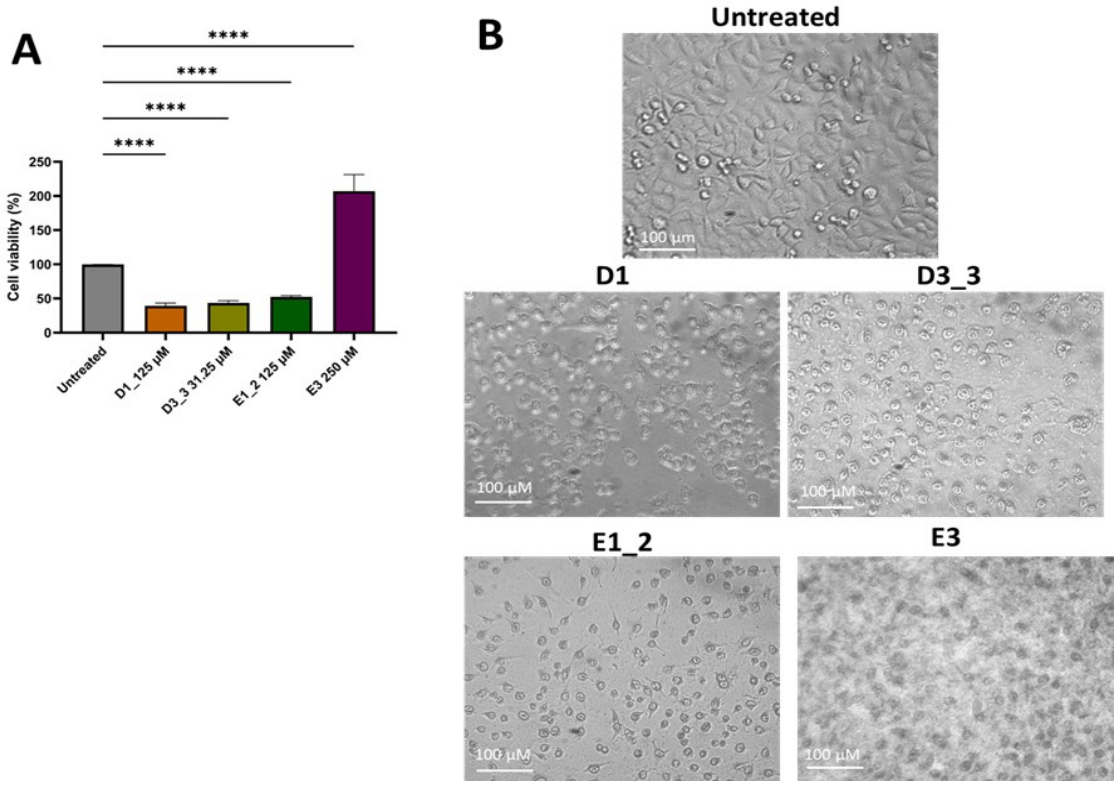

Figure 7.6. Viability of A549 cell monolayers following 24 h exposure to selected NPs-based molecules. (A) The metabolic activity of cells treated with NPs formulations at the indicated concentrations was assessed using the MTT assay. Untreated control cells were used as negative controls. Data are presented as mean ± SD, from at least three independent experiments; statistical significance was assessed using ANOVA; ****$p < 0.0001$. (B) Representative microscopy images of cell morphology after 24 h of exposure to the same concentrations as in panel A. Images were acquired using the 20X objective on Motic AE21 microscope connected with a ZZCAT digital camera scale bar: 100 µm.

7.4 Discussion

Gemini surfactants are widely known for their ability to form vesicular aggregates with low CMC and can assemble into cationic vesicles when mixed with anionic or zwitterionic partners such as 8-8Ser, DMPG, and DMPC [7,14,17,18]. In this study, serine-based gemini NPs combine with DMPG was used to provide a bacterial-like, phosphatidylglycerol-rich environment, which mimics envelope of gram-positive and gram-negative bacteria [19–21]; in contrast, the combination with DMPC (zwitterionic PC) mimics mammalian phosphatidylcholine-rich zwitterionic lipid membranes, yet it might reduce direct antibacterial activity compared to DMPG [22]. To our knowledge, the specific combinations of serine-based ester and amide gemini surfactants with DMPC or DMPG investigated in this study have not been reported previously, although they are conceptually grounded in the earlier self-assembly and membrane-interaction studies [7,14,20,22].

The microdilution assays, MIC based OD reading was unreliable because all serine-based formulations generated intrinsic turbidity both at bactericidal concentration and even in uninoculated conditions. Consequently, CFU enumeration was adopted as the primary readout for antibacterial activity in subsequent experiments. Preliminary screening at 500 μM identified several active formulations and highlighted a pronounced susceptibility of *S. aureus* compared with *E. coli*, *A. baumannii* and *P. aeruginosa*. Further experiments with four selected formulations (D1, E1_2, D3_3, and E3) in a broad range of concentrations revealed similar species-formulation patterns.

It has been described that cationic serine-based gemini vesicles are first electrostatically attracted to negatively charged cell-surface components, such as teichoic acids and phosphatidylglycerol (PG) in Gram-positive envelopes and lipopolysaccharide and PG in Gram-negative envelopes [6,23]. Among these, the gemini-rich, DMPG-containing formulations, especially D3_3, which incorporate a high proportion of dimeric surfactant, generate a higher local positive charge density and stronger hydrophobic features drive for insertion than the corresponding monomer-containing formulations D1 and E1_2 [6,11]. Once bound, the twin C12 chains and dimeric headgroups of the gemini-formulations possibly insert more efficiently into the lipid bilayer, disturb packing, and generating curvature stress and defects; the catanionic vesicles are expected to fuse with or partially disintegrate into the membrane [24–26]. This leads to increased permeability, ion leakage and loss of membrane potential, and, at sufficiently high local concentrations, to large defects or lysis [7,8,11,19]. Rapid, multi-log bactericidal effect is particularly evident result for D3_3 in *S. aureus*, whereas D1 and E1_2 might produce the same outcome but only at higher bulk concentrations. In Gram-negative bacteria, the bactericidal effect of almost all formulations is weaker, which may be explained by the outer-membrane/LPS barrier limiting NPs access to the inner membrane. The structure is in contrast with the thick and porous peptidoglycan layer in *S. aureus* that allows NPs to accumulate [21,27,28] . These results are in line with previous reports showing that cationic surfactants and nanoparticles often display higher potency against Gram-positive species [9,12], whereas the outer membrane and associated structures of Gram-negative pathogens limit access of amphiphilic agents to the cytoplasmic membrane [29,30].

Although these mechanisms were not directly assessed here, the differential susceptibility between *S. aureus* and the Gram-negative strains is consistent with the model of multidimensional envelope-based protection [29]. The proposed antibacterial mechanism of serine-based NPs is showed by schematic diagram on Figure 7.7.

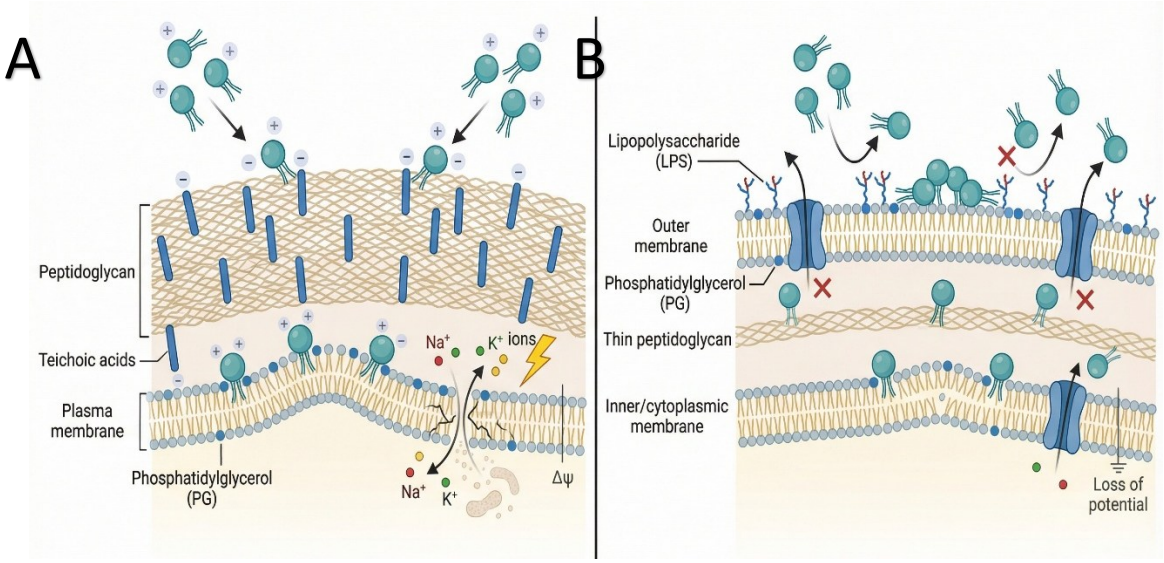

Figure 7.7. Proposed bactericidal mechanism of serine-based NPs in Gram-positive and Gram-negative bacteria. The NPs accumulate and bind to negatively charged cell envelopes, induce membrane curvature stress and defects, and cause ion leakage and loss of membrane potential. The result is rapid multi-log killing of Gram-positive bacteria (A) and weaker LPS-limited bactericidal effects in Gram-negative species (B). Figure was created using FigureLabs.

Evaluation of A549 cell viability revealed that the four selected formulations compromise host-cell metabolic activity and monolayer integrity at concentrations similar to those required for antibacterial effects. MTT assays showed a reduction in cell viability up to 50-60 % relative to untreated controls following 48 h exposure. The serine-based NPs formulations are expected to exert toxicity primarily through non-selective disruption of the plasma membrane, followed by secondary intracellular stress responses [31,32]. At bactericidal concentrations, cationic gemini-rich vesicles adsorb onto the slightly negatively charged, phosphatidylcholine-rich outer leaflet of the A549 plasma membrane and insert their twin hydrophobic chains into the bilayer [33,34]. This insertion perturbs lipid packing, increases membrane curvature stress and leads to the formation of transient or stable defects, resulting in membrane thinning, leakage of ions and loss of membrane integrity [33]. Once the membrane is compromised, this NPs possibly enter the cell, where they are likely disturb mitochondrial function and promote the generation of reactive oxygen species, as reported for other inorganic and metallic nanoparticles in A549 and related lung cell lines [35,36]. The combined effects of membrane damage, ionic imbalance, mitochondrial dysfunction, oxidative stress and downstream DNA or protein injury ultimately drives cell death [31,33,34,37]. As a results, these effects lead to appearance of marked rounding, detachment and

loss of monolayer under microscopic inspection (Figure 7.6B). All these possible mechanisms of NP activities on host cells are depicted in Figure 7.8.

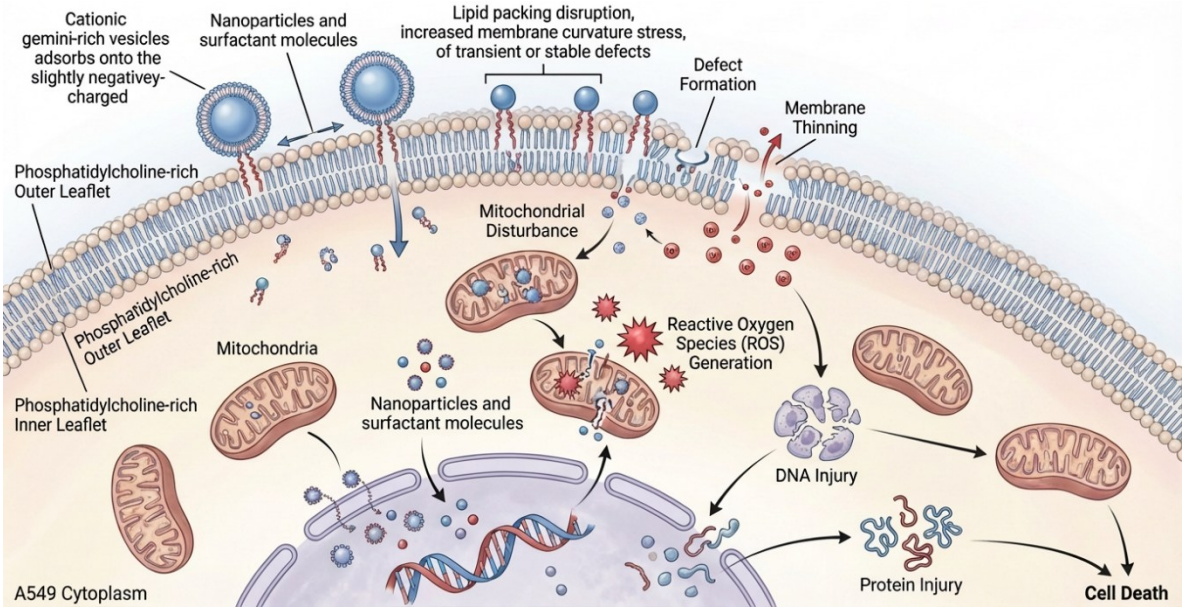

Figure 7.8. Proposed Cytotoxicity Mechanism of Serine-Based Nanoparticle Formulations in A549 Cells. Cationic gemini-rich vesicles adsorb onto the phosphatidylcholine-rich plasma membrane of A549 cells, disrupt lipid packing and membrane integrity, and trigger mitochondrial dysfunction, reactive oxygen species generation, macromolecular damage and loss of monolayer viability. Figure was created using FigureLabs.

Furthermore, the apparent increase in OD_{570} for the highest E3 concentration reflects optical interference from turbid suspensions due to aggregation rather than true preservation of cell viability, which possibly caused by several reasons. First, the high gemini:DMPG molar ratio (4:1) yields strongly cationic aggregates with a large hydrophobic core; such gemini-rich catanionic systems may undergo vesicle–vesicle association, fusion or transition to larger, more heterogeneous aggregates, which could increases light scattering and turbidity [17,38]. Second, DMPG is an anionic phospholipid that mimics phosphatidylglycerol; at high ratios of cationic surfactant to DMPG, charge neutralization and over-charging may promote flocculation or formation of multilamellar structures increasing medium turbidity [17,39]. Third, the presence of salts, proteins and other components in the culture medium may induce electrostatic repulsion and favours NP aggregation, a phenomenon widely documented for inorganic and polymeric nanoparticles in biological media [31,40,41].

Previous studies also demonstrated that exposure to NPs from various substances significantly reduced the viability of human cell lines. For instance, metal oxide NPs caused viability loss of A549 cells by up to 50% after treatment at higher concentrations, primarily through DNA damage, oxidative stress, and apoptosis [42]. Similarly, experiments with silica and silver NPs showed a

decrease in the viability of A549 cells, which depended on both dosage and duration of exposure. This is indicated by a significant percentage of cell death at higher concentrations and longer incubation periods, along with increased production of reactive oxygen species (ROS) and membrane damage [35,43]. In addition, studies on Caco-2 cells have demonstrated similar trends: exposure to silver NPs results in significant alterations in the cell cycle, cell morphology, cellular function, and cell maintenance in the short term at higher concentrations. Meanwhile, continuous NPs uptake over the long term, even at the lowest concentrations, poses a potential carcinogenic risk [44,45].

This study has several limitations that should be consider. All data were obtained only from planktonic cultures of reference strains and cytotoxicity was evaluated by using a single epithelial cell type. Moreover, the evaluation of serine-gemini NPs with DMPC integration is missing among representative tested formulations, adding the uncomplete finding for contrasting the effect of DMPG and DMPC in serine-based gemini NP formulation. In future work, these limitations could be addressed by evaluating the most promising ester-based formulations in additional human cell types or another complex tissue models, assessing activity against clinical isolates and biofilms, and performing pharmacologically relevant studies to examine efficacy, biodistribution and toxicity in infection models.

7.5 Conclusion

Serine-based gemini surfactant NPs combining ester-linked dimers with DMPG or 8-8Ser co-lipids exhibited potent bactericidal activity, with particularly strong effects against *S. aureus* and a lower to moderate, species-dependent impact on Gram-negative pathogens. At the same time, the overlap between antibacterial and cytotoxic concentration ranges in A549 cells indicates that the current formulations require further optimization. Altogether, these findings support serine-based gemini NPs as a promising platform for the development of next-generation antimicrobial nanomaterials, while also highlighting the importance of integrated physicochemical, microbiological and toxicological evaluation for their future translation.

References

1. Yusuf, A., Almotairy, A. R. Z., Henidi, H., Alshehri, O. Y. & Aldughaim, M. S. Nanoparticles as Drug Delivery Systems: A Review of the Implication of Nanoparticles' Physicochemical Properties on Responses in Biological Systems. *Polymers* **15**, 1596 (2023).
2. Joudeh, N. & Linke, D. Nanoparticle classification, physicochemical properties, characterization, and applications: a comprehensive review for biologists. *J. Nanobiotechnology* **20**, 262 (2022).
3. Selmani, A., Kovačević, D. & Bohinc, K. Nanoparticles: From synthesis to applications and beyond. *Adv. Colloid Interface Sci.* **303**, 102640 (2022).
4. Shaban, S. M., Kang, J. & Kim, D.-H. Surfactants: Recent advances and their applications. *Compos. Commun.* **22**, 100537 (2020).
5. Qin, F., Ma, Y., Miao, L., Wang, Z. & Gan, L. Influence of Metal–Ligand Coordination on the Elemental Growth and Alloying Composition of Pt–Ni Octahedral Nanoparticles for Oxygen Reduction Electrocatalysis. *ACS Omega* **4**, 8305–8311 (2019).
6. Kowalczyk, I., Koziróg, A., Szulc, A., Komasa, A. & Brycki, B. Antimicrobial Properties of Monomeric and Dimeric Catanionic Surfactant System. *Molecules* **30**, 164 (2025).
7. Kowalczyk, I., Szulc, A. & Brycki, B. Gemini Surfactants: Advances in Applications and Prospects for the Future. *Molecules* **30**, 4599 (2025).
8. Brycki, B. E., Szulc, A., Kowalczyk, I., Koziróg, A. & Sobolewska, E. Antimicrobial Activity of Gemini Surfactants with Ether Group in the Spacer Part. *Molecules* **26**, 5759 (2021).
9. Mechken, K. A., Menouar, M., Talbi, Z., Saidi-Besbes, S. & Belkhodja, M. Self-assembly and antimicrobial activity of cationic gemini surfactants containing triazole moieties. *RSC Adv.* **14**, 19185–19196 (2024).
10. Dahal, H., Roy, S., Dey, J. & Bose Dasgupta, S. Impact of the Hydrocarbon Chain Length of Biodegradable Ester-Bonded Cationic Gemini Surfactants on Self-Assembly, In Vitro Gene Transfection, Cytotoxicity, and Antimicrobial Activity. *Langmuir* **40**, 2242–2253 (2024).
11. Kowalczyk, I., Szulc, A., Koziróg, A., Komasa, A. & Brycki, B. Surface and Antimicrobial Properties of Ester-Based Gemini Surfactants. *Molecules* **30**, 2648 (2025).
12. Sousa, F. F. O. D. *et al.* Arginine Gemini-Based Surfactants for Antimicrobial and Antibiofilm Applications: Molecular Interactions, Skin-Related Anti-Enzymatic Activity and Cytotoxicity. *Molecules* **28**, 6570 (2023).
13. Wu, J. *et al.* Cationic gemini surfactants containing both amide and ester groups: Synthesis, surface properties and antibacterial activity. *J. Mol. Liq.* **299**, 112248 (2020).
14. Silva, S. G. *et al.* Serine-based surfactants as effective antimicrobial agents against multiresistant bacteria. *Biochim. Biophys. Acta BBA - Biomembr.* **1864**, 183969 (2022).
15. Dahal, H., Paswan, A. M., Dey, J. & Raj, C. R. Harnessing the Potential of Amide-Linked Gemini Surfactants for Corrosion Inhibition and Antimicrobial Activity: From Molecular Design to Functional Performance. *Langmuir* **41**, 5455–5466 (2025).
16. Neubauer, D. *et al.* Biological and Physico-Chemical Characteristics of Arginine-Rich Peptide Gemini Surfactants with Lysine and Cystine Spacers. *Int. J. Mol. Sci.* **22**, 3299 (2021).
17. Oliveira, I., Silva, S., Do Vale, M. & Marques, E. Model Catanionic Vesicles from Biomimetic Serine-Based Surfactants: Effect of the Combination of Chain Lengths on Vesicle Properties and Vesicle-to-Micelle Transition. *Membranes* **13**, 178 (2023).
18. Silva, S. G., Oliveira, I. S., Do Vale, M. L. C. & Marques, E. F. Serine-based gemini surfactants with different spacer linkages: from self-assembly to DNA compaction. *Soft Matter* **10**, 9352–9361 (2014).

19. Modi, S. K., Gaur, S., Sengupta, M. & Singh, M. S. Mechanistic insights into nanoparticle surface-bacterial membrane interactions in overcoming antibiotic resistance. *Front. Microbiol.* **14**, 1135579 (2023).

20. Shahzadi, I. *et al.* Lipophilic Arginine Esters: The Gateway to Preservatives without Side Effects. *Mol. Pharm.* **17**, 3129–3139 (2020).

21. Wang, L., Hu, C. & Shao, L. The antimicrobial activity of nanoparticles: present situation and prospects for the future. *Int. J. Nanomedicine* **Volume 12**, 1227–1249 (2017).

22. Oñate-Garzón, J. *et al.* Antimicrobial activity and interactions of cationic peptides derived from Galleria mellonella cecropin D-like peptide with model membranes. *J. Antibiot. (Tokyo)* **70**, 238–245 (2017).

23. Tripathi, V., Bhadra, J. & Bhattacharya, S. Structure–Activity Relationships and Practical Aspects of Cationic Gemini Surfactants as Antimicrobial Agents. *J. Surfactants Deterg.* jsde.70007 (2025) doi:10.1002/jsde.70007.

24. Dehsorkhi, A., Castelletto, V., Hamley, I. W., Seitsonen, J. & Ruokolainen, J. Interaction between a Cationic Surfactant-like Peptide and Lipid Vesicles and Its Relationship to Antimicrobial Activity. *Langmuir* **29**, 14246–14253 (2013).

25. Tesauro, D. *et al.* Peptide-Based Drug-Delivery Systems in Biotechnological Applications: Recent Advances and Perspectives. *Molecules* **24**, 351 (2019).

26. Munusamy, S., Conde, R., Bertrand, B. & Munoz-Garay, C. Biophysical approaches for exploring lipopeptide-lipid interactions. *Biochimie* **170**, 173–202 (2020).

27. Nam-Cha, S. H. *et al.* Methacrylate Cationic Nanoparticles Activity against Different Gram-Positive Bacteria. *Antibiotics* **12**, 533 (2023).

28. Lai, X. *et al.* Polysaccharide-Targeting Lipid Nanoparticles to Kill Gram-Negative Bacteria. *Small* **20**, 2305052 (2024).

29. Sharma, P., Vaiwala, R., Gopinath, A. K., Chockalingam, R. & Ayappa, K. G. Structure of the Bacterial Cell Envelope and Interactions with Antimicrobials: Insights from Molecular Dynamics Simulations. *Langmuir* **40**, 7791–7811 (2024).

30. Carnero Canales, C. S. *et al.* Combating Gram-negative infections: The role of antimicrobial peptides and nanotechnology in overcoming antibiotic resistance. *Mater. Today Bio* **35**, 102381 (2025).

31. Pérez, L., Pinazo, A., Morán, M. C. & Pons, R. Aggregation Behavior, Antibacterial Activity and Biocompatibility of Catanionic Assemblies Based on Amino Acid-Derived Surfactants. *Int. J. Mol. Sci.* **21**, 8912 (2020).

32. Parikh, K. *et al.* Physico-biochemical studies on cationic gemini surfactants: Role of spacer. *J. Mol. Liq.* **206**, 19–28 (2015).

33. Awashra, M. & Młynarz, P. The toxicity of nanoparticles and their interaction with cells: an *in vitro* metabolomic perspective. *Nanoscale Adv.* **5**, 2674–2723 (2023).

34. Qian, P. *et al.* Recent Progress in Gene Delivery Systems Based on Gemini-Surfactant. *MedComm – Future Med.* **4**, e70027 (2025).

35. Lin, W., Huang, Y., Zhou, X.-D. & Ma, Y. In vitro toxicity of silica nanoparticles in human lung cancer cells. *Toxicol. Appl. Pharmacol.* **217**, 252–259 (2006).

36. Peivandi, Z. *et al.* Silica nanoparticles-induced cytotoxicity and genotoxicity in A549 cell lines. *Sci. Rep.* **14**, 14484 (2024).

37. Massa, M. *et al.* Chemico-Physical Properties of Some 1,1′-Bis-alkyl-2,2′-hexane-1,6-diyl-bispyridinium Chlorides Hydrogenated and Partially Fluorinated for Gene Delivery. *Molecules* **28**, 3585 (2023).

38. Silva, S. G., Vale, M. L. C. D. & Marques, E. F. Size, Charge, and Stability of Fully Serine-Based Catanionic Vesicles: Towards Versatile Biocompatible Nanocarriers. *Chem. – Eur. J.* **21**, 4092–4101 (2015).

39. Chen, Y., Qiao, F., Fan, Y., Han, Y. & Wang, Y. Interactions of Cationic/Anionic Mixed Surfactant Aggregates with Phospholipid Vesicles and Their Skin Penetration Ability. *Langmuir* **33**, 2760–2769 (2017).

40. Bélteky, P. *et al.* Silver nanoparticles: aggregation behavior in biorelevant conditions and its impact on biological activity. *Int. J. Nanomedicine* **Volume 14**, 667–687 (2019).

41. Raasakka, A., Jones, N. C., Hoffmann, S. V. & Kursula, P. Ionic strength and calcium regulate membrane interactions of myelin basic protein and the cytoplasmic domain of myelin protein zero. *Biochem. Biophys. Res. Commun.* **511**, 7–12 (2019).

42. Mahmoud, A., Ezgi, Ö., Merve, A. & Özhan, G. In Vitro Toxicological Assessment of Magnesium Oxide Nanoparticle Exposure in Several Mammalian Cell Types. *Int. J. Toxicol.* **35**, 429–437 (2016).

43. Suliman Y, A. O. *et al.* Evaluation of cytotoxic, oxidative stress, proinflammatory and genotoxic effect of silver nanoparticles in human lung epithelial cells. *Environ. Toxicol.* **30**, 149–160 (2015).

44. Gioria, S. *et al.* Proteomics study of silver nanoparticles on Caco-2 cells. *Toxicol. In Vitro* **50**, 347–372 (2018).

45. Vila, L., Marcos, R. & Hernández, A. Long-term effects of silver nanoparticles in caco-2 cells. *Nanotoxicology* 1–10 (2017) doi:10.1080/17435390.2017.1355997.

Chapter 8. General Discussion

High-impact clinical pathogens such as *A. baumannii*, UPEC, and *S. agalactiae* continued to develop persistence mechanisms under antibiotic pressure. To survive in their preferable niches, these pathogens undergo multidimensional adaptation by connecting genomic, phenotypic, and ecological changes.

Our data showed that *A. baumannii* developed a marked variability over a decade of circulation. This superbug can express an XDR phenotype even utilizing a limited set of resistance genes for specific antibiotic classes, together with multiple efflux pump-related genes, to resist to a broad range of antimicrobials. One of the most studied features is the interchangeable roles of different of bla_{oxa} variants, supported by bla_{ADC} and bla_{TEM}, which represent major drivers for carbapenem resistance. In the respiratory niche, the strains showed temporal divergence in their phenotypes, where the older strains had higher antibiotic resistance, desiccation tolerance, and bladder cell invasiveness, while the recent respiratory strains had faster growth, biofilm formation, and invasiveness in the lung cells. However, the positive correlation between the fast growth, biofilm formation, and invasiveness in the lung cells implies co-selection of the strains in the respiratory niche. Although a large core set of virulence genes was conserved over time, respiratory isolates also acquired and lost accessory genes, including old-specific adhesion and nutrient-uptake genes and a few genes unique to recent respiratory strains, indicating ongoing genomic remodelling in the respiratory niche. In contrast, the urinary strains showed no major temporal differences in invasiveness towards bladder or lung cells, implying a generalist invasive phenotype. However, the absence of shared virulence genes between the old and recent urinary strains points to substantial changes in their genome over time.

Longitudinal and comparative genomic studies similarly show that dynamic genomic adaptation in *A. baumannii* increases the risk of carbapenem resistance, particularly through the acquisition and reshaping of mobile genetic elements carrying bla_{OXA} variants over time [1–3]. Our observation that XDR phenotypes can arise from relatively restricted ARG repertoires is consistent with the idea that focusing resistance on a smaller set of key determinants and combination with global regulatory systems can reduce fitness costs and favour long-term persistence in clinical environments, as suggested for strains exposed to different historical antibiotic regimes [4]. This trade-off between resistance properties and fitness also aligns with reports that modern clinical isolates, which carry more unique and less conserved genes, thereby contributing to a broader spectrum of persistence phenotypes and complicating the extrapolation of data from references strains to contemporary clinical population [4–6]. In addition, an experimental work indicates that human urine can trigger extensive adaptive changes in gene expression among carbapenem-resistant *A. baumannii* (CRAB), including metabolic and biofilm-related functions. This finding is compatible with the variability in metabolic and biofilm-associated genes we observed among urinary isolates and supports the notion that urinary tract environment modulates CRAB behaviour

in a niche-specific manner [7]. In the airway context, the distinct phenotype properties among our respiratory isolates may facilitate prolonged colonization of the airway surface and protection from host defences, in line with in vivo pneumonia models showing that *A. baumannii* maintains airway colonization through host-cell modulation and intracellular persistence [8]. Moreover, clinical data indicate that patients colonized by biofilm-producing *A. baumannii* have a high risk of ventilator associated pneumonia, which are less susceptible to antibiotic treatments, further supporting the idea that niche-adapted respiratory lineages may require different preventive strategies from those targeting urinary CRAB [9]. Altogether, these findings underscore that *A. baumannii* genomic plasticity is tightly interconnected to niche-specific phenotypic rewiring, reinforcing its status as an outstanding opportunistic nosocomial pathogen and a priority organism on the WHO list.

In the first study, correlations between quantitative phenotypes and genomic/phenotypic features of *A. baumannii* were explored, but the heterogeneous nature of the variables (continuous MIC values, semi-quantitative phenotypes, and presence/absence of genes) represents an important concern. To address skewness, some variables were transformed before applying Pearson correlation. However, several remained non-Gaussian and sample sizes were modest, which may compromise the assumptions underlying Pearson's coefficient and increase the risk of biased estimates. Therefore, the reported correlation coefficients should be interpreted as exploratory association rather than definitive evidence of linear relationships. Future investigations should validate these relationships using Spearman's rank correlation or other non-parametric approaches, which make fewer distributional assumptions and are more robust for ordinal and mixed-scale data [10,11]. Such analysis will be essential to translate these associations into predictive models of *A. baumannii* behaviour across clinical niches.

Given that nosocomial pneumonia represents the primary clinical manifestation of *A. baumannii* infection, an air-liquid interface (ALI) model of differentiated human bronchial epithelial cells was employed for the first time to investigate the impact of *A. baumannii* strain AB5075 on the airway epithelium during both early and late stages of infection. In this model, we demonstrated that pathogen induces early structural damage to the bronchial epithelium and goblet cells even at relatively low bacterial loads and after short infection periods, while simultaneously triggering a robust inflammatory response. Over time, this host response progressively impaired epithelial barrier function by disrupting cytoskeletal organization and cell-matrix interactions, ultimately weakening cell junctions and compromising barrier integrity. The most pronounced damage occurred at the level of goblet cells, which constitute a first line of defense in the airway epithelium. Transcriptomic profiling further confirmed this intense inflammatory response, revealing activation of cytokine signaling cascades involved in the recruitment of neutrophils and macrophages, which contributed to extensive epithelial damage. At later time points, goblet cells exhibited marked dysfunction, characterized by a swollen, granular, and irregular morphology, impaired apical mucus secretion, and loss of barrier integrity. It is tempting to speculate that the strong inflammatory response elicited by *A. baumannii* is a key strategy used by the pathogen to facilitate its dissemination within the airways. These histopathological observations are biological

important, but they should be complemented by quantitative analysis, for example, cellular morphometry, blinded scoring, and the percentage of alter cells per field. Combining qualitative and quantitative morphology assessment not only would increase rigor and reproducibility but also provide more comprehensive understanding of the extend of epithelial damage caused by *A. baumannii* during early infection.

It is interestingly to note that other respiratory pathogens often require higher inocula and/or more extensive replication to cause comparable epithelial injury. For example, *Klebsiella pneumonia* typically needs higher MOI to induce marked intracellular ROS production, nuclear condensation, loss of plasma membrane integrity and cytotoxicity [12], with capsulated strains requiring even higher MOI to exert strong cytotoxic effect [13]. Similarly, *Streptococcus pneumonia* needs high MOI in the range of 10-35 to leave lasting epigenetic and transcriptional memory in host cells after infection and repeated rounds of bacterial proliferation [14], and even higher MOI (MOI 200-400) and longer infection duration (4-7 h) to cause more severe damage such as DNA double-strand breaks and cell death [15]. Furthermore, this low-burden high-damage behavior of *A. baumannii* contrasts with other toxin-heavy respiratory pathogens such as *P. aeruginosa*, where type III (T3SS) and type VI secretion systems (T6SS) drives goblet-cell invasion, triggers cytotoxicity and epithelial rupture [16]. *A. baumannii*, by comparison, lacks a canonical T3SS and often repress or inactivates T6SS in clinical contexts and in the presence of multidrug resistance plasmids, yet still achieves significant barrier disruption, implying a greater reliance on alternative secretion systems, surface components and inflammation-mediated tissue remodelling to secure airway persistence [17–19]. The sustained transcriptional reprogramming observed in our ALI model, together with previous evidence that *A. baumannii* can persist within modified macrophage vacuoles [20,21], dictates neutrophil influx and function at infectious sites [22,23], supports a "persist-and-damage" strategy that can underlie chronic or relapsing pneumonia despite targeted antibiotic therapy. When the transcriptomic and functional observations are viewed alongside the genomic evidence of multiple secretion systems, they underline a subtle destructive strategy: *A. baumannii* remodels the airway niche and host immunity to its advantage without relying on very high bacterial loads or classical toxin arsenals typical of other respiratory priority pathogens [12,13,15,16,24]. In this context, clinical isolates enriched in a mosaic of virulence traits would be expected to cause even more pronounced epithelial disruption and dysregulated inflammation in ALI models, further explaining the severe outcomes observed in ventilator-associated pneumonia.

Although our ALI data and the available genomic evidence support this model of low-burden and high-damage adaptation, an important issue of the present system is that all three independent experiments used cells from the same donor. This strategy reduced technical variability and was less time-consuming; however, it also limits the biological robustness of the data and may lead to generalized the conclusions. Several reports have shown that including multiple donors can still yield comparable epithelial composition, ciliary distribution and function, and expression of secretory markers, while enhancing the characterization of inflammatory responses [25–27]. Integrating cells from multiple donors is therefore more promising, as it may reveal mechanistic

insights within donor-to-donor variability and capture a broader range of physiological responses to *A. baumannii,* as has been demonstrated shown for other respiratory pathogens [27,28]. Future work should validate the present findings using ALI cultures derived from multiple donors and, ideally, from individuals with different clinical backgrounds (e.g. smokers, patients with chronic airway disease) to better capture inter-individual variability in host–pathogen interactions.

Beyond the respiratory tract, UPEC possessed third-generation cephalosporin and carbapenem-resistance, demonstrating complex and multidimensional adaptation to support its persistence and spread in both hospital and community settings. Together with *A. baumannii*, they belong to the critical priority group in the WHO BPPL. In our study, we highlighted a near-uniform distribution of antibiotic-resistance genes between inpatient and outpatient isolates, together with their genetic relatedness. These results suggesting cross-contamination and comparable selective pressures in the two environments. Genes encoding ESBL production and cefotaxime inactivation were highly prevalent in both groups, whereas carbapenem resistance was largely restricted to hospital isolates. Community-acquired strains generally displayed greater virulence, with higher motility and biofilm production. Virulence genes, particularly those involved in iron acquisition, were common in both settings, while genes critical for bladder-cell isolates, biofilm maturation and heme uptake were more prevalent among outpatient isolates. Specific virulence factors also correlated with resistance to ciprofloxacin and gentamicin. Overall, these observations support a model in which virulence determinants compensate for the energetic cost of resistance, enhancing the overall fitness and persistence of UPEC across diverse ecological niches.

The near-uniform distribution of resistance genes and close genetic relatedness between inpatient and outpatient UPEC isolates suggests that the same successful lineages circulate across hospital and community settings, with ESBL and cefotaxime-resistant isolates sharing resistance profile rather than being confined to one environment. This pattern is consistent with epidemiological studies showing that cefotaxime-resistant and ESBL-producing *E. coli* display highly similar resistance. In addition, ESBL gene profiles across clinical, community and even wastewater compartments, with CTX-M–type ESBLs and associated multidrug resistance appearing in both hospital-acquired and community-acquired UTI isolates [29–31]. In contrast, carbapenem resistance remain restricted to hospital UPEC isolates, fitting with the strong selective pressures imposed by carbapenem therapy and invasive procedures, as demonstrated by risk-factor analyses of nosocomial carbapenem-resistant *E. coli* infections, and with the emergence of carbapenemase-producing high-risk ExPEC clones such as ST131 and ST167 in hospital outbreaks and surveillance studies [32,33]. In comparison with hospital isolates, community-acquired strains were more motile, stronger biofilm formers, and carried a higher frequency of heme-, iron-uptake and invasive genes; these features, to our knowledge, revealed an under-recognised facet of the UPEC ecology. Previous experimental infection models indicate that UPEC rely on multiple adhesins and redundant iron acquisition systems to survive in the iron-limited and high-shear urinary tract [34,35]; our data extend these findings by showing that such traits can be enriched in community-circulating lineages. Such redundancy helps maintaining their growth and colonisation

capacity under urinary tract conditions and likely reduces the fitness costs associated with multidrug resistance during transmission and relapse [36]. In support of this, our study showed that the third-generation cephalosporin resistance in UPEC was linked to iron-scavenging genes (*fyuA*, *iutA*), and that biofilm formation was significantly associated with *fyuA*, suggesting that both these features jointly promote reduced antibiotic susceptibility and persistence in the urinary tract [37].

UPEC study also has important methodological limitations that should be considered when interpreting the observed associations between virulence content and resistance. Because odds ratios were reported without 95% confidence intervals, the precision and statistical stability of these estimates cannot be fully assessed, particularly for very large Ors, such as those observed for *papC* (OR 80.500), *papAH* (OR 61.600), and *ompT* (OR 23.800) in association with gentamicin resistance. Given the relatively small sample size and the large number of parallel comparisons performed between genes and antibiotics, these extreme values are especially linked to type I error and overestimation [38,39]. As a result, these findings should be regarded as exploratory and hypothesis-generating rather than definitive evidence of causal links. Future studies with larger samples and formal estimation of confidence intervals will be required to verify these predictions, refine their effect sizes and clarify the biological mechanisms. This methodological approach will provide strong biological reason to explains community-circulating UPEC lineages may contribute to treatment failure and recurrent infection.

The emergence of MDR *S. agalactiae* add further concern because this pathogen is recognised as a major cause of neonatal sepsis and meningitis, and resistant lineages indeed threaten the effectiveness of IAP. Colonising *S. agalactiae* isolates from pregnant women displayed heterogenous aggregation capacity and β-hemolytic activity, together with a mosaic of capsular serotypes and pilus island profiles. In our study, this structural diversity was mirrored at the genetic level: core adhesins, hemolysin and immune-evasion genes were widely conserved, whereas alpha-like surface proteins and the hypervirulence marker *hvgA* defined subgroups with distinct virulence architectures. In particular, the *hvgA*-positive strains emerged as dual-threat lineages that combine a rich virulence-gene repertoire with high-level gentamicin resistance (HLGR). Notably, even relatively low bacterial load was sufficient to induce epithelial cytotoxicity over the short infection period. Taken together, these features indicate typical *S. agalactiae* survival strategies, and when coupled with diverse antibiotic-resistance phenotypes could increase the risk of ascending infection in favourable host conditions.

Our data that *hvgA*-positive, MDR/HLGR *S. agalactiae* are already established among colonising vaginal isolates from pregnant women fits into a broader picture emerging from invasive disease and genomic studies, in which hypervirulent clones (such as CC17, ST283 and related lineages) accumulate both complex virulence repertoires and multidrug resistance [40–43]. The maintenance of high cytotoxicity even at low inocula challenges a simple virulence-fitness trade-off, thereby suggesting that these strains harbor survival mechanisms similar to the invasive phenotypes that actively exploit human macrophages to evade immune recognition [44]. This structural and genetic

adaptation is clinically significant, as the combination of complex virulence factors with antimicrobial resistance genes is consistent with convergent evolution toward highly adapted MDR, hypervirulent clones in human hosts [43].

Beyond genomic and functional traits, our study also underlines practical limitation. In particular, β-hemolysis and the co-plating inhibition assays were evaluated visually to classify hemolytic heterogeneity and to screen for Lactobacillus–*S. agalactiae* competition. While this approach is widely used in exploratory settings, standardised semi-quantitative methods, such as scoring systems or halo diameters measurement, would further increase reproducibility and comparability, as previously adopted in inhibition and hemolysis assays [45–47]. Incorporating such semi-quantitative approach together with the current phenotypic and genomic analyses would allow a more robust definition of *S. agalactiae* virulence heterogeneity and probiotic antagonism, without changing the biological conclusions of the present study.

Furthermore, to mitigate the transmission risk of MDR pathogens, several innovative strategies have been proposed. One promising option is the use of probiotics as adjunct or alternative approaches to conventional therapy. A key advantage of employing probiotic strains that are native or closely related to the resident microbiota of a given anatomical sites is the possibility of ecologically engineering the host environment to resist and resolve infection, rather than simply killing pathogens in a non-selective manner [48,49]. Within this framework, *Lactobacillus* spp. were evaluated for their ability to inhibit colonisation by *S. agalactiae* isolates with diverse characteristics, including MDR and hypervirulent phenotypes. We demonstrated that single *Lactobacillus* strains significantly reduced *S. agalactiae* survival in co-culture, although their inhibitory activity was strain-dependent. By contrast, a multi-strain *Lactobacillus* combination produced broader and more robust effects, acting through a combination of direct antimicrobial activity, protection of host cell viability, and impairment of pathogen adhesion.

While probiotic therapy offers a promising ecological strategy against key Gram-positive pathogens such as MDR *S. agalactiae*, the challenges posed by Gram-negative bacteria often demands more direct antimicrobial approaches. In this context, advanced nanoplatforms based on serine-derived nanoparticle (NP) were designed to target the distinctive cell-envelope structures of bacteria such as *E. coli*, *A. baumannii* and *P. aeruginosa,* as well as to tackle resilient Gram-positive threats like MRSA. Serine-based NP exhibited composition-dependent bactericidal activity, demonstrating substantial potential as antimicrobial agents but also raising concerns regarding cytotoxicity and selectivity. These formulations exerted antibacterial effects possibly through a membrane-centric mechanisms, involving electrostatic attraction to negatively charged bacterial surfaces, insertion of the amphiphilic molecules into the lipid bilayer, disruption of lipid packing and curvature stress, that increase permeability which further promote ion leakage and culminate in cell lysis [50–52]. In our study, a strong bactericidal effect was consistently observed against *S. aureus*, with all tested formulations causing undetectable colony counts; on the contrary, the effects against Gram-negative bacteria were weaker. It has been reported that the outer-membrane/LPS barrier and efflux systems in Gram-negative species limit NPs access to the

cytoplasmic membrane and resulted in weaker bactericidal effects [51,52]. Unfortunately, serine-based NP formulations compromised A549 cells metabolic activity and monolayer integrity at concentrations similar to those required for antibacterial activity, failing to offer an alternative treatment option. Although clinical isolates of *A. baumannii* and UPEC were not directly tested, these findings suggest that similar or even higher concentrations would likely be required to overcome the additional resistance and virulence traits of XDR/MDR clinical strains.

Interestingly, among the Gram-negative species tested, *A. baumannii* showed a comparatively greater reduction in CFU in response to serine-based NP formulations, whereas *E. coli* and *P. aeruginosa* remained more tolerant under the same conditions. This pattern suggests that, despite its notorious multidrug resistance, *A. baumannii* retains a degree of vulnerability to strong membrane-active agents that are able overcome the outer-membrane barrier, as previously reported [51,52]. When considered together with the ALI model, in which *A. baumannii* causes early epithelial and goblet-cell damage without massive replication, these findings raise the possibility that optimised serine-based NPs with acceptable cytotoxicity levels might be effective in preventing or reducing the initial stages of pathogen interaction within the airway epithelium, to avoid extensive tissue destruction and dysregulated inflammation.

Collectively, this thesis shows that *A. baumannii*, UPEC and *S. agalactiae* achieve persistence under antibiotic pressure through tightly coupled genomic, phenotypic and ecological adaptations that are tuned to adapt within the airway, urinary and vaginal niches. Across these pathogens, multidrug resistance does not simply accumulate on a neutral background but is embedded within virulence architectures that can compensate for resistance-associated fitness costs and sustain transmission in both hospital and community settings. At the same time, the evaluation of *Lactobacillus*-based probiotic strategies and serine-based NP highlights the need for complementary approaches that either reinforce colonisation resistance in stable microbiota or directly target the pathogen in their ideal niches. Together, these findings argue for integrated surveillance of resistance-virulence combinations across niches, alongside translational efforts that combine optimised antibiotic regimens with ecological (e.g., probiotics) and membrane-targeted (e.g., NPs) interventions to suppress high-priority MDR pathogens. While these novel strategies still encounter significant practical and regulatory challenges before clinical application, the extensive research efforts dedicated to this field make them highly promising solutions to effectively complement or replace traditional antibiotics in the near future.

References

1. López, M. *et al.* Evolution of the Quorum network and the mobilome (plasmids and bacteriophages) in clinical strains of Acinetobacter baumannii during a decade. *Sci. Rep.* **8**, 2523 (2018).
2. López, M. *et al.* Genomic Evolution of Two Acinetobacter baumannii Clinical Strains from ST-2 Clones Isolated in 2000 and 2010 (ST-2_clon_2000 and ST-2_clon_2010). *Genome Announc.* **4**, e01182-16 (2016).
3. Opazo-Capurro, A. *et al.* Evolutionary dynamics of carbapenem-resistant *Acinetobacter baumannii* circulating in Chilean hospitals. Preprint at https://doi.org/10.1101/467589 (2018).
4. Rokes, A. B., Santos-Lopez, A. & Cooper, V. S. History shapes regulatory and evolutionary responses to tigecycline in strains of *Acinetobacter baumannii* from the pre- and post-antibiotic eras. Preprint at https://doi.org/10.1101/2025.01.22.634413 (2025).
5. Valcek, A. *et al.* Genomic Analysis of a Strain Collection Containing Multidrug-, Extensively Drug-, Pandrug-, and Carbapenem-Resistant Modern Clinical Isolates of Acinetobacter baumannii. *Antimicrob. Agents Chemother.* **66**, e00892-22 (2022).
6. Valcek, A. *et al.* Phenotypic Characterization and Heterogeneity among Modern Clinical Isolates of Acinetobacter baumannii. *Microbiol. Spectr.* **11**, e03061-22 (2023).
7. Escalante, J. *et al.* Carbapenem-resistant Acinetobacter baumannii (CRAB): metabolic adaptation and transcriptional response to human urine (HU). *Sci. Rep.* **14**, 19145 (2024).
8. Jackson-Litteken, C. D. *et al.* InvL, an Invasin-Like Adhesin, Is a Type II Secretion System Substrate Required for Acinetobacter baumannii Uropathogenesis. *mBio* **13**, e00258-22 (2022).
9. Chukamnerd, A. *et al.* Association of biofilm formation, antimicrobial resistance, clinical characteristics, and clinical outcomes among *ACINETOBACTER BAUMANNII* isolates from patients with ventilator-associated pneumonia. *Clin. Respir. J.* **18**, e13732 (2024).
10. Schober, P., Boer, C. & Schwarte, L. A. Correlation Coefficients: Appropriate Use and Interpretation. *Anesth. Analg.* **126**, 1763–1768 (2018).
11. Janse, R. J. *et al.* Conducting correlation analysis: important limitations and pitfalls. *Clin. Kidney J.* **14**, 2332–2337 (2021).
12. Leone, L. *et al.* Klebsiella pneumoniae Is Able to Trigger Epithelial-Mesenchymal Transition Process in Cultured Airway Epithelial Cells. *PLOS ONE* **11**, e0146365 (2016).
13. Cano, V., Moranta, D., Llobet-Brossa, E., Bengoechea, J. A. & Garmendia, J. Klebsiella pneumoniae triggers a cytotoxic effect on airway epithelial cells. *BMC Microbiol.* **9**, 156 (2009).
14. Chevalier, C. *et al.* Epithelial cells maintain memory of prior infection with Streptococcus pneumoniae through di-methylation of histone H3. *Nat. Commun.* **15**, 5545 (2024).
15. Rai, P. *et al. Streptococcus pneumoniae* secretes hydrogen peroxide leading to DNA damage and apoptosis in lung cells. *Proc. Natl. Acad. Sci.* **112**, (2015).
16. Swart, A. L. *et al.* Pseudomonas aeruginosa breaches respiratory epithelia through goblet cell invasion in a microtissue model. *Nat. Microbiol.* **9**, 1725–1737 (2024).
17. Bhowmik, S. *et al. Acinetobacter baumannii* represses type VI secretion system through a manganese-dependent small RNA-mediated regulation. *mBio* **16**, e03025-24 (2025).
18. Zhang, Y. *et al.* The Negative Regulatory Role of Transcriptional Regulator H-NS on the Type VI Secretion System in Acinetobacter baumannii. *Infect. Drug Resist.* **Volume 18**, 2997–3011 (2025).
19. Weber, B. S., Ly, P. M., Irwin, J. N., Pukatzki, S. & Feldman, M. F. A multidrug resistance plasmid contains the molecular switch for type VI secretion in *Acinetobacter baumannii*. *Proc. Natl. Acad. Sci.* **112**, 9442–9447 (2015).

20. Janet-Maitre, M., Di Venanzio, G., Jackson-Litteken, C. D., Scott, N. E. & Feldman, M. F. Intracellular *Acinetobacter baumannii* Acts as a Reservoir in Lung Infection *via* a 'Persist and Resist' Strategy. Preprint at https://doi.org/10.1101/2025.04.28.651116 (2025).

21. Distel, J. S., Di Venanzio, G., Mackel, J. J., Rosen, D. A. & Feldman, M. F. Replicative Acinetobacter baumannii strains interfere with phagosomal maturation by modulating the vacuolar pH. *PLOS Pathog.* **19**, e1011173 (2023).

22. Bhuiyan, M. S. *et al. Acinetobacter baumannii* phenylacetic acid metabolism influences infection outcome through a direct effect on neutrophil chemotaxis. *Proc. Natl. Acad. Sci.* **113**, 9599–9604 (2016).

23. Liu, A.-R. *et al.* Role of immunodeficiency in Acinetobacter baumannii associated pneumonia in mice. *Chin. Med. J. (Engl.)* **133**, 2161–2169 (2020).

24. Soong, G., Parker, D., Magargee, M. & Prince, A. S. The Type III Toxins of *Pseudomonas aeruginosa* Disrupt Epithelial Barrier Function. *J. Bacteriol.* **190**, 2814–2821 (2008).

25. Cardinale, D. *et al.* Donor-derived airway ALI model for high-throughput screening of antiviral combinations with concurrent analysis of antiviral efficacy and epithelial toxicity using ciliR. *ERJ Open Res.* 01283–02025 (2026) doi:10.1183/23120541.01283-2025.

26. Awatade, N. T. *et al.* Comparison of commercially available differentiation media on cell morphology, function, and anti-viral responses in conditionally reprogrammed human bronchial epithelial cells. *Sci. Rep.* **13**, 11200 (2023).

27. Fisher, C. R. *et al.* A High-Throughput, High-Containment Human Primary Epithelial Airway Organ-on-Chip Platform for SARS-CoV-2 Therapeutic Screening. *Cells* **12**, 2639 (2023).

28. De Rudder, C., Calatayud Arroyo, M., Lebeer, S. & Van De Wiele, T. Dual and Triple Epithelial Coculture Model Systems with Donor-Derived Microbiota and THP-1 Macrophages To Mimic Host-Microbe Interactions in the Human Sinonasal Cavities. *mSphere* **5**, e00916-19 (2020).

29. Rohde, A. M. *et al.* Prevalence of third-generation cephalosporin-resistant Enterobacterales colonization on hospital admission and pmaESBL genotype-specific risk factors: a cross-sectional study in six German university hospitals. *J. Antimicrob. Chemother.* **75**, 1631–1638 (2020).

30. Liedhegner, E. *et al.* Similarities in Virulence and Extended Spectrum Beta-Lactamase Gene Profiles among Cefotaxime-Resistant Escherichia coli Wastewater and Clinical Isolates. *Antibiotics* **11**, 260 (2022).

31. Ruppé, E. *et al.* CTX-M β-Lactamases in *Escherichia coli* from Community-acquired Urinary Tract Infections, Cambodia. *Emerg. Infect. Dis.* **15**, 741–748 (2009).

32. Kohlenberg, A. *et al.* Emergence of Escherichia coli ST131 carrying carbapenemase genes, European Union/European Economic Area, August 2012 to May 2024. *Eurosurveillance* **29**, (2024).

33. Zhang, X., Miao, S., Ji, C. & Hu, W. Risk factors and treatment advances for carbapenem-resistant Enterobacteriaceae infections in the urinary tract. *Front. Cell. Infect. Microbiol.* **15**, 1724851 (2026).

34. Garcia, E. C., Brumbaugh, A. R. & Mobley, H. L. T. Redundancy and Specificity of *Escherichia coli* Iron Acquisition Systems during Urinary Tract Infection. *Infect. Immun.* **79**, 1225–1235 (2011).

35. Frick-Cheng, A. E. *et al.* Ferric Citrate Uptake Is a Virulence Factor in Uropathogenic Escherichia coli. *mBio* **13**, e01035-22 (2022).

36. Khan, F. Z., Palmer, K. & Dillon, N. Siderophores mediate antibiotic resistance. *Nat. Microbiol.* **9**, 587–588 (2024).

37. Karam, M. R. A., Habibi, M. & Bouzari, S. Relationships between Virulence Factors and Antimicrobial Resistance among <italic>Escherichia coli</italic> Isolated from Urinary Tract Infections and Commensal Isolates in Tehran, Iran. *Osong Public Health Res. Perspect.* **9**, 217–224 (2018).

38. Yilmaz, A. E. How reliable are the multiple comparison methods for odds ratio? *J. Appl. Stat.* **49**, 3141–3163 (2022).

39. Knol, M. J., Le Cessie, S., Algra, A., Vandenbroucke, J. P. & Groenwold, R. H. H. Overestimation of risk ratios by odds ratios in trials and cohort studies: alternatives to logistic regression. *Can. Med. Assoc. J.* **184**, 895–899 (2012).

40. Creti, R. *et al.* Group B Streptococcus (GBS) Carriage in Pregnant Women: Possible Emergence of Rare Serotypes and Antibiotic Resistance in Neonatal Disease. *Microorganisms* **13**, 1496 (2025).

41. Plainvert, C. *et al.* Multidrug-Resistant Hypervirulent Group B *Streptococcus* in Neonatal Invasive Infections, France, 2007–2019. *Emerg. Infect. Dis.* **26**, 2721–2724 (2020).

42. Chaguza, C. *et al.* Population genomics of Group B Streptococcus reveals the genetics of neonatal disease onset and meningeal invasion. *Nat. Commun.* **13**, 4215 (2022).

43. Ouancharee, W. *et al.* Predomination of hypervirulent ST283 and genetic diversity of levofloxacin resistance in multidrug-resistant, hypervirulent Streptococcus agalactiae in Thailand. *J. Med. Microbiol.* **74**, (2025).

44. Janžič, L. *et al.* Macrophage polarization during Streptococcus agalactiae infection is isolate specific. *Front. Microbiol.* **14**, 1186087 (2023).

45. Moran, J. C., Crank, E. L., Ghabban, H. A. & Horsburgh, M. J. Deferred Growth Inhibition Assay to Quantify the Effect of Bacteria-derived Antimicrobials on Competition. *J. Vis. Exp.* 54437 (2016) doi:10.3791/54437.

46. Sabersky-Müssigbrodt, H., Russell, S., Wantia, N. & Hayden, O. Rapid direct disk diffusion testing for antibiotic resistance in urinary tract infections: a bacterial concentration-adjusted approach. *Microbiol. Spectr.* **13**, e00888-25 (2025).

47. Hansen, S. M. & Sørensen, U. B. S. Method for Quantitative Detection and Presumptive Identification of Group B Streptococci on Primary Plating. *J. Clin. Microbiol.* **41**, 1399–1403 (2003).

48. Mazziotta, C., Tognon, M., Martini, F., Torreggiani, E. & Rotondo, J. C. Probiotics Mechanism of Action on Immune Cells and Beneficial Effects on Human Health. *Cells* **12**, 184 (2023).

49. Zhao, X. *et al.* Harnessing dual-channel probiotics to synergistically correct intestinal and vaginal dysbiosis after antibiotic disruption. *Npj Biofilms Microbiomes* **11**, 174 (2025).

50. Kowalczyk, I., Szulc, A., Koziróg, A., Komasa, A. & Brycki, B. Surface and Antimicrobial Properties of Ester-Based Gemini Surfactants. *Molecules* **30**, 2648 (2025).

51. Tripathi, V., Bhadra, J. & Bhattacharya, S. Structure–Activity Relationships and Practical Aspects of Cationic Gemini Surfactants as Antimicrobial Agents. *J. Surfactants Deterg.* jsde.70007 (2025) doi:10.1002/jsde.70007.

52. Modi, S. K., Gaur, S., Sengupta, M. & Singh, M. S. Mechanistic insights into nanoparticle surface-bacterial membrane interactions in overcoming antibiotic resistance. *Front. Microbiol.* **14**, 1135579 (2023).

Acknowledgments

Some dreams seem far beyond reach. Yet, never bury a dream, even when the road toward it appears almost impossible to find.

This PhD journey is one of those dreams that eventually became a reality. Along the way, many people became part of this journey with kindness, support, prayers, and trust, allowing me to stand where I am today.

With profound gratitude, I would like to express my sincere appreciation to:

1. The Indonesia Endowment Fund for Education (LPDP), for the investment, trust, and mandate granted through this doctoral scholarship. Thank you for opening the path for someone who was born and raised in a remote corner of the country, surrounded by limitations in access to information and technology, to pursue knowledge as far as possible and one day return home to serve.
2. My supervisors, Prof. Cecilia Ambrosi and Dr. Daniela Scribano. No words will ever be enough to express my gratitude for the dedication, patience, guidance, encouragement, and values you shared throughout these years. I came with nothing; even the foundations of microbiology and basic laboratory skills were not truly mine at the beginning. Yet, because of you, today I leave with knowledge, experience, and a profound love for bacteriology that I will carry for the rest of my life.
3. Professors and senior researchers in the section of Microbiology and Parasitology: Prof. Lucia Nencioni, Prof. Catia Longhi, Prof. Stefano D'Amelio, Prof. Serena Cavarello, Dr. Giulia Radocchia, and Dr. Ilaria Bellini, thank you for your collaboration and support.
4. Dr. Amina Bougouizi, for your willingness to collaborate. I truly hope you have found a stable position, and I hope our paths will cross again in the future.
5. My supportive and energetic lab-mates, Silvia Iannarelli, Giuseppe Di Cosimo, and Fransesca Giannotti, who constantly filled the laboratory with joy, laughter, and positive energy. *Grazie per questa bellissima amicizia.*
6. My ecclesia family in Rome, thank you for always making me feel at home whenever I came to you. Your kindness, care, and prayers meant far more than words can express.
7. Voor mijn tante en oom in Almelo, Netherland (Tante Ema, Tante Evie, Tante Tina, Tante Syane, en Oom Jhony) bedankt voor jullie onophoudelijke gebeden, steun, en de warmte van familie die zelfs op afstand altijd voelbaar bleef.
8. Last but not least, my greatest support system: my parents, my baby boys, my husband, and my brother. Thank you for every prayer, sacrifice, tear, encouragement, and unwavering support throughout these years. I may never be able to fully express my gratitude for your patience, endurance and unconditional love. Mom and Dad, thank you for everything. El and Natan, thank you for having such brave and loving heart!